The Pennsylvania State University

The Graduate School

Department of Energy and Geo-Environmental Engineering

MULTIPHASE ANALYSIS OF THREE-PHASE (GAS-CONDENSATE-WATER) FLOW IN PIPES

A Thesis in

Petroleum and Natural Gas Engineering

by

Jose S. Zaghloul

Submitted in Partial Fulfillment
of the Requirements
for the Degree of

Doctor of Philosophy

December 2006

The thesis of Jose S. Zaghloul was reviewed and approved* by the following:

Michael Adewumi
Professor of Petroleum and Natural Gas Engineering
Thesis Co-Adviser
Chair of Committee

M. Thaddeus Ityokumbul
Associate Professor of Mineral Processing and Geo-Environmental Engineering
Thesis Co-Adviser

Turgay Ertekin
Professor of Petroleum and Natural Gas Engineering
Program Chair, Petroleum & Natural Gas Engineering

Robert W. Watson
Associate Professor of Petroleum and Natural Gas and Geo-Environmental Engineering

Osama Awadelkarim
Professor of Engineering Science and Mechanics

*Signatures are on file in the Graduate School.

ABSTRACT

The transport of unprocessed gas streams in transmission pipelines is becoming more attractive for new developments. Transporting gas, oil, and water together from wells in satellite fields to existing processing facilities would reduce the investments required for expanding production. However, engineers often face several problems when designing these systems. These problems include reduced flow capacity, corrosion, emulsion, asphaltene or wax deposition, and hydrate formation.

Engineers need a tool to understand how the fluids travel together, quantify the flow reduction in the pipe, and determine where, how much, and the type of liquid that would form in a pipe. The present work addresses these needs, gaining a fundamental understanding of the thermodynamics, and hydrodynamic mechanisms for two- and three-phase flow.

The current study presents a flow model that couples complex hydrodynamic and thermodynamic models for describing the behavior of fluids traveling in near-horizontal pipes. This work includes:

- A hydrodynamic formulation for three-phase flow in pipes

- A thermodynamic model capable of performing two-phase and three-phase flow calculations in an accurate, fast and reliable manner.

- A new theoretical approach for determining flow pattern transitions in three-phase (gas-condensate-water) flow, and closure models that effectively handle different three-phase flow patterns and their transitions.

The unified two-fluid model developed herein is shown to be capable of handling systems exhibiting two-phase (gas-water and gas-condensate) and three-phase (gas-condensate-water) flow. Model predictions were compared against field and experimental data with excellent matches.

The hydrodynamic model allows: 1) the determination of flow reduction due to the condensation of liquid(s) in the pipe, 2) assessment of the potential for forming substances that might affect the integrity of the pipe, and 3) evaluation of the possible measures for improving the deliverability of the pipeline.

This work develops the framework for a robust thermodynamic-hydrodynamic model capable of simulating two and three-phase flow in typical gas transmission pipelines. The flow model developed herein represents an outstanding tool that allows engineers to improve the design of lines, liquid collection, and separation facilities.

TABLE OF CONTENTS

LIST OF FIGURES

LIST OF TABLES

NOMENCLATURE

A	Peng-Robinson EOS parameter [*unitless*]
A_{pipe}	Cross sectional area of the pipe $[L^2]$
A_g	Cross sectional area of the pipe occupied by the gas phase $[L^2]$
A_{Lh}	Cross sectional area of the pipe occupied by the condensate phase $[L^2]$
A_{Lw}	Cross sectional area of the pipe occupied by the aqueous phase $[L^2]$
$A_{g\text{-}Lh}$	Surface area between gas – condensate phases per unit volume $[1/L]$
$A_{g\text{-}Lw}$	Surface area between gas – water phases per unit volume $[1/L]$
$A_{Lw\text{-}Lh}$	Surface area between condensate-aqueous phases per unit volume $[1/L]$
A_w	Pipe area in contact to a fluid per unit volume $[1/L]$
A_{wa}	Pipe area in contact to phase 'a' per unit volume $[1/L]$
A_{wg}	Pipe area in contact to the gas phase per unit volume $[1/L]$
A_{wLh}	Pipe area in contact to the condensate phase per unit volume $[1/L]$
A_{wLw}	Pipe area in contact to the aqueous phase per unit volume $[1/L]$
A_{PD}	Passut & Danner ideal enthalpy coefficient
$[A_m]$	Coefficient Matrix of the hydrodynamic formulation (implicit form)
a_i^F	Fehlberg parameter (Runge-Kutta method)
$(a\alpha)_i$	Peng-Robinson parameter for the *i*-th element $[L^5/m\text{-}t^2]$
$(a\alpha)_m$	Peng-Robinson parameter for the mixture $[L^5/m\text{-}t^2]$
B	Peng-Robinson EOS parameter [*unitless*]
B_{PD}	Passut & Danner ideal enthalpy coefficient
$[B_m]$	Coefficient Vector of the hydrodynamic formulation (implicit form)
b_i	Peng-Robinson co-volume parameter for the *i*-th component $[L^3/m]$
b_m	Peng-Robinson co-volume parameter for the mixture $[L^3/m]$
b_i^F	Fehlberg parameter (Runge-Kutta method)
Cd	Drag coefficient *[unitless]*

C_{PD} Passut & Danner ideal enthalpy coefficient

C_{Pg} Gas heat capacity at constant pressure $[L^2/t^2\text{-}T]$

C_{PLh} Condensate heat capacity at constant pressure $[L^2/t^2\text{-}T]$

C_{PLw} Aqueous phase heat capacity at constant pressure $[L^2/t^2\text{-}T]$

C_{Pl} Liquid heat capacity at constant pressure $[L^2/t^2\text{-}T]$

c_i Mole fraction of the *i*-th component *[unitless]*

c_i^{*F} Fehlberg parameter (Runge-Kutta method)

c_i^{F} Fehlberg parameter (Runge-Kutta method)

D_{PD} Passut & Danner ideal enthalpy coefficient

d Diameter of the pipe *[L]*

dp Droplet diameter *[L]*

d_i^{F} Fehlberg parameter (Runge-Kutta method)

d_h Hydraulic diameter *[L]*

d_{ha} Hydraulic diameter of phase '*a*' *[L]*

d_{hg} Hydraulic diameter of the gas phase *[L]*

d_{hl} Hydraulic diameter of the liquid phase *[L]*

d_{hLh} Hydraulic diameter of the condensate phase *[L]*

d_{hLw} Hydraulic diameter of the aqueous phase *[L]*

E_{PD} Passut & Danner ideal enthalpy coefficient

e_i^{F} Fehlberg parameter (Runge-Kutta method)

F_i Interfacial force between gas – liquid phases per unit volume $[m/L^2\text{-}t^2]$

$F_{ig\text{-}Lh}$ Interfacial force between gas – condensate phases per unit volume $[m/L^2\text{-}t^2]$

$F_{iLw\text{-}Lh}$ Interfacial force b/w condensate –aqueous phases per unit volume $[m/L^2\text{-}t^2]$

F_g Gravitational force per unit volume $[m/L^2\text{-}t^2]$

F_{gg} Gas gravitational force per unit volume $[m/L^2\text{-}t^2]$

$F_{g\text{-}Lh}$ Condensate gravitational force per unit volume $[m/L^2\text{-}t^2]$

$F_{g\text{-}Lw}$ Aqueous phase gravitational force per unit volume $[m/L^2\text{-}t^2]$

$F_{mg\text{-}l}$ Mass transfer force b/w gas – liquid phases per unit volume $[m/L^2\text{-}t^2]$

$F_{mg\text{-}Lh}$ Mass transfer force b/w gas – condensate phases per unit volume *[m/ L^2-t^2]*

$F_{mLw\text{-}Lh}$ Mass transfer force b/w cond. –aqueous phases per unit volume *[m/ L^2-t^2]*

F_{PD} Passut & Danner ideal enthalpy coefficient

F_{tg} Net forces acting on the gas phase per unit volume *[m/ L^2-t^2]*

F_{tLh} Net forces acting on the condensate phase per unit volume *[m/ L^2-t^2]*

F_{tLw} Net forces acting on the aqueous phase per unit volume *[m/ L^2-t^2]*

F_{tl} Net forces acting on the liquid phase per unit volume *[m/ $L^{2\text{-}}t^2$]*

F_w Wall friction forces per unit volume *[m/ $L^{2\text{-}}t^2$]*

F_{wa} Wall friction forces acting on phase '*a*' per unit volume *[m/ L^2-t^2]*

F_{wg} Wall friction forces acting on the gas phase per unit volume *[m/ L^2-t^2]*

F_{wl} Wall friction forces acting on the liquid phase per unit volume *[m/ L^2-t^2]*

F_{wLh} Wall friction forces acting on the condensate phase per unit volume *[m/ L^2-t^2]*

F_{wLw} Wall friction forces acting on the aqueous phase per unit volume *[m/ L^2-t^2]*

F_i^F Fehlberg parameter (Runge-Kutta method)

f_i Interfacial friction factor *[unitless]*

$f_{ig\text{-}Lh}$ Gas – Condensate interfacial friction factor *[unitless]*

$f_{iLh\text{-}Lw}$ Condensate – Aqueous phase interfacial friction factor *[unitless]*

f_{ai} Fugacity of the component '*i*' in phase '*a*'

f_{gi} Fugacity of the component '*i*' in the gas phase

f_{li} Fugacity of the component '*i*' in the liquid phase

f_{Lhi} Fugacity of the component '*i*' in the condensate phase

f_{Lwi} Fugacity of the component '*i*' in the aqueous phase

f_{mg} Gas mass fraction *[unitless]*

f_{ml} Liquid mass fraction *[unitless]*

f_{mLh} Condensate mass fraction *[unitless]*

f_{ng} Gas molar fraction *[unitless]*

f_{nl} Liquid molar fraction *[unitless]*

f_{nLh} Condensate molar fraction *[unitless]*

f_{nLw} Aqueous phase molar fraction *[unitless]*

f_{vg} Gas volumetric fraction *[unitless]*

f_{vl} Liquid volumetric fraction *[unitless]*

f_{vLh} Condensate volumetric fraction *[unitless]*

f_{vLw} Aqueous phase volumetric fraction *[unitless]*

f_w Fanning friction factor *[unitless]*

f_{wa} Fanning friction factor of phase '*a*' *[unitless]*

f_{wg} Fanning friction factor of the gas phase *[unitless]*

f_{wl} Fanning friction factor of the liquid phase *[unitless]*

f_{wLh} Fanning friction factor of the condensate phase *[unitless]*

f_{wLw} Fanning friction factor of the aqueous phase *[unitless]*

f_{vi} Fugacity of the *i*-th component in the gas phase

f_{LAi} Fugacity of the *i*-th component in the hydrocarbon-rich liquid

f_{LBi} Fugacity of the *i*-th component in the water-rich liquid

G_m Total mass flux entering the pipe per unit area *[m/L^2-t]*

g Gravitational acceleration *[m/t^2]*

g_c Unit conversion factor *[32.174 lbm-ft/lbf-s^2]*

g_{∞}^{E} Excess Gibbs energy at infinite pressure

g_{ij} Interaction energy parameters (thermodynamic model)

hl Equilibrium liquid level in the pipe *[L]*

H Enthalpy per unit mass *[L^2/t^2]*

H_g Gas enthalpy per unit mass *[L^2/t^2]*

H_l Liquid enthalpy per unit mass *[L^2/t^2]*

H_{Lh} Condensate enthalpy per unit mass *[L^2/t^2]*

H_{Lw} Aqueous phase enthalpy per unit mass *[L^2/t^2]*

H^* Ideal gas enthalpy *[L^2/t^2]*

J Energy conversion factor *[778.17 lbf-ft/Btu]*

K_i Distribution coefficient of component '*i*'

KA_i	Distribution coefficient of component '*i*' for the hydrocarbon-rich phase
KB_i	Distribution coefficient of component '*i*' for the water-rich phase
k_v	Lee & González gas viscosity parameter
k_{ij}	Binary interaction coefficients (Peng-Robinson EOS)
L_{pipe}	Total Length of the pipe *[L]*
LA	Mole fraction of the hydrocarbon-rich liquid phase
LB	Mole fraction of the water-rich liquid phase
$\tilde{M}_g$	Total Mass transferred into the gas phase *[m/s-L^3]*
$\tilde{M}_{Lh}$	Total Mass transferred into the condensate phase *[m/s-L^3]*
$\tilde{M}_{Lw}$	Total Mass transferred into the aqueous phase *[m/s-L^3]*
Mw	Molecular weight
Mw_a	Molecular weight of phase 'a'
Mw_v	Molecular weight of the gas phase
Mw_{LA}	Molecular weight of the condensate phase
Mw_{LB}	Molecular weight of the aqueous phase
Mw_i	Molecular weight of the *i*-th component
Mw_l	Molecular weight of the liquid phase
n	Number of components
On	Ohnesorge or viscosity stability number *[unitless]*
P	Pressure *[m/L-t^2]*
Pcr_i	Parachor of the *i*-th component *[m/L-t^2]*
P_{ci}	Critical pressure of the *i*-th component *[m/L-t^2]*
P_{ri}	Reduced pressure of the *i*-th component *[m/L-t^2]*
Q_w	Water flow rate injected into the pipe *[bbl/s]*
Q_{gLh}	Heat exchanged from the gas to the condensate phase *[m/L-t^3]*
Q_{gLw}	Heat exchanged from the gas to the aqueous phase *[m/L-t^3]*
Q_{Lhg}	Heat exchanged from the condensate to the gas phase *[m/L-t^3]*

Q_{LhLw} Heat exchanged from the condensate to the aqueous phase *[m/L-t^3]*

Q_{Lwg} Heat exchanged from the aqueous to the gas phase *[m/L-t^3]*

Q_{LwLh} Heat exchanged from the aqueous to the condensate phase *[m/L-t^3]*

Q_{sg} Heat exchanged between the surroundings and the gas phase *[m/L-t^3]*

Q_{sLh} Heat exchanged between the surroundings and the condensate phase *[m/L-t^3]*

Q_{sLw} Heat exchanged between the surroundings and the aqueous phase *[m/L-t^3]*

Q_{st} Total heat input per unit volume *[m/L-t^3]*

r Droplet radius *[L]*

r_p Mean droplet radius *[L]*

r_{max} Maximum droplet radius *[L]*

R Radius of the pipe [L] / Universal Gas Constant (In thermodynamics)

$[R_m]$ Vector of the hydrodynamic system of equations (explicit form)

Re Reynolds number *[unitless]*

Re_a Reynolds number of phase '*a*' *[unitless]*

Rr_i Fugacity ratio of the *i*-th component *[unitless]*

s Jeffrey's sheltering coefficient *[unitless]*

S_g Pipe surface wetted by the gas phase *[L^2]*

S_{Lh} Pipe surface wetted by the condensate phase *[L^2]*

S_{Lw} Pipe surface wetted by the aqueous phase *[L^2]*

$S_{iLw\text{-}Lh}$ Surface of the interface b/w condensate – aqueous phase *[L^2]*

$S_{ig\text{-}Lh}$ Surface of the interface b/w gas - condensate phase *[L^2]*

T Temperature *[T]*

T_{ci} Critical temperature of the *i*-th component *[T]*

T_{ri} Reduced temperature of the *i*-th component *[unitless]*

T_{pc} Pseudo-critical temperature *[T]*

T_s Temperature of the surroundings *[T]*

t Time *[t]*

$[U]$ Vector containing the unknowns of the hydrodynamic formulation

U	Overall heat transfer coefficient *[m/t^3-T]]*
V	Molar fraction of the vapor phase (thermodynamic model) *[unitless]*
V_{ci}	Critical volume of the *i*-th component *[L^3]*
V_{pc}	Pseudo critical volume *[L^3]*
$\tilde{v}$	Specific volume of a fluid *[L^3/m]*
v	Local fluid velocity *[L/t]*
v_a	Velocity of phase '*a*' *[L/t]*
v_g	Gas velocity *[L/t]*
v_{Lh}	Velocity of the condensate phase *[L/t]*
v_{Lw}	Velocity of the aqueous phase *[L/t]*
v_l	Liquid velocity *[L/t]*
w_i	Acentric factor of the *i*-th component *[unitless]*
We	Webber number *[unitless]*
We_{sl}	Superficial Webber number *[unitless]*
Wf	Wetted wall fraction (Grolman and Fortuin correlation) *[unitless]*
x	Distance *[L]*
x_i	Mole composition of the *i*-th component in the liquid phase
XA_i	Mole composition of the *i*-th component in the hydrocarbon-rich liquid phase
XB_i	Mole composition of the *i*-th component in the aqueous liquid phase
x_v	Lee & González gas viscosity parameter
y_i	Mole composition of the *i*-th component in the vapor phase
y_v	Lee & González gas viscosity parameter
Z	Compressibility factor *[unitless]*
Z_a	Compressibility factor of phase '*a*' *[unitless]*
Z_v	Compressibility factor of the gas phase *[unitless]*
Z_{Lh}	Compressibility factor of the condensate phase *[unitless]*
Z_{Lw}	Compressibility factor of the aqueous phase *[unitless]*
z_i	Mole composition of the *i*-th component in a mixture

GREEK

α_a	Holdup of phase '*a*' *[unitless]*
α_g	Gas holdup *[unitless]*
α_ℓ	Liquid holdup *[unitless]*
α_{Lh}	Holdup of the condensate phase *[unitless]*
α_{Lw}	Holdup of the aqueous phase *[unitless]*
β	Pipe inclination
β_{ij}	Non-randomness parameters (NRTL model)
Δ	Truncation error value
Δ_{ij}	Kroeneker delta
Δ_0	Maximum truncation error allowed
Δx	Length of a pipe block *[L]*
ε	Pipe roughness *[L]*
ε_i	Interface roughness *[L]*
ϕ_1	Wetting angle of the aqueous phase
ϕ_2	Wetting angle of the liquid phases
$\overline{\phi}_i$	Fugacity coefficient of the *i*-th component
$\overline{\phi}_{LAi}$	Fugacity coefficient of the *i*-th component in the condensate phase
$\overline{\phi}_{LBi}$	Fugacity coefficient of the *i*-th component in the aqueous phase
$\gamma_{i\infty}$	Activity coefficient at infinite pressure for the *i*-th component
η_g	Joule-Thomson coefficient for the gas phase *[L-t^2-T/m]*
η_{Lh}	Joule-Thomson coefficient for the condensate phase *[L-t^2-T/m]*
η_{Lw}	Joule-Thomson coefficient for the aqueous phase *[L-t^2-T/m]*
λ_i	ASSM exponent
μ_g	Gas viscosity *[m/L-t]*

μ_{Lh}	Viscosity of the condensate phase *[m/L-t]*
μ_{Lw}	Viscosity of the aqueous phase *[m/L-t]*
μ_l	Liquid viscosity *[m/L-t]*
μ^*	Viscosity at atmospheric pressure (Lohrenz et al. correlation) *[m/L-t]*
μ_i^*	Viscosity of the *i*-th comp. at low pressure (Lohrenz et al. correlation) *[m/L-t]*
θ	Inclination angle of the pipe with respect to the horizontal *[rad]*
ρ_a	Density of phase '*a*' *[m/L^3]*
ρ_g	Gas density *[m/L^3]*
ρ_{Lh}	Density of the condensate phase *[m/L^3]*
ρ_{Lw}	Density of the aqueous phase *[m/L^3]*
ρ_r	Reduced density *[unitless]*
θ	Pipe wetted angle in stratified flow regime
θ_i	Interface angle in the double circle model
∇	Divergence or gradient operator
φ	Fractional error
ξ_m	Mixture viscosity parameter (Lohrenz et al. correlation) *[L-t/m]*
σ	Surface tension
σ_l	Surface tension of the liquid *[m/t^2]*
σ_m	Surface tension of the mixture *[m/t^2]*
σ_{Lh}	Surface tension of the condensate phase *[m/t^2]*
σ_{Lw}	Surface tension of the aqueous phase *[m/t^2]*

SUBSCRIPT

a	Phase '*a*'
c	Critical
calc	Calculated
dg	Dense gas
eq	Equivalent

exp	Experimental
i, j, k	*i*-th, *j*-th, or *k*-th component
g, v	Gas
LA, L_h	Condensate phase , Hydrocarbon-rich liquid phase
LB, L_w	Aqueous phase, Water-rich liquid phase
l	Liquid
PD	Passut & Danner
pc	Pseudo-critical
r	Reduced
s	Surroundings
sc	Standard conditions
t	Total

CHAPTER 1

INTRODUCTION

1.1 Introduction

Flow assurance engineers face several challenges when designing multiphase flow systems. These challenges include: assessing the flow capacity reduction due to the formation of liquid(s) in the pipe, and evaluating the potential for forming undesirable substances (acids, waxes, emulsions and hydrates) in the lines.

Perhaps, one of the most severe problems is the reduced flow capacity. Multiphase flow in pipes might result in a significant increase in pressure drop when compared to single phase flow. Hart et al. (1989) reported that pressure drop could increase up to 30% for systems flowing gas/gas-condensate at low liquid loadings (0.5%). Currently, most numerical models are designed for evaluating flow reduction in two-phase (gas-liquid) flow systems. Therefore, there is the need for a tool capable of estimating flow reduction when more than one liquid is formed in the pipe.

Another flow assurance issue is the potential formation of hydrates. Transporting water and light hydrocarbons together might create the conditions for forming these crystals. The formation of these solid compounds might create a restriction to the flow or even plug the pipe. Methanol, glycol and other alcohols are commonly injected in pipelines for inhibiting hydrate formation. These substances can easily mix with the

water phase promoting the formation of a liquid phase. Engineers need to assess how much the inclusion of inhibitors affects the flow capacity of the lines.

Corrosion is another problem found in unprocessed gas streams. Transporting water along with CO_2 and/or H_2S might create the conditions for forming acids, that could affect the mechanical integrity of the lines. Therefore, it is important to estimate the composition of the aqueous liquid phase formed in order to evaluate the possibility of acid formation.

In summary, engineers need a tool to understand how the fluids travel together, quantify the flow reduction in the pipe, and determine where, how much, and the type of liquid(s) that form in the pipe. The present work addresses these needs, gaining a fundamental understanding of the thermodynamics, and hydrodynamic mechanisms for three-phase flow.

1.2 Statement of the problem

Three-phase flow in pipes is a topic of practical importance in the oil and gas industry. Most gas wells produce small fractions of condensate and water that are transported simultaneously to processing facilities. Even though this flow is of practical research importance, it is an area that has not received much attention.

Much of the research work has focused on developing an understanding of two-phase (gas-liquid) flow, and then extrapolates the two-phase behavior to liquid mixtures containing water. This assumption is, most of the time, unpractical or erroneous. Three-

phase flow is a challenging and complex problem. Modeling this flow involves the solution of complex thermodynamic and hydrodynamic mathematical formulations.

The main problem to be addressed in this work is the reduced flow capacity due to the formation of two liquid phases in a gas pipeline. This work focuses on developing a model to describe the hydrodynamic behavior of three-phase flow in pipes.

The impact that three-phase flow (gas-oil-water) could have on the deliverability of a piping system could be better explained with an example. Figure 1.1 explains the typical behavior of a system entering the three-phase region. This figure shows that a well might be producing gas at certain conditions (point A), but at a certain point in the pipe, this gas will start to form condensate (point B). The formation of this liquid phase will increase the pressure losses in the pipe. This liquid will continue to accumulate in the pipe until a second liquid phase starts to occur (Point C). At this point we would have three phases traveling simultaneously inside the pipe, increasing the pressure gradient in the pipe even more. The two liquids formed continue to accumulate until reaching a maximum liquid holdup. Then, as the pressure drops the liquids start re-vaporizing until they reach a point where one of the liquid phases disappears (Point D). As pressure continues to drop, the liquid still present continues to revaporize until it leaves only a single vapor phase in the piping system (Point E). Then, the pipe will operate with a single phase until reaching its final destination (Point F). These series of events would explain a high pressure drop and a reduced flow capacity, and would allow engineers to decide beforehand the actions to take in order to improve the deliverability of the pipe.

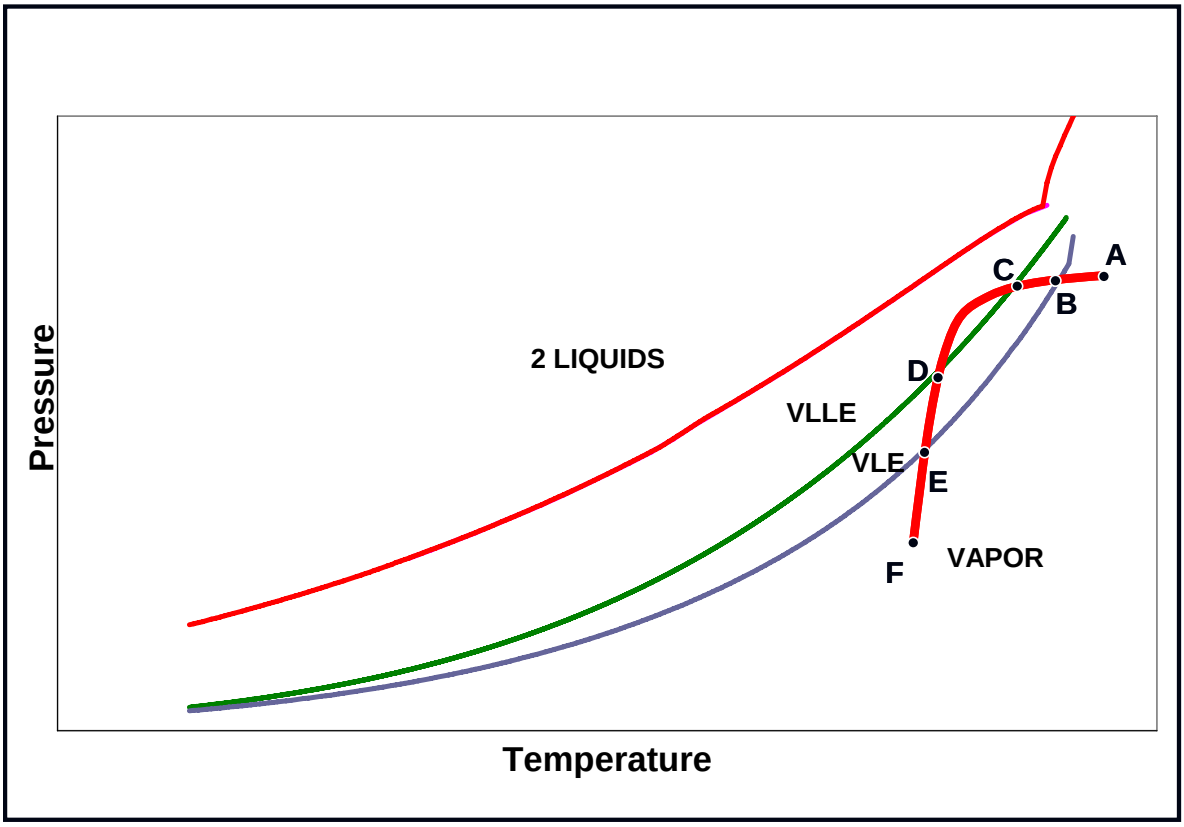

Figure 1.1 Behavior of a system entering the three-phase condition

This example showed that an operator could be producing gas from a reservoir and obtaining gas at the processing plant. However, the deliverability of the system is not that expected for single phase flow. With the current tools, this operator would not be able to provide an explanation for the reduced flow capacity, since he lacks a tool to adequately describe what is happening between the two points.

There are other flow assurance issues that could be addressed through the understanding of the thermodynamic and hydrodynamic behavior of this kind of flow. These flow assurance issues are related to the potential formation of undesirable

substances inside the transport system. These substances could be acids, hydrates, emulsions, waxes, or asphaltene compounds. These issues could be properly addressed by estimating the composition of the phases traveling inside the pipe. This information allows engineers to assess the possibility of forming these substances, and how to avoid their occurrence. These analyses minimize production losses and maintenance investments required to keep these piping systems operating properly.

The model provides engineers with a tool for understanding the flow mechanisms involved in three-phase flow in pipes, and help them make better assessments on the actions required to prevent any flow restrictions in a pipe.

1.3 Research objectives

The objective of this study is to develop a one-dimensional compositional hydrodynamic model for three-phase flow (gas-condensate-water) in pipes. This model provides the means for gaining a fundamental understanding of the thermodynamic and hydrodynamic mechanisms involved.

The model described herein is used for determining the effect of hydrate inhibitors on the flow performance of a system. It is also used to estimate the composition of the phases precipitating in the pipe and their potential to form substances that might affect the mechanical integrity of the pipe. The tool developed allows performing a fundamental representation of three-phase flow that will help engineers make better

assessments on the actions required to prevent or minimize the reduction in flow capacity of pipes.

CHAPTER 2

BACKGROUND

Multiphase flow technology in the petroleum industry has experienced dramatic improvements over the last sixty years. This state of the art technology has evolved from simple correlations and charts for estimating pressure losses and flow regimes in the early 50's, to the complex numerical simulators used nowadays.

Multiphase flow simulation tools couple complex hydrodynamic and thermodynamic models to describe the behavior of fluids flowing simultaneously in a pipe. This work will briefly summarize the background of each one of the major disciplines involved in the development of these tools; namely, hydrodynamic modeling and multiphase equilibria.

2.1 Hydrodynamic modeling

Brill and Arirachakaran (1992) presented a brief summary of the history of the development of multiphase flow technology. They divided the development of multiphase flow technology into three periods: the empirical period, the awakening years, and the modeling period. This work will explain the evolution of the technology for these three periods.

The empirical period (Late 40's-early 80's)

During this period, researchers focused their work on correlating experimental and field data for estimating pressure losses and determining flow patterns at different operating conditions. There were two different approaches used for modeling multiphase flow. These approaches were classified by Adewumi and Mucharam (1987) as Single-Phase-Safety-Factor (SPSF) and the Steady-Empirical-Two-Phase (SETP) approaches.

The SPSF approaches considered the multi-fluid system as a homogeneous mixture and used the equations for single phase flow in pipes for determining pressure losses. These approaches propose the use of a "correction or safety factor" to account for the increase in pressure drop when compared to single phase flow.

The SETP approaches are basically empirical correlations relating liquid holdup, superficial velocities, flow patterns, and pressure drop in pipes. Many of these correlations are still in use in the petroleum industry. The most popular and extensively used correlations in the petroleum industry were the Lockhart-Martinelli (1949), Baker (1953), Eaton et al. (1967), and Beggs & Brill (1973). These correlations provided a practical tool for estimating pressure drop and identifying flow regimes, but did not contribute to the fundamental understanding of the multiphase flow mechanisms.

Many comparative studies of SPSF and SETP models have been performed over the years. Among these studies can be cited the works of Dukler (1969), Gregory & Aziz

(1975), Danesh & Noghrehkar (1976), Fayed & Otten (1983), Adewumi & Bukacek (1985), and Cawkwell & Charles (1985). These studies show wide differences between the predictions, and significant deviations between the calculated and measured data. These studies show that both, SPSF and SETP, empirical approaches have failed due to their lack of universal applicability.

The awakening years (Late 70's – Mid 80's)

These years were signed by the introduction of the PC during the early 80's, and the increase of the computational power at a reasonable cost. The introduction of the PC allowed engineers to have tools for discretizing problems and numerically integrating pressure gradients over long segments of pipes. By the early 80's most of the major oil companies had computational tools that predicted pressure drop in pipelines based on the empirical methods previously proposed (Brill and Arirachakaran, 1992).

During this period, many of the inconsistencies between different empirical methods proposed were identified, making clear the need for a new approach that took into account the physics behind multi-phase transport. Taitel & Dukler (1976) were one of the first researchers that introduced the use of the fundamental conservation equations into multiphase flow modeling. They introduced physical concepts for predicting pressure losses and understanding how the transitions between the different flow regimes occur.

The modeling years (Mid 80's – Today)

The increase in oil prices and promising offshore developments in places like the Gulf of Mexico and North Sea triggered the need for a fundamental understanding of the multiphase flow processes and phenomena. Models based on the fundamental conservation equations were available (Hughes et al. (1976)). They were more advanced and theoretically sound than the previous approaches, but required significantly more computational power to be implemented. The expansion in affordable computational power allowed researchers to implement solution approaches for using numerical modeling techniques.

The Two-Fluid model (Hughes et al. (1976)) was originally developed and successfully implemented for problems in the nuclear industry. This approach was based on solving the mass, momentum, and energy conservation equations for pipes transporting water and air. This formulation provided the framework for integrating the thermodynamic behavior and the retrograde condensation effects in the simulation of gas/gas-condensate systems.

Since the early 90's, several mechanistic models have been proposed for simulating two-phase flow in pipes. Xiao et al. (1990) proposed a comprehensive model for near horizontal pipes, Ansari et al. (1990) suggested a model for vertical pipes, and Kaya et al. (1999) introduced a model for deviated pipes. However, these models have an important limitation. They assume that the fluids traveling in the pipe are immiscible, since no mass transfer is considered between the phases in the formulation of the

continuity equations. This assumption makes these models inappropriate for simulating gas/gas-condensate systems.

Successful modeling of multiphase flow (gas/gas-condensate) has been systematically developed at Penn State (Adewumi et al., 1993). The chronology of the studies performed at Penn State is described in Table 2.1. The thermodynamic-hydrodynamic models developed at Penn State sought a fundamental understanding of two-phase (gas-condensate) flow in pipes and the solution of practical problems faced by the natural gas industry.

Table 2.1 Chronology of the multiphase flow studies developed at Penn State

Year	Author	Summary
1988	Vincent	Successfully modeled steady-state two-phase flow (gas/condensate) in a horizontal pipeline operating under mist flow conditions.
1990	Mucharam	Incorporated the effect of undulating terrain into Vincent's work, and expanded his formulation for un-steady state flow. Mucharam still retained the mist flow assumption.
1994	Boriyantoro	Expanded the steady state formulation by including stratified flow regime and handling the transitions between flow regimes.
1994	Martinez	Proposed an extension of Boriyantoro's work for modeling open-network systems.
1996	Dukhovnaya	Incorporated for the first time the energy balance equation into the formulation.
1997	Nordin	Developed a thermodynamic model capable of predicting the behavior of natural gas systems containing Polychlorinated-Biphenyl components.
1999	Carrillo	Incorporated stream blending into Martinez's work.
2000	Antonini	Presented a simplified non-isothermal hydrodynamic model for two-phase (gas-condensate) flow in pipelines.
2001	Ayala	Performed the most comprehensive study on steady-state two-phase flow at Penn State. Expanded the formulation for all low liquid loading flow regimes (mist, annular, stratified smooth, and stratified wavy), and incorporated the energy balance into the set of equations.
2003	Eltohami	Developed a thermodynamic-hydrodynamic model for simulating PCB removal processes from natural gas transmission lines.

All the previous efforts at Penn State have focused on modeling gas/gas-condensate flow. No attempt has been made at Penn State to model three-phase flow (gas-condensate-water) using the mechanistic approach developed.

Three-phase flow (gas-oil-water) in pipes is a common occurrence in the petroleum and natural gas industry. Gas pipelines typically contain small fractions of condensate and water that are transported together to the processing plants. Moreover, water and condensate production may increase dramatically as reservoirs are depleted. Using the two-phase assumption for modeling three-phase flow does not appear to be a sound practice. In spite of the practical importance of three-phase flow in pipes, it is surprising how little work has been dedicated to study these systems (Taitel et al., 1995).

A limited number of experimental studies for understanding the occurrence and transition of three-phase flow regimes are available. Açikgöz et al. (1992) proposed the first flow regime map for horizontal three-phase flow. This flow regime map divides the three-phase flow spectrum into ten complex flow patterns. Since then, other authors have performed similar studies. Lee et al. (1993) and Pan et al. (1995) performed flow pattern studies for horizontal air-oil-water flow, and classified three-phase flow regimes into seven flow patterns, namely: stratified smooth, stratified wavy, rolling wave, plug flow, bubble flow, slug flow, and annular flow. These studies were empirical in nature and the correlation developed did not provide a sound theoretical basis for the transition from one flow regime to the other.

One of the first attempts at modeling three-phase flow in horizontal pipes using fundamental equations was performed by Taitel, Barnea, and Brill in 1995. These researchers proposed a simplified approach for estimating pressure losses in stratified three-phase flow that only considered the momentum balance of the three phases. Khor et al. (1997) compared predictions for the three-phase stratified flow proposed by Taitel et al. (1995) using different options for calculating the shear stresses between the phases. Zhang et al. (2005) proposed a unified model of gas/oil/water flow. Zhang et al. (2005) treated the three-phase flow as being equivalent to two-phase flow when turbulence is sufficient to mix the liquids or as a three-layer stratified flow at low flow rates in horizontal or near horizontal pipes. The Zhang et al. model makes several simplifications to the three-phase flow problem. These authors did not take into account mass transfer between the flowing phases, and assumed isothermal flow conditions.

2.2 Multiphase equilibria

Numerous researchers have proposed modifications to the Van Der Waals Equation of State (EOS) ever since it was published in 1873. The objectives of these variations have been calculating vapor-liquid equilibria using the same EOS, and obtaining a better representation of liquid and vapor densities for the entire spectrum of operating conditions that could exist in a chemical system. These issues were discussed by Van Der Waals as early as 1873 and they are still important areas of research.

One of the most popular and extensively used modifications of the Van Der Waals EOS was proposed by Redlich and Kwong (1949). Since that time, hundreds of

modifications have been proposed for representing different mixtures at different operating conditions.

Heidemann (1974) showed that a single equation of state could be used to describe three-phase (vapor-liquid-liquid) equilibrium. He used a simple approach based on free energy minimization to perform three-phase flash calculations for a water-paraffin system and a methane-n-butane-water system. For his calculations, he used Wilson's version of Redlich-Kwong EOS. Nevertheless, he indicated that his approach could be used with almost any other equation of state.

Soave (1972) proposed a modification to the Redlich-Kwong EOS that was rapidly adopted by the petroleum industry due to its simplicity and reasonable accuracy predicting liquid and vapor densities. However, the proposed modification could not accurately predict the liquid density near the critical point.

Peng and Robinson (1976a) proposed an EOS that improved the liquid density calculations near the critical point. That same year, Peng and Robinson (1976b) expanded the use of their newly proposed equation of state for performing two and three-phase equilibrium calculations in hydrocarbon/water systems. They based their phase equilibria calculations on the use of distribution coefficients. The method proposed had two limitations: the need to know a priori the number of phases in equilibrium, and the poor accuracy of the flash calculations using the classical mixing rules.

Nelson (1987) suggested an algorithm for rapid determination of the number of phases. His method was based on the Rachford-Rice formulation and a multiphase generalization of the dew and bubble point criteria. This algorithm proved to be fast and reliable for many applications during twelve years of use in the Shell Process Engineering Calculation System, but it had its limitations. For example, the method required an educated initial guess for the composition of the second liquid phase that may form, and did not evaluate the thermodynamic stability of the phases predicted.

Bunz et al. (1991) incorporated the algorithm proposed by Nelson into a program for calculating high-pressure phase equilibria. The method proposed in their work includes an a priori determination of the phases using the Nelson approach and an iterative method for solving the multiphase Rachford-Rice set of equations. Specifically, the authors performed flash calculations on mixtures capable of splitting into three phases, and illustrated the method using ternary systems. However, this work did not address the problem of verifying the thermodynamic stability of the solution obtained.

In 1982, Michelsen presented two publications that are perhaps the most cited in phase equilibria journals. Michelsen (1982a) presented a numerical method for checking phase stability using the concept of the tangent plane criterion, and successfully implemented several algorithms for Gibbs energy minimization. This work provided a fast and reliable method for determining stability of phases in multiphase equilibria. Michelsen (1982b) focused on the method for performing phase-split calculations. He suggested the use of the stability analysis described in the previously cited paper to

generate the initial guess of the distribution coefficients, and used second-order convergence methods for performing the equilibria calculations. His results show that this method yields a rapid solution even near the critical point.

Michelsen (1986) described a calculation method for multiphase equilibrium assuming composition independent fugacity coefficients. He formulated the problem as a Gibbs free energy minimization problem, and made a few simplifications for handling a limited number of pure phases.

Peng-Robinson (1976b), verified the poor accuracy of the classical mixing rules for determining hydrocarbon solubility in an aqueous phase. The results of their calculations were several orders of magnitude lower than the experimental data. Therefore, Peng and Robinson (1980) introduced two modifications in their previous calculation procedure. They suggested modifying the temperature-dependent attraction parameter (α) for the water phase for temperatures below 0.85 T_r, and the introduction of temperature-dependent binary interaction parameters. These modifications improved the accuracy of the prediction for two and three phase calculations; however, this approximation was still not enough to capture the effect of the strong interactions between the water and hydrocarbon molecules over a large range of pressures and temperatures.

Two approaches have been extensively researched for representing the thermodynamic behavior of strongly non-ideal mixtures. The first of these approaches

represents the strong molecular interactions by incorporating a local composition or "activity model" into the mixing rules of an EOS. The second suggests the formulation of a new type of EOS called Association Equation of State (AEOS) for representing the attraction (association) and repulsion of different molecules in a mixture.

Huron and Vidal (1979) performed the first successful attempt for representing vapor-liquid-equilibria (VLE) of strongly non-ideal mixtures. They proposed a new set of mixing rules that incorporated an activity model into an EOS. These authors based their formulation on the observation that deviation from a linear weighting rule of the attraction parameter (a) of an EOS was related to the excess free energy at infinite pressure.

One of the main advantages of the Huron-Vidal (HV) mixing rule is its capacity of representing polar and non-polar systems. The authors suggested the use of a modified version of the Non-Random-Two-Liquids (NRTL) activity coefficient model (Renon et al., 1968) that allows the mixing rules to collapse to the classical expression when no polar substances are present.

The introduction of the Huron-Vidal mixing rules represented a significant progress for modeling the behavior of strongly non-ideal mixtures. It was able to reasonably predict the behavior of systems at high pressures, but this model had some problems. The Huron-Vidal mixing breaks down at low pressures. It is noted that this mixing rule assumes that the excess Gibbs free energy of a system does not change

significantly with pressure, and thus estimates the activity coefficient of the mixture from the excess Gibbs free energy at infinite pressure. Experimental data shows that the excess Gibbs free energy is a function of pressure.

Mollerup (1986) suggested a possible solution to the limitation of the HV mixing rule. He proposed the idea of combining activity coefficient models and equations of state at low pressures. This approach required solving for liquid density at zero pressure from the explicit EOS for each species of a mixture. This complication opened the door for formulating approximate solutions for this problem.

Michelsen (1990) proposed two methods for improving the accuracy of the Huron-Vidal mixing rules, trying to account for the variation of excess Gibbs free energy with pressure. These methods used a linear (MHV1) or quadratic (MHV2) expression for extrapolating excess free energy at different pressures. These procedures provide an excellent representation of strongly non-ideal systems but do not collapse to the classical mixing rules in the absence of polar components.

Another problem of the Huron-Vidal mixing rules is its inconsistency with the statistical mechanical theory. This model does not satisfy the criterion that the second virial coefficient has to be a quadratic function of the composition. Vidal (2003) recognizes the problem, but indicates that he has never observed practical consequences due to this deficiency.

Wong and Sandler (1992) suggested a new mixing rule that corrected the mechanistic inconsistency found in the Huron-Vidal model. They related the temperature-dependent attraction parameter to the excess Helmholtz energy at infinite pressure. This assumption proves to be more theoretically sound since the Helmholtz energy is a weak function of pressure. However, at high pressures, the results obtained using the Wong-Sandler model does not differ significantly from the ones obtained using the Huron-Vidal mixing rules. This model also has an important limitation. It fails to collapse to the classical mixing rule when small fractions of polar components are present in the mixture.

Pedersen et al. (1996) employed the Soave-Redlich-Kwong EOS along with the Huron-Vidal mixing rule for modeling the thermodynamic behavior of systems containing hydrocarbons, water, and methanol. For this purpose, these authors used experimental data obtained by Kristensen et al. (1993) for characterizing the Huron-Vidal binary energy interaction coefficients and the non-randomness number. The results verified that the Huron-Vidal mixing rule can represent, “reasonably well”, the mutual solubility of hydrocarbon and aqueous phases. Lindeloff, et al. (2003) used this method in an algorithm for calculating pressure-temperature phase diagrams for hydrocarbon-water mixtures.

Orbey and Sandler (1998), and Ghosh (1999) performed a comprehensive review of the methods available for modeling vapor-liquid equilibria. These authors discussed in depth the equations of state and the mixing rules applicable for each specific problem.

Another approach for representing polar systems is the use of an association equation of state (AEOS). The concept of AEOS consists of splitting the effects that cause the deviation from ideal behavior in two parts. The first part, also called physical compressibility factor, is calculated using the commonly used approach of an equation of state for non-polar systems. The second part, or chemical compressibility, tries to account for the chemical interaction for highly polar molecules. Shinta et al. (1994) and Yakoumis et al. (1997) have shown that the AEOS methods improve the accuracy of the flash calculations of several mixtures containing large water fractions.

The use of AEOS models present some disadvantages. In most cases, the AEOS models are not cubic but of higher degree. This complicates the calculation and selection of the actual compressibility factors.

Numerous researchers have proposed expressions and models for characterizing these AEOS. A comprehensive review of these methods can be found in the work of Economou and Tsonopoulos (1997), and Economou and Donohue (1991).

The present work is the first attempt to develop a fully compositional hydrodynamic model for three-phase flow in pipes. It developed and coupled state-of-the-art thermodynamic and hydrodynamic calculators for describing the behavior of two- and three-phase flow in a pipe. It minimized assumptions and simplifications commonly

introduced into other studies, and focuses on understanding the mechanisms and phenomena occurring in this type of flow.

CHAPTER 3

HIDRODYNAMIC MODEL FOR THREE-PHASE FLOW IN PIPES

3.1 Description of the approach

Multiphase flow simulation tools couple complex hydrodynamic and thermodynamic models to describe the behavior of fluids flowing simultaneously in a pipe. Multiphase flow models assume that the phases transported in a pipe constitute a continuum and, thereby, invoke the basic laws of continuum mechanics for the solution of the system. This assumption along with a volume averaging technique allows the formulation of the governing mass, momentum and energy balance equations for each phase.

Hydrodynamic modeling consists of solving the governing mass, momentum, and energy equations for different fluids traveling simultaneously in a pipe. The solution of the hydrodynamic equations requires coupling this model with a thermodynamic model in order to account for the mass transfer between the fluids transported and the changes in fluid properties along the pipe.

3.2 Hydrodynamic equations for three-phase flow

The formulation of the governing equations for three-phase flow in pipes may consist of up to nine partial differential equations that should be solved simultaneously. The system of equations may consist of three mass conservation, three momentum

balance, and three energy balance equations. This set of equations completely describes the behavior of this type of flow.

3.2.1 Conservative form of the governing equations

Continuity Equations

Mass conservation equations are formulated for each phase flowing in a pipe. Equations 3.1a through 3.1c express these equations in a conservative manner.

Gas phase:

$$\frac{\partial(\alpha_g \rho_g)}{\partial t} + \frac{\partial(\alpha_g \rho_g v_g)}{\partial x} = \tilde{M}_g \qquad (3.1a)$$

Condensate phase:

$$\frac{\partial(\alpha_{Lh} \rho_{Lh})}{\partial t} + \frac{\partial(\alpha_{Lh} \rho_{Lh} v_{Lh})}{\partial x} = \tilde{M}_{Lh} \qquad (3.1b)$$

Aqueous phase:

$$\frac{\partial(\alpha_{Lw} \rho_{Lw})}{\partial t} + \frac{\partial(\alpha_{Lw} \rho_{Lw} v_{Lw})}{\partial x} = \tilde{M}_{Lw} \qquad (3.1c)$$

In this work the system under study is assumed to be in steady state condition, therefore, the time dependent terms in equations (3.1a) through (3.1c) are equal to zero. This consideration allows expressing the material balance as a set of ordinary differential equations.

Gas phase:

$$\frac{d\left(\alpha_g \rho_g v_g\right)}{dx} = \tilde{M}_g \qquad (3.2a)$$

Condensate phase:

$$\frac{d\left(\alpha_{Lh} \rho_{Lh} v_{Lh}\right)}{dx} = \tilde{M}_{Lh} \qquad (3.2b)$$

Aqueous phase:

$$\frac{d\left(\alpha_{Lw} \rho_{Lw} v_{Lw}\right)}{dx} = \tilde{M}_{Lw} \qquad (3.2c)$$

Equations 3.2 take into account the mass transfer between the phases coexisting in the pipe. The right hand side of these expressions includes the total mass per unit volume transferred into a phase. The mass transfer terms include the contributions from all the phases coexisting in the system.

This work does not include blending streams, chemical reactions, or any form of mass generation at any point of the pipe. Therefore, the sum of the mass transfer terms between the phases is equal to zero.

$$\tilde{M}_g + \tilde{M}_{Lh} + \tilde{M}_{Lw} = 0 \qquad (3.3)$$

$$\alpha_g + \alpha_{Lh} + \alpha_{Lw} = 1 \qquad (3.4)$$

Momentum equations

The momentum equations represent balances of the work done by the forces acting on the fluids flowing in the pipe. These balances include the work done by body and surface forces. The surface forces consist of the wall friction and interfacial forces,

while the body forces include the pressure and gravity forces. The conservative form of the momentum equations can be written as follows:

Gas phase

$$\frac{\partial\left(\alpha_g \rho_g v_g\right)}{\partial t} + \frac{\partial\left(\alpha_g \rho_g v_g^2\right)}{\partial x} = -\alpha_g \frac{dP}{dx} - F_{tg} \tag{3.5a}$$

Condensate phase

$$\frac{\partial\left(\alpha_{Lh} \rho_{Lh} v_{Lh}\right)}{\partial t} + \frac{\partial\left(\alpha_{Lh} \rho_{Lh} v_{Lh}^2\right)}{\partial x} = -\alpha_{Lh} \frac{dP}{dx} - F_{tLh} \tag{3.5b}$$

Aqueous phase

$$\frac{\partial\left(\alpha_{Lw} \rho_{Lw} v_{Lw}\right)}{\partial t} + \frac{\partial\left(\alpha_{Lw} \rho_{Lw} v_{Lw}^2\right)}{\partial x} = -\alpha_{Lw} \frac{dP}{dx} - F_{tLw} \tag{3.5c}$$

The second right-hand-side term of these expressions includes the work done by wall friction, interfacial, and gravitational forces. The methods for determining these forces are described in section 3.2.3.

Since the system is considered to be in steady state conditions, the accumulation terms are equal to zero. Therefore, the resulting equations are a sole function of space.

Gas phase

$$\frac{d\left(\alpha_g \rho_g v_g^2\right)}{dx} = -\alpha_g \frac{dP}{dx} - F_{tg} \tag{3.6a}$$

Condensate phase

$$\frac{d\left(\alpha_{Lh}\rho_{Lh}v_{Lh}^2\right)}{dx} = -\alpha_{Lh}\frac{dP}{dx} - F_{tLh} \tag{3.6b}$$

Aqueous phase

$$\frac{d\left(\alpha_{Lw}\rho_{Lw}v_{Lw}^2\right)}{dx} = -\alpha_{Lw}\frac{dP}{dx} - F_{tLw} \tag{3.6c}$$

Energy balance equations

Equations 3.7a through 3.7c represent the conservative form of the energy equations at steady state conditions. These equations are written in terms of the enthalpy, kinetic energy, the work done by the fluids, and the heat exchange between the fluids and with the surroundings.

Gas phase

$$\frac{d}{dx}\left[\alpha_g\rho_g v_g\left(H_g + \frac{v_g^2}{2}\right)\right] = Q_{sg} + Q_{gLh} + Q_{gLw} - v_g F_{tg} \tag{3.7a}$$

Condensate phase

$$\frac{d}{dx}\left[\alpha_{Lh}\rho_{Lh}v_{Lh}\left(H_{Lh} + \frac{v_{Lh}^2}{2}\right)\right] = Q_{sLh} + Q_{Lhg} + Q_{LhLw} - v_{Lh}F_{tLh} \tag{3.7b}$$

Aqueous phase

$$\frac{d}{dx}\left[\alpha_{Lw}\rho_{Lw}v_{Lw}\left(H_{Lw}+\frac{v_{Lw}^2}{2}\right)\right]=Q_{sLw}+Q_{Lwg}+Q_{LwLh}-v_{Lw}F_{tLw} \qquad (3.7c)$$

These equations are obtained through application of the first law of thermodynamics to each fluid in the pipe. Equations 3.7a through 3.7c include terms that account for the heat exchange between the phases ($Q_{gLh}, Q_{gLw}, Q_{Lhg}, Q_{LhLw}, Q_{Lwg}, Q_{LwLh}$), and other terms considering the heat exchange between each phase and the surroundings (Q_{sg}, Q_{sLh}, Q_{sLw}). These terms are extremely difficult to determine individually. However, it is assumed that the summation of the heat exchange between the phases is equal to zero.

$$Q_{gLh}+Q_{gLw}+Q_{Lhg}+Q_{LhLw}+Q_{Lwg}+Q_{LwLh}=0 \qquad (3.8)$$

This assumption makes possible to formulate the energy balance as a combined energy equation. Summation of the energy equations will allow canceling out the interfacial heat exchanges. The sum of the heat exchange between the phases and the surroundings represents the total heat gained or lost by the pipe. This term can be properly estimated using an overall heat exchange coefficient. This coefficient will take into consideration the convective and conductive heat exchange between the pipe and the environment.

$$Q_{sg}+Q_{sLh}+Q_{sLw}=Q_{st} \qquad (3.9)$$

Based on this considerations and assumptions, the energy balance is formulated using a combined energy equation. This equation is defined as:

$$\frac{d}{dx}\left[\alpha_g \rho_g v_g \left(H_g + \frac{v_g^2}{2}\right) + \alpha_{Lh}\rho_{Lh} v_{Lh}\left(H_{Lh} + \frac{v_{Lh}^2}{2}\right) + \alpha_{Lw}\rho_{Lw} v_{Lw}\left(H_{Lw} + \frac{v_{Lw}^2}{2}\right)\right]$$

$$= Q_t - v_g F_{tg} - v_{Lh} F_{tLh} - v_{Lw} F_{tLw} \qquad (3.10)$$

The use of a combined energy equation simplifies the multiphase flow problem. This consideration allows formulating the multiphase flow problem using only seven equations. They include three mass balances, three momentum balances, and one combined energy equation. The system of ordinary differential equations are formulated in terms of the following seven unknowns: pressure (*P*), temperature (*T*), mole fraction of condensate (α_{Lh}), mole fraction of aqueous phase (α_{Lw}), and the velocities of the three phases (v_g, v_{Lh}, v_{Lw}).

3.2.2 Non-conservative form of the governing equations

Continuity Equations

Equations 3.2a through 3.2c can be rewritten in terms of the selected unknowns of the problem. In order to do so, the left hand side of these expressions is expanded performing the product differentiation, and the chain rule is applied to the density derivative terms obtained. It is assumed that density is only a function of pressure and temperature. Equation 3.11 shows the application of the chain rule to the density derivative term obtained for phase "g".

$$\frac{d\rho_g}{dx} = \left[\frac{\partial \rho_g}{\partial P}\right]_T \frac{dP}{dx} + \left[\frac{\partial \rho_g}{\partial T}\right]_P \frac{dT}{dx} \qquad (3.11)$$

The resulting mass balance equations are expressed as:

Gas Phase

$$\rho_g v_g \frac{d\alpha_g}{dx} + \alpha_g v_g \left[\frac{\partial \rho_g}{\partial P}\right]_T \frac{dP}{dx} + \alpha_g v_g \left[\frac{\partial \rho_g}{\partial T}\right]_P \frac{dT}{dx} + \alpha_g \rho_g \frac{dv_g}{dx} = \tilde{M}_g \tag{3.12a}$$

Condensate Phase

$$\rho_{Lh} v_{Lh} \frac{d\alpha_{Lh}}{dx} + \alpha_{Lh} v_{Lh} \left[\frac{\partial \rho_{Lh}}{\partial P}\right]_T \frac{dP}{dx} + \alpha_{Lh} v_{Lh} \left[\frac{\partial \rho_{Lh}}{\partial T}\right]_P \frac{dT}{dx} + \alpha_{Lh} \rho_{Lh} \frac{dv_{Lh}}{dx} = \tilde{M}_{Lh} \tag{3.12b}$$

Aqueous phase

$$\rho_{Lw} v_{Lw} \frac{d\alpha_{Lw}}{dx} + \alpha_{Lw} v_{Lw} \left[\frac{\partial \rho_{Lw}}{\partial P}\right]_T \frac{dP}{dx} + \alpha_{Lw} v_{Lw} \left[\frac{\partial \rho_{Lw}}{\partial T}\right]_P \frac{dT}{dx} + \alpha_{Lw} \rho_{Lw} \frac{dv_{Lw}}{dx} = \tilde{M}_{Lw} \tag{3.12c}$$

Equation 3.12a can be expressed in terms of the liquid fractions by recalling that the sum of the mass fractions of phases in the system is equal to one. Therefore, the derivative of the gas fraction with respect to space can be expressed as:

$$\frac{d\alpha_g}{dx} = -\frac{d\alpha_{Lh}}{dx} - \frac{d\alpha_{Lw}}{dx} \tag{3.13}$$

The mass transfer terms in equations 3.12a to 3.12c can be expressed in terms of the mass fraction change with respect to pressure and temperature. The chain rule is

applied for expressing the mass transfer term as a function of the mass fraction derivative with respect to pressure and temperature. Equation 3.14 shows how this is performed for the gas phase.

$$\tilde{M}_g = G_m \left[\frac{\partial f_{mg}}{\partial P} \right]_T \frac{dP}{dx} + G_m \left[\frac{\partial f_{mg}}{\partial T} \right]_P \frac{dT}{dx} \tag{3.14}$$

Where:

f_{mg} = Mass fraction of phase "g"

G_m = Total mass flux entering the pipe *[lb_m/s]*

Similar treatment is applied to the other two phases coexisting in equilibrium. The expressions for the mass balance equations are finally recast as:

Gas phase

$$\rho_g v_g \frac{d\alpha_g}{dx} + \left[\alpha_g v_g \left(\frac{\partial \rho_g}{\partial P} \right)_T - G_m \left(\frac{\partial f_{mg}}{\partial P} \right)_T \right] \frac{dP}{dx} + \left[\alpha_g v_g \left(\frac{\partial \rho_g}{\partial T} \right)_P - G_m \left(\frac{\partial f_{mg}}{\partial T} \right)_P \right] \frac{dT}{dx} + \alpha_g \rho_g \frac{dv_g}{dx} = 0 \tag{3.15a}$$

Condensate phase

$$\rho_{Lh} v_{Lh} \frac{d\alpha_{Lh}}{dx} + \left[\alpha_{Lh} v_{Lh} \left(\frac{\partial \rho_{Lh}}{\partial P} \right)_T - G_m \left(\frac{\partial f_{mLh}}{\partial P} \right)_T \right] \frac{dP}{dx} + \left[\alpha_{Lh} v_{Lh} \left(\frac{\partial \rho_{Lh}}{\partial T} \right)_P - G_m \left(\frac{\partial f_{mLh}}{\partial T} \right)_P \right] \frac{dT}{dx} + \alpha_{Lh} \rho_{Lh} \frac{dv_{Lh}}{dx} = 0 \tag{3.15b}$$

Aqueous phase

$$\rho_{Lw} v_{Lw} \frac{d\alpha_{Lw}}{dx} + \left[\alpha_{Lw} v_{Lw} \left(\frac{\partial \rho_{Lw}}{\partial P} \right)_T - G_m \left(\frac{\partial f_{mLw}}{\partial P} \right)_T \right] \frac{dP}{dx} +$$

$$\left[\alpha_{Lw} v_{Lw}\left(\frac{\partial \rho_{Lw}}{\partial T}\right)_P - G_m\left(\frac{\partial f_{mLw}}{\partial T}\right)_P\right]\frac{dT}{dx} + \alpha_{Lw}\rho_{Lw}\frac{dv_{Lw}}{dx} = 0 \qquad (3.15c)$$

The mass fraction of the gas phase is not one of the unknowns selected for the system of equations. Therefore, equations 3.4 and 3.13 are used for expressing equation 3.15a in terms of the liquid fractions.

Momentum equations

A similar treatment to the mass balance expressions is applied to the momentum equations. The left hand side of equations 3.6a-c is expanded performing the product differentiation, and the chain rule is applied to the density derivative term as illustrated in equation 3.11. These manipulations allow rewriting the governing momentum equations as:

Gas phase

$$\left[\alpha_g v_g^2\left(\frac{\partial \rho_g}{\partial P}\right)_T + \alpha_g\right]\frac{dP}{dx} + 2\alpha_g v_g \rho_g \frac{dv_g}{dx} + \rho_g v_g^2 \frac{d\alpha_g}{dx} + \alpha_g v_g^2\left(\frac{\partial \rho_g}{\partial T}\right)_P \frac{dT}{dx} = -F_{tg} \qquad (3.16a)$$

Condensate phase

$$\left[\alpha_{Lh} v_{Lh}^2\left(\frac{\partial \rho_{Lh}}{\partial P}\right)_T + \alpha_{Lh}\right]\frac{dP}{dx} + 2\alpha_{Lh} v_{Lh}\rho_{Lh}\frac{dv_{Lh}}{dx} + \rho_{Lh} v_{Lh}^2 \frac{d\alpha_{Lh}}{dx} + \alpha_{Lh} v_{Lh}^2\left(\frac{\partial \rho_{Lh}}{\partial T}\right)_P \frac{dT}{dx} = -F_{tLh} \qquad (3.16b)$$

Aqueous phase

$$\left[\alpha_{Lw}v_{Lw}^2\left(\frac{\partial\rho_{Lw}}{\partial P}\right)_T+\alpha_{Lw}\right]\frac{dP}{dx}+2\alpha_{Lw}v_{Lw}\rho_{Lw}\frac{dv_{Lw}}{dx}+\rho_{Lw}v_{Lw}^2\frac{d\alpha_{Lw}}{dx}+$$
$$\alpha_{Lw}v_{Lw}^2\left(\frac{\partial\rho_{Lw}}{\partial T}\right)_P\frac{dT}{dx}=-F_{tLw} \qquad (3.16c)$$

Similarly to the mass balance, equations 3.4 and 3.13 are used for expressing equation 3.16a in terms of the liquid fractions. The right hand side terms of equations 3.16 contain the contributions of the external forces applied to each phases. The methods for determining these forces are discussed in detail in section 3.2.3.

Combined energy equation

The non-conservative energy equation is obtained by differentiating the left hand side of equation 3.10. The resulting expression contains enthalpy derivative terms that need to be formulated in terms of the unknowns of the problem. The enthalpy derivatives with respect to space can be expressed in terms of the specific heat at constant pressure (C_p) and the definition of the Joule Thompson effect (η) as shown in equation 3.17.

$$\frac{dH_g}{dx}=C_{pg}\frac{dT}{dx}-\eta_g C_{pg}\frac{dP}{dx} \qquad (3.17)$$

The use of this expression allows recasting the energy equation as follows:

$$\left[\alpha_g v_g\left[H_g+\frac{v_g^2}{2}\right]\left(\frac{\partial\rho_g}{\partial P}\right)_T+\alpha_{Lh}v_{Lh}\left[H_{Lh}+\frac{v_{Lh}^2}{2}\right]\left(\frac{\partial\rho_{Lh}}{\partial P}\right)_T+\alpha_{Lw}v_{Lw}\left[H_{Lw}+\frac{v_{Lw}^2}{2}\right]\left(\frac{\partial\rho_{Lw}}{\partial P}\right)_T\right]\frac{dP}{dx}+$$

$$-\left[\alpha_g v_g \rho_g \eta_g Cp_g + \alpha_{Lh} v_{Lh} \rho_{Lh} \eta_{Lh} Cp_{Lh} + \alpha_{Lw} v_{Lw} \rho_{Lw} \eta_{Lw} Cp_{Lw}\right]\frac{dP}{dx} +$$

$$\left[\alpha_g v_g \left[H_g + \frac{v_g^2}{2}\right]\left(\frac{\partial \rho_g}{\partial T}\right)_P + \alpha_{Lh} v_{Lh}\left[H_{Lh} + \frac{v_{Lh}^2}{2}\right]\left(\frac{\partial \rho_{Lh}}{\partial T}\right)_P + \alpha_{Lw} v_{Lw}\left[H_{Lw} + \frac{v_{Lw}^2}{2}\right]\left(\frac{\partial \rho_{Lw}}{\partial T}\right)_P\right]\frac{dT}{dx} +$$

$$-\left[\alpha_g v_g \rho_g Cp_g + \alpha_{Lh} v_{Lh} \rho_{Lh} Cp_{Lh} + \alpha_{Lw} v_{Lw} \rho_{Lw} Cp_{Lw}\right]\frac{dT}{dx} +$$

$$\left[\alpha_g \rho_g \left[H_g + \frac{3v_g^2}{2}\right]\frac{dv_g}{dx} + \alpha_{Lh}\rho_{Lh}\left[H_{Lh} + \frac{3v_{Lh}^2}{2}\right]\frac{dv_{Lh}}{dx} + \alpha_{Lw}\rho_{Lw}\left[H_{Lw} + \frac{3v_{Lw}^2}{2}\right]\frac{dv_{Lw}}{dx}\right] +$$

$$\left[\rho_g v_g \left[H_g + \frac{v_g^2}{2}\right]\frac{d\alpha_g}{dx} + \rho_{Lh} v_{Lh}\left[H_{Lh} + \frac{v_{Lh}^2}{2}\right]\frac{d\alpha_{Lh}}{dx} + \rho_{Lw} v_{Lw}\left[H_{Lw} + \frac{v_{Lw}^2}{2}\right]\frac{d\alpha_{Lw}}{dx}\right] =$$

$$Q_t - v_g F_{tg} - v_{Lh} F_{tLh} - v_{Lw} F_{tLw} \qquad (3.18)$$

This equation requires using equations 3.4 and 3.13 in order to express it in terms of the selected unknowns of the system.

Equations 3.15 a-c, 3.16 a-c, and 3.18 represent the system of governing equations for three-phase flow. Appendix A presents the matrix of governing equations for three-phase flow in pipes.

Using a similar approach the governing equations for single and two-phase (gas-liquid) flow in pipes can be derived. Appendix B summarizes the equations required for modeling two-phase flow, while appendix C summarizes the equations formulated for single phase (gas) flow in pipes.

3.2.3 Closure relationships

Formulation of the momentum equations requires determining the forces acting on the fluids transported in the pipe. The forces acting on the system include gravitational, frictional, and interfacial forces. The magnitude of the forces acting on the fluids depends on the geometry of the prevailing flow configuration.

The present work summarizes the potential flow regimes that could result in two- and three-phase flow, and proposes a theoretical method for estimating flow patterns in near horizontal, three-phase (gas-condensate-water) flow in pipes. This method is described in detail in Chapter 5.

The current study analyzes the geometry and flow conditions for each potential flow pattern and proposes closure relationships for different two- and three-phase flow patterns. These closure relationships are described in Chapter 6.

3.3 Solution approach

Modeling three-phase flow in pipes requires solving a system of seven first-order ordinary differential equations (ODEs). The expressions describing this type of flow are presented as equations 3.15 a-c, 3.16 a-c, and 3.18. This system of ODEs is implicit and can be expressed in a matrix form as follows:

$$[A_m]\frac{d}{dx}[U]=[B_m] \tag{3.19}$$

In this expression, A_m is a square matrix of 7x7 elements representing the coefficients in the previously mentioned equations, B_m is the independent term vector, and U is the vector of unknowns. Appendix A defines the coefficients of matrix $[A_m]$, and vector $[B_m]$. Vector $[U]$ consists of the following variables: pressure, temperature, liquid holdups, and velocity for each phase.

The solution of the governing equations requires the implementation of an ODE solver. Most ODE solvers require expressing the derivatives of the unknowns in an explicit form. This is achieved solving for $\frac{d}{dx}[U]$ using the Gaussian elimination method.

$$\frac{d}{dx}[U] = [R_m] \tag{3.20}$$

Where:

$$[R_m] = [B_m][A_m]^{-1} \tag{3.21}$$

$[R_m]$ is the resulting vector obtained from multiplying matrix $[A_m]^{-1}$ by vector $[B_m]$. Once the system of equations is expressed in an explicit manner, an ODE solver is implemented. This study proposes the use of the Fifth-order Cash & Karp Embedded Runge-Kutta method. This method has been successfully implemented for solving two-phase flow problems in pipes at Penn State (Ayala, 2001). Therefore, as a logical extension, this work will test the appropriateness of ODE solver for three-phase flow in pipes. Press et al. (1994) presents a detailed description of the ODE solver that will be used in this study.

3.3.1 Marching algorithm

The changes in the fluid properties along the pipe do not allow performing hydrodynamic calculations for the entire pipe length in one single step. Therefore, the pipe length is discretized into small segments called blocks, in which the fluid properties are assumed to be constant. The calculations are conducted progressively, block by block, over the length of the pipe. This solution approach is typically called as the “marching” algorithm. This approach takes into account the fluid property changes along the pipe, as the results for the calculations of a block are used for estimating the fluid properties and hydrodynamic behavior at the inlet of the next block. Figure 3.1 illustrates the implementation of the “marching” algorithm. As shown in Figure 3.1, this algorithm contains four main sections or “subroutines”. They are: Input data, determination of the boundary conditions, formulation of the system of equations, and solution of the system of ODEs. This section outlines the implementation of the marching algorithm describing in detail the calculations performed in each subroutine.

The marching algorithm can be described as follows;

a) Input data subroutine

This subroutine reads the data required for performing the calculations. It must contain the following information:

- Pipe data: Length, diameter, roughness, and inclination of each pipe section.
- Inlet conditions: Overall inlet stream composition, flow rate at standard conditions, inlet pressure and temperature.

- Energy data: Temperature of the surroundings and overall heat transfer coefficient.

In addition to this information, the calculations require physical and thermodynamic properties of the substances present in the overall inlet stream composition. This study uses a database containing physical and thermodynamic properties of 46 pure substances. This database was extracted from work of Erdogmus (2000).

b) Determination of the boundary conditions

Pressure, temperature, liquid holdup(s), and the velocity of the phases in equilibrium represent the boundary conditions required for solving the set of equations for steady state flow in pipes. Inlet pressure and temperature are part of the input data required by the algorithm. The liquid holdups at the inlet are assumed to be equal to the volumetric fractions of each phase and they are calculated using the thermodynamic package. Estimating the velocity of the fluids at the pipe inlet requires the determination of the total mass flux entering the system (Gm).

$$G_m = 3.0493 \cdot 10^{-8} \frac{Q_{sc} \cdot Mw}{A_{pipe}} \qquad (3.22)$$

b.1) For single phase flow the inlet velocity is calculated as:

$$v_g = \frac{G_m}{\rho_g} \qquad (3.23)$$

b.2) For two and three-phase flow the velocity of the phases entering the pipe is determined as:

$$v_a = \frac{f_{ma} G_m}{\alpha_a \rho_a} \tag{3.24}$$

At the pipe inlet, it is assumed that the holdups of the phases are equal to the volumetric fractions. ($\alpha_a = f_{ma}$).

These expressions are formulated for phase "*a*", however, they should be applied for those phases coexisting in equilibrium.

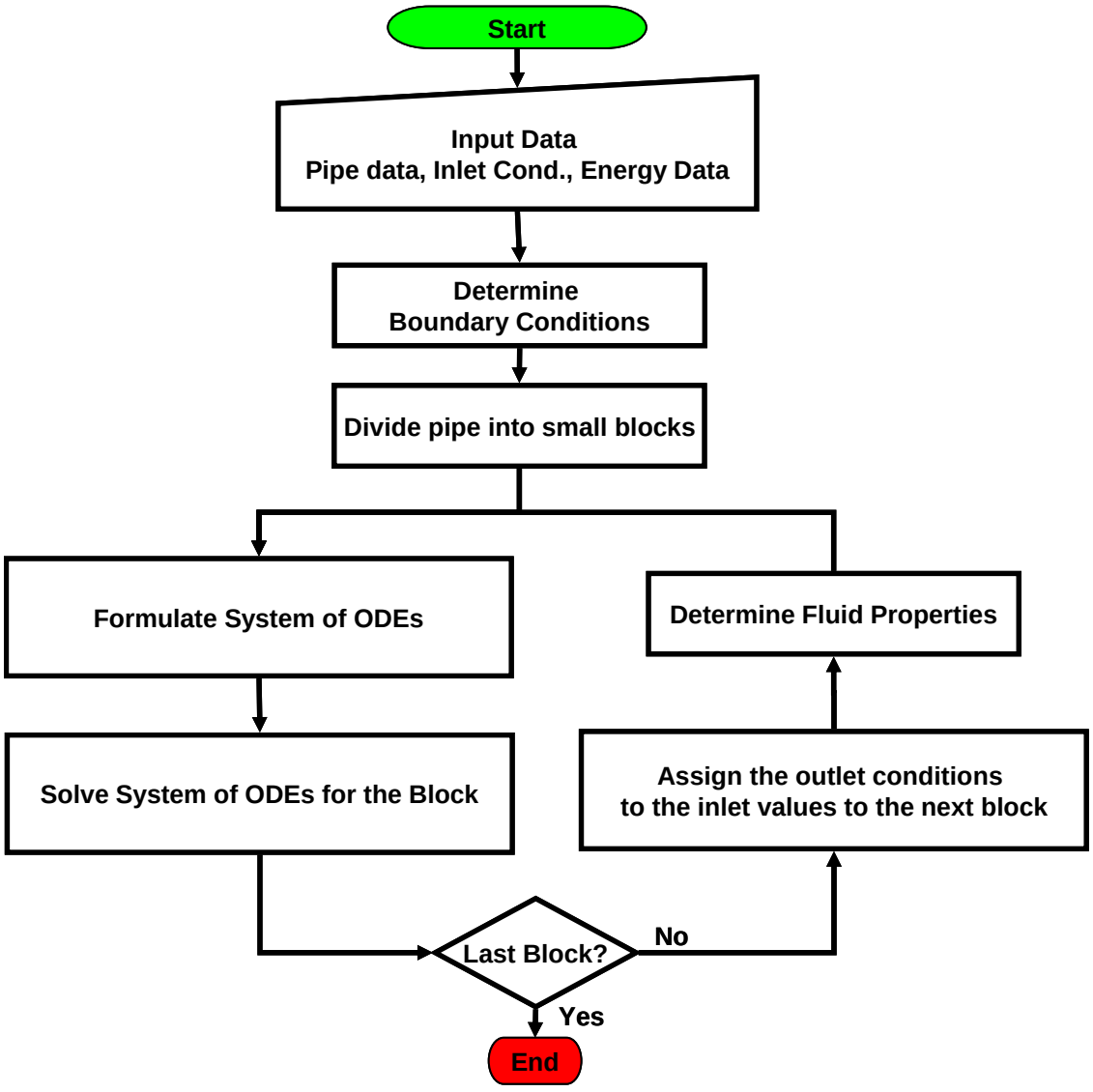

Figure 3.1 Description of the "marching" algorithm

c) The total pipe length is divided into small blocks.

d) Formulation of the system of ODEs. The system of ODEs can be expressed in matrix form as shown in equation 3.19. The coefficient matrices (A_m, B_m) defining the governing equations for single, two-phase, or three-phase flow in pipes are calculated as outlined in appendices C, B, and A respectively.

$$[A_m]\frac{d}{dx}[U]=[B_m] \tag{3.19}$$

e) Solution of the system of ODEs. Equation 3.19 is numerically solved using the fifth-order Cash & Karp embedded Runge-Kutta method. For applying the RK methods, it is required to express the system of ODEs in an explicit manner. The derivative of each unknown is determined using the Gaussian elimination method.

$$\frac{d}{dx}[U]=[R_m] \tag{3.20}$$

The resultant system has an explicit form, which is then solved with the mentioned Runge-Kutta method. The Runge-Kutta method selected uses an automatic step-size procedure for satisfying the desired accuracy of the calculations. The application of the fifth-order Cash & Karp embedded Runge-Kutta method is discussed in the next section.

f) The values of the outlet conditions calculated are assigned to the inlet of the next block. The thermodynamic package is invoked for calculating the fluid properties at the entry of the upcoming block. The algorithm progresses to the

next block and repeats steps **d** and **e** until the entire length of the pipe is covered. For each block, individual and cumulative material balance calculations are performed.

3.4 Fifth-order Cash & Karp Runge-Kutta Method

Runge-Kutta (RK) methods are the most popular numerical procedures for integrating systems of ordinary differential equations. These methods propagate a solution over an interval by combining the information from several Euler-style steps, and then using this information to match a Taylor series expansion up to some higher degree (Press et al., 1994). The Runge-Kutta methods are robust procedures that succeed for most calculations. However, they are not the fastest or most accurate methods. Other methods, such as the Bulirsch-Stoer routines, and the corrector-predictor methods are typically more efficient and accurate than the Runge-Kutta methods. Nevertheless, these methods are not as stable as the Runge-Kutta methods and, therefore, they are not the most adequate formulations for solving the multiphase flow problem.

Runge-Kutta methods are typically classified in terms of the truncation error of the procedure. A Runge-Kutta method is called of n^{th} order if its truncation error term is of n+1 order. A higher order Runge-Kutta method usually implies higher accuracy of the calculations for the same step size. However, this is at the expense of computational cost.

The fifth-order embedded Runge-Kutta method with six function evaluations was first proposed by Fehlberg (1968). The embedded method proposed by Fehlberg

consisted of calculating two estimates for the unknowns of the problem, one of fourth and another one of fifth order, for determining the truncation error of the solution. Then, Fehlberg proposed to adjust the step size of the calculation in order to obtain a specified accuracy. The form of the fifth-order Runge-Kutta method proposed by Fehlberg is expressed as:

$$U(x+\Delta x) = U_0 + \sum_{i=1}^{6} c_i^F F_i^F \tag{3.25}$$

While the fourth-order estimate is determined by:

$$U(x+\Delta x) = U_0 + \sum_{i=1}^{6} c_i^{*F} F_i^F \tag{3.26}$$

In these expressions, c_i^F, c_i^{*F}, and d_{ij}^F are parameters proposed by Fehlberg, while F_i^F are variables calculated using vector $[R]$ defined in equation 3.20. The values of F_i^F are determined as:

$$F_1^F = \Delta x \cdot R(U_0) \tag{3.27}$$

$$F_2^F = \Delta x \cdot R\left(U_0 + d_{21}^F F_1^F\right) \tag{3.28}$$

$$F_3^F = \Delta x \cdot R\left(U_0 + d_{31}^F F_1^F + d_{32}^F F_2^F\right) \tag{3.29}$$

$$F_4^F = \Delta x \cdot R\left(U_0 + d_{41}^F F_1^F + d_{42}^F F_2^F + d_{43}^F F_3^F\right) \tag{3.30}$$

$$F_5^F = \Delta x \cdot R\left(U_0 + d_{51}^F F_1^F + d_{52}^F F_2^F + d_{53}^F F_3^F + d_{54}^F F_4^F\right) \tag{3.31}$$

$$F_6^F = \Delta x \cdot R\left(U_0 + d_{61}^F F_1^F + d_{62}^F F_2^F + d_{63}^F F_3^F + d_{64}^F F_4^F + d_{65}^F F_5^F\right) \tag{3.32}$$

Cash & Karp (1990) suggested a new set of parameters that yielded more accurate results than those proposed by Fehlberg. The value of these parameters is presented in Table 3.1.

Equations 3.25 and 3.26 allow calculating the fifth and fourth order estimates of the solution for the unknowns of the problem. The difference between these estimates represents the truncation error. The truncation error is expressed as:

$$\Delta = \sum_{i=1}^{6} \left(c_i^F - c_i^{*F} \right) F_i^F = \sum_{i=1}^{6} e_i^F F_i^F$$

Table 3.1 Cash & Karp parameters for the embedded fifth-order Runge-Kutta method

i	$c^F{}_i$	$d^F{}_{ij}$					$e^F{}_i$
1	$\frac{37}{378}$	0					$-\frac{277}{64512}$
2	0	$\frac{1}{5}$					0
3	$\frac{250}{621}$	$\frac{3}{40}$	$\frac{9}{40}$				$\frac{6925}{370944}$
4	$\frac{125}{594}$	$\frac{3}{10}$	$-\frac{9}{10}$	$\frac{6}{5}$			$-\frac{6925}{202752}$
5	0	$-\frac{11}{54}$	$\frac{5}{2}$	$-\frac{70}{27}$	$\frac{35}{27}$		$-\frac{277}{14336}$
6	$\frac{512}{1771}$	$\frac{1631}{55296}$	$\frac{175}{512}$	$\frac{575}{13824}$	$\frac{44275}{110592}$	$\frac{253}{4096}$	$\frac{277}{7084}$

The determination of the truncation error allows selecting a step size that satisfies the required accuracy of the calculations. Press et al. (1994) suggested using the following expressions for determining the appropriate step size.

$$\Delta x_0 = \begin{cases} S \cdot \Delta x_1 \cdot \left| \dfrac{\Delta_0}{\Delta_1} \right|^{0.20} & \Delta_0 \geq \Delta_1 \\ S \cdot \Delta x_1 \cdot \left| \dfrac{\Delta_0}{\Delta_1} \right|^{0.25} & \Delta_0 < \Delta_1 \end{cases}$$

In these equations, S is a safety factor (considered to be 0.95) proposed to avoid exceeding the maximum truncation error in the calculations. Δ_0 is the desired accuracy

of the calculations and Δ_1 is the truncation error obtained for a step size Δx_1. Once the step size is determined, the solution of the ODE system is calculated using equation 3.25.

CHAPTER 4

THERMODYNAMIC MODEL

Equations of state (EOS) are analytical expressions that provide fundamental relationships among pressure, temperature and volume of a system (Ayala, 2001). These relationships are commonly used to describe the thermodynamic behavior of complex mixtures. In the oil and gas industry, one of the most popular EOS is that proposed by Peng and Robinson (1976a). This EOS has been widely employed in the petroleum industry due to its simplicity and accuracy for performing phase equilibria calculations of complex hydrocarbon systems.

4.1 Equation of state and mixing rules

This study uses the Peng-Robinson equation of state (PR EOS) for performing two and three-phase equilibria calculations. This EOS is used because it can accurately model the behavior of non-polar systems, can provide acceptable liquid density predictions (even near critical conditions), and has the capacity to handle polar components when using an appropriate set of mixing rules. These qualities make the PR EOS appropriate for representing the behavior of typical reservoir fluids.

Peng and Robinson originally expressed their two-constant pressure-explicit EOS as follows:

$$P = \frac{RT}{\tilde{v} - b_i} - \frac{a_{ci}\,\alpha_i(T)}{\tilde{v}^2 + 2b_i\tilde{v} - b_i^2} \tag{4.1}$$

This equation provides a relationship among pressure (P), temperature (T) and molar volume ($\tilde{v}$) of a system. The two constants in this EOS are called attraction parameter ($a_{ci}\,\alpha_i(T)$) and the co-volume factor (b_i). These constants are defined by the next equations:

$$a_{ci} = 0.45724\frac{R^2 T_{ci}^{\ 2}}{P_{ci}} \tag{4.2}$$

$$\alpha_i = \left[1 + f(w_i)\left(1 - T_{ri}^{0.5}\right)\right]^2 \qquad T_{ri} = \frac{T}{T_{ci}} \tag{4.3}$$

$$f(w_i) = 0.37464 + 1.54226w_i - 0.26992w_i \tag{4.4}$$

$$b_i = 0.07780\frac{RT_{ci}}{P_{ci}} \tag{4.5}$$

The equation proposed by Peng and Robinson can also be expressed as a cubic expression in terms of the compressibility factor $Z = \frac{P\tilde{v}}{RT}$ (Equation 4.6). This analytical expression is a convenient way of representing the EOS, because it can be easily solved either analytically or numerically.

$$Z^3 - (1 - B)Z^2 + \left(A - 3B^2 - 2B\right)Z - \left(AB - B^2 - B^3\right) = 0 \tag{4.6}$$

Where:

$$A = \frac{a_{ci}\,\alpha_i(T)P}{R^2T^2} \tag{4.7}$$

$$B = \frac{b_i P}{RT} \tag{4.8}$$

Peng and Robinson suggested a set of mixing rules for performing phase equilibria calculations of complex hydrocarbon mixtures. These mixing rules are typically referred to as the classical mixing rules.

$$b_m = \sum_i c_i b_i \tag{4.9}$$

$$(a\alpha)_m = \sum_i \sum_j c_i c_j \sqrt{(a\alpha)_i (a\alpha)_j}\left(1 - k_{ij}\right) \tag{4.10}$$

In these equations, c_i is the mole fraction of component "*i*" in the mixture, and k_{ij} are the binary interaction parameters (BIP) between the different components of the mixture. BIP are parameters correlated from experimental data for improving the accuracy of the phase equilibria predictions.

The classical mixing rules have been shown appropriate for representing hydrocarbon systems. However, these mixing rules break down in systems containing strongly polar substances, such as water and methanol. In fact, Peng-Robinson (1976b), verified the poor accuracy of the classical mixing rules for determining hydrocarbon solubility in an aqueous phase. The results of their calculations were several orders of magnitude lower than experimental data.

Several researchers have proposed new mixing rules that improve the predictions for strongly polar systems. Perhaps the most commonly used are those suggested by Huron and Vidal (1979), Michelsen (1990a,b), and Wong and Sandler (1992). All these

mixing rules have the capacity to represent polar mixtures. They incorporate parameters that allow correlating solubility data, and are thermodynamically consistent because the same model can be applied to all the phases. However, only the Huron-Vidal mixing rule has the capacity of representing polar and non-polar systems (Lindeloff & Michelsen, 2003). This mixing rule collapses to the classical mixing rules in the absence of polar components.

The mixing rule proposed by Huron and Vidal (1979) are expressed as follows:

$$b_m = \sum_i c_i b_i \tag{4.11}$$

$$a_m = b_m \left[\sum_i c_i \frac{(a\alpha)_i}{b_i} + \frac{\sqrt{2}\, g_\infty^E}{\ln\left(\sqrt{2}-1\right)} \right] \tag{4.12}$$

These authors correlated the deviation of the attraction parameter $(a\alpha)_m$ from the classical mixing rules with the excess Gibbs energy at infinite pressure, and calculate the excess Gibbs energy in a way similar to the NRTL model proposed by Renon et al. (1968).

$$\frac{g_\infty^E}{RT} = \sum_{i=1}^{n} c_i \frac{\sum_{j=1}^{n} c_j G_{ji} \tau_{ji}}{\sum_{k=1}^{n} c_k G_{ki}} \tag{4.13}$$

With

$$\tau_{ji} = \frac{\left(g_{ji} - g_{ii}\right)}{RT} \tag{4.14}$$

And

$$G_{ji} = b_j \exp\left(-\beta_{ji}\tau_{ji}\right) \tag{4.15}$$

In this formulation, g_{ji} and g_{ii} are defined as the interaction energies between unlike and like molecules respectively, and β_{ji} is defined as a non-randomness parameter. The only difference between the NRTL model proposed by Renon et al. (1968) and that used in the Huron-Vidal formulation is the incorporation of the co-volume factor (b_j) in the calculation of the local composition parameters G_{ji}.

The Huron-Vidal mixing rules are able to reduce to the classical mixing rules when no polar components are present in the mixture. However, in order to obtain an exact reduction to the classical mixing rules the energy interactions and the non-randomness parameters must be calculated as follows:

$$\beta_{ij} = 0 \tag{4.16}$$

$$g_{ii} = \left[\frac{\ln\left(\sqrt{2}-1\right)}{\sqrt{2}}\right]\frac{(a\alpha)_i}{b_i} \tag{4.17}$$

$$g_{ij} = -2\frac{\sqrt{b_i b_j}}{b_i + b_j}\sqrt{g_{ii}g_{jj}}\left(1-k_{ij}\right) \tag{4.18}$$

As suggested by Lindeloff & Michelsen (2003), this work calculates the interaction energies and non-randomness parameters between non-polar components using the equations shown above, while the parameters required for polar components are assigned according to values correlated from experimental data by Kristensen et al. (1993). Tables 4.1 and 4.2 show the interaction energies and non-randomness parameters

between polar – non-polar and polar-polar components. These parameters were used in a series of phase equilibria calculations of systems including hydrocarbons, water and methanol with reasonable results (Kristensen et al., 1993).

Table 4.1 Interaction Energy and Non-randomness parameters for binary mixtures of water and the indicated second component

Second Component	$(g_{12}-g_{22})/R$ [°R]	$(g_{21}-g_{11})/R$ [°R]	β_{12}
Nitrogen	1240.20	7057.80	0.15
Carbon Dioxide	28.80	2973.60	0.15
Hydrogen Sulfide	212.40	2329.20	0.15
Methane	738.00	4123.80	0.15
Ethane	885.60	4105.80	0.15
Propane	1524.60	4770.00	0.15
i-Butane	1427.40	4501.80	0.15
n-Butane	1427.40	4501.80	0.15
i-Pentane	2016.00	5220.00	0.15
n-Pentane	1996.20	5221.80	0.15
n-Hexane	2136.60	5180.40	0.15
n-Heptane	-145.80	4933.80	0.15

Table 4.2 Interaction Energy Parameters and Non-randomness parameters for binary mixtures of methanol and the indicated second component

Second Component	$(g_{12}-g_{22})/R$ [°R]	$(g_{21}-g_{11})/R$ [°R]	β_{12}
Water	518.40	496.80	1.2
Nitrogen	642.60	2034.00	0.4
Carbon Dioxide	444.60	5346.00	0.4
Hydrogen Sulfide	104.40	1594.80	0.4
Methane	138.60	3769.20	0.4
Ethane	459.00	2898.00	0.4
Propane	837.00	2552.40	0.4
i-Butane	928.80	1888.20	0.4
n-Butane	928.80	1888.20	0.4
i-Pentane	1215.00	1900.80	0.4
n-Pentane	1393.20	2151.00	0.4
n-Hexane	1492.20	2095.20	0.4
n-Heptane	9000	2809.8	0.48

4.2 Fugacity

Chemical equilibrium is usually expressed in terms of fugacities. Therefore, multiphase equilibria determination requires the calculation of fugacity coefficients. Typically, these coefficients are calculated from an EOS. In this study, the introduction of the Huron-Vidal mixing rules into the PR EOS collapses the fugacity coefficient expression to:

$$\ln \bar{\phi}_i = \frac{b_i}{b_m}(Z-1) - \ln(Z-B) - \frac{1}{2\sqrt{2}}\left[\frac{(a_{ci}\alpha_i)}{b_i RT} - \frac{\ln \gamma_{i\infty}}{0.62323}\right]\ln\left[\frac{Z+(1+\sqrt{2})B}{Z+(1-\sqrt{2})B}\right] \tag{4.19}$$

The fugacity coefficient is defined as:

$$\bar{\phi}_i = \frac{f_i}{c_i P}$$

Where:

f_i is the fugacity of component "*i*" in the mixture.

This formulation requires calculating the activity coefficient at infinite pressure for all the components present in a mixture. Huron and Vidal suggested calculating these coefficients by means of the following expression:

$$\ln \gamma_{i\infty} = \frac{1}{RT}\left[g_{\infty}^{E} + \sum_{j=1}^{n} \frac{\partial g_{\infty}^{E}}{\partial c_j}(\Delta_{ij} - c_j)\right] \tag{4.20}$$

However, the equation above requires determining the derivative of the excess Gibbs energy at infinite pressure with respect to composition. This derivative can be expressed as:

$$\frac{1}{RT}\frac{\partial g_{\infty}^{E}}{\partial c_j} = \frac{\sum_j c_j \tau_{ji} G_{ji}}{\sum_k c_k G_{ki}} + \sum_j \frac{c_j G_{ij}}{\sum_k c_k G_{kj}} \left[\tau_{ij} - \frac{\sum_l c_l \tau_{li} G_{li}}{\sum_k c_k G_{kj}} \right] \tag{4.21}$$

Where:

$$\tau_{ji} = \frac{g_{ji} - g_{ii}}{RT}$$

$$G_{ij} = b_i \cdot EXP\left(-\beta_{ij}\tau_{ij}\right)$$

4.3 Flash Calculations

This work presents an algorithm for performing Vapor-Liquid-equilibria (VLE), Liquid-Liquid-equilibria (LLE), and Vapor-Liquid-Liquid-equilibria (VLLE) calculations for typical compositions of unprocessed gas well streams. The model is capable of identifying up to three phases in equilibrium, estimating their composition, quantifying their mass fraction in the system, and estimating their physical and thermodynamic properties.

4.3.1 Description of the multiphase equilibria algorithm

Figure 4.1 presents a simplified representation of the proposed model. This algorithm calculates phase equilibria based on the traditional technique of matching the fugacities for each component in each phase. The model only requires the input of

composition, and operating conditions (pressure and temperature) for performing flash calculations. The output includes the number, type and fraction of the phases in equilibrium, and the following thermophysical properties for each fluid: density (ρ), viscosity (μ), compressibility factor (Z), specific heat at constant pressure (Cp), and Joule-Thomson coefficient (η). This output includes all the fluid properties required for performing the hydrodynamic calculations.

This model contains five important calculation processes or "routines". These routines include: 1) initialization, 2) determination of number and type of phases, 3) determination of phase compositions and fugacities, 4) phase stability verification, and 5) calculation of thermophysical properties. These calculation processes will be described in this chapter.

4.3.2 Initialization

Figure 4.1 shows that the first step taken by the model is estimating the values of the distribution coefficients for every component in the mixture. Distribution coefficients (K_i) are defined as the ratio between the mole fractions of component "*i*" in the vapor phase and the mole fractions of that component in a liquid phase. One set of distribution coefficients is required for each potential liquid phase that may be formed in a system. Therefore, three-phase (VLLE) equilibrium requires the definition of two sets of distribution coefficients (KA_i and KB_i). In this study, KA_i is a set of distribution coefficients for a hydrocarbon-rich liquid phase, while KB_i are the coefficients for a water-rich liquid phase. Two sets of distribution coefficients are required by the model,

even if less than three phases can coexist in equilibrium. These coefficients are defined as:

$$KA_i = \frac{y_i}{XA_i} \quad , \qquad KB_i = \frac{y_i}{XB_i} \tag{4.22}$$

Where y_i is the mole fraction of component "*i*" in the vapor phase, XA_i is the mole fraction of that component in the hydrocarbon-rich liquid, and XB_i *is* the mole fraction of the same component in a water-rich (aqueous) liquid phase.

The distribution coefficients are not known a priori, in fact, one of the objectives of this algorithm is their calculation in order to determine the compositions of the splitting phases. The initial estimation of these coefficients is not critical. However, a good initial selection reduces the number of iterations required for converging to a solution.

KA_i is initially estimated using Wilson's empirical equation, While KB_i is initialized using an expression suggested by Peng and Robinson (1976b). These equations are defined as:

$$KA_i = \frac{1}{P_{ri}} EXP\left(5.3727(1+\omega_i)\left(1-\frac{1}{T_{ri}}\right)\right) \tag{4.23}$$

$$KB_i = 10^6\left(\frac{P_{ri}}{T_{ri}}\right) \tag{4.24}$$

This initialization procedure has been employed for a wide range of two and three-phase equilibria calculations, and it has proven an appropriate starting point for the

calculations. Once the distribution coefficients are initialized the algorithm proceeds to estimate the number, type, and mole fractions of the phases coexisting in equilibrium.

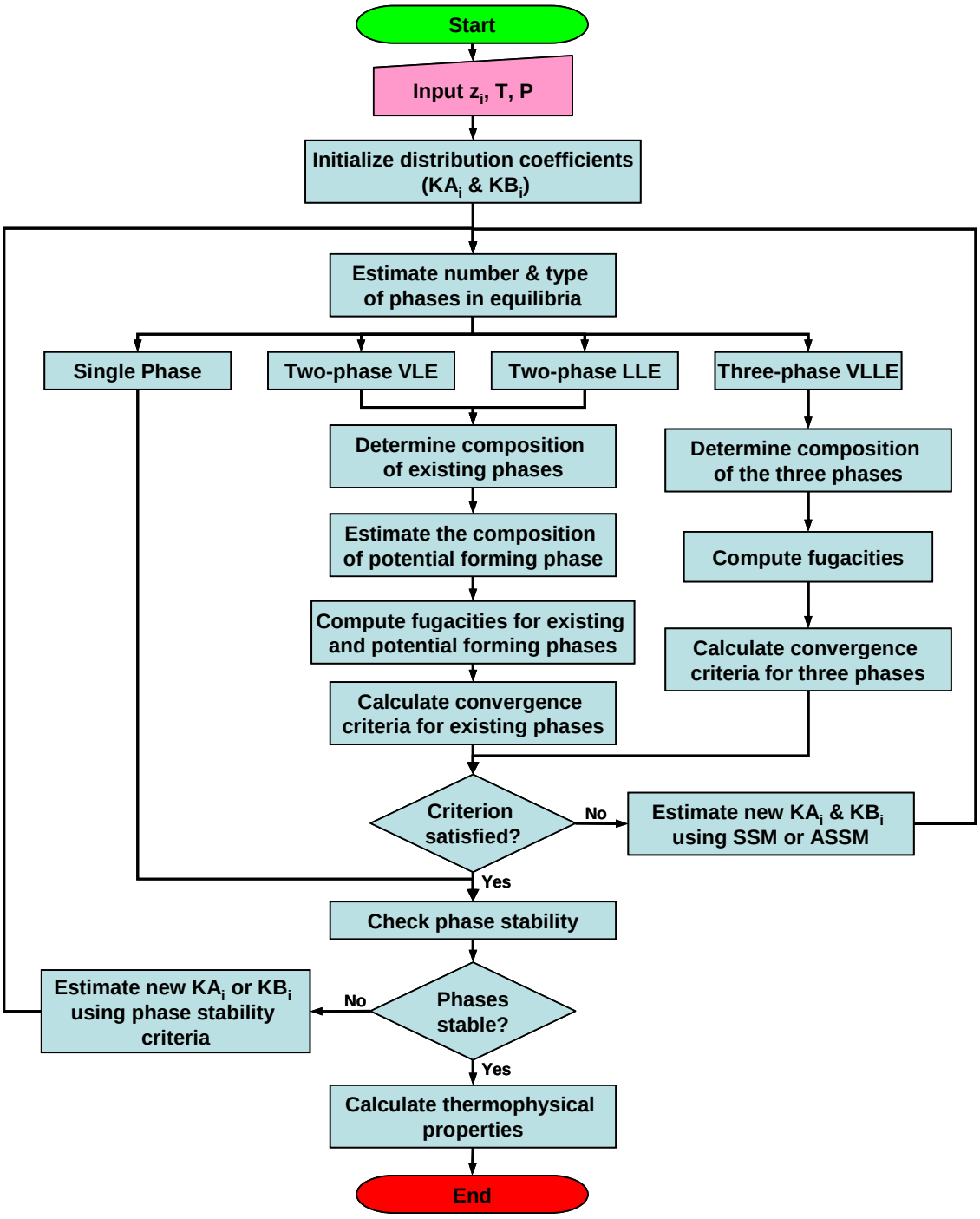

Figure 4.1 Flowchart of the multiphase equilibria algorithm

4.3.3 Determination of number and type of phases in equilibrium

This algorithm implements a method for rapid phase determination in multiphase flash calculations suggested by Nelson (1987). The method is based on the generalization of the Rachford-Rice formulation and a multiphase generalization of the dew and bubble point criteria. This section focuses on the description of this method.

Three material balance equations and the definition of the distribution coefficients are the elements required for fully describing three-phase flash calculations. These equations are defined as:

Component material balance:

$$Vy_i + XA_i LA + XB_i LB = z_i \tag{4.25}$$

Total material balance:

$$LA + LB + V = 1 \tag{4.26}$$

Stoichiometric balance:

$$\sum_{i=1}^{n} y_i = \sum_{i=1}^{n} XA_i = \sum_{i=1}^{n} XB_i = 1 \tag{4.27}$$

In these expressions *V, LA,* and *LB* are the molar fractions of the vapor, hydrocarbon-rich liquid and water-rich liquid phases respectively.

Equations 4.22, 4.25 and 4.26 are combined in order to obtain an expression for the composition of each phase in terms of the mole fractions of the liquid phases and the distribution coefficients. The expressions obtained are:

$$y_i = \frac{z_i KA_i}{LA(1-KA_i) + LB\left(\frac{KA_i}{KB_i} - KA_i\right) + KA_i} \tag{4.28}$$

$$XA_i = \frac{z_i}{LA(1-KA_i) + LB\left(\frac{KA_i}{KB_i} - KA_i\right) + KA_i} \tag{4.29}$$

$$XB_i = \frac{z_i\left(\frac{KA_i}{KB_i}\right)}{LA(1-KA_i) + LB\left(\frac{KA_i}{KB_i} - KA_i\right) + KA_i} \tag{4.30}$$

A system of algebraic equations can be defined applying Stoichiometric balances (Equation 4.27). These equations must be satisfied at the solution of a three-phase system. The system of algebraic equations obtained is represented as follows:

$$F_1 = \sum_i y_i - 1$$

$$= \sum_i \frac{z_i KA_i}{LA(1-KA_i) + LB\left(\frac{KA_i}{KB_i} - KA_i\right) + KA_i} - 1 = 0 \tag{4.31}$$

$$F_2 = \sum_i XA_i - 1$$

$$= \sum_i \frac{z_i}{LA(1-KA_i) + LB\left(\frac{KA_i}{KB_i} - KA_i\right) + KA_i} - 1 = 0 \qquad (4.32)$$

$$F_3 = \sum_i XB_i - 1$$

$$= \sum_i \frac{z_i\left(\frac{KA_i}{KB_i}\right)}{LA(1-KA_i) + LB\left(\frac{KA_i}{KB_i} - KA_i\right) + KA_i} - 1 = 0 \qquad (4.33)$$

These equations contain two independent variables; therefore, only two of them are linearly independent. These equations are combined to define two independent functions more suitable for numerical solution.

$$Q_1(LA, LB) = \sum_{i=1}^{n} XA_i - \sum_{i=1}^{n} y_i \qquad (4.34)$$

$$Q_1(LA, LB) = \sum_{i=1}^{n} \frac{z_i KB_i(1-KA_i)}{KA_i KB_i + LAKB_i(1-KA_i) + LBKA_i(1-KB_i)} = 0 \qquad (4.35)$$

$$Q_2(LA, LB) = \sum_{i=1}^{n} XB_i - \sum_{i=1}^{n} y_i \qquad (4.36)$$

$$Q_2(LA, LB) = \sum_{i=1}^{n} \frac{z_i KA_i(1-KB_i)}{KA_i KB_i + LAKB_i(1-KA_i) + LBKA_i(1-KB_i)} = 0 \qquad (4.37)$$

Equations 4.35 and 4.37 are the three-phase equivalent of the Rachford-Rice functions. A three-phase system solution is satisfied if it is identified at a point in the domain of interest where Q_1 and Q_2 are equal to zero. The domain of interest is a triangular region with vertices (0,0), (0,1), and (1,0). Figure 4.2 illustrates a typical solution for a three phase system. The dashed lines show the points at which Q_1 and Q_2 are equal to zero. The intersection of these lines shows the point at which the system is in equilibrium.

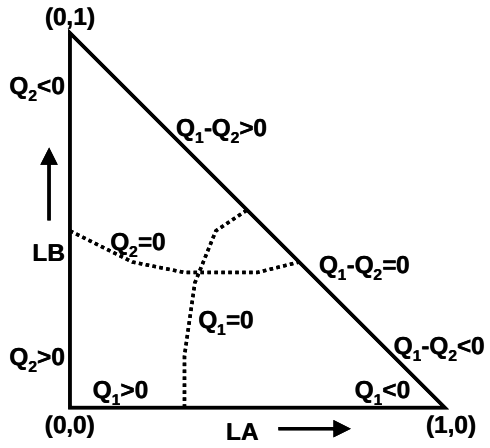

Figure 4.2 Location of zeros of Q_1 and Q_2 for normal three phase behavior

In three-phase systems, Q_1 is positive at (0,0) and negative at (1,0) changing signs along the LA axis. Analogously, Q_2 is positive at (0,0) and negative at (0,1) changing signs along the LB axis. Similarly, $Q_1 - Q_2$ is larger than zero at (1,0) and less than zero at (0,1) changing signs along the diagonal, thus defining the domain of interest.

A better understanding of three phase systems can be obtained by evaluating functions Q_1, Q_2, and $Q_1 - Q_2$ at the vertices of the triangular domain described in Figure

4.2. Table 4.3 shows the results of this evaluation. These results allow the determination of the conditions under which Q_1 has a root along the *LA* axis, Q_2 has a root along the *LB* axis, or $Q_1 - Q_2$ has a zero along the diagonal.

Table 4.3. Evaluation of Q_1, Q_2, and Q_1-Q_2 at the vertices of the domain of interest

LA	***LB***	Q_1	Q_2	Q_1-Q_2
0	0	$\sum_{i=1}^{n} \frac{z_i}{KA_i} - 1$	$\sum_{i=1}^{n} \frac{z_i}{KB_i} - 1$	$\sum_{i=1}^{n} \frac{z_i}{KA_i} - \sum_{i=1}^{n} \frac{z_i}{KB_i}$
1	0	$1 - \sum_{i=1}^{n} z_i KA_i$	$\sum_{i=1}^{n} z_i \frac{KA_i}{KB_i} - \sum_{i=1}^{n} z_i KA_i$	$1 - \sum_{i=1}^{n} z_i \frac{KA_i}{KB_i}$
0	1	$\sum_{i=1}^{n} z_i \frac{KB_i}{KA_i} - \sum_{i=1}^{n} z_i KB_i$	$1 - \sum_{i=1}^{n} z_i KB_i$	$\sum_{i=1}^{n} z_i \frac{KB_i}{KA_i} - 1$

Table 4.3 shows that Q_1 has a zero value along the *LA* axis if $\sum_{i=1}^{n} \frac{z_i}{KA_i} > 1$ and $\sum_{i=1}^{n} z_i KA_i > 1$, Q_2 has a root along the *LB* axis if $\sum_{i=1}^{n} \frac{z_i}{KB_i} > 1$ and $\sum_{i=1}^{n} z_i KB_i > 1$, and Q_1-Q_2 has a root along the diagonal edge if $\sum_{i=1}^{n} z_i \frac{KA_i}{KB_i} > 1$ and $\sum_{i=1}^{n} z_i \frac{KB_i}{KA_i} > 1$.

The analysis of Figure 4.2 and Table 4.3 allows defining the criteria for the existence of single, two, and three-phases in equilibrium. These criteria can be summarized as follows:

4.3.3.1 Test for verifying the existence of two-phase equilibrium

Vapor – hydrocarbon-rich liquid:

Vapor and hydrocarbon- rich liquid are in equilibrium if the following criteria are satisfied:

$$\sum_{i=1}^{n}\frac{z_i}{KA_i}>1;\ \sum_{i=1}^{n}z_i KA_i>1;\ \text{and}\ Q_2(LA,0)<0\ \text{at the point where}\ Q_1(LA,0)=0.$$

For this test, $Q_1(LA,0)$ collapses to the classical Rachford-Rice (RR) expression along the *LA* axis.

$$Q_1(LA,0)=\sum_{i=1}^{n}\frac{z_i(1-KA_i)}{KA_i+LA(1-KA_i)} \qquad (4.38)$$

Q_1 is a non-linear equation that can be solved with the implementation of a numerical technique. In this work, the Newton-Raphson method was used for this purpose. Appendix D shows how this method is implemented for solving the classical Rachford-Rice equation. Once the point where Q_1 is equal to zero is determined, the evaluation of Q_2 at $(LA,0)$ is straightforward using equation 4.37.

Vapor phase and aqueous liquid:

Vapor and a water- rich liquid are in equilibrium if the following criteria are satisfied:

$$\sum_{i=1}^{n}\frac{z_i}{KB_i}>1\ ;\ \sum_{i=1}^{n}z_i KB_i>1;\ \text{and}\ Q_1(0,LB)<0\ \text{at the point where}\ Q_2(0,LB)=0.$$

Analogously to the previous test, Q_2 also collapses to the classical Rachford-Rice (RR) expression along the *LB* axis. This expression is defined as follows for the point *(0,LB):*

$$Q_2(0, LB) = \sum_{i=1}^{n} \frac{z_i(1 - KB_i)}{KB_i + LB(1 - KB_i)} \tag{4.39}$$

Q_2 is solved using the Newton-Raphson method described in Appendix D. Once the root of Q_2 along the *LB* axis is determined, Q_1 at *(0,LB)* can be easily evaluated using equation 4.35.

Hydrocarbon-rich liquid and aqueous liquid:

Two liquids (condensate and water) are in equilibrium if the following conditions are met:

$\sum_{i=1}^{n} z_i \frac{KA_i}{KB_i} > 1$; $\sum_{i=1}^{n} z_i \frac{KB_i}{KA_i} > 1$; and $Q_1(LA,1-LA) > 0$ or $Q_2(LA,1-LA) > 0$ at the point where $Q_1(LA,1-LA) - Q_2(LA,1-LA) = 0$.

In this test, $Q_1(LA,1-LA) - Q_2(LA,1-LA)$ collapse to a Rachford-Rice type similar to that presented above. The expression derived is the typical RR equation for two-liquid systems.

$$Q_1(LA,1-LA) = \sum_{i=1}^{n} \frac{z_i KB_i(1 - KA_i)}{KA_i + LA(KB_i - KA_i)} \tag{4.40}$$

The expression shown above is solved using the Newton-Raphson method. Then, Q_1 at *(LA,1-LA)* is evaluated using equation 4.35.

4.3.3.2 Test for verifying the existence of only one phase

The existence of a single phase is verified by evaluating the objective functions at the vertices of the domain of interest. Evaluation of Q_1 and Q_2 at (0,0), (0,1), and (1,0) allows identifying the existence of single-phase vapor, hydrocarbon-rich liquid, and water-rich liquid respectively. The tests required are presented as follows:

Single vapor phase:

The existence of vapor phase is detected if the following conditions are met:

$$\sum_{i=1}^{n} \frac{z_i}{KA_i} < 1 \quad \text{And} \quad \sum_{i=1}^{n} \frac{z_i}{KB_i} < 1$$

Hydrocarbon-rich liquid:

The criteria for detecting the sole presence of a hydrocarbon rich –liquid are defined as:

$$\sum_{i=1}^{n} z_i KA_i < 1 \quad \text{And} \quad \sum_{i=1}^{n} z_i \frac{KA_i}{KB_i} < 1$$

Water-rich liquid:

A water-rich phase is identified if the following criteria are satisfied:

$$\sum_{i=1}^{n} z_i KB_i < 1 \quad \text{And} \quad \sum_{i=1}^{n} z_i \frac{KB_i}{KA_i} < 1$$

These single-phase detection tests verify whether the generalized Rachford-Rice equations (Q_1 and Q_2) are both negative at the vertices. This condition guarantees that there is no root for these functions in the domain of interest, and allows the identification of the type of phase encountered in the system.

4.3.3.3 Detection of three phases in equilibrium

The failure to satisfy any of the tests previously presented indicates that there is a root for the RR equations in the triangular domain described in Figure 4.2. Then, the algorithm can proceed to perform the three-phase flash calculation.

This flash calculation requires the simultaneous solution of a system of non-linear equations (4.35 and 4.37). Therefore, a numerical method is required to solve the system:

$$Q_1(LA, LB) = \sum_{i=1}^{n} \frac{z_i KB_i (1 - KA_i)}{KA_i KB_i + LAKB_i (1 - KA_i) + LBKA_i (1 - KB_i)} = 0 \quad (4.35)$$

$$Q_2(LA, LB) = \sum_{i=1}^{n} \frac{z_i KA_i (1 - KB_i)}{KA_i KB_i + LAKB_i (1 - KA_i) + LBKA_i (1 - KB_i)} = 0 \quad (4.37)$$

The Newton-Raphson procedure for non-linear systems of equations was implemented for locating a solution. This method is an iterative procedure that requires determining the partial derivative of the objective functions with respect to *LA* and *LB*. These derivatives are expressed as follows:

$$\frac{\partial Q_1}{\partial LA} = \sum_{i=1}^{n} \frac{-z_i KB_i^2 \left(1 - KA_i\right)^2}{\left[KA_i KB_i + LAKB_i \left(1 - KA_i\right) + LBKA_i \left(1 - KB_i\right)\right]^2} = 0 \qquad (4.41)$$

$$\frac{\partial Q_1}{\partial LB} = \frac{\partial Q_2}{\partial LA} = \sum_{i=1}^{n} \frac{-z_i KB_i^2 \left(1 - KA_i\right)^2}{\left[KA_i KB_i + LAKB_i \left(1 - KA_i\right) + LBKA_i \left(1 - KB_i\right)\right]^2} = 0 \qquad (4.42)$$

$$\frac{\partial Q_1}{\partial LA} = \sum_{i=1}^{n} \frac{-z_i KA_i^2 \left(1 - KB_i\right)^2}{\left[KA_i KB_i + LAKB_i \left(1 - KA_i\right) + LBKA_i \left(1 - KB_i\right)\right]^2} = 0 \qquad (4.43)$$

The Newton-Raphson method for non-linear systems of equations consists of finding successive estimates of the unknowns (*LA* and *LB*) by the iterative calculation of:

$$\begin{pmatrix} LA \\ LB \end{pmatrix}_{t+1} = \begin{pmatrix} LA \\ LB \end{pmatrix}_{t} - \begin{bmatrix} \frac{\partial Q_1}{\partial LA} & \frac{\partial Q_1}{\partial LB} \\ \frac{\partial Q_2}{\partial LA} & \frac{\partial Q_2}{\partial LB} \end{bmatrix}_{t}^{-1} \cdot \begin{pmatrix} Q_1 \\ Q_2 \end{pmatrix}_{t} \qquad (4.44)$$

This identity can also be expressed as follows in terms of the determinant of the Jacobian matrix:

$$\begin{pmatrix} LA \\ LB \end{pmatrix}_{t+1} = \begin{pmatrix} LA \\ LB \end{pmatrix}_{t} - \frac{1}{D} \begin{bmatrix} \frac{\partial Q_1}{\partial LA} & -\frac{\partial Q_1}{\partial LB} \\ -\frac{\partial Q_2}{\partial LA} & \frac{\partial Q_2}{\partial LB} \end{bmatrix}_{t}^{-1} \times \begin{pmatrix} Q_1 \\ Q_2 \end{pmatrix}_{t} \qquad (4.45)$$

Where:

$$D = \frac{\partial Q_1}{\partial LA}\frac{\partial Q_2}{\partial LB} - \frac{\partial Q_1}{\partial LB}\frac{\partial Q_2}{\partial LA} \tag{4.46}$$

This method requires repeating the calculation procedure until the values of Q_1 and Q_2 are within a specified tolerance. Then, convergence has been achieved and the values of *LA* and *LB* have, therefore, been properly determined.

4.3.4 Determination of phase compositions and fugacities

The distribution coefficients are not known a priori. This model proposes an iterative procedure for their determination. This procedure is based on the traditional technique of matching the fugacities for each component in each phase.

The method described in the previous section allows estimating the configuration and fraction of phases in equilibrium. If a single phase is detected, the model does not perform additional phase split calculations. However, the model tests the thermodynamic stability of that phase. If the single-phase estimated is not stable, the phase stability routine will allow estimating new distribution coefficients that will be used to find a thermodynamically stable multiphase solution. This process is illustrated in Figure 4.1.

If a two or three-phase configuration is estimated, the compositions of three phases are calculated based on equations (4.28, 4.29, and 4.30).

$$y_i = \frac{z_i KA_i}{LA(1 - KA_i) + LB\left(\frac{KA_i}{KB_i} - KA_i\right) + KA_i} \tag{4.28}$$

$$XA_i = \frac{z_i}{LA(1-KA_i)+LB\left(\frac{KA_i}{KB_i}-KA_i\right)+KA_i} \tag{4.29}$$

$$XB_i = \frac{z_i\left(\frac{KA_i}{KB_i}\right)}{LA(1-KA_i)+LB\left(\frac{KA_i}{KB_i}-KA_i\right)+KA_i} \tag{4.30}$$

For two-phase systems, two of these compositions correspond to the predicted phases in equilibrium while the composition of the third phase estimated is assumed to be that of a potentially forming phase. This assumption will allow the model to update the two sets of distribution coefficients and determine if more than two phases form as these coefficients are recalculated.

The sum of the mole fractions of the phases predicted in equilibrium is equal to one. However, the initial set of distribution coefficients could yield to initial composition estimations where the sum of the mole fractions might be less than one. Therefore, the composition of this phase has to be normalized. Equation 4.47 describes the method for normalizing the composition of this phase.

$$c_{i,norm} = \frac{c_i}{\sum_{i=1}^{n} c_i} \tag{4.47}$$

Fugacity is a measure of the chemical potential of a component in a mixture. Equal fugacities imply the lack of a driving force to transfer a component from one phase to another. Hence, phase equilibria imply equal fugacities.

The algorithm proposed verifies whether thermodynamic equilibrium has been achieved. To do so, it calculates the fugacity for each component in all phases (using the method described in section 4.1), and compares them for those phases in equilibrium. Two or more phases are in equilibrium when the fugacity ratios for all components in the phases in equilibrium are equal to one. This criterion can be expressed as follows for two and three-phase systems.

Two-phase systems are said to be in equilibrium when the following inequality is satisfied.

$$\sum_{i=1}^{n}\left(\frac{f_{ai}}{f_{bi}}-1\right)^2 < 10^{-12} \tag{4.48}$$

Where:

f_{ai} is the fugacity of component "*i*" in phase "*a*" and f_{bi} the fugacity of the same component in phase "*b*".

Three-phase systems are considered to be in equilibrium when the following convergence criterion is satisfied.

$$\sum_{i=1}^{n}\left(\frac{f_{LAi}}{f_{vi}}-1\right)^2 < 10^{-12} \quad \text{And} \quad \sum_{i=1}^{n}\left(\frac{f_{LBi}}{f_{vi}}-1\right)^2 < 10^{-12} \tag{4.49}$$

Where:

f_{LAi} is the fugacity of component "*i*" in the hydrocarbon-rich liquid phase, f_{LBi} the fugacity of the same component in the water-rich liquid phase, and f_{vi} the fugacity of that component in the vapor phase.

Fugacity match is a necessary condition for phase equilibria. However, it is not the only criterion that has to be satisfied. Several phase configurations in the domain of interest might satisfy the fugacity match criterion. However, the system is in equilibrium for the phase configuration that represents the lowest Gibbs energy. The algorithm presented here addresses the phase stability issue by checking that the phase configuration obtained does not have the capacity to split into a lower energy phase configuration. Section 4.3.5 describes the phase stability verification routine.

The fugacity match method implemented in this model consists of finding successive estimates of the distribution coefficients, determining the number of phases, and recalculating fugacities until convergence is attained. The iterative procedure permits the model to form or remove phases as the distribution coefficients are updated. New estimates of the distribution coefficients are calculated using the successive substitution method (SSM) or the accelerated successive substitution method (ASSM).

The successive substitution method (SSM)

Distribution coefficients can also be expressed in terms of fugacity coefficients. This definition introduces the fugacity ratio into the calculation of new estimates for the distribution coefficients.

$$KA_i = \frac{\phi_{LAi}}{\phi_{vi}} = \frac{f_{LAi}/(XA_i P)}{f_{vi}/(y_i P)} = \frac{y_i}{XA_i}\left(\frac{f_{LAi}}{f_{vi}}\right) \tag{4.50}$$

$$KB_i = \frac{\phi_{LBi}}{\phi_{vi}} = \frac{f_{LBi}/(XB_i P)}{f_{vi}/(y_i P)} = \frac{y_i}{XB_i}\left(\frac{f_{LBi}}{f_{vi}}\right) \tag{4.51}$$

The SSM consists of performing new estimates of distribution coefficients in terms of the previous estimates and the fugacity ratios calculated from the equation of state.

$$KA_i^{t+1} = \left(\frac{y_i}{XA_i}\right)^t \left(\frac{f_{LAi}}{f_{vi}}\right)^t = KA_i^t \left(\frac{f_{LAi}}{f_{vi}}\right)^t \tag{4.52}$$

$$KB_i^{t+1} = \left(\frac{y_i}{XB_i}\right)^t \left(\frac{f_{LBi}}{f_{vi}}\right)^t = KB_i^t \left(\frac{f_{LBi}}{f_{vi}}\right)^t \tag{4.53}$$

The SSM is an efficient method for most calculations. However, it has been shown to be inefficient for flash calculations in the region close to the critical points. Therefore, an acceleration technique is implemented in order to overcome this deficiency.

The accelerated successive substitution method (ASSM)

This method is an accelerated version of the SSM presented by Risnes et al. (1981). This method consists of updating the distribution coefficients by multiplying the old coefficients by the fugacity ratios elevated to a factor. This factor is defined to be a function of the improvement ratio obtained for the solution of the problem. This method is independently employed for each set of distribution coefficients. It is expressed as follows:

$$K_i^{new} = K_i^{old}\left(\frac{f_{li}}{f_{vi}}\right)^{\lambda_i} \tag{4.54}$$

Where:

$$\lambda_i = \left[\frac{\left(\frac{f_{li}}{f_{vi}}\right)^{old} - 1}{\left(\frac{f_{li}}{f_{vi}}\right)^{old} - \left(\frac{f_{li}}{f_{vi}}\right)^{new}}\right] \tag{4.55}$$

The ASSM is implemented for those conditions where the SSM starts to be inefficient. Therefore, there are certain criteria that have to be satisfied in order to proceed with its implementation. These criteria are:

$$\frac{\sum_{i=1}^{n}\left(\left(\frac{f_{li}}{f_{vi}}\right)^{new} - 1\right)^2}{\sum_{i=1}^{n}\left(\left(\frac{f_{li}}{f_{vi}}\right)^{old} - 1\right)^2} > 0.8 \tag{4.56}$$

$$\left| f_{nl}^{new} - f_{nl}^{old} \right| < 0.1 \tag{4.57}$$

$$10^{-5} < \sum_{i=1}^{n}\left(\left(\frac{f_{li}}{f_{vi}}\right)^{new} - 1\right)^2 < 10^{-3} \tag{4.58}$$

In these expressions, f_{li} is the fugacity of component "*i*" in a liquid phase, f_{vi} is the fugacity of that component in the vapor phase, and f_{nl} is the molar fraction of liquid in the system.

The ASSM should be tested in order to verify that it leads to an improved solution. If not, the calculations should switch back to the SSM.

4.3.5 Phase stability verification

Multiphase equilibrium can be formulated as a Gibbs free energy minimization problem. Fugacity match is a necessary but not unique condition to guarantee phase stability. Several phase configurations in the domain of interest might satisfy the fugacity match criterion. These solutions to the fugacity match represent local minima to the Gibbs energy in the domain of interest. However, the system is in equilibrium for that phase configuration showing a global minimum of Gibbs energy.

Once a solution to the fugacity match is achieved, the algorithm needs to check that the phases obtained do not have the capacity to split into a lower energy phase configuration. Phase stability is verified using the method suggested by Michelsen (1982a).

This model requires verifying the stability of all phases detected to be in equilibrium. Therefore, the algorithm has to be able to test if: a vapor phase has the potential of forming a second liquid phase, a liquid phase has the potential to form a vapor phase, or a liquid phase has the potential of forming a second liquid phase. If a potential for phase split is detected, the algorithm uses the distribution coefficients estimated for new equilibria calculations. The satisfaction of the fugacity match and the

phase stability criteria verifies that the solution is a global minimum in terms of free Gibbs energy.

These phase-stability tests are performed following the next procedure:

1. Calculate the mixture fugacity using the composition of the phase being tested.
2. Create a second phase; it could be vapor or liquid. This phase is created using the distribution coefficients estimated. Table 4.4 summarizes the equation used to estimate the composition of a potentially splitting phase.
    a. For a vapor phase, two stability tests are required. The first test verifies whether this composition has the potential of forming a hydrocarbon-rich liquid, while the second test is for determining the potential for splitting into a water-rich liquid phase.

    b. For each liquid phase, a check is performed to determine whether it can split into a vapor phase or a second liquid phase. For a hydrocarbon-rich liquid, it is checked if it might form a vapor or a second water-rich phase, while for a water-rich liquid, it is checked if it might form a vapor or a second hydrocarbon-rich phase.

3. Sum the numbers of moles for phase(s) created. The sum of the mole fractions is calculated by $S = \sum_{i=1}^{n} y_i'$ for a potential vapor phase, as $S = \sum_{i=1}^{n} XA_i'$ for a potential hydrocarbon-rich liquid, or by $S = \sum_{i=1}^{n} XB_i'$ for a water-rich liquid.

Table 4.4 Equations for estimating composition of a potentially splitting phase

Phase Tested	***Potential phase splitting***		
	Vapor	***Hydrocarbon-rich liquid***	***Water-rich liquid***
Vapor	---	$XA_i' = \frac{c_i}{KA_i}$	$XB_i' = \frac{c_i}{KB_i}$
Hydrocarbon-rich liquid	$y_i' = c_i KA_i$	---	$XB_i' = c_i \frac{KA_i}{KB_i}$
Water-rich liquid	$y_i' = c_i KB_i$	$XB_i' = c_i \frac{KB_i}{KA_i}$	---

4. The phases obtained are normalized, and the fugacity of the potentially splitting phase is determined from the EOS.

5. The SSM is used for calculating the updated distribution coefficients. These coefficients are estimated by using one of the following expressions:

$$KA_i^{t+1} = KA_i^t \left(R_i\right)^t \tag{4.59}$$

$$KB_i^{t+1} = KB_i^t \left(R_i\right)^t \tag{4.60}$$

$$\left(\frac{KB_i}{KA_i}\right)^{t+1} = \left(\frac{KB_i}{KA_i}\right)^t \left(R_i\right)^t \tag{4.61}$$

Where:

R_i is defined as the fugacity ratio of component "*i*".

6. Convergence is attained if:

$$\sum_{i=1}^{n}\left(R_i - 1\right)^2 < 10^{-12} \tag{4.62}$$

7. A trivial solution is achieved if:

$$\sum_{i=1}^{n}\left(\ln\left(K_i\right)\right)^2 < 10^{-4} \tag{4.63}$$

8. If convergence or a trivial solution is attained, the procedure is stopped. If convergence is not achieved, the new K_i values are used to re-evaluate the splitting phases and the process is repeated from step 2.

A phase is stable if for all tests $S \leq 1$. Only one test violating this criterion proves that the phase is unstable and the new distribution coefficients estimated are used for determining the new phase split configuration.

4.4 Thermophysical properties

Multiphase flash calculation provides composition and molar fraction of the phases in equilibrium. This information is used for estimating the physical and thermodynamic fluid properties required by a hydrodynamic model. The thermophysical properties required by a hydrodynamic model include: density (ρ), viscosity (μ), enthalpy (H), specific heat at constant pressure (Cp), and Joule-Thomson coefficient (η) for each phase. This section is devoted to explain how the model estimates these properties based on the information provided by the flash calculator.

4.4.1 Molecular weight

The molecular weight of each phase is calculated using Kay's mixing rule. Kay's mixing rule relates the molecular weight of a mixture to the mole fraction and the individual molecular weight of each component.

$$Mw_a = \sum_{i=1}^{n} c_i Mw_i \tag{4.64}$$

Where:

Mw_a is the molecular weight of phase "a", c_i the mole fraction of component "i" in phase "a", and Mw_i the individual molecular weight of component "i".

4.4.2 Density

The density of each phase is calculated using the real gas law. The real gas law relates the density to the pressure, temperature, molecular weight, and compressibility factor of a mixture. The compressibility factor is calculated from the PR EOS as indicated in section 4.1. The real gas law is used for calculating the density of both vapor and liquid phases.

$$\rho_a = \frac{P}{RT}\left(\frac{Mw_a}{Z_a}\right) \tag{4.65}$$

Where:

ρ_a is the density of phase "a",and Z_a the compressibility factor of that phase.

4.4.3 Mass fraction

Multiphase flash calculations provide the molar fraction of each phase present in equilibrium. However, a hydrodynamic model requires the mass fraction of each phase in order to determine the mass exchange between the phases. The mass fraction of each phase is calculated as follows for two and three-phase systems.

$$f_{mv} = \frac{Mw_v f_{nv}}{Mw_v f_{nv} + Mw_{LA} f_{nLA} + Mw_{LB} f_{nLB}} \tag{4.66}$$

$$f_{mLA} = \frac{Mw_{LA} f_{nLA}}{Mw_v f_{nv} + Mw_{LA} f_{nLA} + Mw_{LB} f_{nLB}} \tag{4.67}$$

$$f_{mLB} = 1 - f_{mLA} - f_{mv} \tag{4.68}$$

Where:

f_{mv}, f_{nv}, f_{mLA}, f_{nLA} f_{mLB}, f_{nLB} are the mass and molar fractions of the vapor, hydrocarbon-rich liquid, and aqueous liquid phase respectively.

4.4.4 Viscosity of the gas

The viscosity of the gas is determined using an empirical correlation proposed by Lee, Gonzalez and Eakin (1966). These authors correlated the viscosity of a natural gas with the density, molecular weight, and temperature of a fluid. The correlation suggested by these authors is defined as:

$$\mu_g = 1 \cdot 10^{-4} k_v EXP\left(x_v \left(\frac{\rho_v}{62.4} \right)^{y_v} \right) \tag{4.69}$$

Where:

$$k_v = \frac{(9.4 + 0.02Mw_v)T^{1.5}}{209 + 19Mw_v + T} \tag{4.70}$$

$$y_v = 2.4 - 0.2x_v \tag{4.71}$$

$$x_v = 3.5 + \frac{986}{T} + 0.01Mw_v \tag{4.72}$$

For these expressions, the viscosity results are obtained in [cp], the temperature is required in [R], and the density is used in $\left[Lb_m / ft^3\right]$.

4.4.5 Viscosity of the Hydrocarbon-rich liquid

Lohrenz, Bray, and Clark (1964) proposed a method for calculating viscosity of hydrocarbon fluids from their composition. In this study, their method is used for calculating the viscosity of hydrocarbon-rich liquid that may condense in a pipe. The Lohrenz et al. method adapted a correlation originally developed for pure components by Jossi, Stiel, and Thodos (1962) for handling liquid mixtures. The following expression was originally proposed by Jossi et al.:

$$\mu_l = \mu^* + \xi_m^{-1}\left[\left(0.1023 + 0.023364\rho_r + 0.058533\rho_r^2 - 0.040758\rho_r^3 + 0.0093724\rho_r^4\right)^4 - 1\cdot 10^{-4}\right] \tag{4.73}$$

For mixtures, Lorenz, Bray and Clark proposed to use the following equations for defining viscosity of the mixtures as a gas at low pressure μ^*, the reduced density ρ_r., and the mixture viscosity parameter ξ_m.

The expression for μ^* was originally proposed by Herning and Zipperer (1936).

$$\mu^* = \frac{\sum_{i=1}^{n} x_i \mu_i^* \sqrt{Mw_i}}{\sum_{i=1}^{n} x_i \sqrt{Mw_i}} \tag{4.74}$$

Where:

x_i is the mole fraction of the "*i-th*" component

Mw_i is the molecular weight of component "*i*"

μ_i^* is the viscosity of component "*i*" as a gas at low pressure [cp]. For μ_i^*, Lohrenz et al. recommend the use of a correlation formulated by Jossi et al. (1962).

$$\mu_i^* = \frac{34 \cdot 10^{-5} T_{ri}^{0.94}}{\xi_i} \qquad \left(\text{For } \frac{T}{T_{ci}} \leq 1.5\right) \tag{4.75}$$

$$\mu_i^* = \frac{17.78 \cdot 10^{-5} \left(4.58 T_{ri} - 1.67\right)}{\xi_i} \qquad \left(\text{For } \frac{T}{T_{ci}} > 1.5\right) \tag{4.76}$$

In these equations, ξ_i is defined as:

$$\xi_i = \frac{5.4402 T_{ci}^{1/6}}{\sqrt{Mw_i} P_{ci}^{2/3}} \tag{4.77}$$

Where:

T_{ci} is the critical temperature of the "*i-th*" component [R]

P_{ci} is the critical pressure of the "*i-th*" component [psia]

The reduced density (ρ_r), and mixture viscosity parameter (ξ_m) were defined by Lohrenz et al. (1964) as follows:

$$\xi_m = \frac{5.4402 T_{pc}^{1/6}}{\sqrt{Mw_l}\, P_{pc}^{2/3}} \tag{4.78}$$

$$\rho_m = \left(\frac{\rho_l}{Mw_l} \right) V_{pc} \tag{4.79}$$

Where:

P_{pc}, T_{pc}, and V_{pc} are the pseudocritical pressure, temperature, and volume calculated using Kay's mixing rule. The units of these parameters are [*psia*], [*R*], and [$ft^3/lbmol$] respectively.

Mw_l is the molecular weight of the liquid [*lbm/lbmol*]

ρ_l is the density of the liquid phase [lbm/ft^3].

4.4.6 Viscosity of the aqueous liquid

The viscosity correlation proposed by Lohrenz et al. is only applicable to hydrocarbon mixtures. Therefore, a different calculation method is required for the viscosity of an aqueous liquid phase. Teja and Rice (1981) proposed a semi-theoretical method for calculating viscosity of polar liquids based on the corresponding states principles. The equation proposed by these authors is defined as:

$$\ln\left(\mu_m \varepsilon_m\right) = \ln\left(\mu\varepsilon\right)^{(R1)} + \left[\ln\left(\mu\varepsilon\right)^{(R2)} - \ln\left(\mu\varepsilon\right)^{(R1)}\right]\left(\frac{\omega_m - \omega^{(R1)}}{\omega^{(R2)} - \omega^{(R1)}} \right) \tag{4.80}$$

In this expression (*R1*) and (*R2*) refer to two reference fluids, and ε is a parameter similar to the previously defined ξ. This parameter is defined as:

$$\varepsilon = \frac{V_c^{2/3}}{\left(T_{ci} Mw_i\right)^{1/2}} \tag{4.81}$$

For liquid mixtures, the authors suggested to calculate ε_m in a similar manner, but introducing the following mixing rules parameters:

$$V_{cm} = \sum_{i=1}^{n}\sum_{j=1}^{n} x_i x_j V_{cij} \tag{4.82}$$

$$T_{cm} = \frac{\sum_{i=1}^{n}\sum_{j=1}^{n} x_i x_j T_{cij} V_{cij}}{V_{cm}} \tag{4.83}$$

$$Mw_m = \sum_{i=1}^{n} x_i Mw_i \tag{4.84}$$

$$\omega_m = \sum_{i=1}^{n} x_i \omega_i \tag{4.85}$$

$$V_{cij} = \frac{\left(V_{ci}^{1/3} + V_{cj}^{1/3}\right)}{8} \tag{4.86}$$

$$T_{cij} V_{cij} = \psi_{ij} \left(T_{ci} T_{cj} V_{ci} V_{cj}\right)^{1/2} \tag{4.87}$$

The parameter ψ_{ij} in the last expression is an interaction parameter that the authors suggest must be correlated from experimental data. This parameter is approximately one for the interactions involving non-polar components. However, it differs significantly from unity for interactions between water and other polar substances. In this study, this parameter was set to one for all the interactions involving non-polar components, while for water-methanol interactions this parameter was set to 1.34, as suggested by Teja and Rice in their study.

Equation 4.80 requires the knowledge of the viscosity of the two reference substances at a specified temperature. The two reference substances selected in this study were water and methanol. These substances were selected because they will be the dominant components in the aqueous mixture.

This study correlated the viscosity of the reference substances with the reduced temperature by means of the Andrade equation. The results obtained are:

For water:

$$\ln(\mu\varepsilon)^{(R1)} == -7.4392 + 2.4585T_r^{-1} \quad (4.88)$$

For methanol

$$\ln(\mu\varepsilon)^{(R2)} = -6.5806 + 2.4935T_r^{-1} \quad (4.89)$$

Water-methanol mixtures exhibit an atypical behavior in terms of viscosity. Experimental data (Isdale et al, 1985, and Guo et al., 2003) show a dramatic increase of the viscosity of an aqueous mixture when containing low quantities of methanol. The increase in viscosity is up to one and a half times the viscosity of water at the same conditions. Figure 4.3 shows the viscosity of water-methanol mixtures at 20 and 50 °C. This figure was extracted from the publication presented by Teja and Rice (1981).

The calculation method proposed by Teja and Rice was tested against experimental data with satisfactory results. This method was able to represent satisfactorily the strongly non-ideal behavior of water-methanol mixtures.

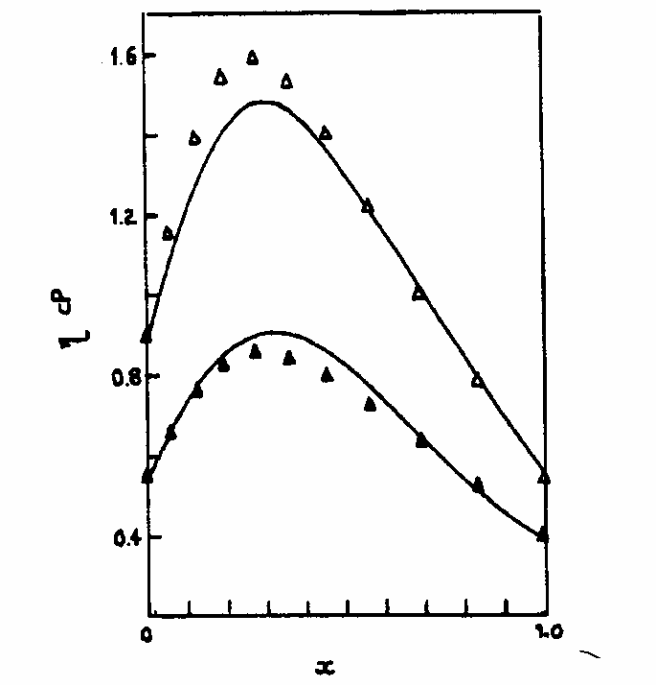

Figure 4.3. Viscosity of water-methanol mixtures at 20 and 50 °C.

From Teja & Rice, 1981

Where:

x represents the mole fraction of methanol

4.4.7 Enthalpy

Peng and Robinson (1976a) presented an expression for the enthalpy departure of a fluid from ideal behavior. This expression was given by these authors as:

$$H - H^* = RT(Z-1) + \frac{T\dfrac{d(a\alpha)_m}{dT} - (a\alpha)_m}{2\sqrt{2}b_m} \ln\left|\frac{Z + (\sqrt{2}+1)B}{Z - (\sqrt{2}-1)B}\right| \qquad (4.90)$$

Equation 4.90 relates the enthalpy of a fluid to the ideal gas enthalpy (H^*) of that mixture, and the departure from ideality presented in the right hand term of the equation.

Ideal gas enthalpy has been correlated by many authors over the years. One of the most remarkable efforts to accurately correlate this property was performed at Penn State University by Passut and Danner (1972). These authors correlated ideal gas enthalpy for 89 compounds (Mostly hydrocarbons) using an equation of the form:

$$H^* = A_{PD} + B_{PD}T + C_{PD}T^2 + D_{PD}T^3 + E_{PD}T^4 + F_{PD}T^5 \qquad (4.91)$$

Where: A_{PD}, B_{PD}, C_{PD}, D_{PD}, E_{PD}, *and* F_{PD} are derived coefficients, with the enthalpy in *Btu/lbm* and temperature in *R*. Erdogmus (2000) presents a summary of the coefficients derived by Passut and Danner for most of the components typically encountered in reservoir fluids.

Equation 4.91 allows determining the ideal gas enthalpy of each component in a mixture (H_i^*). Then, the ideal gas of the mixture is determined using Kay's mixing rule. This mixing rule is expressed as follows:

$$H_m^* = \sum_{i=1}^{n} c_i H_i^* \qquad (4.92)$$

Equation 4.90 requires parameters calculated using the EOS. The only additional parameter required is the derivative of the attraction parameter with respect to temperature ($d(a\alpha)_m / dT$). Peng and Robinson suggested an analytical expression for calculating this parameter based on the use of the classical mixing rules. This expression is not applicable in this case. This study calculates this derivative numerically using a perturbation analysis.

$$\frac{d(a\alpha)_m}{dT} \cong \frac{(a\alpha)_m^{T+\Delta T} - (a\alpha)_m^{T}}{\Delta T} \tag{4.93}$$

4.4.8 Constant pressure specific heat, C_p

This property is defined as the derivative of the enthalpy of a fluid with respect to temperature at constant pressure. This expression is defined as:

$$C_p = \left(\frac{\partial H}{\partial T}\right)_P \tag{4.94}$$

In this work, this derivative is calculated numerically using a perturbation analysis. The numerical approximation obtained for this property is expressed as follows:

$$C_p = \frac{H(P, T+\Delta T) - H(P,T)}{\Delta T} \tag{4.95}$$

The determination of this property requires determining fluid enthalpy at the perturbed temperature. Therefore, the thermodynamic algorithm has to be invoked at least twice for calculating this property.

4.4.9 Joule-Thomson coefficient

The Joule-Thomson coefficient is defined as the derivative of temperature with respect to pressure at constant enthalpy. Mathematically, this property is expressed as:

$$\eta = \left(\frac{\partial T}{\partial P}\right)_H \tag{4.96}$$

Using Maxwell's relationships, it is obtained that:

$$\left(\frac{\partial T}{\partial P}\right)_H \left(\frac{\partial H}{\partial T}\right)_P \left(\frac{\partial P}{\partial H}\right)_T = -1$$

Therefore, the following relationship can be derived for the Joule-Thomson coefficient.

$$\eta = -\frac{1}{C_P}\left(\frac{\partial H}{\Delta P}\right)_T$$

This expression is solved numerically, again, using the perturbation analysis.

$$\eta = -\frac{1}{C_P}\left(\frac{H(P+\Delta P,T)-H(P,T)}{\Delta P}\right) \tag{4.97}$$

4.4.10 Density derivatives

The hydrodynamic model demands determining density derivatives of the fluids flowing with respect to pressure and temperature. In this study, these derivatives are calculated numerically using the perturbation analysis as expressed in equations 4.98 and 4.99.

$$\left(\frac{\partial \rho}{\partial P}\right)_T \cong \left(\frac{\rho(P+\Delta P,T)-\rho(P,T)}{\Delta P}\right) \tag{4.98}$$

$$\left(\frac{\partial \rho}{\partial T}\right)_P \cong \left(\frac{\rho(P,T+\Delta T)-\rho(P,T)}{\Delta T}\right) \tag{4.99}$$

Determining the density derivatives requires the invocation of the thermodynamic model at least three times. The thermodynamic model is called the first time for determining the density at the operating conditions, after that, it is called twice more for calculating the densities at the perturbed conditions.

4.4.11 Surface Tension

Surface tension is commonly defined as the force exerted in the plane of a surface per unit length (Poling et al., 2001). This property is usually expressed in units of lbf/in or dynes/cm.

Over the past century, determination of surface tension has posed a difficult and interesting challenge for scientists and engineers. Typical methods for estimating this property include empirical correlations and thermodynamic-based methods.

Empirical correlations are perhaps the most commonly employed method for estimating surface tension due to their simplicity and acceptable accuracy. These methods are built upon correlating the limited existing data. They have shown to be simple and reliable tools when the deviation from ideal solution behavior is not large. Among the most popular of these correlations could be cited the works of Macleod (1923), Sugden (1924), Weinaug & Katz (1943), Hough & Stegemeier (1961), Lee & Chien (1984), Hugill & van Welseness (1986) and Zuo & Stenby (1997).

The correlations previously mentioned have been shown to provide a reasonable estimate of the surface tension of hydrocarbon systems. However, they have also proven to be inadequate for estimating surface tension of strongly polar or non-ideal substances such as water or water-methanol mixtures.

From the molecular point of view, the boundary layer between two different phases (gas and liquid) could be considered to be a third phase with properties different than those of the bulk of the fluids in contact (Poling et al, 2001). Thermodynamic-based calculation methods solve complex systems of non-linear equations for estimating the composition of the boundary layer, and then develop models for estimating the surface tension based on the composition of the surface layer.

One of the pioneering works on the development of thermodynamic-based models for surface tension is that of Sprow & Prausnitz in 1965b. This method uses the regular solution theory for estimating the composition of the surface layer between fluids. This method was particularly successful for those liquid mixtures showing a behavior close to ideality. However, it shown to be inappropriate for those cases where the deviation from ideality was significant (i.e. aqueous mixtures). Other calculation methods have been developed since then, the most remarkable efforts being that of Suarez et al. (1989). Suarez et al. used Sprow & Prausnitz's formulation but calculated the deviation from ideality using the UNIFAC model. Suarez was able to report average deviations of up to 4% for ternary systems. In 1991, Zhibao et al. used a different version of the UNIFAC

method and reported similar results to those obtained by Suarez. Since then, many other efforts have been performed for estimating surface tension of liquid mixtures using different solution theories, among them could be cited the works of Chunxi et al. (2000), Zhibao & Lu (2001), and Miqueau et al. (2005).

Thermodynamic-based methods represent a reliable and fundamentally based procedure for estimating surface tension. However, they require computationally expensive methods of calculation. This characteristic makes them unattractive for calculating surface tension in this work.

4.4.11.1 Surface Tension of Hydrocarbon-Rich Liquids

Perhaps one of the most popular empirical correlations for estimating surface tension of hydrocarbon systems is that proposed by Weinaug & Katz (1943). This correlation is popular due to its simplicity and the fact that it was derived from the Sugden correlation, which was extensively tested on pure component data (Fawcett, 1994). The Weinaug & Katz correlation is usually expressed as follows:

$$\sigma^{1/n} = \sum_i Pcr_i \left(\frac{\rho_l X_i}{Mw_l} - \frac{\rho_g Y_i}{Mw_g} \right)$$

However, the Weinaug & Katz (WK) correlation has shown to give poor surface tension predictions for multicomponent systems (Danesh et al., 1991). In order to improve the predicted capabilities of the WK correlation, modifications have been suggested by several authors.

Fawcett (1994) performed a comparative analysis of three of the most popular empirical correlations. His analyses included the Hough & Stegemeier (HS), Lee & Chien (LC), and the Weinaug & Katz (WK) correlations. The author reported that the best fit was that provided by the Stegemeier & Hough correlation and proposed a new set of parachors for low interfacial tension data. Fawcett claims that the new set of parachors provide very small systematic errors for multicomponent systems.

In the present study, we estimate the surface tension of hydrocarbon-rich liquids using the Hough & Stegemeier correlation and the new set of parachors suggested by Fawcett (1994). The Hough & Stegemeier correlation has exactly the same form of the Weinaug and Katz correlation. The only difference is the definition of the scaling coefficient “n”. WK uses an “n” value of 4.0, LC uses an n value of 3.91, and HS uses a value of 3.66 which was fitted from experimental data. Table 4.5 indicates the Parachor values suggested by Fawcett.

Fawcett observed that the HS Parachor values could be estimated using a linear expression. For alkanes, Fawcett suggested estimating the Parachor values using the following equation:

$$Pcr_i = 3.148 \times Mw_i + 12.18$$

While for crude oil cuts, the author suggested estimating the HS parachor as follows:

$$Pcr_i = 2.448 \times Mw_i + 81.2$$

For methanol, this works uses a parachor value of 88.25 suggested by Campbell & Anand (1972).

Table 4.5. Stegemeier & Hough Parachors

Component	Parachor
Nitrogen	63.2
Carbon Dioxide	80.7
Hydrogen Sulfide	90.2
Water	57.2
Methane	74.1
Ethane	116.4
Propane	158.1
i-Butane	203.7
n-Butane	203.9
i-Pentane	244.5
n-Pentane	246.2
n-Hexane	283.5
n-Heptane	327.9
n-Octane	371.5
n-Decane	460.7
n-C12	547.9
n-C16	721.3
n-C17	769.9
n-C18	818.9
n-C19	855.6
n-C20	900.5

Schechter & Guo (1998) proposes the use of a new scaling exponent (n = 3.88) based on the critical scaling theory for interfacial tension, and suggested a new set of parachors. They performed a comparative analysis of the correlations found in the literature, based on the scaling exponents. Schechter & Guo observed that “the question of applicability of critical scaling exponents well away from the critical point has been speculated upon, but no evidence can be found in the literature that proves or disproves the extent of critical scaling and what governs deviations from critical scaling”. This observation implies that even though the Hough & Stegemeier was developed for near critical conditions it might still be applicable for those conditions far away from criticality.

4.4.11.2 Surface Tension of Aqueous Mixtures

When organic substances are dissolved in water, these compounds are strongly adsorbed at the surface. In other words, the organic substances are rejected from the bulk of the water phase tending to accumulate at the surface.

Meissner & Michaels (1949) suggests using the Szyszkowski equation (1908) for estimating the surface tension of dilute aqueous solutions. The Szyszkowski equation is expressed as:

$$\frac{\sigma_m}{\sigma_w} = 1 - 0.411 \log\left|1 + \frac{x}{a}\right| \qquad \text{For } x < 0.01$$

Where:

σ_m is the surface tension of the aqueous mixture

σ_w is the surface tension of pure water at the specified temperature

x is mole fraction of the solute in the mixture

In this expression, a is an empirical constant which is characteristic of the solute. Szyszkowski was able to correlate the behavior of a number of dilute solutions using this expression. The solutions correlated include aqueous mixtures of acids, alcohols, esters, ketones, and amines. The author proposed a limited number of values for the empirical coefficient "a". These coefficients are listed in Table 4.6. Szyszkowski recognized that the organic species are oriented in the surface in a nearly identical manner, and suggested the use of the same constants for organic compounds containing the same number of carbon atoms.

The solubility of hydrocarbons in water is very small. Therefore, the concentration of hydrocarbon at the surface of the aqueous solution will be very limited. Inspecting the Szyszkowski equation for those substances it could be seen that the logarithmic term will tend to one, making the surface tension of the solutions containing very small amounts of hydrocarbons approximately equal to that of pure water.

For the purposes of this work, the surface tension of aqueous solutions containing small amounts of "almost insoluble" hydrocarbons is estimated to be equal to that of pure water at the corresponding temperature. Surface tension of water at various temperatures was correlated, and the following expression was derived:

$$\sigma_w = -2.15374\times10^{-8}\,T^3 - 3.56283\times10^{-5}\,T^2 - 0.0300061\,T + 101.642$$

Where:

T is temperature in R.

This expression correlates the surface tension of water for temperatures ranging from 32 to 212 F. The maximum error observed for this correlation is 0.2%.

Table 4.6. Constants for the Szyszkowski equation. From Meissner & Michaels (1949)

Compound	***Carbon atoms***	$a \times 10^4$
Propionic acid	3	26
n-Propyl alcohol	3	26
Isopropyl alcohol	3	26
Methyl acetate	3	26
n-Propyl amine	3	19
Methyl ethyl ketone	4	19
n-Butyric acid	4	7.0
Isobutyric acid	4	7.0
n-Butyl alcohol	4	7.0
Isobutyl alcohol	4	7.0
Propyl formate	4	8.5
Ethyl acetate	4	8.5
Methyl Propionate	4	8.5
Diethyl ketone	5	8.5
Ethyl propionate	5	3.1
Propyl acetate	5	3.1
n-Valeric acid	5	1.7
Isovaleric acid	5	1.7
n-Amyl alcohol	5	1.7
Isoamyl alcohol	5	1.7
Propyl propionate	6	1.0
n-Caproic acid	6	0.75
n-Heptanoic acid	7	0.17
n-Octanoic acid	8	0.034
n-Decanoic acid	10	0.0025

When methanol or other soluble organic substance is present in an aqueous solution the previous simplification is no longer applicable. Therefore, a different approach is required for estimating surface tension. When methanol is present, surface tension is estimated by means of the Tamura method (1955). The Tamura method is commonly used to estimate surface tension of aqueous binary mixtures over a wide range of concentrations.

The Tamura method requires determining the surface tension of the substances found in the binary mixture. Surface tension of water is calculated using the previously mentioned correlation, while surface tension of methanol is determined using the Sastri-Rao correlation (1995). The Sastri-Rao correlation for methanol can be expressed as follows;

$$\sigma_o = 18.94329\left[\frac{512.78-\left(\frac{T}{1.8}\right)}{174.8967}\right]^{0.8}$$

For water-methanol mixtures, the Tamura method reduces to:

$$\sigma_m = \left[\psi_w^{\sigma}\left(\sigma_w^{0.25}\right)+\psi_o^{\sigma}\left(\sigma_o^{0.25}\right)\right]^4$$

In this expression, ψ_w^{σ} and ψ_o^{σ} represent superficial volume fraction of water and methanol respectively. Tamura estimates the superficial volume fraction of water using the following expression:

$$\psi_w^\sigma = \frac{10^C}{1+10^C}$$

Where:

$$C = B + W$$

$$B = \log\left|0.439\frac{(1-x_{CH3OH})}{x_{CH3OH}}\right|$$

$$W = \frac{0.7938}{T}\left[11.89\sigma_o - 6.868\sigma_w\right]$$

While the superficial volume fraction of methanol is calculated as:

$$\psi_o^\sigma = 1 - \psi_w^\sigma$$

The values reported by the Tamura method are in dynes/cm, this expression must be multiplied by 6.85218 x 10-5 to obtain Lbf/ft.

CHAPTER 5

FLOW REGIMES AND THEIR TRANSITIONS

Flow regime can be defined as the geometrical configuration in which two or more fluids travel simultaneously in a pipe or any other conduit. Flow regime determination is a key step in calculating the forces acting on the fluids, and thereby modeling the hydrodynamic behavior of the fluids.

5.1 Two-Phase (Gas-Liquid) Flow

Introduction

Since Lockhart & Martinelli introduced their pioneering work in late 1940's, much efforts have been put forth to determine flow regimes over a wide range of conditions. Traditional approaches consist of collecting experimental data by visualizing the prevailing flow regimes, and creating a two-dimensional plot (based on dimensionless parameters) for mapping flow regime transitions.

The most successful efforts to create a "reliable" map using this technique were performed by Baker (1953), Hubbard & Dukler (1966), Beggs & Brill (1973) and Mandhane et al. (1974). However, the development of these maps relied strongly on the visual inspections made by the researchers, and their criteria for identifying the prevailing flow pattern. Moreover, these publications failed to provide any physical explanation for supporting the occurrence of flow regime transitions. Therefore, the applicability of these

maps for a wide range of operating conditions cannot be ascertained (Taitel & Dukler, 1976).

Taitel & Dukler (1976) proposed a model for predicting flow regime transitions in horizontal and near horizontal gas-liquid flow. These authors focused their analysis on understanding the physics behind the flow regime transitions. Taitel & Dukler's work represented a breakthrough from the typical approach for performing research in the field, and this publication is among the most cited in multiphase flow literature.

Taitel & Dukler's work remains one of most employed criteria for estimating the flow regimes in horizontal and near horizontal gas-liquid flow in pipes. The applicability of Taitel & Dukler's model has been extensively tested by the work of several other researchers. Among them are the works of Barnea (1987), Xiao et al. (1991), Chen et al. (1997), and Meng et al. (1999).

Flow Regime Determination in Two—Phase (Gas-Liquid) flow

This work proposes identifying two-phase (gas-liquid) flow regimes using the unified model proposed by Ayala (2001). Ayala's approach combines the Brauner (2001), Taitel & Dukler (1976), and Barnea (1987) models for determining two-phase flow regime transitions. The method proposed uses the Brauner model for determining the transition between mist and annular flow, the Taitel & Dukler model for the transitions between stratified wavy and annular flow, and the approach suggested by

Barnea for transitions from stratified smooth to stratified wavy flow. This approach has been tested and shown to be appropriate for gas-liquid flow in near horizontal pipes exhibiting low liquid loading.

Transition from Stratified Smooth to Stratified Wavy

Stratified smooth is the prevailing flow regime when the gas motion is not sufficient to disturb the liquid surface. This flow pattern exhibits a smooth and flat gas-liquid interface. A smooth liquid surface may be disturbed by contact with flowing gas. Gas flow may create a "wind" effect, forming waves on a liquid surface. Taitel & Dukler suggest that waves are formed when pressure and shear forces exceed viscous dissipation forces. These authors introduced the following criterion as a threshold for wave formation:

$$v_g > \sqrt{\frac{4\gamma\mu_l(\rho_l - \rho_g)gCos\beta}{s\rho_l\rho_g v_l}} \qquad (5.1)$$

In this inequality, γ is a unit conversion factor ($\gamma = 6.72x10^{-4}$ lbm-ft^{-1}-s^{-1}-cp^{-1}), and s is defined as Jeffrey's (1926) "sheltering" coefficient. This work uses a sheltering coefficient of 0.06 recommended by Xiao et al. (1991).

Barnea et al. (1982) observed that waves might also be formed due to the effect of gravity, and suggested an additional criterion for downward inclined pipes. Barnea

suggested that waves may be formed when liquid velocity satisfies the following expression:

$$v_l > 1.5\sqrt{gh_l} \tag{5.2}$$

Where:

h_l is defined as the liquid level on the pipe.

Satisfaction of the criteria presented in expressions 5.1 or 5.2 indicates that the prevailing flow pattern is not stratified smooth. Therefore, additional verification is required for determining the prevailing flow regime.

Transition from Stratified Wavy to Annular flow

At high gas rates and low liquid loading, Taitel & Dukler suggested that waves may grow and be "swept up and around" the internal surface of a pipe forming a flow pattern known as annular flow. This transition is triggered by the growing potential of waves. Taitel & Dukler used the Kelvin-Helmholtz theory for proposing a criterion for predicting wave growth. They proposed that annular flow may exist when the following criterion is satisfied:

$$v_g > \left(1 - \frac{h_l}{d}\right)\sqrt{\frac{(\rho_l - \rho_g) g \cos(\beta) A_g}{\rho_g \frac{dA_l}{dh_l}}} \tag{5.3}$$

In this expression, A_g is the area available for gas flow, and dA_l/dh_l represents the derivative of the area available for liquid flow with respect to liquid height in the pipe. These quantities are determined as follows:

$$A_g = \frac{2(\pi - \theta) + \sin 2\theta}{8} d^2 \tag{5.4}$$

$$\frac{dA_l}{dh_l} = d\sqrt{1 - \left(2\frac{h_l}{d} - 1\right)^2} \tag{5.5}$$

Where:

θ is the pipe wetted angle in a stratified smooth regime.

This transition criterion was proposed by Taitel & Dukler not only as the threshold for forming annular flow but also as the criterion for intermittent flow. Taitel & Dukler claim that for high liquid loading ($h_l > 0.5d$), waves may reach the top of the pipe forming a “liquid bridge” creating the conditions for intermittent flow. This condition of intermittent flow is typically known as slug flow.

Slug flow is not likely to occur in gas transmission applications exhibiting low liquid loading. In most cases, the liquid in the pipe is not enough to create the “liquid bridge” required for intermittent flow. Therefore, the criterion previously described is restricted for predicting annular flow.

Ayala (2001) proposed incorporating an additional criterion suggested by Grolman & Fortuin (1997b) for estimating occurrence of annular flow. This criterion assumes that annular flow exists when the wetted pipe wall fraction exceeds 80%. For implementing this criterion, Grolman & Fortuin proposed a correlation for estimating the wetted wall fraction (W_f) of a pipe. Their correlation can be expressed as:

$$W_f = 0.624\alpha_l^{0.374} + We_{sl}^{0.25} Fr_g^{0.8} \frac{\rho_g}{(\rho_l - \rho_g) Cos\beta} \tag{5.6}$$

Where:

$$We_{sl} = \frac{\rho_l (\alpha_l v_{sl})^2 d}{\sigma g_c} \tag{5.6a}$$

$$Fr_g = \frac{(\alpha_g v_{sg})^2}{\alpha_g^2 g d} \tag{5.6b}$$

$$v_{sg} = \alpha_g v_g \tag{5.6c}$$

$$v_{sl} = \alpha_l v_l \tag{5.6d}$$

The dimensionless numbers We_{sl} and Fr_g are defined as superficial liquid Weber number and gas-phase Froude number respectively.

Stratified wavy flow is assumed when the inequality presented in equation 5.3 is not satisfied, and the wetted pipe wall area does not exceed 80% ($W_f < 0.8$). Otherwise, additional analysis is required for estimating the prevailing flow pattern.

Transition from Annular to Mist flow

Brauner (2001) proposed a unified model for predicting dispersed flow boundaries in liquid-liquid and gas-liquid systems. Brauner's work performed a complete review of the methods available for predicting the occurrence of dispersed flow in gas-liquid systems, and proposed an approach for predicting the occurrence of mist flow.

Brauner (2001) proposed that the transition to mist flow occurs when the turbulence of the continuous gas phase is "sufficiently intense" to break the liquid phase into droplets smaller than a critical size. The transitional mechanism implies that gas velocity must be high enough to detach the fluid from liquid surface forming droplets small enough to be dragged by the gas phase. Therefore, the maximum drop size that can be formed must be smaller than the maximum drop size that can be dragged by the gas phase. The proposed transitional criterion can be formulated as:

$$d_{\max} \leq d_{crit} \tag{5.7}$$

Brauner (2001) proposes the critical drop size to be the minimum between the maximum drop diameter above which drops are deformed ($d_{c\sigma}$), and the maximum drop diameter above which migration to the tube walls due to buoyant forces takes place (d_{cb}).

$$\frac{d_{crit}}{d} = \min\left\{\frac{d_{c\sigma}}{d}, \frac{d_{cb}}{d}\right\} \tag{5.8}$$

As suggested by Brauner (2001), this work calculates $d_{c\sigma}$ using an approach proposed by Brodkey (1967), and d_{cb} employing an expression suggested by Barnea (1987).

$$\frac{d_{c\sigma}}{d} = \sqrt{\frac{0.4\sigma_l}{\left|\rho_g - \rho_l\right| g\, Cos\beta\, d^2}} \tag{5.9}$$

$$\frac{d_{cb}}{d} = \frac{3}{8}\frac{\rho_g}{\left|\rho_g - \rho_l\right|}\frac{f_{wg} v_g^2}{d\, g\, Cos\beta} \tag{5.10}$$

The maximum drop diameter is calculated as the maximum between the maximum drop size that could exist in a dilute dispersion $(d_{max})_\varepsilon$ and the maximum drop diameter that could exist in a dense dispersion $(d_{max})_o$ (Brauner, 2001).

$$\frac{d_{\max}}{d} = \max\left\{\left(\frac{d_{\max}}{d}\right)_o, \left(\frac{d_{\max}}{d}\right)_\varepsilon\right\} \tag{5.11}$$

The maximum drop diameters are calculated by Hinze's model (1955). Hinze's correlation for dilute dispersion is expressed as:

$$\left(\frac{d_{\max}}{d}\right)_o = 0.55\left(\frac{\rho_g v_g^2 d}{\sigma g_c}\right)^{-0.6}\left(\frac{\left(\alpha_g \rho_g + \alpha_l \rho_l\right)}{\alpha_g \rho_g} f_{wg}\right)^{-0.4} \tag{5.12}$$

While Hinze's correlation for dense dispersions can be written as:

$$\left(\frac{d_{\max}}{d}\right)_{\varepsilon} = 2.22\left(\frac{\rho_g v_g^2 d}{\sigma g_c}\right)^{-0.6}\left(\frac{\left(\alpha_g \rho_g + \alpha_l \rho_l\right)}{\alpha_g \rho_g} f_{wg}\right)^{-0.4}\left(\frac{\alpha_l}{\alpha_g}\right)^{0.6} \qquad (5.13)$$

When the criterion expressed in equation 5.7 is satisfied the prevailing flow regime is mist flow, otherwise, the flow pattern is assumed to be annular.

5.2 Three-Phase (Gas-Liquid-Liquid) Flow

Introduction

The literature available shows only a limited number of experimental studies on three-phase flow. This section describes the most relevant work performed for understanding flow transitions in this type of flow.

The first publication on three-phase (gas-liquid-liquid) flow in horizontal pipes was presented by Sobocinski (1955). In his pioneering work, this author performed the first attempt to classify three-phase flow regimes.

Sobocinski performed a limited number of experiments for observing the flow patterns, and classified flow regimes in three-phase flow in nine categories. Table 5.1 shows the early classification presented by Sobocinski.

From 1955 to 1988, the literature shows a very limited number of publications on three-phase flow in horizontal or near horizontal pipes. During this period most researchers in the field focused their efforts on analyzing flow patterns, developing correlations and models for understanding two-phase flow. To the author's knowledge, in this period only the works of Guzhov et al. (1974), Malinowski et al. (1975), and Laflin & Oglesby (1976) could be cited. These studies focused on determining the occurrence of intermittent three-phase flow (slug and/or plug flow), and correlating their pressure drops and liquid holdups. These authors treated the two liquid phases (oil and water) as a single liquid, and proposed using two-phase mapping techniques for three-phase flow.

Table 5.1 Three-phase flow regime classification (Sobocinski, 1955)

No.	Flow Pattern Description
1	No liquid mixing Stratified
2	No liquid mixing Ripple
3	Inception of oil & water mixing surface waves
4	Incipient emulsion light waves
5	Incipient emulsion w/ waves
6	Partial emulsion w/ waves
7	Partial emulsion w/ heavy waves
8	Partial emulsion w/ light crests
9	Emulsified / semi annular

Most of the studies for identifying flow patterns in three-phase flow have been performed in the last fifteen years. Stapelberg & Mewes (1990a,b, and 1991) conducted three-phase (air-oil-water) experiments and proposed adapting Baker's two-phase map for estimating flow transitions in three-phase flow. Again, Stapelberg & Mewes treated

the two liquid phases (oil and water) as a single liquid of “volume-averaged” properties. This approach assumes that the liquid phases form an emulsion. Therefore, this assumption is not appropriate when the two liquids travel independently through the pipes.

Açikgöz et al. (1992) identified several flow patterns in horizontal three-phase flow, and presented one of the most comprehensive three-phase flow regime maps developed to date. Açikgöz’s flow regime map divided the three-phase flow spectrum into ten complex flow patterns. These flow patterns are listed in Table 5.2.

Açikgöz et al. (1992) conducted their experiments at near atmospheric conditions, and plotted their flow regime maps using superficial velocities as coordinates. These features make this flow regime map only applicable for the conditions for which it was designed. These conditions are far from representing the wide spectrum of conditions that exist in typical natural gas transmission operations.

Table 5.2 Three-phase flow regime classification (Açikgöz et al., 1992)

No.	Flow Pattern Description
1	Oil-based dispersed plug flow
2	Oil-based dispersed slug flow
3	Oil-based dispersed stratified/wavy flow
4	Oil-based separated stratified/wavy flow
5	Oil-based separated stratifying/annular flow
6	Separated/dispersed stratifying/annular flow
7	Water-based dispersed slug flow
8	Water-based dispersed stratified/wavy flow
9	Water-based separated/dispersed incipient stratifying/annular flow
10	Water-based dispersed stratifying-annular flow

Lunde et al. (1993) performed three-phase flow experiments using a dense gas (refrigerant 12 or sulfur hexafluoride), oil, and water in upward inclined pipes. Their experiments focused on determining flow regimes, pressure drop and liquid holdups. The flow patterns observed and described in these experiments were mainly slug and stratified wavy flow.

Lee et al. (1992) performed flow pattern studies for horizontal air-oil-water flow. These authors classified three-phase flow regimes into seven flow patterns, namely: stratified smooth, stratified wavy, rolling wave, plug flow, bubble flow, slug flow and annular flow.

Pan (1996) conducted extensive experimentation on a three-phase (air-oil-water) system, and prepared flow regime maps for horizontal flow at three different pressures. Pan proposed defining fifteen different three-phase flow patterns. However, his experiments were able to identify only eight of them. Table 5.3 lists the flow regimes identified by Pan.

Table 5.3 Three-phase flow regimes identified by Pan (1996)

No.	Flow Pattern Description
1	Separated Slug flow
2	Dispersed water-continuous slug flow
3	Dispersed oil-continuous slug flow
4	Separated stratified flow
5	Dispersed oil-continuous stratified flow
6	Dispersed oil-continuous annular flow
7	Dispersed water-continuous stratified flow
8	Dispersed water-continuous annular flow

Pan (1996) compared his experimental data with the three-phase flow map of Açikgöz et al., and the two-phase flow maps of Stapelberg et al. (1990a,b), Baker (1953), Beggs & Brill (1973), Mandhane et al. (1974), Taitel & Dukler (1976), and Weisman et al. (1979). His flow map comparison showed important differences. Pan (1996) identified two main reasons for these differences. This author observed that two-phase flow maps are "fundamentally unsuitable" for correlating three-phase flow patterns because their flow configurations are inconsistent with those observed in his three-phase experiments. Moreover, he verified that the three-phase flow map of Açikgöz et al. (1992) is not "comprehensive enough" to be applied under for wide range of operating conditions.

Khor (1998) conducted extensive three-phase (air-oil-water) experimentation under various operating conditions. His experiments varied pipe inclination, pressure and flow rates. Khor's work did not present a comprehensive flow regime map. However, he identified the flow patterns observed during his experiments, and provided a more detailed flow regime description than that previously presented by Açikgöz et al. (1992) and Pan (1996).

Khor compared flow regimes observed against the predictions of the Taitel & Dukler map. For this purpose he treated the two liquid phases (oil and water) as a single liquid of "average" properties. The author approximated liquid density and viscosity using a volumetric average of the fluid properties. Khor concluded that the Taitel & Dukler model can give a rough qualitative indication of the transitions. However, he suggests that more specific models are required to obtain accurate predictions.

Currently, there is no generalized flow regime map for horizontal three-phase flow. All the flow regime maps described in the literature are purely empirical, and did not attempt to explain the physical mechanisms behind flow regime transitions. The present work summarizes the potential flow regimes that could result in three-phase flow, and proposes a theoretical method for estimating flow patterns in near horizontal three-phase (gas-condensate-water) flow in pipes.

Terminology for identifying three-phase flow regimes

The typical terminology used for identifying flow regimes in three-phase flow is different from that used for two-phase flow. Even though there is no "standard" nomenclature for identifying three-phase flow patterns, most authors use a three-part designation for describing these patterns (Açikgöz et al.(1992), Pan (1996), Khor (1998)).

This study will employ a terminology similar to that proposed by Pan (1996). The terminology proposed by Pan consists of three parts. The first part specifies whether the two liquid phases travel separately, or if one liquid is dispersed in the other. If one liquid phase is dispersed, the second part of the designation indicates the continuous phase in the emulsion. Obviously, the second part of the designation will be necessary only if one of the liquid phases is dispersed. The third part describes the flow pattern depicted by the gas and total liquid, using the same terminology used in two-phase flow. Figure 5.2 illustrates an example of this designation.

Pan's terminology seems appropriate for describing flow patterns exhibiting dispersed flow in one of the liquid phases. However, it requires an additional element for describing flow patterns where the liquid phases travel separately.

Açikgöz et al. (1992) and Khor (1998) have observed flow configurations where the two-phase flow regime depicted by the gas and total liquid phases does not appropriately describe the three-phase flow configuration. Figures 5.3 and 5.8 illustrate examples of these flow regimes. As suggested by Açikgöz et al. and Khor, the description of these flow regimes will require incorporating an additional element into the designations.

This study proposes adding the following modification to Pan's terminology. When the liquid phases are separated, the third part of the identification should include the flow pattern described by a "dense" gas phase (gas + condensate) and the water phase, and the flow regime depicted by the gas and the oil phase. Figures 5.3 and 5.8 present examples of this terminology.

Flow regimes in three-phase flow

The literature reports up to ten different flow patterns observed under low liquid-loading conditions. These flow configurations have been identified and reported by several researchers (Sobocinski (1955), Açikgöz et al. (1992), Pan (1996), and Khor (1998)). Table 5.4 lists the flow patterns identified, while Figures 5.1 through 5.10 illustrate the flow patterns observed.

Table 5.4 Three-phase flow regimes reported in the literature

No.	Flow Pattern Description
1	Separated stratified smooth – stratified smooth
2	Dispersed oil-continuous stratified smooth
3	Separated stratified smooth – stratified wavy
4	Separated stratified wavy – stratified wavy
5	Dispersed oil-continuous stratified wavy (partially dispersed)
6	Dispersed oil-continuous stratified wavy (fully dispersed)
7	Dispersed water-continuous stratified wavy (fully dispersed)
8	Separated stratified wavy – annular
9	Dispersed oil-continuous annular
10	Dispersed water-continuous annular

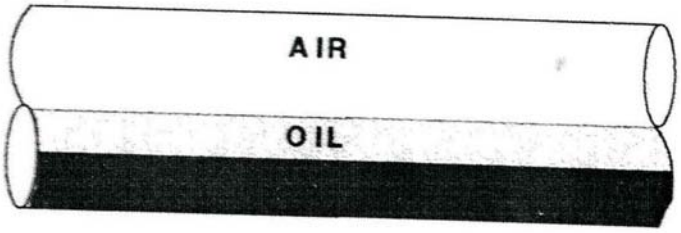

Figure 5.1 Separated Stratified Smooth – Stratified Smooth. Khor (1998)

The flow regime illustrated in Figure 5.1 is perhaps the first flow pattern that comes to mind when discussing three-phase flow. In this flow configuration, the interfaces exhibit smooth and flat surfaces. Several authors have reported the occurrence of this type of flow (Açikgöz et al. (1992), Pan (1996), and Khor (1998)), which has been observed in horizontal and downward inclined pipes operating at low gas and liquid flow rates.

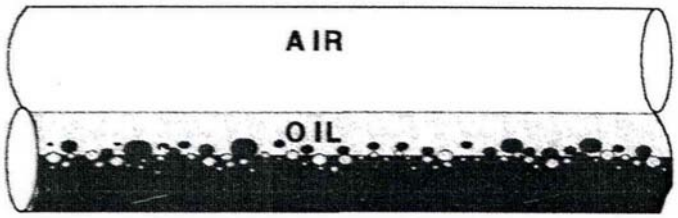

Figure 5.2 Dispersed Oil Continuous Stratified Smooth. Khor (1998)

Figure 5.2 shows a stratified smooth flow pattern where an emulsification process is starting to take place. Oil and water droplets are observed in the vicinity of the oil-water interface. This flow pattern has been reported only by Khor (1998).

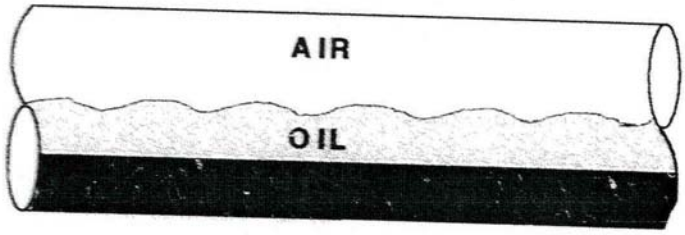

Figure 5.3 Separated Stratified Smooth – Stratified Wavy. Khor (1998)

The flow pattern illustrated in Figure 5.3 shows a wavy and concave gas–oil interface and a smooth and flat oil-water interface. This flow configuration was observed by Khor (1998).

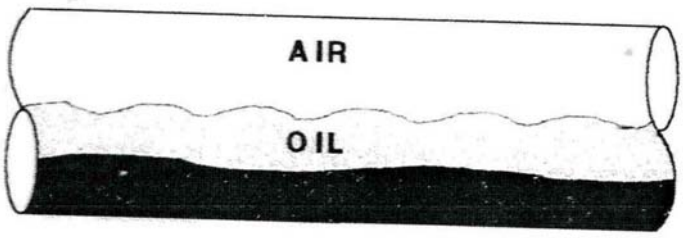

Figure 5.4 Separated Stratified Wavy – Stratified Wavy. Khor (1998)

Figure 5.4 illustrates a flow pattern exhibiting waves in the gas-oil and oil-water interfaces. Furthermore, these interfaces show a concave surface. It has been observed by several researchers, among them Açikgöz et al., Pan, and Khor.

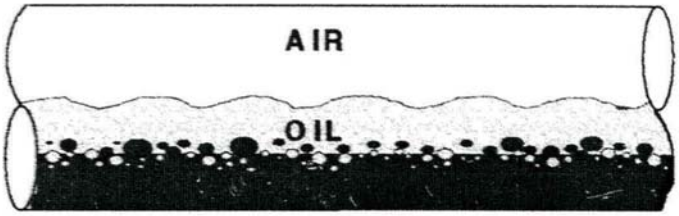

Figure 5.5 Dispersed Oil Continuous Stratified Wavy (Partially dispersed).

From Khor (1998)

The flow pattern shown in Figure 5.5 suggests that an incipient emulsification process is taking place. Oil and water droplets are starting to form in the vicinity of the oil-water interface. This flow pattern has been observed by Açikgöz et al. (1992) and Khor (1998).

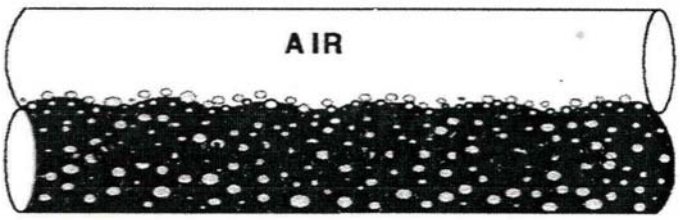

Figure 5.6 Dispersed Oil Continuous Stratified Wavy (Fully Dispersed). Khor (1998)

Figure 5.6 shows a flow pattern in which water is completely dispersed in an oil phase. This flow regime resembles two-phase gas-oil flow.

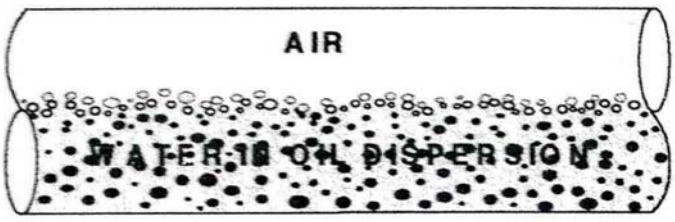

Figure 5.7 Dispersed Water Continuous Stratified Wavy (Fully Dispersed). Khor (1998)

The flow regime presented in Figure 5.7 shows an oil phase completely emulsified in a water phase. This flow regime resembles two-phase gas-water flow.

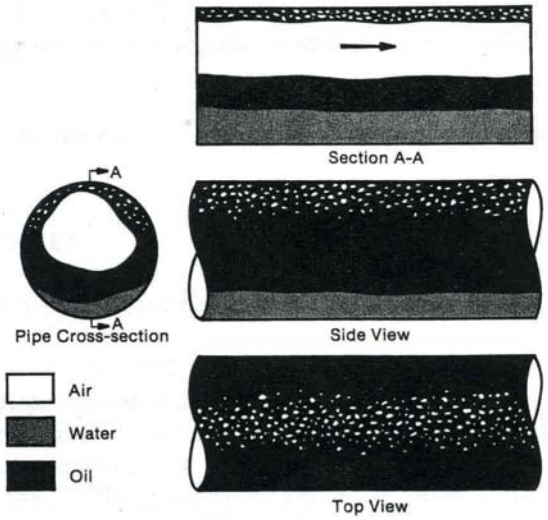

Figure 5.8 Separated Stratified Wavy – Annular. Açikgöz et al. (1992)

Figure 5.8 shows a water phase traveling at the bottom of the pipe resembling stratified wavy flow, while an oil phase wets the upper parts of the pipe resembling

annular flow. For this flow configuration Açikgöz et al. (1992) observed that the liquid wetting the upper part of the tube may exhibit waves, or contain entrained gas bubbles, while Khor (1998) visualized an incipient emulsification process starting to take place at the oil-water interface.

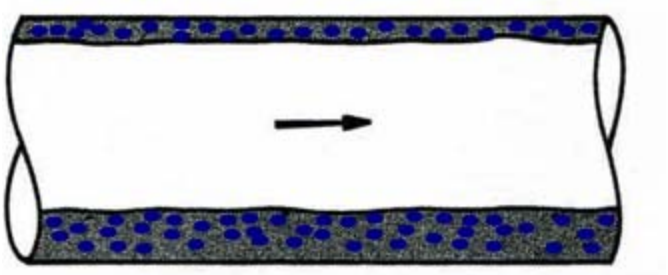

Figure 5.9 Dispersed Oil Continuous Annular. Adapted from Açikgöz et al. (1992)

Figure 5.9 shows water completely dispersed in a continuous oil phase. This flow regime resembles two-phase gas-oil annular flow. As in two-phase annular flow, this flow pattern may also exhibit droplets entrained in the gas core.

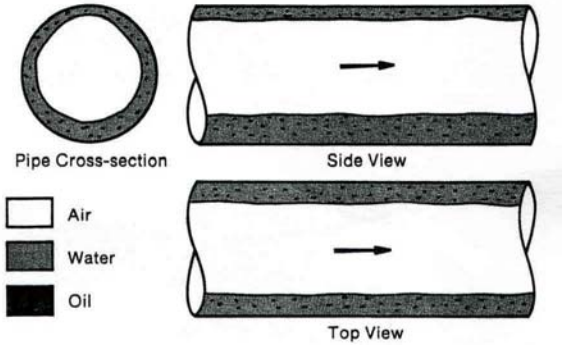

Figure 5.10 Dispersed Water Continuous Annular. Açikgöz et al. (1992)

Figure 5.10 illustrates oil completely dispersed in water. This flow regime resembles two-phase gas-oil annular flow. As in the previous case, this flow pattern may also exhibit droplets entrained in the gas core.

The previously described flow patterns have been reported for low and moderate gas and liquid flow rates. However, this study goes beyond that point, and suggests that at least three other flow configurations may be formed at higher flow rates. At high water cuts and superficial gas velocity, this study suggests that it may be possible to obtain a flow configuration where water travels in a stratified wavy fashion, while condensate droplets are entrained in the gas stream. This would occur because the first droplets to form will correspond to the liquid having lower density and surface tension. Figure 5.11 illustrates the flow pattern idealized. This flow configuration will be called Separated Stratified Wavy – Mist flow.

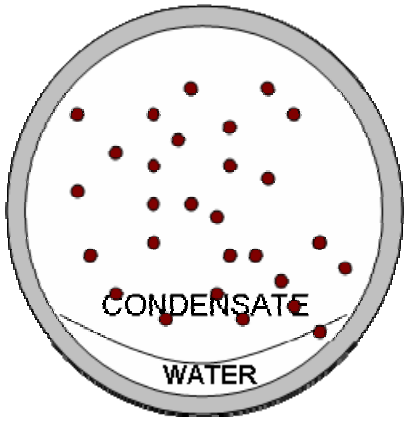

Figure 5.11 Separated Stratified Wavy – Mist flow

Upon transition from annular to mist flow, this study suggests that liquid droplets will be detached from the pipe walls and will be entrained in the gas stream due to the high gas velocity. As in the previous case, it is hypothesized that the first droplets to detach will be those of the liquid having low density and surface tension. Therefore, the formation of a flow configuration where water will exhibit annular flow behavior while the condensate travels as mist flow is predicted. Figure 5.12 illustrates the predicted flow pattern. This idealized flow regime will be identified as Separated Annular – Mist flow.

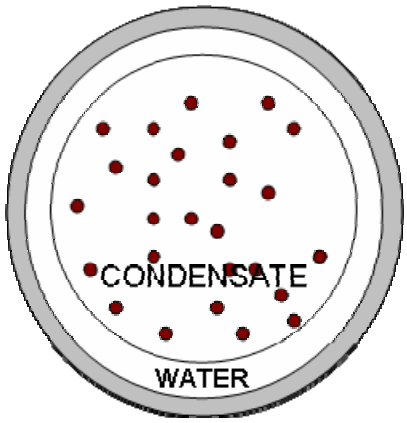

Figure 5.12 Separated Annular – Mist flow

At sufficiently high flow rates, it is predicted that the liquids will detach from the pipe walls and travel separately as entrained droplets in the gas phase. However, these droplets might wet the internal walls of the pipe to a certain extent. This flow pattern will be called Separated Mist-Mist and is illustrated in Figure 5.13.

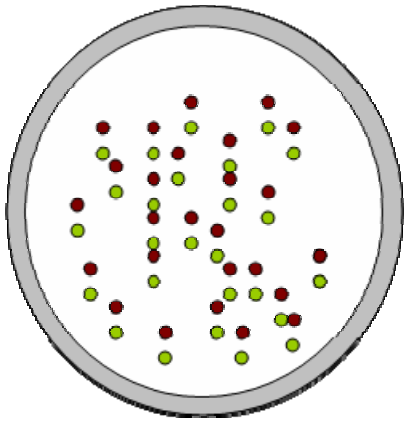

Figure 5.13 Separated Mist – Mist flow

For modeling purposes, this study simplifies the three-phase flow problem assuming that the condensate and water phases are immiscible. Therefore, it will be considered that the three phases travel separately in the pipe.

Given that all flow patterns considered are separated; the terminology used in this work will consist of two parts. The first part will indicate the flow pattern described by the water and “dense” gas phases. The dense gas phase consists of treating gas and condensate as a pseudo fluid exhibiting volume averaged properties. The second part will indicate the flow regime described by the gas and oil phases.

Three-phase flow patterns considered in this study can be summarized in eight idealized configurations. These flow configurations are listed in Table 5.5, while their cross-sectional areas are illustrated in Figure 5.14.

Table 5.5 Three-phase flow patterns idealized for this study

Flow Pattern Description		
Flow pattern described by water & hydrocarbons	**Flow pattern described by gas & condensate**	**Designation**
Stratified smooth	Stratified smooth	SS-SS
Stratified smooth	Stratified wavy	SS-SW
Stratified wavy	Stratified wavy	SW-SW
Stratified wavy	Annular	SW-AN
Stratified wavy	Mist	SW-MT
Annular	Annular	AN-AN
Annular	Mist	AN-MT
Mist	Mist	MT-MT

This work performs a qualitative description of three-phase flow regime transitions considering that in typical gas transmission operations superficial velocities increase as pressure drops along the pipe. Figure 5.14 describes the flow pattern transitions expected for three-phase flow.

As suggested by Taitel & Dukler (1976), flow pattern transitions are analyzed by evaluating the physical mechanisms leading to changes in flow configuration. The process of analyzing the flow pattern transitions starts from a fully stratified flow regime (SS-SS).

Transition to SS-SW flow pattern is expected when the gas superficial velocity is sufficient to disturb the gas-oil interface, while not yet enough to disturb the condensate-water interface. Transition to SW-SW will occur when gas flow could create sufficient

turbulence in the condensate phase to disturb the condensate-water interface. SW-AN or SW-MT will take place when the gas-condensate flow could reach the conditions for annular or mist flow, while water is still traveling stratified at the bottom of the pipe.

Moreover, at high gas superficial velocities oil and water phases could be swept up and around the pipe forming fully annular (AN-AN) flow. SW-AN or AN-AN flow could transition into AN-MT flow as gas velocity reaches sufficient energy to detach the condensate from the pipe walls and drag it as droplets in the gas stream. Eventually, the gas velocity will be sufficient to detach most of the liquid from the pipe walls forming a fully dispersed flow pattern (MT-MT).

Flow regime determination in three-phase flow

Currently, there is no a generalized flow regime map for horizontal three-phase flow. However, several researchers (Malinowski et al. (1975), Stapelberg & Mewes (1990a,b), Pan (1996), Khor (1998), among others) have suggested using two-phase flow maps for estimating three-phase flow regimes. For this purpose, the authors proposed treating the two liquid phases (oil and water) as a single liquid of "volume-averaged" properties.

Treating two liquid phases as a single phase assumes that the liquids form an emulsion, and that the gas and total liquid phases describe the same flow pattern. This assumption is clearly inappropriate when liquids travel separately in the pipe. Gas and oil

may describe a different flow pattern than that exhibited by the hydrocarbon (gas + condensate) and water phases (i.e. stratified wavy – annular or stratified smooth – stratified wavy).

The current work proposes a new method for estimating three-phase (gas-condensate-water) flow patterns in near horizontal pipes exhibiting low liquid loading conditions. The proposed method consists of two steps. The first step determines the flow pattern exhibited by the gas and condensate phases, while the second estimates the flow pattern described by the hydrocarbon (gas + condensate) and aqueous phases.

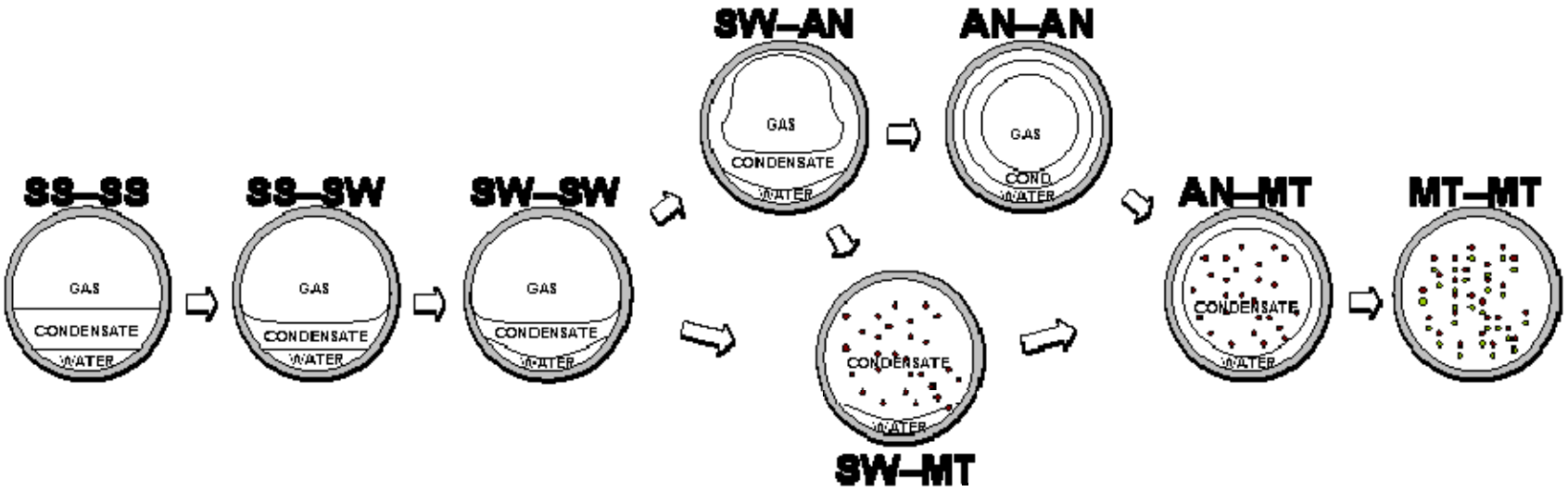

Figure 5.14 Idealized flow regime transitions in three-phase flow

Flow pattern described by the gas and condensate

The present study considers the hydrocarbon and water phases to be virtually immiscible, and recognizes that for all eight flow configurations idealized gas and condensate travel in the pipe as if they were traveling in a separate flow conduit. Figure 5.15 illustrates the flow conduits were gas and condensate travel for the idealized three-phase flow patterns.

The equivalent diameter of hydrocarbon (gas + condensate) flow conduit is proposed to be determined as follows:

$$d_{eq} = \sqrt{(\alpha_g + \alpha_{Lh})}d$$

Gas and condensate holdups in the hydrocarbon flow conduit are estimated by the following expressions:

$$\alpha_{Lh\,eq} = \frac{\alpha_{Lh}}{\alpha_g + \alpha_{Lh}}$$

$$\alpha_{g\,eq} = 1 - \alpha_{Lh\,eq}$$

Once the hydrocarbon flow conduit is characterized, this work identifies the flow regime exhibited by the gas and condensate phases using the unified approach employed for two-phase flow. The properties of the fluids in the hydrocarbon flow conduit are those determined by the thermodynamic model, while the gas and condensate velocities are those reported by the hydrodynamic model.

Flow pattern described by the hydrocarbon and aqueous phases

This work identifies the flow regime described by the hydrocarbon and aqueous phases using the approach proposed for two-phase flow. For this purpose, gas and condensate are treated as a single fluid resembling a “dense gas” phase. This assumption is appropriate given the fact that the system exhibits low condensate loading and the hydrocarbon phases are highly soluble.

The holdup of the dense gas will be equal to the sum of the gas and condensate holdups.

$$\alpha_{dg} = \alpha_{Lh} + \alpha_{g}$$

While the thermodynamic properties of this pseudo-fluid will be determined as follows:

$$\rho_{dg} = \frac{\left(\alpha_{Lh}\rho_{Lh} + \alpha_{g}\rho_{g}\right)}{\alpha_{dg}}$$

$$Mw_{dg} = \frac{\left(LA\ Mw_{Lh} + V\ Mw_{g}\right)}{\left(1 - LB\right)}$$

Once the density and molecular weight of the dense gas are determined, the viscosity can be determined using the Lee et al. (1966) correlation.

In order to satisfy the material balance, the dense gas velocity needs to be defined as:

$$v_{dg} = \frac{\left(\alpha_{Lh}\rho_{Lh}v_{Lh} + \alpha_g \rho_g v_g\right)}{\alpha_{dg}\rho_{dg}}$$

The fluid properties of the aqueous phase are those calculated by the thermodynamic model, while the water velocity is that determined by the hydrodynamic model.

Finally, the three-phase flow pattern is defined as a combination of the flow pattern shown by the hydrocarbon and water phases, and the flow regime described by the gas and condensate phases.

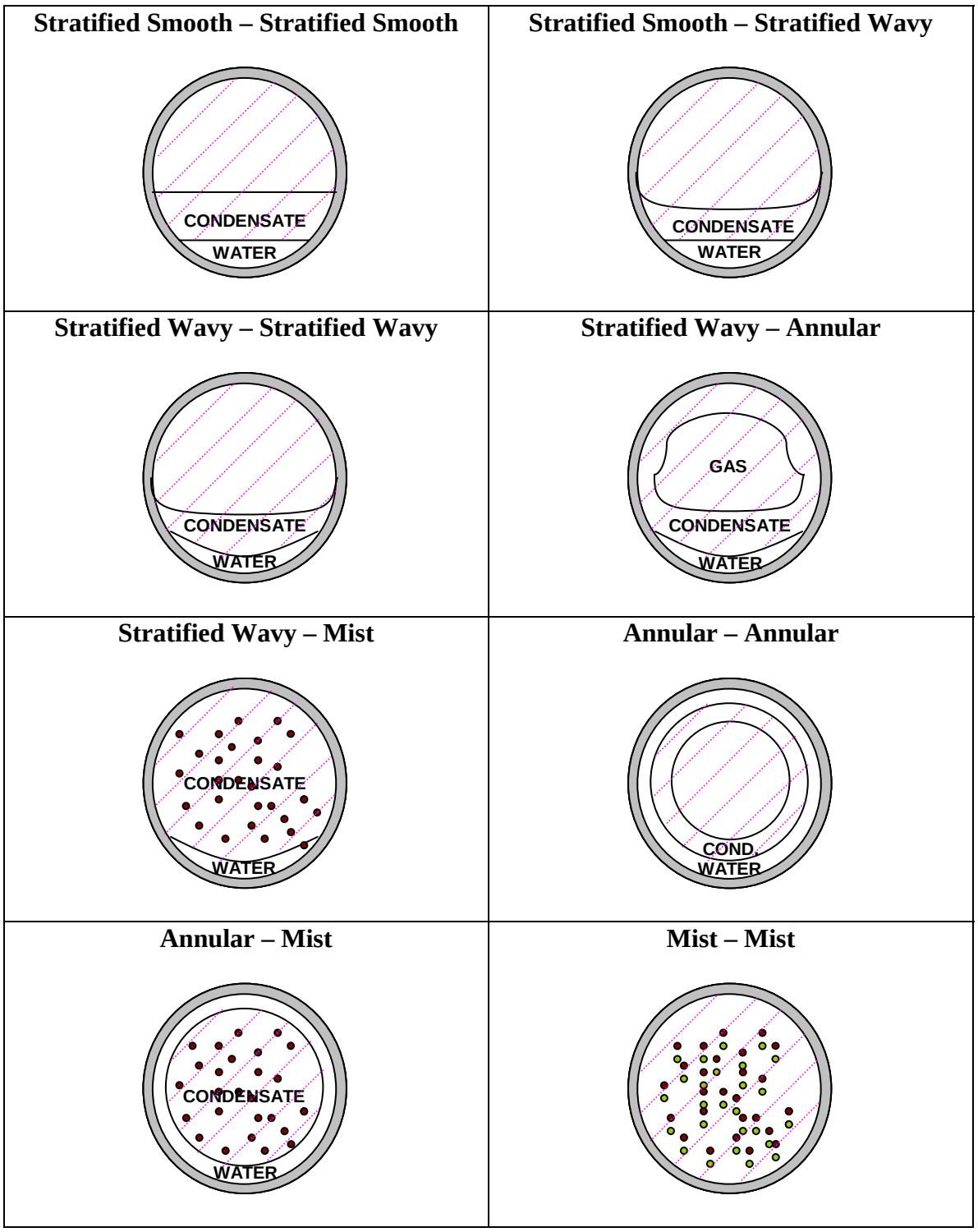

Figure 5.15 Cross-sectional area of the hydrocarbon flow conduit.

CHAPTER 6

CLOSURE RELATIONSHIPS

In hydrodynamic modeling, the expressions for determining the forces acting on the fluids are commonly called closure relationships. Closure relationships include equations for calculating gravitational, frictional, and interfacial forces. Accurate modeling of these forces is fundamental for the appropriate formulation of the momentum equations.

This work uses the guidelines of the two-fluid model (Hughes et al., 1976) for formulating the closure relationships, and includes some adaptations for performing a more accurate description of the problem under study. This chapter describes the closure models used for two and three-phase flow in pipes.

All the forces described in this chapter are calculated on a volumetric average basis and their units are expressed in [lbf/ft^3]. That is the form required by the equations of the hydrodynamic model presented in Chapter 3.

6.1 Wall friction forces

Contact between the fluids and the pipe walls cause shear forces. These forces are usually determined using the Fanning equation. Below, this equation is formulated in general terms for a fluid "*a*".

$$F_{wa} = f_{wa} A_{wa} \frac{\rho_a v_a^2}{2 g_c} \tag{6.1}$$

Where:

F_{wa} = Forces between fluid "*a*" and the pipe walls

f_{wa} = Fanning frictional factor

A_{wa} = Pipe surface wetted by fluid "*a*" per unit volume

ρ_a = Density of fluid "*a*"

v_a = Velocity of fluid "*a*"

The Fanning equation requires determining the pipe surface wetted by a fluid per unit volume (A_{wa}). This quantity is defined as follows:

$$A_{wa} = \frac{Pipe\ surface\ wetted\ by\ \ fluid\ "a"}{Total\ volume} \qquad (6.2)$$

The pipe surface wetted by a fluid is calculated from the flow patterns' geometry. The geometrical considerations for each flow regime are discussed in detail in section 6.4.

The concept of hydraulic diameter is commonly used for estimating pressure losses through non-circular conduits. This concept consists of equaling the frictional pressure losses of a non-circular conduit to the losses of an "equivalent" circular conduit of diameter d_{ha} (Wilkes, 1999).

The Fanning friction factor (f_{wa}) is a function of conduit roughness and Reynolds number of a fluid (Re_a). The Reynolds number is expressed in terms of the hydraulic diameter (d_{ha}) as:

$$\mathrm{Re}_a = \frac{\rho_a v_a d_{ha}}{\mu_a} \tag{6.3}$$

Where:

d_{ha} = Equivalent hydraulic diameter of fluid "*a*"

μ_a = Viscosity of fluid "*a*"

The hydraulic diameter concept allows estimating friction factors using the typical relationships employed for single phase flow through circular conduits. For a circular pipe, hydraulic diameter can be expressed as:

$$d_{ha} = 4\frac{Volume\ of\ \ fluid\ "a"}{Pipe\ surface\ wetted\ by\ \ fluid\ "a"} \tag{6.4}$$

The Fanning friction factor is determined using different expressions for laminar and turbulent flow. For laminar flow ($\mathrm{Re}_a < 2300$), this factor is approximated using the following analytical expression:

$$f_{wa} = \frac{16}{\mathrm{Re}_a} \tag{6.5}$$

While for turbulent flow ($\mathrm{Re}_a > 2300$), the Fanning friction factor is estimated using the Colebrook (1939) correlation. This correlation is widely used in the oil & gas

industry because it provides excellent results for estimating pressure losses in gas and liquid pipelines. Equation 6.6 shows the empirical correlation proposed by Colebrook:

$$\frac{1}{\sqrt{f_{wa}}} = -2.0\log\left[\frac{(\varepsilon/d_{ha})}{3.7} + \frac{2.51}{\mathrm{Re}_a\sqrt{f_{wa}}}\right] \tag{6.6}$$

This correlation is a non-linear equation that must be solved using an iterative numerical method. This work uses the bisection method for this purpose.

6.2 Interfacial Forces

Contact between fluids flowing in a pipe cause shear forces. These forces are calculated using a Fanning-type equation. This Fanning-type equation is expressed in terms of the relative velocity between fluids $(v_a - v_b)$. This relative velocity is typically referred to as slip velocity. In general terms, the Fanning equation for interfacial forces between fluids "*a*" and "*b*" can be expressed as follows:

$$F_{ia-b} = f_{ia-b}A_{a-b}\frac{\rho_a|v_a - v_b|(v_a - v_b)}{2g_c} \tag{6.7}$$

Where:

A_{a-b} represents the total contact surface between fluids "a" and "b" per unit volume. This quantity is defined as:

$$A_{a-b} = \frac{Total\ contact\ surface\ between\ \ fluids\ a\ and\ b}{Total\ volume} \tag{6.8}$$

The total contact surface between fluids and the interfacial friction factors are calculated from the flow pattern geometry. A complete discussion on their determination is presented in section 6.4.

6.3 Gravitational forces

Gravitational forces are calculated as a function of the pipe inclination, liquid holdup, and density of the fluids. These forces are determined using the following equation:

$$F_{ga} = \alpha_a \rho_a \frac{g}{g_c} Sin\theta \qquad (6.9)$$

Where:

$\alpha_a =$ Holdup of fluid "a"

$\theta =$ Inclination angle of the pipe

Equation 6.9 does not contain any geometry-dependent coefficients. Therefore, its application is independent of the flow configuration exhibited by the gas and liquid phases.

6.4 Geometrical definitions and coefficients

6.4.1 Two-phase (gas-liquid) flow

The two-phase flow patterns considered in this study are: stratified smooth, stratified wavy, annular and mist flow. They are the most commonly observed flow

regimes in pipelines exhibiting low liquid-loading. This section presents the calculation of frictional and interfacial coefficients for these flow configurations.

6.4.1.1 Stratified smooth flow

Figure 6.1 illustrates the geometry idealized by Taitel & Dukler (1976) for stratified smooth flow. This geometry exhibits a flat gas-liquid interface.

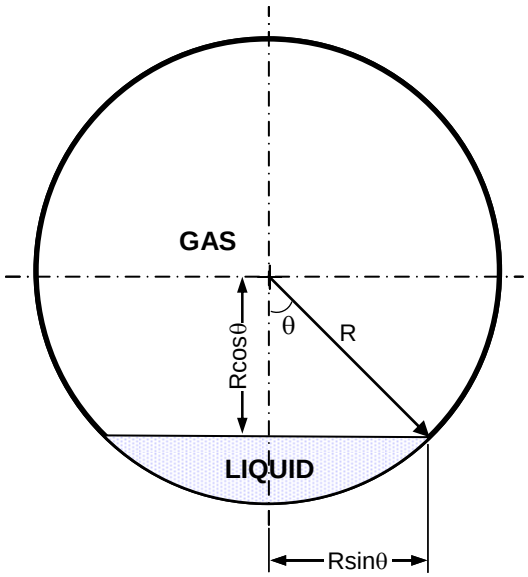

Figure 6.1 Idealized stratified smooth flow pattern

The stratified smooth geometry is completely described by the pipe wetted angle (θ). This angle allows calculating the pipe surface wetted by the fluids, friction factors, and the gas-liquid interface area. The liquid holdup is expressed as a function of the pipe wetted angle as:

$$\alpha_l = \frac{2\theta - \sin 2\theta}{2\pi} \tag{6.10}$$

Equation 6.10 is a non-linear expression that requires a numerical procedure for its solution. This work employs the bisection method for solving this equation.

Wall friction coefficients

Once the pipe wetted angle is obtained, the surfaces wetted by each fluid per unit volume are calculated using basic geometric relationships. These surface areas are given by:

$$A_{wg} = \frac{4(\pi - \theta)}{\pi d} \tag{6.11}$$

$$A_{wl} = \frac{4\theta}{\pi d} \tag{6.12}$$

The hydraulic diameters are evaluated using the approach suggested by Agrawal et al. (1973). Agrawal's approach adds the interfacial surface into the definition of the total pipe wall area wetted by the gas phase. The hydraulic diameters are defined by the next two equations.

$$d_{hg} = \frac{\pi \alpha_g d}{(\pi - \theta + \sin\theta)} \tag{6.13}$$

$$d_{hl} = \frac{\pi \alpha_l d}{\theta} \tag{6.14}$$

Frictional losses are calculated using Colebrook's equation. This empirical correlation requires the Reynolds number and wall roughness of each "equivalent" flow conduit.

The roughness of the "equivalent" liquid conduit is assumed to be equal to that of the pipe. However, that assumption may not be appropriate for the "equivalent" gas conduit.

For stratified flow, Meng et al. (1999) reports liquid deposition in the gas conduit and streamlets draining down the pipe walls. In this flow configuration the gas stream does not have enough energy to drag the liquid along the pipe wall.

Liquid deposition affects the roughness of the "equivalent" gas conduit. However, the conduit roughness has limited impact on the friction factor calculated for stratified smooth flow. Fluid velocities observed for this flow pattern are small (laminar flow), and therefore, in most cases friction factors are almost independent of the conduit roughness. For stratified smooth flow, this study assumes that the roughness of the "equivalent" gas and liquid conduits are equal to that of the pipe wall.

Interfacial coefficients

The interfacial area per unit volume is determined using equation 6.8. The resulting expression for this flow pattern is given by:

$$A_{gl} = \frac{4\sin\theta}{\pi d} \qquad (6.15)$$

The interfacial friction factor is estimated using a correlation proposed by Kowalski (1987). This correlation estimates the interfacial friction factor using an expression similar to that used by Blasius for smooth pipes. Kowalski's correlation is given by:

$$f_{i\,g-l} = 0.96\left(\mathrm{Re}_g^+\right)^{-0.52} \tag{6.16}$$

Where:

$$\mathrm{Re}_g^+ = 1488.16\frac{\alpha_g v_g \rho_g d}{\mu_g} \tag{6.17}$$

6.4.1.2 Stratified wavy flow regime

This work uses the Chen et al. (1997) model for estimating the length of the concave interface exhibited by stratified wavy flow. The Chen et al. model estimates the length of the interface as a portion of a circle eccentric to that of the pipe. The authors refer to their approach as the "double-circle" model. Figure 6.2 illustrates the geometry proposed by Chen's model.

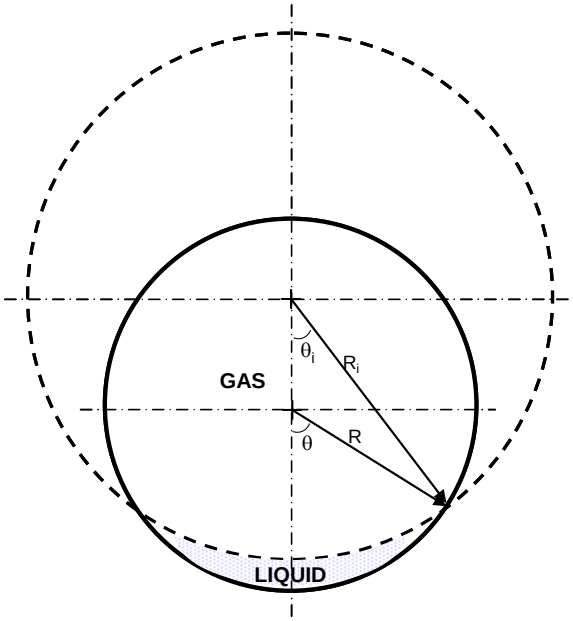

Figure 6.2 Double-circle model (Chen et al., 1997)

The geometrical description of this flow pattern requires two angles "θ" and "θ_i". θ is the pipe wetted angle, while θ_i defines the length of the interface.

As suggested by Meng et al. (1999), this work uses the Grolman & Fortuin correlation for calculating the pipe wall wetted fraction (W_f), and thereby, determining the pipe wetted angle (θ). The correlation proposed by Grolman & Fortuin is expressed as:

$$W_f = 0.624\alpha_l^{0.374} + We_{sl}^{0.25} Fr_g^{0.8} \frac{\rho_g}{(\rho_l - \rho_g) Cos\beta} \tag{6.18}$$

Where:

$$We_{sl} = \frac{\rho_l (\alpha_l v_{sl})^2 d}{\sigma g_c} \tag{6.18a}$$

$$Fr_g = \frac{\left(\alpha_g v_{sg}\right)^2}{\alpha_g^2 gd} \tag{6.18b}$$

$$v_{sg} = \alpha_g v_g \tag{6.18c}$$

$$v_{sl} = \alpha_l v_l \tag{6.18d}$$

The pipe wall fraction (W_f) is related to the pipe wetted angle as:

$$\theta = \pi W_f \tag{6.19}$$

Chen et al. (1997) calculated the interface angle (θ_i) using basic geometric considerations. The resultant is an implicit expression relating liquid holdup (α_l) and pipe wetted angle (θ) to the interface angle (θ_i).

$$\theta_i = \left(\frac{\sin\theta_i}{\sin\theta}\right)^2 \left(\theta + \frac{\sin^2\theta}{\tan\theta_i} - \frac{\sin 2\theta}{2} - \pi\alpha_l\right) \tag{6.20}$$

A numerical method is required for solving this implicit expression. This study uses the bisection method for that purpose.

Wall friction coefficients

The pipe surfaces wetted by the fluids per unit volume are calculated using equation 6.2. The equations derived for this flow regime are the same as those obtained for stratified smooth flow.

$$A_{wg} = \frac{4(\pi - \theta)}{\pi d} \tag{6.21}$$

$$A_{wl} = \frac{4\theta}{\pi d} \tag{6.22}$$

The hydraulic diameters are evaluated using Agrawal's approach (1973). The interfacial area is included as part of the total pipe area wetted by the gas phase. The hydraulic diameters are expressed as follows:

$$d_{hg} = \left(\frac{\pi \alpha_g \sin \theta_i}{(\pi - \theta)\sin \theta_i + \theta_i \sin \theta} \right) d \tag{6.23}$$

$$d_{hl} = \frac{\pi \alpha_l d}{\theta} \tag{6.24}$$

This study considers the roughness of the "equivalent" liquid conduit to be equal to that of the pipe, and suggests that liquid deposition has an effect on the "equivalent" gas conduit roughness. For stratified flow, Meng et al. (1999), Chen et al. (1997) and Sutharshan et al. (1995) reported liquid deposition in the gas conduit. Meng et al. noticed liquid detaching from the gas-liquid interface, droplets depositing in the upper parts of the pipe and rivulets draining down the pipe walls. Jamari (2006) reported that entrainment and liquid deposition mechanisms dominate the stratified-wavy to annular flow transition.

In gas-condensate systems, this study suggests that condensation will also contribute to liquid deposition in the pipe walls. Liquid deposition forms a "rough" surface in the "equivalent" gas conduit that has significant impact on the friction factor.

Existing models for stratified wavy flow do not consider the effect of liquid deposition on the gas conduit roughness. The current study suggests that this roughness is greater than that of the pipe walls, and suggests that it can be related to the density and surface tension of the liquid deposited.

Another effect observed in stratified flow is liquid droplet entrainment in the gas flow. Even though significant droplet entrainment has been reported by several researchers (Meng et al., Chen et al. and Sutharshan et al.) this study does not consider this phenomenon in the model. The stratified wavy flow conditions are far from satisfying Hinze's criteria for diluted or dense dispersions. Therefore, the droplets detached from the liquid will eventually hit the pipe walls or return to the liquid bulk because the gas turbulence is not sufficient to support a stable dispersed flow pattern.

Interfacial coefficients

The interfacial area per unit volume is related to the pipe wetted and interface angles. The expression for the idealized stratified wavy flow pattern is given by:

$$A_{gl} = \frac{4}{d}\left(\frac{\theta_i \sin\theta}{\pi \sin\theta_i}\right) \tag{6.25}$$

The interfacial friction factor is determined by the following correlation proposed by Chen et al. (1997).

$$f_i = \left[1 + 3.17\left(\frac{\alpha_l}{W_f}\right)^{0.20}\left(\left(\frac{\rho_g \rho_l v_l}{\gamma \mu_l (\rho_l - \rho_g) g}\right)^{0.50} - 8.165\right)^{0.08}\right] f_{wg} \qquad (6.26)$$

6.4.1.3 Annular flow

Several researchers in the field treat annular and mist flow as a combined configuration called annular-mist flow (Bendiksen et al. (1991), Issa & Tang (1994), Xiao et al. (1991) and Meng et al. (1999)). This method treats the gas and entrained liquid droplets as a core pseudo-fluid of volumetric averaged properties. For this purpose, these authors assume that gas and entrained liquid travel at the same velocity (no-slip condition) and rely on empirical correlations for estimating the liquid entrainment fraction.

Several liquid entrainment correlations are available in the literature. The most commonly used for modeling horizontal annular flow are those of Wallis (1969), Oliemans et al. (1986), and Ishii & Mishima (1989). Meng et al. (1999) compared some of these correlations against experimental data, and recognized that they provide good estimations for entrainment fractions up to 40% but fail to predict higher entrainment fractions.

Current liquid entrainment correlations are not accurate for the whole spectrum of annular and mist flow conditions. Therefore, this work treats annular and mist flow as separate flow patterns, and considers annular-mist a transitional configuration between these flow patterns.

Transition from annular to mist flow occurs when the turbulent dispersive forces overcome the resistant forces due to surface tension and gravity (Brauner, 2001). The current work argues that limited droplet entrainment will take place before reaching the annular/mist transition threshold. Therefore, the current work does not consider a liquid droplet field in annular flow.

Bendiksen et al. (1991) recognized that neglecting a droplet field in horizontal annular-mist flow could result in large deviations in liquid holdup predictions. When neglecting the droplet field, Bendiksen et al. reported liquid holdup predictions that were higher by a factor of two in extreme cases. However, these extreme cases are those exhibiting high liquid entrainment which this work treats as a different flow pattern (mist flow).

Figure 6.3 illustrates the idealized configuration for annular flow. This configuration considers uniform film thickness distribution, no bubbles entrained in the liquid film and no liquid entrained in the gas core. Therefore, the complete geometrical description of this flow pattern only requires determining the radius to the gas-liquid interface (R_i).

This idealization assumes that all the liquid is in the film flowing along the pipe walls. Therefore, the interface radius can be related to the liquid holdup as:

$$R_i = \left(\sqrt{\alpha_l}\right)\frac{d}{2} \tag{6.27}$$

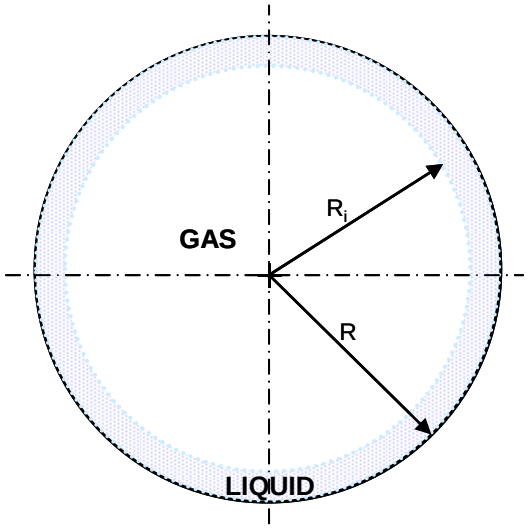

Figure 6.3. Idealized Annular flow configuration

Wall friction coefficients

In this flow configuration there is no contact between the gas and the pipe walls. Therefore, no wall shear forces act on the gas phase. In contrast, the liquid contacts fully the pipe walls and significant shear forces act on this phase.

The surface wetted by the liquid per unit volume is the same as in single phase flow, and is represented by:

$$A_{wl} = \frac{4}{d} \tag{6.28}$$

The liquid hydraulic diameter is determined using equation 6.4 obtaining:

$$d_{hl} = (\alpha_l)d \tag{6.29}$$

The roughness in the equivalent liquid conduit is equal to that of the pipe walls.

Interfacial coefficients

The geometry of annular flow allows expressing the interfacial area per unit volume as:

$$A_{gl} = \left(\sqrt{\alpha_l}\right)\frac{4}{d} \tag{6.30}$$

The current work uses the interfacial friction factor proposed by Meng et al. (1999). Meng et al. suggested approximating the interfacial friction factor to a constant value (f_i=*0.0089*). This value was correlated from experimental data obtained from systems exhibiting low liquid-loading annular flow.

6.4.1.4 Mist flow

Mist flow is idealized as droplets of the same size and shape dispersed in a gas stream. The current work assumes the droplets to be spherical and uses widely accepted stability criteria for estimating their size. Figure 6.4 illustrates this idealized flow structure.

The Weber number is a dimensionless parameter relating inertial and surface forces acting on a single droplet. This dimensionless number is a commonly used parameter for determining stability of a droplet in a gas stream. It is commonly expressed as:

$$We = \frac{2\rho_g \left(v_g - v_l\right)r}{\sigma_l g_c} \tag{6.31}$$

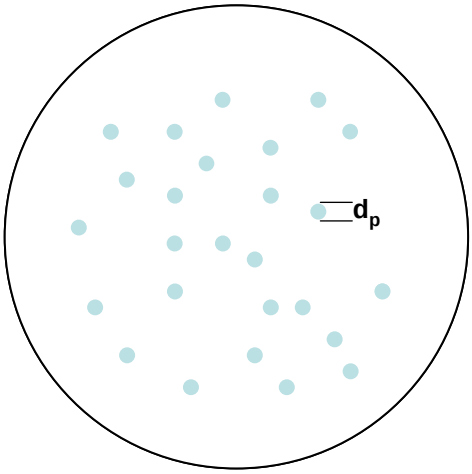

Figure 6.4 Idealized mist flow pattern

The Weber number for the largest droplet size in equilibrium is defined as critical Weber number. For an inviscid fluid, Wallis (1969) suggested that this critical number has a value of approximately 12. Therefore, the maximum droplet diameter for an inviscid fluid could be estimated as:

$$r_{\max}^{inv} = \frac{12\sigma g}{2\rho_g \left(v_g - v_l\right)} \tag{6.32}$$

Hinze (1995) suggested that the Ohnesorge number (*On*) can be related to the droplet stability increase due to viscous effects. Based on this suggestion, Wallis (1969) proposed the following expression for estimating the critical Weber number of viscous fluids:

$$We_{visc} = 12\left(1 + On^{0.72}\right) \tag{6.33}$$

Where:

$$On = \frac{0.000672\,\mu_l}{2\rho_l r_{\max} \sigma_l g_c} \tag{6.34}$$

Determining the Ohnesorge number requires a preliminary estimation for the maximum droplet radius. This preliminary estimation is that of the maximum droplet radius for an inviscid fluid (equation 6.32). Once the critical Weber number is estimated, the maximum droplet size is calculated using the Weber number definition.

$$r_{\max} = \frac{We_{visc}\,\sigma_l\, g}{2\rho_g \left(v_g - v_l\right)} \tag{6.35}$$

The mean droplet radius is related to the maximum droplet radius by means of an expression proposed by Ulke (1984).

$$r_p = 0.06147\, r_{\max} \tag{6.36}$$

Wall friction coefficients

For mist flow, the pipe surface in contact with each fluid is assumed to be proportional to the fluid holdup in the dispersed flow regime. Therefore, the wetted pipe areas per unit volume can be expressed as:

$$A_{wl} = \left(\alpha_l\right)\frac{4}{d} \tag{6.37}$$

$$A_{wg} = \left(\alpha_g\right)\frac{4}{d} \tag{6.38}$$

The hydraulic diameters are calculated using the concept expressed in equation 6.4. The resulting “equivalent” hydraulic diameters are given by:

$$d_{hl} = d \tag{6.39}$$

$$d_{hg} = d \tag{6.40}$$

Interfacial coefficients

The interfacial area per unit volume is equal to the surface area of the droplets entrained in the gas stream divided by the total volume of the fluids. This area is calculated based on basic geometric considerations. The expression for the volumetric interfacial areas is given by:

$$A_{gl} = \frac{3\alpha_l}{r_p} \tag{6.41}$$

As suggested by Ayala (2001), this model treats the dispersed droplets in the gas stream as rigid spheres and uses a correlation proposed by Clift et al. (1978) for estimating the interfacial friction factor. Clift et al. used a critical compilation of experimental data found in the literature for correlating drag coefficients (C_d) over the whole range of Reynolds numbers. His correlation divides the whole range of Reynolds numbers in ten intervals and provides a distinct equation for each one of them. The correlation proposed by Clift et al. is presented in Table 6.1.

Table 6.1 Recommended drag correlations

Range	**Correlation**
Re < 0.01	$C_d = 3/16 + 24/\mathrm{Re}$

$0.01 < \text{Re} \le 20$	$\log_{10}\left\lvert\frac{C_d\,\text{Re}}{24}-1\right\rvert = -0.881 + 0.82w - 0.05w^2$
$20 < \text{Re} \le 260$	$\log_{10}\left\lvert\frac{C_d\,\text{Re}}{24}-1\right\rvert = -0.7133 + 0.6305w$
$260 < \text{Re} \le 1500$	$\log_{10}\lvert C_d\rvert = 1.6435 - 1.1242w + 0.1558w^2$
$1500 < \text{Re} \le 12000$	$\log_{10}\lvert C_d\rvert = -2.4571 + 2.5558w - 0.9295w^2 + 0.1049w^3$
$12000 < \text{Re} \le 44000$	$\log_{10}\lvert C_d\rvert = -1.9198 + 0.6370w - 0.0636w^2$
$44000 < \text{Re} \le 3.38\times10^5$	$\log_{10}\lvert C_d\rvert = -4.3390 + 1.5809w - 0.1546w^2$
$3.38\times10^5 < \text{Re} \le 4.0\times10^5$	$C_d = 29.78 - 5.3w$
$4.0\times10^5 < \text{Re} \le 10^6$	$C_d = -0.49 + 0.1w$
$10^6 < \text{Re}$	$C_d = 0.19 - 8\times10^{-4}/\text{Re}$

The parameters to be employed in this correlation are defined as:

$$\text{Re} = 1488.16\frac{\rho_g\left(2r_p\right)\left(v_g - v_l\right)}{\mu_g} \tag{6.42}$$

$$w = \log_{10}\text{Re} \tag{6.43}$$

For this idealized flow pattern, the drag coefficient is related to the interfacial friction factor as:

$$f_i = \frac{1}{4}C_d \tag{6.44}$$

6.4.2 Three-phase (gas-liquid-liquid) flow

Most studies in the field limit the study of separated three-phase flow patterns to stratified flow exhibiting flat interfaces (Hall (1992), Taitel et al. (1995), Roberts (1996) and Zhang et al. (2005)). The current study proposes a methodology which provides a more detailed description of the flow patterns that may exist in three-phase (gas-condensate-water) flow. This methodology is based on expanding two-phase models and correlations for use in three-phase flow.

The closure relationships for three-phase flow consist of three gravitational forces, three wall shear forces, and three interfacial friction forces. The interfacial forces include: gas-condensate, gas-water and condensate-water friction forces. The calculation of closure relationships follow the guidelines presented in sections 6.1 through 6.3. This section presents the calculation of frictional and interfacial coefficients for eight idealized fully-separated three-phase flow configurations.

6.4.2.1 Stratified smooth – stratified smooth flow (SS-SS)

This flow pattern is idealized having flat interfaces between the fluids. Figure 6.5 illustrates this flat-interface model.

The geometrical considerations presented in this work follow the general guidelines discussed by Taitel et al. (1995). The current work assumes that water is accumulated at the bottom of the pipe, while condensate flows on top of the water. This

flow configuration requires defining two wetting angles. As shown in Figure 6.5, ϕ_1 represents the angle wetted by the water, while ϕ_2 is the angle wetted by the liquids.

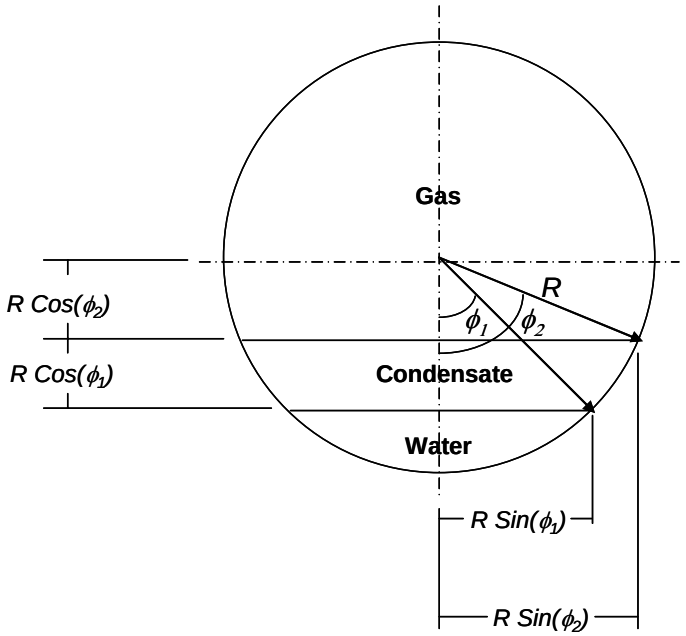

Figure 6.5 Stratified smooth idealized flow structure

Expressions for the area occupied by the water phase and the liquid phases are derived from the geometry presented in Figure 6.5. These expressions assume a strictly flat interface between fluids.

$$A_{Lw} = \phi_1 R^2 - \frac{R^2 Sin(2\phi_1)}{2} \tag{6.45}$$

$$A_{Lw} + A_{Lh} = \phi_2 R^2 - \frac{R^2 Sin(2\phi_2)}{2} \tag{6.46}$$

Equations 6.47 and 6.48 relate the water holdup (α_{Lw}) and total liquid holdup ($\alpha_{Lw} + \alpha_{Lh}$) to the wetting angles (ϕ_1, ϕ_2).

$$\alpha_{Lw} = \frac{A_{Lw}}{A_{pipe}} = \frac{2\phi_1 - Sin(2\phi_1)}{2\pi} \tag{6.47}$$

$$\alpha_{Lw} + \alpha_{Lh} = \frac{A_{Lh} + A_{Lw}}{A_{pipe}} = \frac{2\phi_2 - Sin(2\phi_2)}{2\pi} \tag{6.48}$$

The expression for condensate holdup (α_{Lh}) is derived from the previous equations.

$$\alpha_{Lh} = \frac{A_{Lh}}{A_{pipe}} = \frac{2(\phi_1 + \phi_2) - (Sin(2\phi_1) + Sin(2\phi_2))}{2\pi} \tag{6.49}$$

$$\alpha_g = 1 - \alpha_{Lh} - \alpha_{Lw} \tag{6.50}$$

Equations 6.47 and 6.49 are non-linear expressions that require a numerical method for their solution. This work uses the bisection method for that purpose.

Equations 6.47, 6.49, and 6.50 fully describe the geometry of the system. They allow calculating the pipe surface wetted by the fluids and the interfacial surface areas. Equations 6.51 through 6.53 describe the pipe surface wetted by the fluids, while equations 6.54 and 6.55 represent the interfacial surface areas.

$$S_{Lw} = 2\phi_1 R\Delta x \tag{6.51}$$

$$S_{Lh} = 2(\phi_2 - \phi_1)R\Delta x \tag{6.52}$$

$$S_g = 2(\pi - \phi_2)R\Delta x \tag{6.53}$$

$$S_{iLw-Lh} = 2RSin(\phi_1)\Delta x \tag{6.54}$$

$$S_{ig-Lh} = 2RSin(\phi_2)\Delta x \tag{6.55}$$

Wall shear force coefficients

The Fanning equation requires determining the pipe surface wetted by each phase per unit volume. The concept of these areas is presented in equation 6.2. Based on basic geometrical considerations, these areas are expressed as:

$$A_{Wg} = \frac{2(\pi - \phi_2)R\Delta x}{\pi R^2 \Delta x} = \frac{4(\pi - \phi_2)}{\pi d} \tag{6.56}$$

$$A_{WLh} = \frac{2(\phi_2 - \phi_1)R\Delta x}{\pi R^2 \Delta x} = \frac{4(\phi_2 - \phi_1)}{\pi d} \tag{6.57}$$

$$A_{WLw} = \frac{2\phi_1 R\Delta x}{\pi R^2 \Delta x} = \frac{4\phi_1}{\pi d} \tag{6.58}$$

The hydraulic diameters are obtained using the definition presented by equation 6.4. The results obtained for the three-phases are expressed as:

$$d_{hg} = \frac{4\frac{\pi d^2}{4}\alpha_g \Delta x}{(S_g + S_{ig-Lh})} = \frac{\pi d \alpha_g}{(\pi - \phi_2 + Sin(\phi_2))} \tag{6.59}$$

$$d_{hLh} = \frac{4\frac{\pi d^2}{4}\alpha_{Lh} \Delta x}{(S_{Lh} + S_{iLw-Lh})} = \frac{\pi d \alpha_{Lh}}{(\phi_2 - \phi_1 + Sin(\phi_1))} \tag{6.60}$$

$$d_{hLw} = \frac{4\frac{\pi d^2}{4}\alpha_{Lw} \Delta x}{S_{Lw}} = \frac{\pi d \alpha_{Lw}}{\phi_1} \tag{6.61}$$

As suggested by Taitel & Dukler (1976), the definition of the gas hydraulic diameter includes the gas-condensate interface as part of the pipe surface wetted by the gas. This work proposes an analogous treatment for the condensate phase, where the water-condensate interface is included as part of the pipe surface wetted by the condensate. The definition of the hydraulic diameter of the water phase does not include the interfacial area between liquids.

Stratified smooth flow is idealized as if the fluids moving in the pipe were traveling through non-circular conduits. Therefore, the definition of hydraulic diameter provides the means for extrapolating the use of single-phase frictional loss equations in circular conduits for multiphase flow.

Interfacial coefficients

The interface areas per unit volume are calculated using the guidelines presented in section 6.2. The interfacial areas are determined using equations 6.54 and 6.55.

$$A_{g-Lh} = \frac{S_{ig-Lh}}{\pi R^2 \Delta x} = \frac{4Sin(\phi_1)}{\pi d} \tag{6.62}$$

$$A_{Lw-Lh} = \frac{S_{iLw-Lh}}{\pi R^2 \Delta x} = \frac{4Sin(\phi_2)}{\pi d} \tag{6.63}$$

$$A_{g-Lw} = 0 \tag{6.64}$$

Interfacial forces require estimating an interfacial friction factor. The literature presents several models and correlations for gas-liquid interfacial friction factors. Among these studies are the works of Kowalski (1987), Andratsios and Hanraty (1987), and

Baker et al. (1988). This study uses a correlation proposed by Kowalski for estimating the gas-condensate interfacial friction factor. Kowalski's Blasius-type correlation is expressed as:

$$f_{i\,g-Lh} = 0.96\left(\mathrm{Re}_g^{+}\right)^{-0.52} \tag{6.16}$$

Where:

$$\mathrm{Re}_g^{+} = \frac{\alpha_g v_g \rho_g d}{\mu_g} \tag{6.17}$$

Limited information is available for determining the water-condensate interfacial friction factor. This study assumes a constant value for the water-condensate interfacial friction factor ($f_{i\,Lw-Lh} = 0.0142$). This value was suggested by Taitel et al. (1995). These authors extrapolated this value from the work of Cheremisinoff & Davis (1979), which correlated frictional losses using experimental data obtained by Miya et al. (1971). The estimation of this frictional factor will require further development when more experimental data becomes available.

6.4.2.2 Stratified smooth – stratified wavy flow (SS-SW)

This flow pattern is idealized as exhibiting a smooth and flat water-condensate interface and a rough and concave gas-condensate interface. Figure 6.6 illustrates the geometry of this flow configuration.

As shown in Figure 6.6, the geometrical description of this flow configuration requires determining the pipe angle wetted by the liquids (ϕ_l), the gas-liquid interfacial

angle (ϕ_{1i}) and the pipe angle wetted by the water (ϕ_2). ϕ_{1i} defines the portion of an imaginary circle eccentric to that of the pipe that approximates the concave shape of the gas-condensate interface.

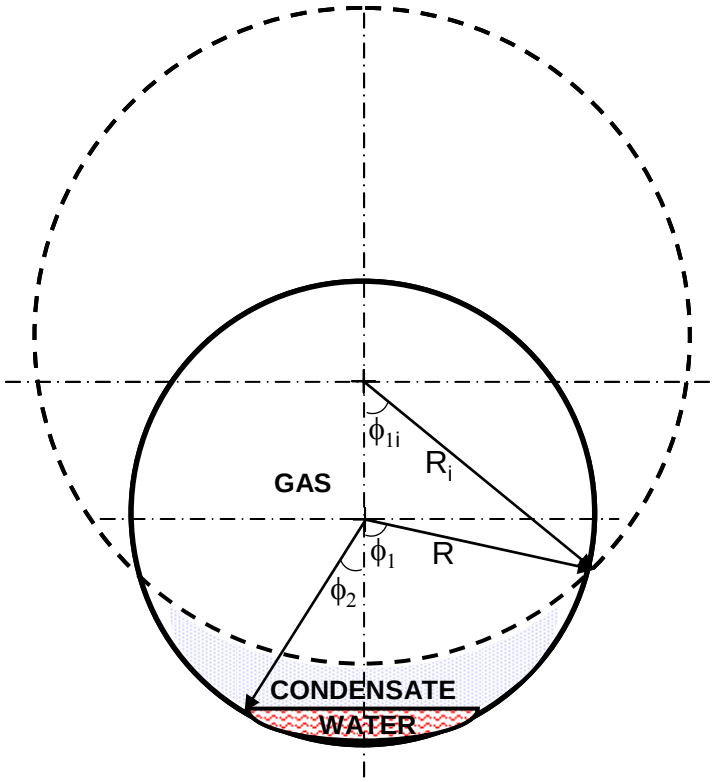

Figure 6.6 Idealized SS-SW flow structure

Given that the water-condensate interface is assumed to be flat, the pipe angle wetted by water (ϕ_2) can be calculated using the same equation derived for SS-SS flow.

$$\alpha_{Lw} = \frac{A_{Lw}}{A_{pipe}} = \frac{2\phi_2 - Sin(2\phi_2)}{2\pi} \tag{6.65}$$

The current work proposes calculating the pipe wetted angle (ϕ_1) and the gas-liquid interfacial angle (ϕ_{1i}) using the Chen et al. model. For that purpose, this study

suggests treating condensate and water as a single liquid of "volume-averaged" properties. The volume averaged properties of this pseudo-fluid are defined as:

$$\alpha_l = \alpha_{Lw} + \alpha_{Lh} \tag{6.66}$$

$$\rho_l = \frac{\left(\alpha_{Lw}\rho_{Lw} + \alpha_{Lh}\rho_{Lh}\right)}{\alpha_l} \tag{6.67}$$

$$\sigma_l = \frac{\left(\alpha_{Lw}\sigma_{Lw} + \alpha_{Lh}\sigma_{Lh}\right)}{\alpha_l} \tag{6.68}$$

While the superficial velocity of the liquid mixture is estimated as:

$$v_{sl} = \alpha_{Lw}v_{Lw} + \alpha_{Lh}v_{Lh} \tag{6.69}$$

The wetted fraction of the pipe (W_f) is estimated using the Grolman & Fortuin (1997b) correlation.

$$W_f = 0.624\alpha_l^{0.374} + We_{sl}^{0.25}Fr_g^{0.8}\frac{\rho_g}{\left(\rho_l - \rho_g\right)Cos\beta} \tag{7.6}$$

Where:

$$We_{sl} = \frac{\rho_l\left(\alpha_l v_{sl}\right)^2 d}{\sigma_l\, g_c} \tag{7.6a}$$

$$Fr_g = \frac{\left(\alpha_g v_{sg}\right)^2}{\alpha_g^2 gd} \tag{7.6b}$$

$$v_{sg} = \alpha_g v_g \tag{7.6c}$$

$$v_{sl} = \alpha_l v_l \tag{7.6d}$$

The pipe wall wetted fraction (W_f) is related to the pipe wetted angle as:

$$\phi_1 = \pi W_f \tag{6.19}$$

The gas-liquid interfacial angle (ϕ_{Ii}) is calculated from an expression derived by Chen et al. (1997). This non-linear expression relating liquid holdup (α_l) and pipe wetted angle (ϕ_I) to the gas-liquid interface angle (ϕ_{Ii}) is solved numerically using the bisection method.

$$\phi_{1i} = \left(\frac{\sin\phi_{1i}}{\sin\phi_1}\right)^2 \left(\phi_1 + \frac{\sin^2\phi_1}{\tan\phi_{1i}} - \frac{\sin 2\phi_1}{2} - \pi\alpha_l\right) \tag{6.20}$$

Wall friction coefficients

Based on this flow pattern's geometry, the following expressions were derived for the pipe surfaces wetted by each fluid per unit volume and for hydraulic diameters of each fluid.

$$A_{Wg} = \frac{4(\pi - \phi_1)}{\pi d} \tag{6.70}$$

$$A_{WLh} = \frac{4(\phi_1 - \phi_2)}{\pi d} \tag{6.71}$$

$$A_{WLw} = \frac{4\phi_2}{\pi d} \tag{6.72}$$

$$d_{hg} = \frac{\pi d\,\alpha_g \sin(\phi_{1i})}{((\pi - \phi_1)\sin(\phi_{1i}) + \phi_{1i}\sin(\phi_1))} \tag{6.73}$$

$$d_{hLh} = \frac{\pi d \alpha_{Lh}}{\left(\phi_1 - \phi_2 + Sin\left(\phi_2\right)\right)} \tag{6.74}$$

$$d_{hLw} = \frac{\pi d \alpha_{Lw}}{\phi_2} \tag{6.75}$$

The definition of the gas hydraulic diameter includes the gas-condensate interface as part of the pipe surface wetted by the gas. The condensate hydraulic diameter includes the water-condensate interface as part of the pipe surface wetted by the condensate. The hydraulic diameter of the water phase does not include the interfacial area between liquids.

Wall shear friction factors are calculated using Colebrook's correlation. The roughness of the "equivalent" water and condensate conduits are assumed to be equal to that of the pipe. Nevertheless, the roughness of the "equivalent" gas conduit may be increased in order to account for liquid deposition in the pipe walls.

Interfacial coefficients

The interface areas per unit volume are calculated using the guidelines presented in section 6.2. The resulting expressions for this flow configuration are expressed as:

$$A_{g-Lh} = \frac{4\phi_{1i} \sin\left(\phi_1\right)}{\pi d \sin\left(\phi_{1i}\right)} \tag{6.76}$$

$$A_{Lw-Lh} = \frac{4Sin\left(\phi_2\right)}{\pi d} \tag{6.77}$$

$$A_{g-Lw} = 0 \tag{6.78}$$

Kowalski's correlation (equation 6.16) was employed for calculating the gas-condensate interfacial friction factor, while the value suggested by Taitel et al. (1995) is used as the water-condensate interfacial friction factor ($f_{i\,Lw-Lh} = 0.0142$).

6.4.2.3 Stratified wavy – stratified wavy flow (SW-SW)

This type of flow shows two rough and concave interfaces. As suggested by Chen et al. the shape of these interfaces is approximated as portions of imaginary circles eccentric to that of the pipe. Figure 6.7 illustrates the idealized geometry for this flow configuration.

Four angles describe the geometry of this flow configuration. These angles define: the pipe portion wetted by the liquids (ϕ_1), the pipe portion wetted by the water (ϕ_2), the gas-liquid interface (ϕ_{1i}) and the condensate-water interface (ϕ_{2i}).

The pipe angle wetted by the liquids (ϕ_1) and the gas-liquid interfacial angle (ϕ_{1i}) are calculated using the same approach described for SS-SW flow. That approach treats condensate and water as a single liquid of "volume-averaged" properties, estimates the pipe wetted fraction with the Grolman & Fortuin correlation (equation 7.6), and solves for the pipe wetted angle and gas-liquid interface angle using Chen et al. model (Equations 6.19 and 6.20).

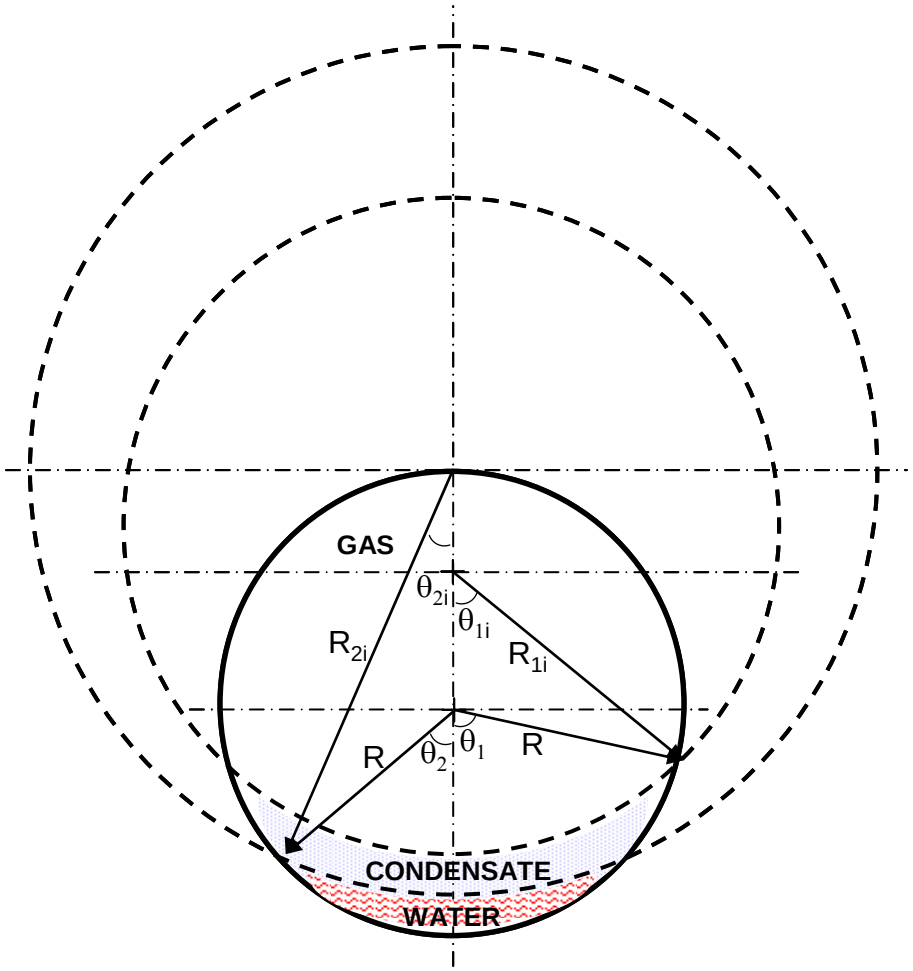

Figure 6.7 Idealized SW-SW flow structure

The current work also estimates the angle wetted by the water (ϕ_2) and the water-condensate interfacial angle (ϕ_{2i}) using the Chen et al. model. However, in this case the proposed method treats gas and condensate as a dense gas phase exhibiting "averaged" properties. The properties of this dense gas are defined as:

$$\alpha_{dg} = \alpha_g + \alpha_{Lh} \tag{6.79}$$

$$\rho_{dg} = \frac{\left(\alpha_g \rho_g + \alpha_{Lh} \rho_{Lh}\right)}{\alpha_{dg}} \tag{6.80}$$

While the superficial velocity of the dense gas is estimated as:

$$v_{sdg} = \alpha_g v_g + \alpha_{Lh} v_{Lh} \tag{6.81}$$

The wetted fraction of the pipe (W_f) is estimated using the Grolman & Fortuin correlation (equation 7.6), while ϕ_2 and ϕ_{2i} are calculated using Chen et al. model.

Wall friction coefficients

The following expressions for the hydraulic diameters and the pipe surfaces wetted per unit volume are derived from the geometry of this flow configuration:

$$A_{Wg} = \frac{4(\pi - \phi_1)}{\pi d} \tag{6.82}$$

$$A_{WLh} = \frac{4(\phi_1 - \phi_2)}{\pi d} \tag{6.83}$$

$$A_{WLw} = \frac{4\phi_2}{\pi d} \tag{6.84}$$

$$d_{hg} = \frac{\pi d \alpha_g \sin(\phi_{1i})}{((\pi - \phi_1)\sin(\phi_{1i}) + \phi_{1i}\sin(\phi_1))} \tag{6.85}$$

$$d_{hLh} = \frac{\pi d \alpha_{Lh} \sin(\phi_{2i})}{((\phi_1 - \phi_2)\sin(\phi_{2i}) + \phi_{2i}\sin(\phi_2))} \tag{6.86}$$

$$d_{hLw} = \frac{\pi d \alpha_{Lw}}{\phi_2} \tag{6.87}$$

These equations are similar to those derived for SS-SW flow. The only difference can be found in the definition of the condensate hydraulic diameter. This is due to the concave nature of the condensate-water interface.

As in SS-SW flow, wall shear friction factors are calculated using Colebrook's correlation. The roughness of the "equivalent" conduits for liquids is assumed to be equal to that of the pipe. While, the roughness of the "equivalent" gas conduit may be increased to account for liquid deposition in the pipe walls.

Interfacial coefficients

The following expressions for interfacial areas were derived from the geometry of this flow configuration:

$$A_{g-Lh} = \frac{4\phi_{1i}\sin(\phi_1)}{\pi d \sin(\phi_{1i})} \tag{6.76}$$

$$A_{Lw-Lh} = \frac{4\phi_{2i}\sin(\phi_2)}{\pi d \sin(\phi_{2i})} \tag{6.77}$$

$$A_{g-Lw} = 0 \tag{6.78}$$

As for interfacial friction factors, Kowalski's correlation (equation 6.16) is employed for the gas-condensate interface, while the value suggested by Taitel et al. (1995) is used as the water-condensate interfacial friction factor ($f_{i\,Lw-Lh} = 0.0142$).

6.4.2.4 Stratified wavy – annular flow (SW-AN)

Figure 6.8 illustrates the geometry idealized for this flow configuration. This flow pattern exhibits a rough and concave condensate-water interface, which is approximated as a portion of an imaginary circle eccentric to that of the pipe using the guidelines presented by Chen et al. (1997). The gas-condensate interface is described as a combination of two geometrical forms. The upper part is idealized as semi-circle concentric to the pipe, while the bottom part is assumed to be parallel to the condensate – water interface.

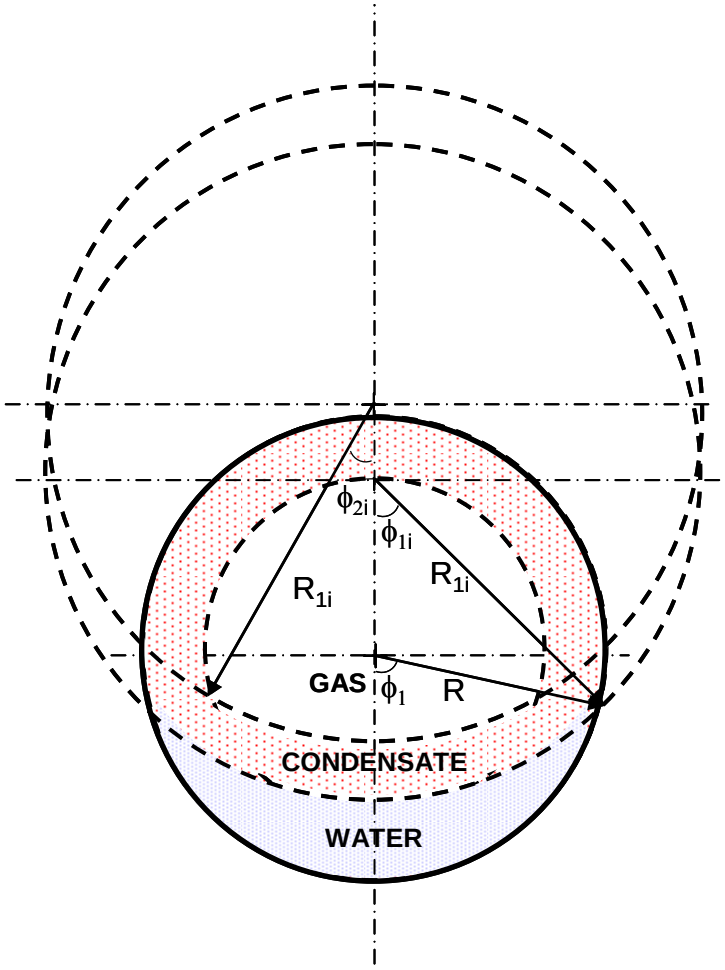

Figure 6.8 Idealized SW-AN flow structure

The condensate film attached to the pipe wall and water above is assumed to have constant thickness. It is assumed that the geometrical forms describing the upper and bottom part of the gas-condensate interface intersect at the same angle of the pipe wetted by the water phase (ϕ_1). Therefore, the liquid film thickness can be related to the gas-condensate interface angle (ϕ_{2t}). The bottom part of the gas-condensate interface is assumed to have the same curvature of the condensate-water interface. Therefore, the radii of the eccentric imaginary circles describing these interfaces are the same.

Three angles are required for fully describing this geometrical configuration. These angles describe: the pipe wetted by the water (ϕ_1), the condensate-water interface (ϕ_{1t}) and the gas-condensate interface (ϕ_{2t}).

The Chen et al. model is used for estimating the angle wetted by the water (ϕ_1) and the water-condensate interfacial angle (ϕ_{1i}). For this purpose, the gas and condensate are treated as a single fluid (dense gas) exhibiting “averaged” properties. The properties of this pseudo-fluid are defined as:

$$\alpha_{dg} = \alpha_g + \alpha_{Lh} \tag{6.79}$$

$$\rho_{dg} = \frac{\left(\alpha_g \rho_g + \alpha_{Lh} \rho_{Lh}\right)}{\alpha_{dg}} \tag{6.80}$$

While its superficial velocity is given by:

$$v_{sdg} = \alpha_g v_g + \alpha_{Lh} v_{Lh} \tag{6.81}$$

As in SW-SW flow, the Grolman & Fortuin correlation (equation 7.6) is used to estimate the pipe fraction wetted by the water. ϕ_1 is calculated from equation 6.19 and ϕ_{1i} from equation 6.20.

From the geometry of the problem, the current study derived an expression relating gas holdup (α_g) to the gas-condensate interfacial angle (ϕ_{2i}). This expression is written as:

$$\alpha_g = \left(\frac{1}{\pi}\right)\left[\left(\frac{\sin\phi_{2i}}{\sin\phi_{1i}}\right)^2\left(\pi - \phi_1 + \frac{\sin 2\phi_1}{2}\right) + \left(\frac{\sin\phi_1}{\sin\phi_{1i}}\right)^2\left(\phi_{2i} - \frac{\sin 2\phi_{2i}}{2}\right)\right] \tag{6.82}$$

Wall friction coefficients

In this flow configuration, the gas does not come in contact with the pipe wall. Therefore, this study only defined expressions for the hydraulic diameters and pipe surfaces wetted by the water and condensate per unit volume. These equations are written as:

$$A_{WLh} = \frac{4(\pi - \phi_1)}{\pi d} \tag{6.83}$$

$$A_{WLw} = \frac{4\phi_1}{\pi d} \tag{6.84}$$

$$d_{hLh} = \frac{\pi d \alpha_{Lh} \sin(\phi_{1i})}{((\pi - \phi_1)\sin(\phi_{1i}) + \phi_{1i}\sin(\phi_1))} \tag{6.86}$$

$$d_{hLw} = \frac{\pi d \alpha_{Lw}}{\phi_1} \tag{6.87}$$

As indicated before, the wall shear friction factors are calculated using Colebrook's correlation. The roughness of the "equivalent" conduits is assumed to be equal to that of the pipe wall.

Interfacial coefficients

The following expressions for interfacial areas were derived from the geometry of this flow configuration:

$$A_{g-Lh} = \left(\frac{4}{\pi d}\right)\left[(\pi - \phi_1)\left(\frac{\sin\phi_{2i}}{\sin\phi_{1i}}\right) + \phi_{2i}\left(\frac{\sin\phi_1}{\sin\phi_{1i}}\right)\right] \tag{6.76}$$

$$A_{Lw-Lh} = \frac{4\phi_{1i}\sin(\phi_1)}{\pi d \sin(\phi_{1i})} \tag{6.77}$$

$$A_{g-Lw} = 0 \tag{6.78}$$

The current study uses the constant value suggested by Meng et al. ($f_{i\,g-Lh} = 0.0089$) as the gas-condensate interfacial friction factor. As for the condensate-water interfacial friction factor, this study uses the value suggested by Taitel et al. ($f_{i\,Lw-Lh} = 0.0142$).

6.4.2.5 Stratified wavy – mist flow (SW-MT)

In this flow configuration condensate droplets travel entrained in the gas stream, while water travels stratified at the bottom of the pipe. Figure 6.9 illustrates this flow configuration.

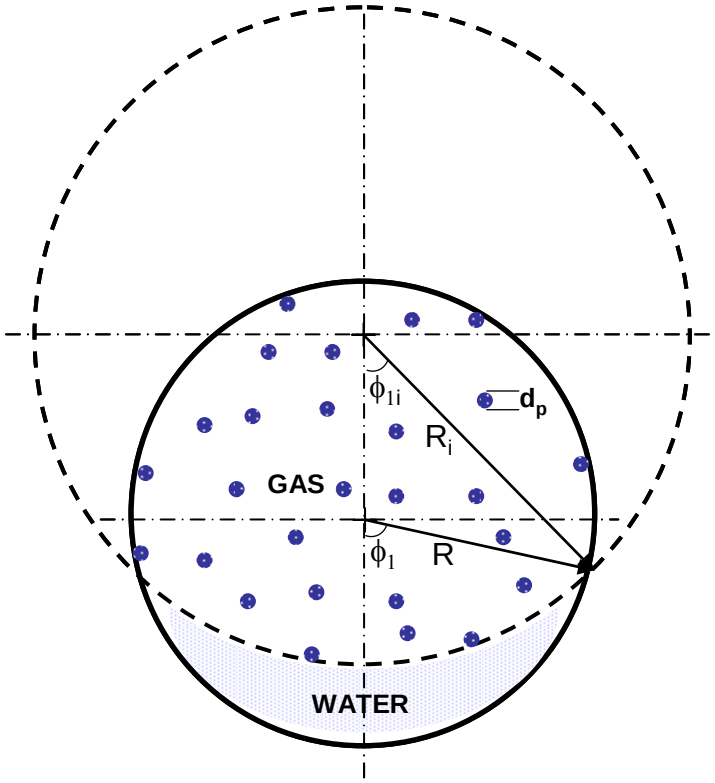

Figure 6.9 Idealized stratified wavy – mist flow configuration

The water exhibits a rough and concave condensate-water interface. As in SW-SW and SW-AN flow, this surface is approximated using the guidelines presented by Chen et al. (1997).

The geometry of this flow configuration is fully described by pipe angle wetted by the water (ϕ_1), the water interface angle (ϕ_{1i}) and condensate mean droplet size (d_p). Condensate droplets contact the water surface and the pipe wall to certain extent.

The angle wetted by the water (ϕ_1) and the water interfacial angle (ϕ_{1i}) are calculated using the same approach described for SW-AN flow. This approach treats gas and entrained condensate as a single fluid (dense gas) exhibiting "averaged" properties (equations 6.79 through 6.81). Then, it employs the Grolman & Fortuin correlation (equation 7.6) for estimating the pipe fraction wetted by water and solves for ϕ_1 and ϕ_{1i} using the Chen et al. model (equations 6.19 and 6.20). The mean condensate droplet diameter (d_p) is estimated using the general guidelines presented for mist flow (section 6.4.1.4).

Wall friction coefficients

Water is assumed to be completely stratified at the bottom of the pipe. Even though limited water entrainment may occur in the gas stream due to liquid deposition, this phenomenon is not considered in this model. Based on this assumption, the pipe surface wetted by the water is approximated by the following expression:

$$A_{WLw} = \frac{4\phi_1}{\pi d} \tag{6.88}$$

While the pipe surface wetted by the gas and condensate is estimated by:

$$A_{W(g+Lh)} = \frac{4(\pi - \phi_1)}{\pi d} \tag{6.89}$$

The current work assumes that the upper part of the pipe is wetted proportionally to the "equivalent" fluid holdup in the dispersed flow regime. The "equivalent" gas and condensate holdups in the upper part of the pipe are defined as:

$$\alpha_g^* = \left(\frac{\alpha_g}{\alpha_g + \alpha_{Lh}} \right) \tag{6.90}$$

$$\alpha_{Lh}^* = \left(\frac{\alpha_{Lh}}{\alpha_g + \alpha_{Lh}} \right) \tag{6.91}$$

Therefore, the following expressions are proposed for the pipe surfaces wetted by the gas and condensate per unit volume:

$$A_{wg} = \frac{4(\pi - \phi_1)}{\pi d} \left(\frac{\alpha_g}{\alpha_g + \alpha_{Lh}} \right) \tag{6.92}$$

$$A_{WLh} = \frac{4(\pi - \phi_1)}{\pi d} \left(\frac{\alpha_{Lh}}{\alpha_g + \alpha_{Lh}} \right) \tag{6.93}$$

As for hydraulic diameters, the following expressions were derived from the geometry shown in Figure 6.9:

$$d_{hLw} = \frac{\pi d \alpha_{Lw}}{\phi_1} \tag{6.94}$$

$$d_{hg} = d_{hLh} = \frac{\pi d (\alpha_g + \alpha_{Lh}) \sin \phi_{1i}}{((\pi - \phi_1) \sin \phi_{1i} + \phi_{1i} \sin \phi_1)} \tag{6.95}$$

The derivation of these expressions included the interfacial areas in the determination of the hydraulic diameters for gas and condensate.

Colebrook's correlation is employed for calculating wall shear friction factors. For this purpose, the roughness of the "equivalent" fluid conduits is assumed to be equal to that of the pipe. This assumption is based on the consideration that limited liquid deposition will occur in the pipe wall because the gas has enough energy to carry liquids along.

Interfacial coefficients

The current work assumes that the water interfacial surface is wetted proportionally to the "equivalent" fluid holdup in the dispersed flow regime. Therefore, the following expressions are proposed for the gas-water and condensate-water interfacial areas:

$$A_{g-Lw} = \frac{4\phi_{1i}\sin(\phi_1)}{\pi d \sin(\phi_{1i})}\left(\frac{\alpha_g}{\alpha_g + \alpha_{Lh}}\right) \tag{6.96}$$

$$A_{Lw-Lh} = \frac{4\phi_{1i}\sin(\phi_1)}{\pi d \sin(\phi_{1i})}\left(\frac{\alpha_{Lh}}{\alpha_g + \alpha_{Lh}}\right) \tag{6.97}$$

The gas-condensate interfacial area per unit volume was determined using the general guidelines presented for mist flow (section 6.4.1.4). The following expression was derived for this interfacial area:

$$A_{g-Lh} = \frac{3\alpha_{Lh}}{r_p} \tag{6.98}$$

As for interfacial friction factors, the Clift et al. correlation (Table 6.1) is employed for determining the droplet drag force coefficients, and thereby, estimating the

gas-condensate interfacial friction factor. The Chen et al. correlation (equation 6.26) is adopted for calculating the gas-water interfacial friction factor, and the constant value suggested by Taitel et al. for stratified flow ($f_{i\,Lw-Lh} = 0.0142$) is assumed for the water-condensate interfacial friction factor.

6.4.2.6 Annular – Annular flow (AN-AN)

For this flow configuration, the literature reports “mixed” liquids and a flow pattern resembling two-phase gas-liquid annular flow (Khor (1998), Pan (1996), Açikgöz et al. (1992)). However, for modeling purposes, this study assumes that the condensate and water phases are immiscible and considers that the three phases travel separately in the pipe.

The idealized configuration proposed in this work exhibits two concentric annular regions where water flows along the pipe wall and condensate in an inner concentric region. Water is considered to be in contact with the pipe walls due to its higher density and surface tension. Figure 6.10 shows this idealized flow configuration.

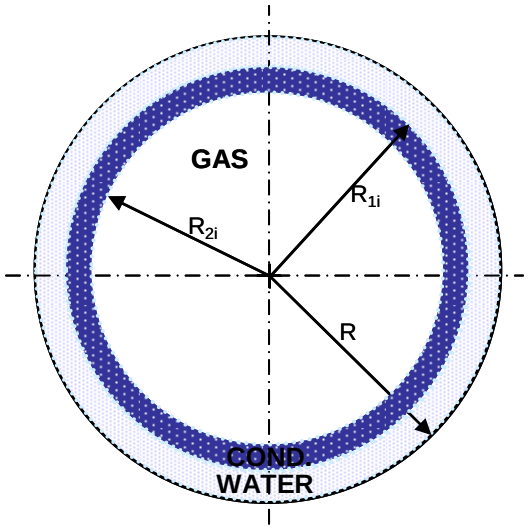

Figure 6.10 Idealized flow structure for annular-annular flow

The thickness of each annular region is considered to be uniform. Therefore, the description of this geometry only requires calculating two radii. These radii identify the condensate-water interface (R_{1i}) and the gas-condensate interface (R_{2i}). From basic geometric considerations, these radii are calculated as:

$$R_{1i} = \sqrt{(\alpha_g + \alpha_{Lh})}R \tag{6.99}$$

$$R_{2i} = \sqrt{\alpha_g}\,R \tag{6.100}$$

Wall friction coefficients

In this idealization, the sole fluid contacting the pipe wall is water. Therefore, the pipe wetted area per unit volume is the same as in single phase flow.

$$A_{wLw} = \frac{4}{d} \tag{6.101}$$

The hydraulic diameter is calculated using the guidelines presented in section 6.2. The resulting diameter for the water in this flow configuration is given by:

$$d_{hLw} = \alpha_{Lw} d \tag{6.102}$$

The wall shear friction factor is estimated by Colebrook's correlation. Water wets the whole pipe; therefore, the roughness of the water conduit is equal to that of the pipe.

Interfacial coefficients

From the geometry described in Figure 6.10, the interfacial areas per unit volume are calculated as:

$$A_{Lh-Lw} = \frac{4}{d}\sqrt{1-\alpha_{Lw}} \tag{6.103}$$

$$A_{g-Lh} = \frac{4}{d}\sqrt{\alpha_g} \tag{6.104}$$

As for interfacial friction factors, the value proposed by Meng et al. is assumed for the gas-liquid interface ($f_{i\,g-Lh} = 0.0089$). No model is available in the literature for calculating the interfacial friction factor between liquids in three-phase annular flow. Therefore, the current work extends the application of the criterion suggested by Taitel et al. (1995) for stratified flow. Taitel et al. suggested approximating the oil-water interfacial friction factor using a constant value ($f_{i\,Lw-Lh} = 0.0142$).

6.4.2.7 Annular – Mist flow (AN-MT)

This idealized flow regime considers that condensate travels dispersed in the gas stream while water flows in the pipe describing an annular pattern. Figure 6.11 illustrates this flow configuration.

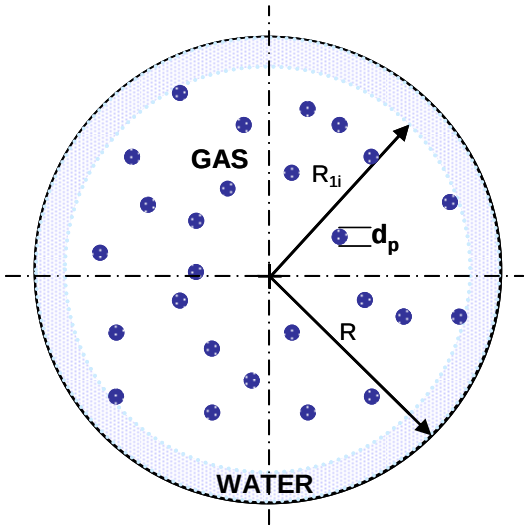

Figure 6.11 Idealized three-phase annular-mist configuration

A uniform thickness is assumed for the annular region. Therefore, the description of the water interface only requires calculating the interface radius (R_{1i}). This radius is calculated from basic geometric considerations as:

$$R_{1i} = \sqrt{(\alpha_g + \alpha_{Lh})}R \qquad (6.105)$$

The mean condensate droplet diameter (d_p) is estimated using the general guidelines presented for mist flow (section 6.4.1.4).

Wall friction coefficients

The sole fluid contacting the pipe wall in this idealization is water. Therefore, it is only required to define wall friction coefficients for this fluid. The pipe wetted area per unit volume is the same as that for single phase flow.

$$A_{wLw} = \frac{4}{d} \tag{6.106}$$

The hydraulic diameter is calculated using the guidelines presented in section 6.2. The resulting diameter for the water in this flow configuration is given by:

$$d_{hLw} = \alpha_{Lw} d \tag{6.107}$$

Even though water entrainment may occur in the gas stream, this phenomenon is not considered in this model. It is assumed that all the water is flowing in an annular fashion along the pipe wall.

Interfacial coefficients

Similarly to SW-AN flow, the current work assumes that the water interfacial surface is wetted proportionally to the "equivalent" fluid holdup in the dispersed flow regime. Therefore, the following expressions are proposed for the gas-water and condensate-water interfacial areas:

$$A_{g-Lw} = \left(\sqrt{1-\alpha_{Lw}}\right)\left(\frac{4}{d}\right)\left(\frac{\alpha_g}{\alpha_g + \alpha_{Lh}}\right) \tag{6.108}$$

$$A_{Lw-Lh} = \left(\sqrt{1-\alpha_{Lw}}\right)\left(\frac{4}{d}\right)\left(\frac{\alpha_{Lh}}{\alpha_g + \alpha_{Lh}}\right) \tag{6.109}$$

The gas-condensate interfacial area per unit volume was determined using the general guidelines presented for mist flow (section 6.4.1.4). The following expression was derived for this interfacial area:

$$A_{g-Lh} = \frac{3\alpha_{Lh}}{r_p} \tag{6.110}$$

As for interfacial friction factors, the Clift et al. correlation (Table 6.1) is employed to determine the droplet drag force coefficients, and thereby, estimate the gas-condensate interfacial friction factor. The value suggested by Meng et al. ($f_{i\,g-Lh} = 0.0089$) is adopted for calculating the gas-water interfacial friction factor, and the constant value suggested by Taitel et al. for stratified flow ($f_{i\,Lw-Lh} = 0.0142$) is assumed for the water-condensate interfacial friction factor.

6.4.2.8 Mist – Mist flow (AN-MT)

In this flow regime the gas turbulence is sufficiently high to drag condensate and water, which travel dispersed in the gas stream. The liquids travel in the gas stream as droplets of different average sizes. Figure 6.12 shows a sketch of this flow configuration.

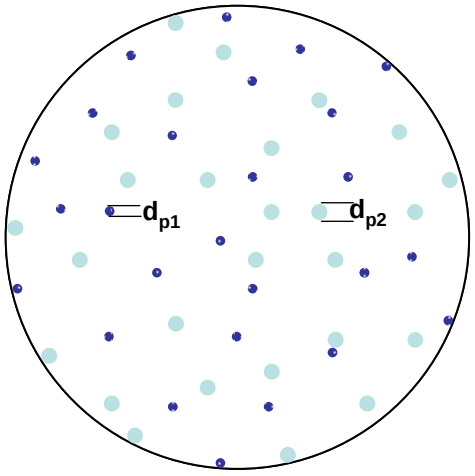

Figure 6.12 Mist-Mist flow structure

The mean droplet diameters for condensate (d_{p1}) and water (d_{p2}) are estimated using the general guidelines presented for mist flow (section *6.4.1.4*). It is important to note that the water droplets are larger than those of condensate which impacts velocity and holdups of the liquids.

Wall friction coefficients

The pipe surface wetted per unit volume is calculated based on the assumption that the pipe wall is wetted proportionally to the fluid holdup in the dispersed flow regime. Therefore, the following expressions are proposed for the pipe surfaces wetted by the gas, condensate and water per unit volume:

$$A_{Wg} = \frac{4\alpha_g}{d} \tag{6.111}$$

$$A_{WLh} = \frac{4\alpha_{Lh}}{d} \tag{6.112}$$

$$A_{WLw} = \frac{4\alpha_{Lw}}{d} \tag{6.113}$$

As for hydraulic diameters, they are derived from the guidelines presented in section 6.2. As shown before, the hydraulic diameters calculated for mist flow are equal to the pipe diameter.

$$d_{hg} = d_{hLh} = d_{hLw} \tag{6.114}$$

The roughness of the "equivalent" fluid conduits is equal to that of the pipe. Liquid deposition in the pipe wall is not likely to occur because the gas can detach and carry liquid droplets dispersed in it.

Interfacial coefficients

The current work predicts limited and random contact between water and condensate droplets traveling in the gas stream. Condensate and water droplets are expected to exhibit similar velocities and low lateral turbulence, as a consequence the contact area and contact frequency between droplets is expected to be small. The interfacial forces caused by these interactions are not considered in the present study. This work assumed no interfacial contact between liquids.

The gas-condensate and gas-water interfacial areas can be expressed as:

$$A_{g-Lh} = \frac{6\alpha_{Lh}}{d_{p1}} \tag{6.115}$$

$$A_{g-Lw} = \frac{6\alpha_{Lw}}{d_{p2}} \tag{6.116}$$

The Clift et al. correlation (Table 6.1) is used for calculating drag force coefficients and interfacial friction factors for water and condensate.

6.5 Transitions in the two-fluid model

The hydrodynamic behavior during flow pattern transitions is one of the most challenging problems still to be addressed in the two-fluid model. Assuming "sudden" flow pattern transitions implies abrupt discontinuities in the force profiles acting on the fluids. These discontinuities lead to wrongful holdup and velocity predictions. Pauchon et al. (1993) indicated that these force discontinuities are not compatible with the averaged nature of the equations of motion and suggested a protocol to avoid them.

As suggested by Ayala (2001), the current work assumes the existence of a transition zone of length '*Lt*' every time flow pattern transition occurs. In this zone, the forces acting on the fluids are considered to be a combination of those exhibited by the initial and ending flow configurations.

The forces in the transition zone are estimated using a weighting function. This function is intended to eliminate abrupt force discontinuities. In this approach, the transitional forces (frictional or interfacial) are calculated as:

$$F_{transition} = \Gamma F_{new} + (1 - \Gamma) F_{old} \qquad (6.117)$$

Γ is a continuous function equal to zero at the beginning of the transition ($x=0$) and to one at the end of the transition interval ($x=Lt$). The nature of this weighting function is still a topic requiring extensive research.

Ayala (2001) suggested that the weighting function (Γ) may be taken as linear, exponential or as hyperbolic tangent. As for Γ, the current study employs a linear function of distance and suggests a transition interval equivalent to 10,000 pipe diameters. Equation 6.118 describes the weighting function used in this study.

$$\Gamma = \frac{x}{Lt} \qquad (6.118)$$

CHAPTER 7

DISCUSSION OF THE RESULTS

Several cases were analyzed for validating and showing the capacity of the one-dimensional compositional model developed. This chapter focuses on comparing the model predictions against field and experimental data obtained from different publications. The case studies analyzed include systems exhibiting two-phase (gas-water and gas-condensate) and three-phase (gas-condensate-water) flow.

7.1 Two-phase (gas-water) flow

Two case studies were selected for analyzing the model performance for systems exhibiting two-phase (gas-water) flow. The first case study compares the model predictions against experimental data obtained by Eaton et al. (1967), while the second presents a numerical experiment for showing the capacity of the model developed.

7.1.1 Eaton et al. two-phase flow experiment

Eaton et al. (1967) performed gas-water flow experiments in high and low liquid loading systems. The focus of their experiments was to develop an empirical pressure drop correlation for two-phase flow in pipelines. Eaton et al. (1967) performed their experiments in a 1700-ft long commercial steel pipe (*2.067" ID*) placed in a horizontal orientation. Their experiments induced two-phase flow by mixing water and natural gas at the pipe inlet. The natural gas used in these experiments was produced from the Tigre

Lagoon field, near Delcambre, LA. The composition of the Tigre Lagoon gas is given in Table 7.1.

Table 7.1 Composition of the Tigre Lagoon natural gas

Component	Mole %
Nitrogen	0.05
Carbon dioxide	0.46
Hydrogen sulfide	0.02
C1	93.00
C2	4.14
C3	1.30
i-C4	0.41
n-C4	0.31
n-C5	0.24
n-C6	0.06
n-C7	0.01

The experiment selected for benchmarking the model mixed *6,179,200 SCFD* of Tigre Lagoon gas with *668.0 BPD* of water at *885.79 psia* and *80 °F*. Then Eaton et al. measured pressure in twelve points along the pipe.

The overall composition and volumetric flow rate of the inlet stream was calculated performing molar and mass balances. The mass flow rate per unit area (G_m) was determined by the following expression:

$$G_m = \frac{\rho_{gsc} Q_{gsc} + 5.615 \rho_{wsc} Q_{wsc}}{A_{pipe}} \tag{7.1}$$

The "G_m" obtained for this piping system was *241.54* lb_m/ft^2-*s*. The overall inlet composition was determined from a molar balance. Table 7.2 shows the resulting inlet

composition. It is interesting to point out that this system contains a high water fraction. The mole fraction of water exceeds *40%*.

Table 7.2 Overall inlet composition

Component	Mole fraction
Nitrogen	0.000299
Carbon dioxide	0.002751
Hydrogen sulfide	0.000120
Water	0.401989
C1	0.556150
C2	0.024758
C3	0.007774
i-C4	0.002452
n-C4	0.001854
n-C5	0.001435
n-C6	0.000359
n-C7	0.000060

The equivalent standard volumetric flow rate entering the system is determined by equation 3.53. This equation relates the mass entering the system and overall molecular weight to the inlet standard volumetric flow rate.

$$G_m = 3.0493 \cdot 10^{-8} \frac{Q_{sc}\, \bar{M}w}{A_{pipe}} \qquad (3.53)$$

The standard volumetric flow rate calculated for this system was *10.339 MMSCFD*. Table 7.3 presents a “data sheet” summarizing all the information required for modeling the system.

Table 7.3 “Data sheet” for Eaton et al. case study

System ID: 2" Eaton et al. system [Mist flow]

Inlet Conditions

Temperature:	***540***	***R***
Pressure:	***885.79***	***psia***
Flow rate:	***10.339***	***MMSCFD***

Gas composition:

Component	zi
Nitrogen	0.000299
Carbon dioxide	0.002751
Hydrogen sulfide	0.000120
Water	0.401989
C1	0.556150
C2	0.024758
C3	0.007774
i-C4	0.002452
n-C4	0.001854
n-C5	0.001435
n-C6	0.000359
n-C7	0.000060

Pipe data

Diameter	***2.067***	***inches***
Abs. Roughness	***0.00041***	***ft***
Terrain Profile	***Horizontal***	

Energy Data

U factor	***10***	***Btu/hr-ft2***
Surr. Temp.	***540***	***R***

The flow pattern estimated by the model (Mist flow) matches that observed by Eaton et al. (1967). The flow pattern detection routine reports that all the liquid is transported as entrained droplets in the gas stream. The identification of the prevailing flow pattern guarantees that the model uses an appropriate closure model.

Figure 7.1 compares the pressure profile calculated with the experimental data presented by Eaton et al. (1967), while Table 7.4 presents the deviation between the calculated and measured values. The results show an excellent match. The pressure profile calculated is within less than *2.0%* of the reported experimental values.

Table 7.4 Deviation between calculated and measured data

Pressure tap location	P_{exp} [psia]	P_{calc} [psia]	Abs. Dev. [%]
50.00	877.53	877.23	0.03
149.80	861.03	859.73	0.15
347.40	823.53	823.70	0.02
548.60	787.13	786.13	0.13
747.00	748.83	746.76	0.28
820.80	734.03	732.50	0.21
867.30	718.13	722.15	0.56
942.30	696.03	707.42	1.64
1142.30	658.13	663.58	0.83
1340.10	615.13	616.71	0.26
1540.40	559.93	566.06	1.10
1639.10	537.13	538.99	0.35

The results obtained show an average absolute deviation (*AAD*) of approximately *0.46%*, and a standard deviation of *0.49%*. In this work, the absolute deviation (*AD*) is calculated as:

$$AD = \left| \frac{P_{\exp} - P_{calc}}{P_{\exp}} \times 100 \right| \qquad (7.2)$$

The hydrodynamic model results show a significant temperature drop along the pipe. This temperature drop is attributed to the Joule-Thomson effect given the fact that the system exhibits a large pressure drop. The calculated temperature profile could not be

compared with experimental data. Eaton et al. did not report a temperature profile in their experiments. Figure 7.2 illustrates the pressure and temperature profiles calculated for this system. The calculated temperature drop along the pipe is approximately *25 °F*.

Figure 7.3 illustrates the liquid holdup profile determined by the hydrodynamic model. The results show liquid holdup declining from *4.3%* at the pipe inlet to *2.5%* at the outlet. The average liquid holdup along the pipe is *3.49%*. The average liquid holdup calculated is in good agreement with the value correlated by Eaton et al. (approximately *4%*).

Figure 7.4 presents the velocity profiles determined by the model. As expected for mist flow, gas and liquid velocity profiles show similar trends. However, the system exhibits significant differences between gas and liquid velocities. The model results show increasing slip velocities. The slip velocity increases from 4 *ft/s* at the pipe inlet to *6.76 ft/s* at the outlet. The average calculated slip velocity is *5.02 ft/s*. Accurate determination of the slip velocity is important for calculating interfacial friction forces.

The reliability of the model was evaluated by calculating a cumulative material balance after each pipe segment analyzed. This material balance is calculated as:

$$MB = \frac{\alpha_g \rho_g v_g + \alpha_l \rho_l v_l}{G_m} \tag{7.3}$$

The results of the cumulative material balance are presented in Figure 7.5. The model exhibits superb behavior. The cumulative material balance is approximately 1.0

along the entire pipe. The maximum deviation observed was less than 10^{-4}. These results prove that the system of equations formulated by the model is accurately solved.

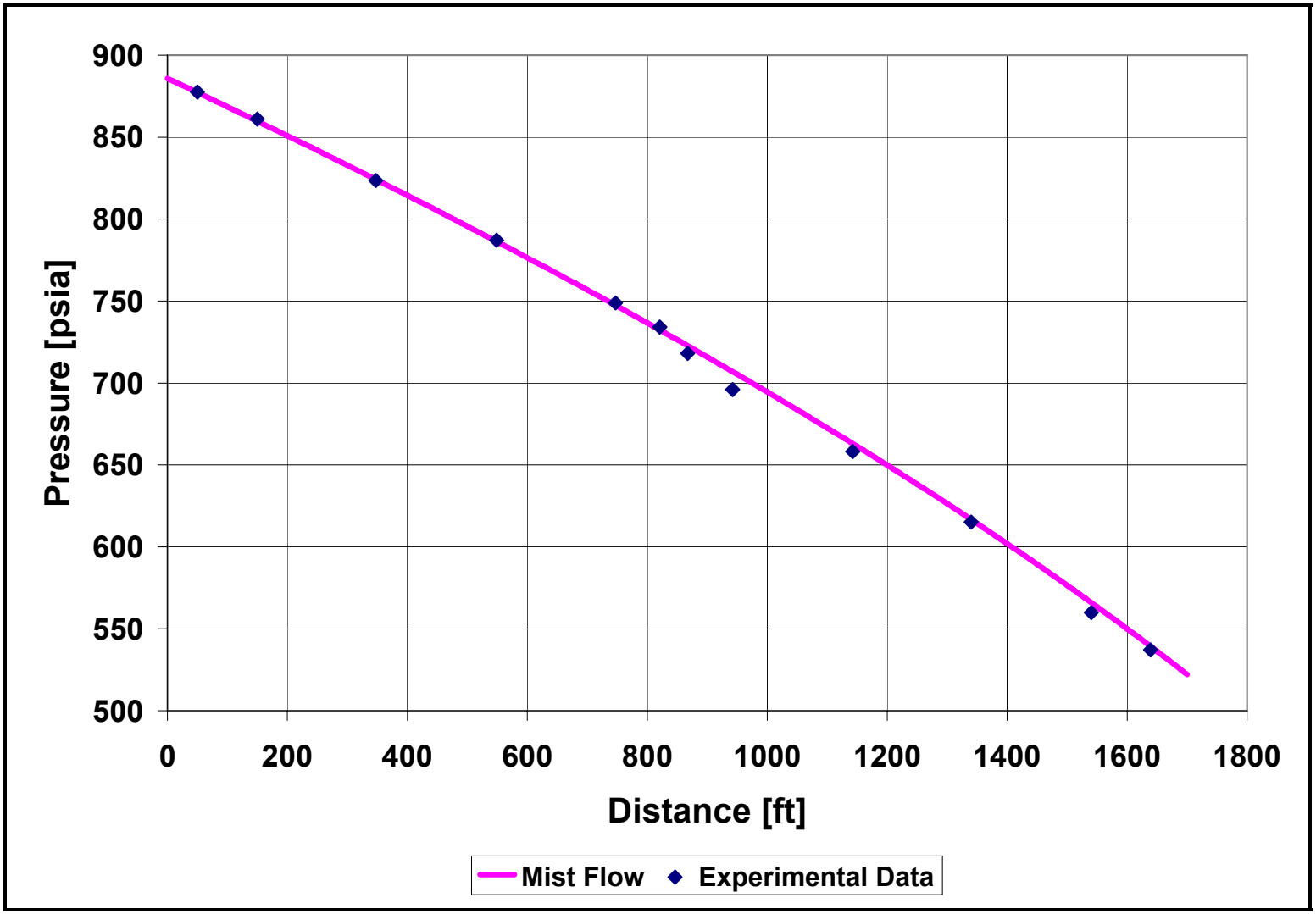

Figure 7.1 Pressure profile calculated vs. experimental data (Eaton et al. experiment)

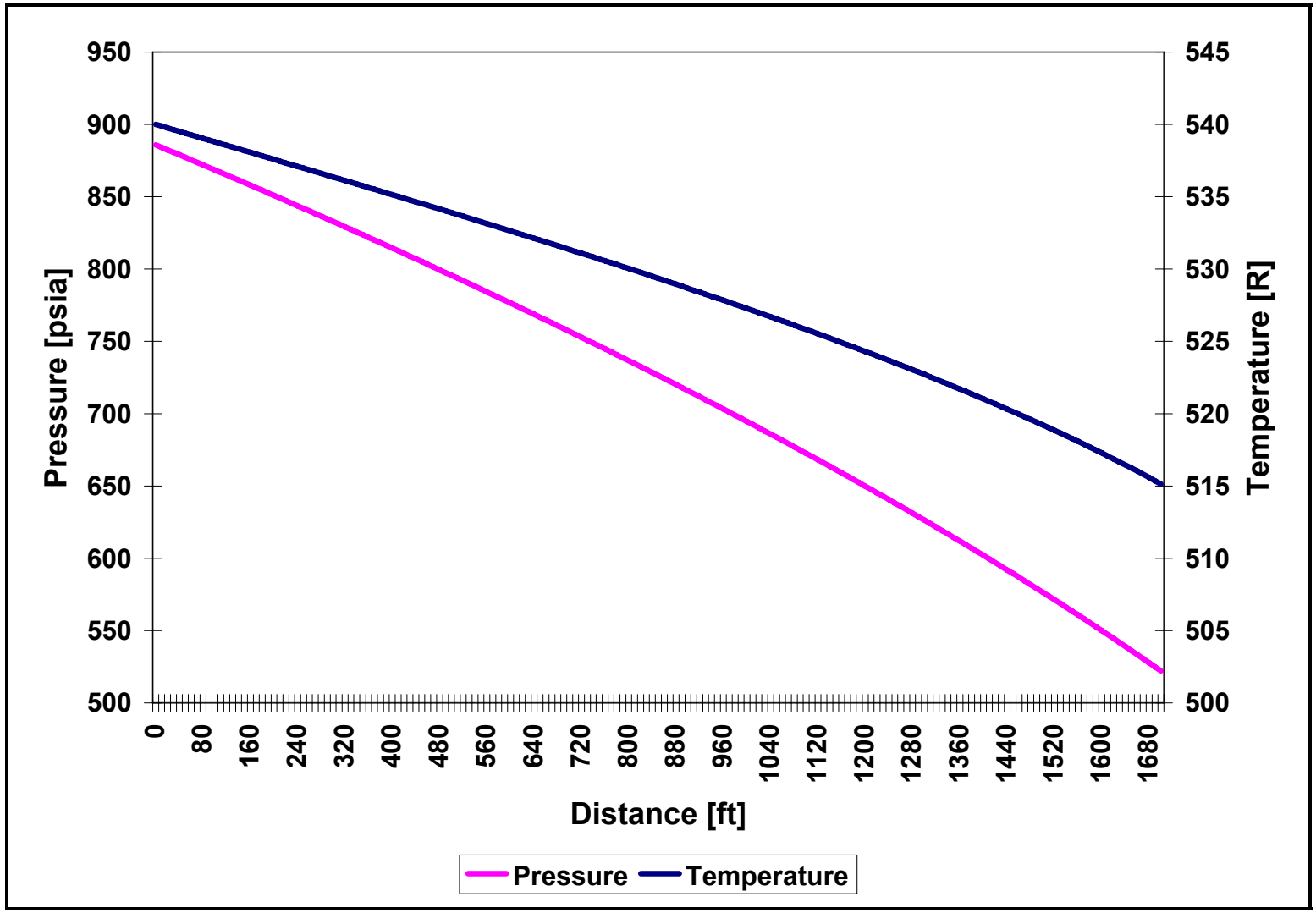

Figure 7.2 Operating conditions of the system (Eaton et al. experiment)

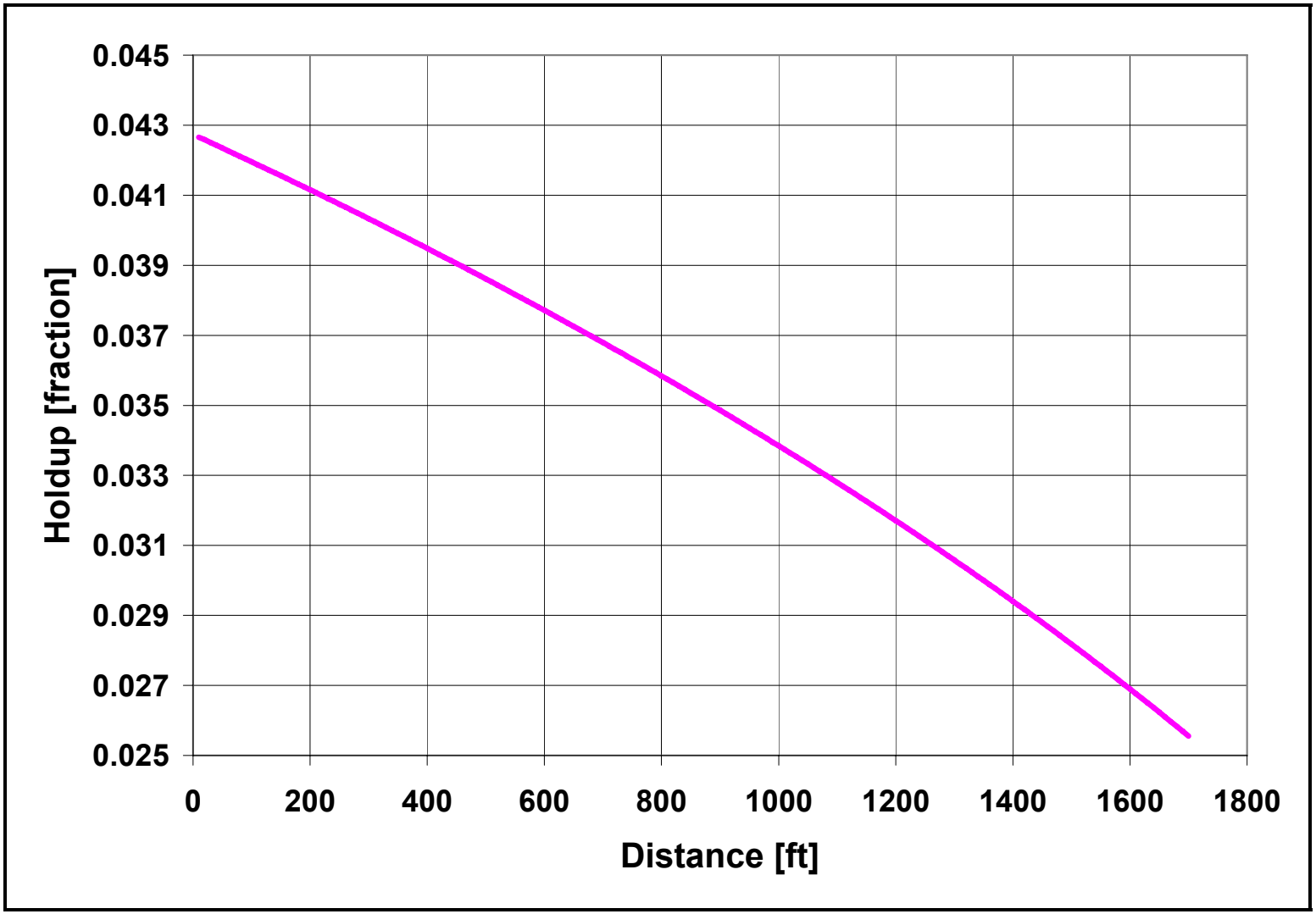

Figure 7.3 Liquid holdup profile (Eaton et al. experiment)

The compositional model developed allows for estimation of the aqueous phase composition being formed. The model has the capacity of estimating the concentration of hydrocarbons, carbon dioxide, hydrogen sulfide, methanol, and other substances dissolved in the aqueous phase. Figures 7.6 through 7.8 show the concentration of methane, carbon dioxide and hydrogen sulfide in the water stream.

Hydrate formation is related to the presence of methane, ethane, propane, butanes and nitrogen in a gas stream, while acid is expected to form when significant amounts of CO_2 or H_2S are present in the aqueous phase. These results provide production engineers with an excellent tool for evaluating the potential formation of hydrates and/or acids in piping systems.

It is known that the gas solubility in water increases as temperature declines and that it decreases as pressure drops. Figures 7.6 through 7.8 present interesting results. They show that even though temperature decreases in the system, the gas concentration in water declines. In this system the pressure drop has a dominant effect on the gas solubility in the water phase.

The compositional model developed was capable of simulating the behavior of gas-water systems. The model does not require assuming, *"a priori"*, the existence of water in the system. It performs phase equilibria calculations for predicting the formation, quantity and composition of liquid phases in equilibrium. These capacities of the model are outstanding tools for flow assurance engineers since they will be able to evaluate the

effectiveness of the hydrate and corrosion inhibition processes. The tool developed will give production engineers great detail about how much hydrate and corrosion inhibitors to inject and where, saving millions of dollars in the design, operation and maintenance of these systems.

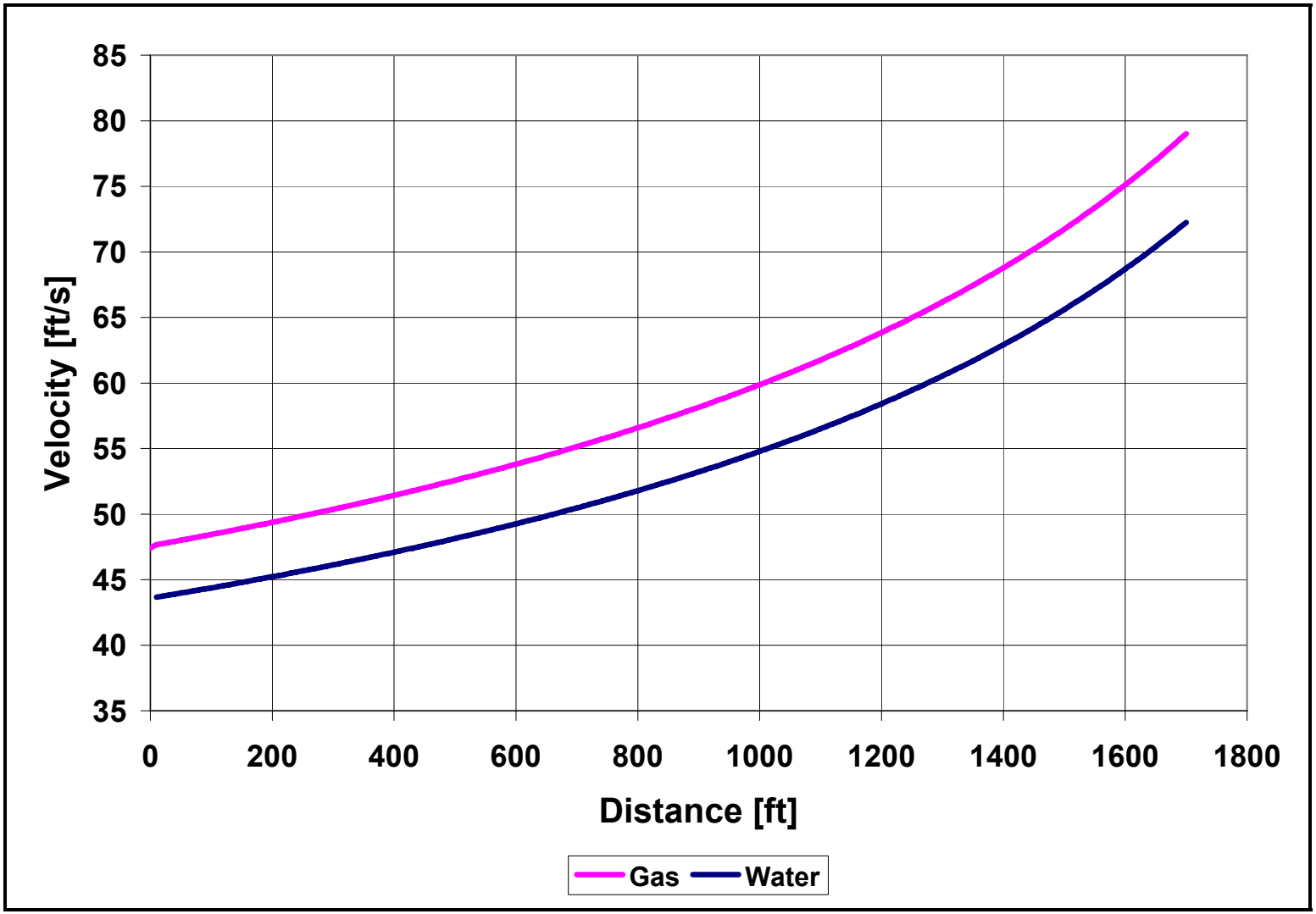

Figure 7.4 Velocity profile (Eaton et al. experiment)

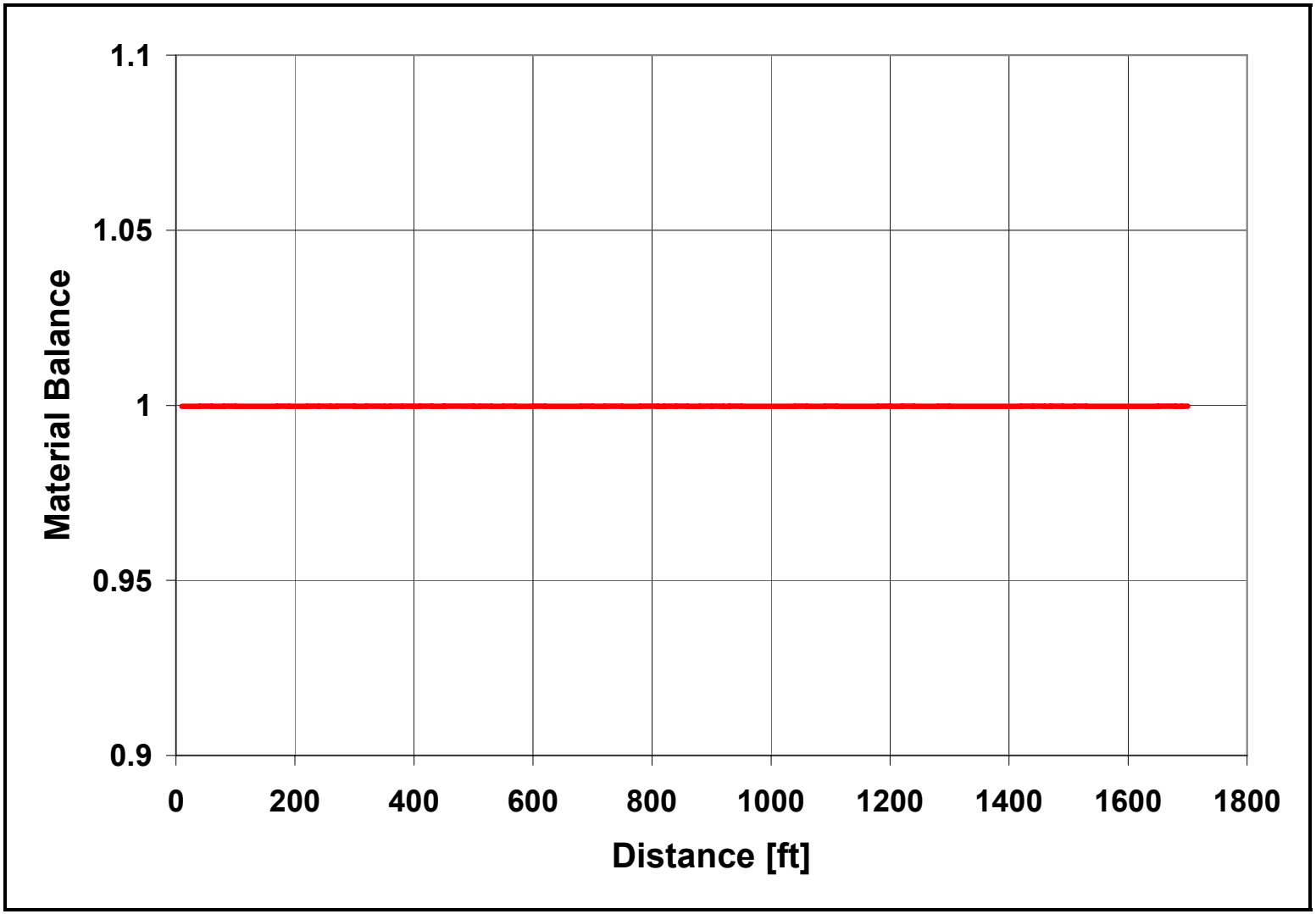

Figure 7.5 Cumulative material balance (Eaton et al. experiment)

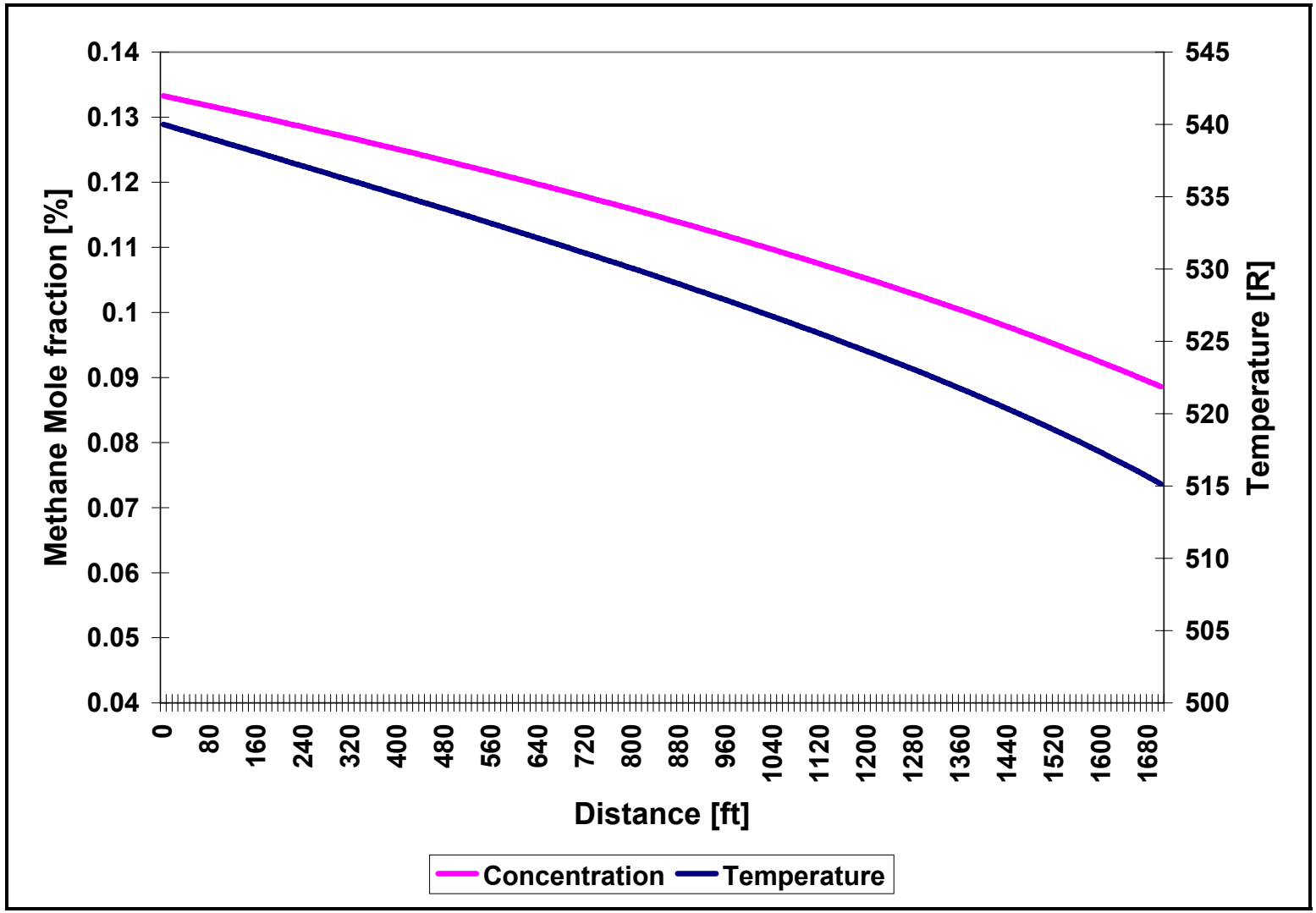

Figure 7.6 Mole fraction of methane in the water phase (Eaton et al. experiment)

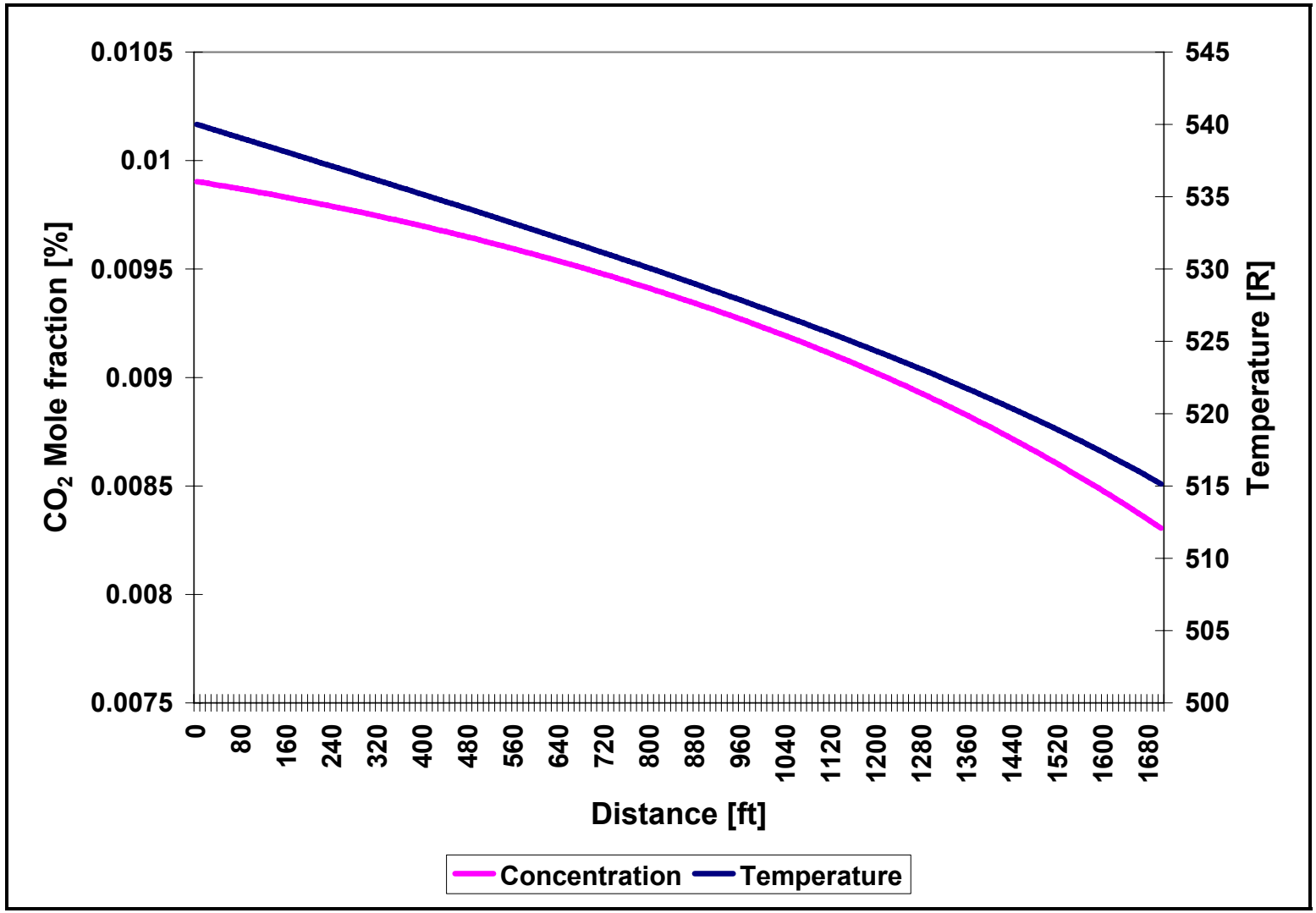

Figure 7.7 Mole fraction of carbon dioxide in the water phase (Eaton et al. experiment)

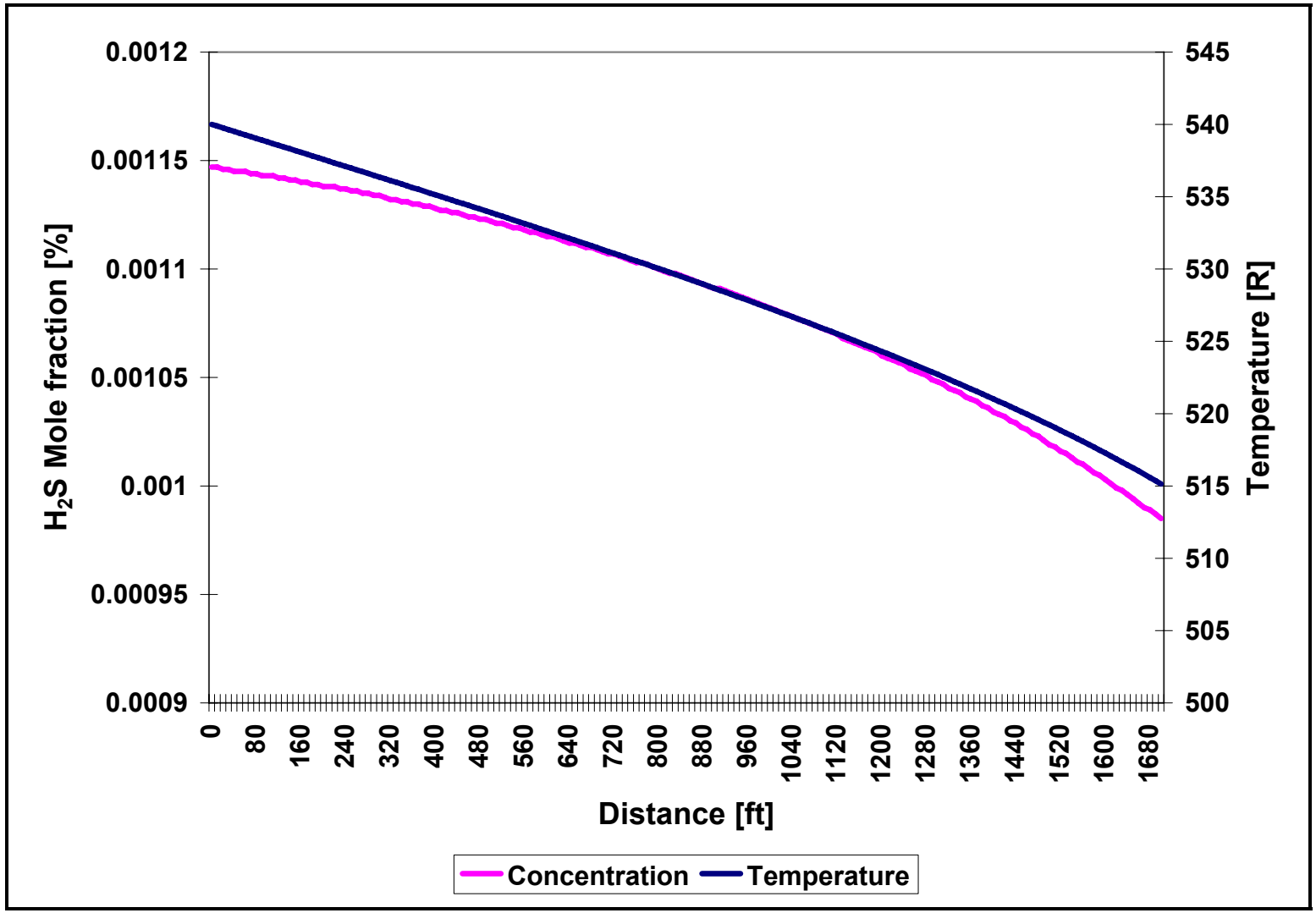

Figure 7.8 Mole fraction of hydrogen sulfide in the water phase (Eaton et al. experiment)

7.1.2 Proposed numerical experiment

Eaton et al. (1967) conducted their experiments with gas compositions containing high water fractions. These high-water compositions are not commonly found in typical transmission systems. Therefore, the current work describes a hypothetical system for showing the capacity for simulating typical transmission operations.

The hypothetical system proposed consists of 7 miles of commercial steel pipeline (*5.461" ID*) placed in an inclined configuration. The inclination is considered uniform and equal to *0.095%* along the entire pipe.

A typical transmission-quality gas is assumed to enter the pipe. The composition of this gas is mainly light hydrocarbons and small fractions of water and CO_2. A hydrate inhibitor (methanol) is added at the pipe inlet in a proportion that would yield *0.2* mole percent in the entering stream. *15 MMSCFD* of this gas are fed into the piping system at *600 psia* and *220 °F*. The temperature surrounding the system is considered to be *60 °F*. Table 7.5 presents the "data sheet" of the proposed hypothetical case. This "data sheet" provides all the information required for modeling this case study.

The objective of this hypothetical case is to illustrate the full capacity of the model. This numerical experiment shows the model's ability to predict the initial water condensation point in the pipeline, determine the composition of the aqueous mixture, and evaluate the effectiveness of a hydrate inhibition process. This numerical experiment also shows the model's capacity for handling transitions between flow patterns.

Table 7.5 “Data sheet” for the proposed numerical experiment

System ID: Proposed numerical experiment

Inlet Conditions

Temperature:	***680***	***R***
Pressure:	***600***	***psia***
Flow rate:	***15***	***MMSCFD***

Gas composition:

Component	zi
Carbon Dioxide	0.020000
Water	0.012000
Methane	0.926000
Ethane	0.020000
Propane	0.015000
n-Butane	0.005000
Methanol	0.002000

Pipe data

Diameter	***5.461***	***inches***
Abs. Roughness	***0.00015***	***ft***
Terrain Profile	***Constant Slope (0.095%)***	

Energy Data

U factor	***1***	***Btu/hr-ft2***
Surr. Temp.	***520***	***R***

Figures 7.9 through 7.12 present the hydrodynamic behavior expected for this system. Figure 7.9 shows the predicted pressure and temperature profiles, and indicates the expected flow pattern in each section of the pipe. This figure shows that the pressure and temperature in the system is expected to decline from *600 psia* and *220 °F* at the pipe inlet to *317.42 psia* and *40.1 °F* at the outlet. The system is expected to show an average pressure drop of *40.35 psi/mile*.

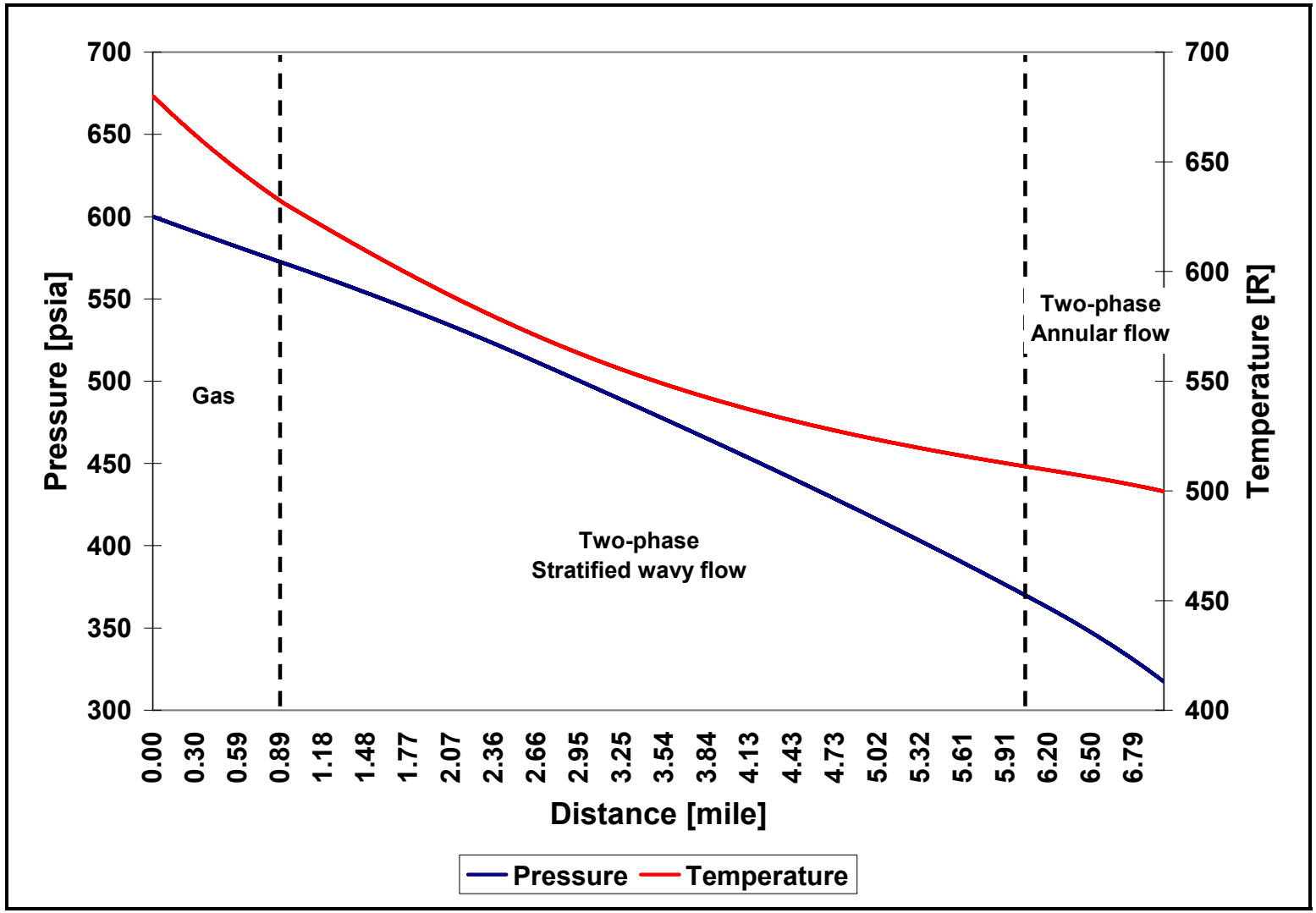

Figure 7.9 Operating conditions (proposed numerical experiment)

The fluid entering the pipe travels as single phase gas until reaching *4880 ft* along the pipe. At that point, water begins to condense and two-phase stratified wavy flow begins to occur. Stratified wavy flow is the prevailing flow pattern until it approaches *32550 ft* along the pipe. At that distance, water wets over eighty percent of the internal pipe surface and the prevailing flow pattern transitions to annular flow. Annular flow prevails until the delivery point of the piping system.

Even though the fluid enters the pipe as single-phase gas, the pipeline is expected to deliver *35.42 BPD* of an aqueous liquid. The liquid produced is expected to contain *11.42%* of methanol in a molar basis, which is equivalent to *19.36%* in a volumetric basis. The density of the liquid delivered is estimated to be *51.3 lbm/ft*^{3}. This information is important to design and operate facilities for treating the produced liquid.

The average pressure drop in the pipe section transporting single-phase gas is approximately *31.16 psi/mile*. As liquid builds up in the pipe, the average pressure losses increase to *39.52 psi/mile* in the pipe section exhibiting stratified wavy flow and to *55.8 psi/mile* in the section exhibiting annular flow. The increasing pressure losses are attributed not only to rising gas velocities but also to liquid building up along the pipe. The occurrence of two-phase flow is known to increase the pressure drop even for systems exhibiting low liquid loading (Hart et al., 1989).

Figure 7.10 shows the expected velocity profiles for this case study. The velocity profile of the gas phase shows the typical behavior expected in transmission operations. Gas velocity declines to a minimum and then drastically increases along the pipe. The changes in gas velocity are related to the variations in gas density along the pipe.

Gas enters the pipe at a velocity of *32.96 ft/s* and reaches a minimum of *31.12 ft/s* after traveling *2.125 miles* along the pipe. After that point, the gas velocity increases almost exponentially until reaching *44.11 ft/s* at the pipe outlet. The gas velocity decline occurs as a consequence of the high temperature drop near the pipe inlet.

Once the dew point is reached, the liquid formed is dramatically accelerated achieving a maximum velocity of *3.99 ft/s* at a point *1.765 miles* along the pipe. After that, liquid velocity declines almost linearly until approaching *2.4 ft/s* at the pipe outlet. Figure 7.10 shows the expected liquid velocity profile.

Figure 7.11 illustrates the expected liquid holdup profile for this system. Liquid holdup increases monotonically along the pipe section exhibiting stratified wavy flow. Liquid holdup presents a “jump” during the flow pattern transition. The “jump” occurs due to the abrupt increase in wall frictional forces. The model assumes that annular flow prevails when the pipe wetted fraction reaches 80%, while the annular flow closure model considers that the whole internal pipe perimeter is wetted by the liquid. Currently, there is no accepted method for modeling flow pattern transitions. It is a topic still requiring extensive experimental investigation.

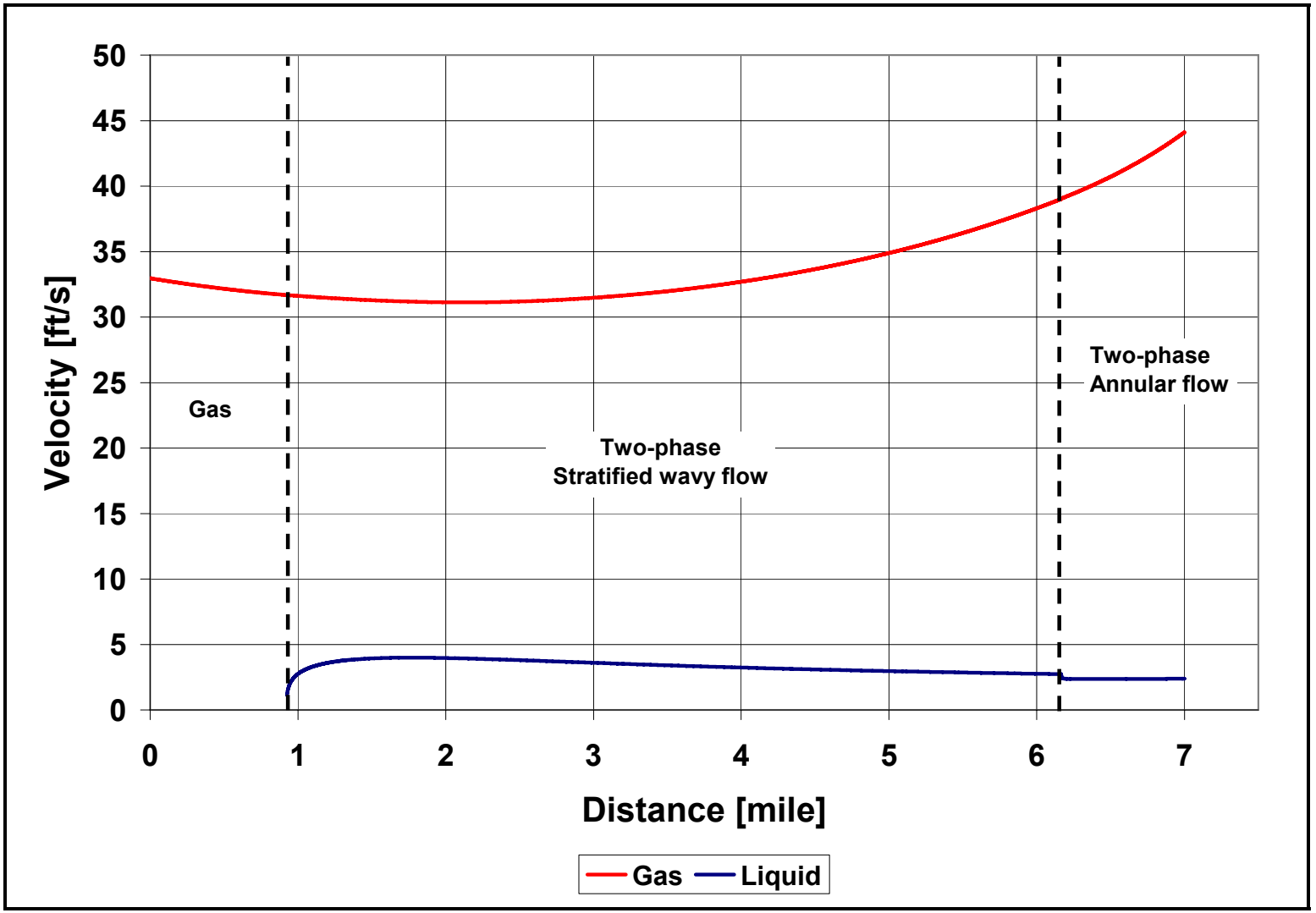

Figure 7.10 Velocity profile (proposed numerical experiment)

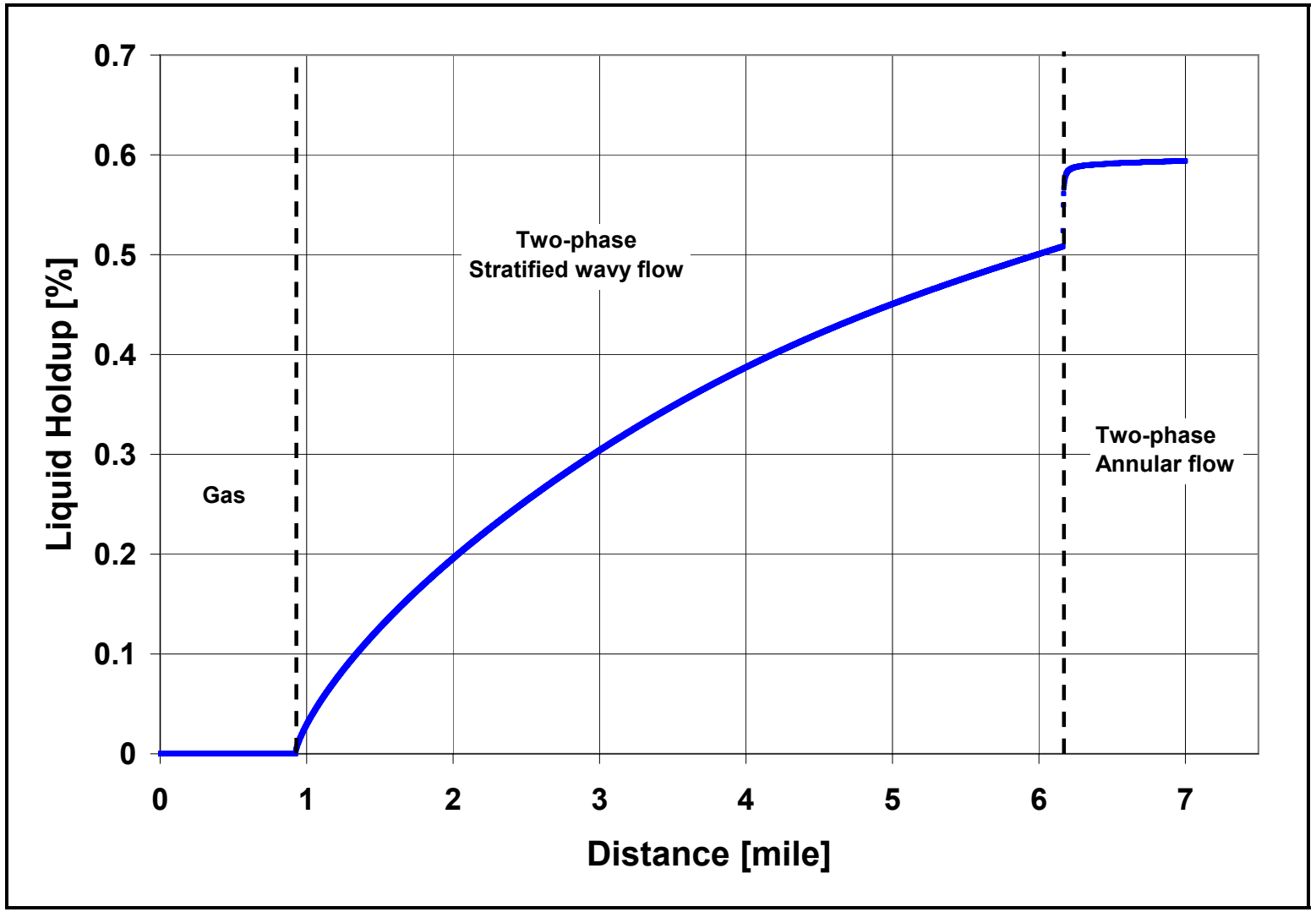

Figure 7.11 Liquid holdup (proposed numerical experiment)

The reliability of the model for handling flow pattern transitions was evaluated by performing the material balance calculations along the pipe. The material balance results are presented in Figure 7.12. The model shows an outstanding behavior for handling transitions from single to two-phase flow and between flow regimes. The cumulative material balance is approximately *1.0* along the entire pipe, with a maximum observed deviation of less than 10^{-4}.

Figures 7.13 through 7.15 show the predicted concentrations of methane, carbon dioxide and methanol in the water stream. Figure 7.13 shows that the methane mole fraction reaches a maximum of *0.126%* in a point located *4.8 miles* from the pipe inlet. The temperature at that point is *66.72 °F*. This graph is a useful tool for identifying the pipe locations having low temperatures and high methane dissolved in the water. These are necessary conditions for hydrate formation and deposition. Figure 7.14 shows mole fraction of CO_2 in the aqueous phase. The results show that the CO_2 concentration in water increases monotonically along the pipe, where its maximum concentration is *0.0477% mole* at the pipe outlet. Figure 7.15 shows the mole fraction of methanol in the aqueous phase. This figure shows an increasing solubility of this substance along the pipe. The maximum methanol concentration (*11.43% mole*) was found at the pipe outlet. This information provides helpful information for evaluating the effectiveness of the hydrate inhibition process along the pipe.

The current numerical experiment demonstrates that the model is capable of predicting water condensation in the pipe, estimating the composition of the aqueous phase, and handling different flow patterns and their transitions.

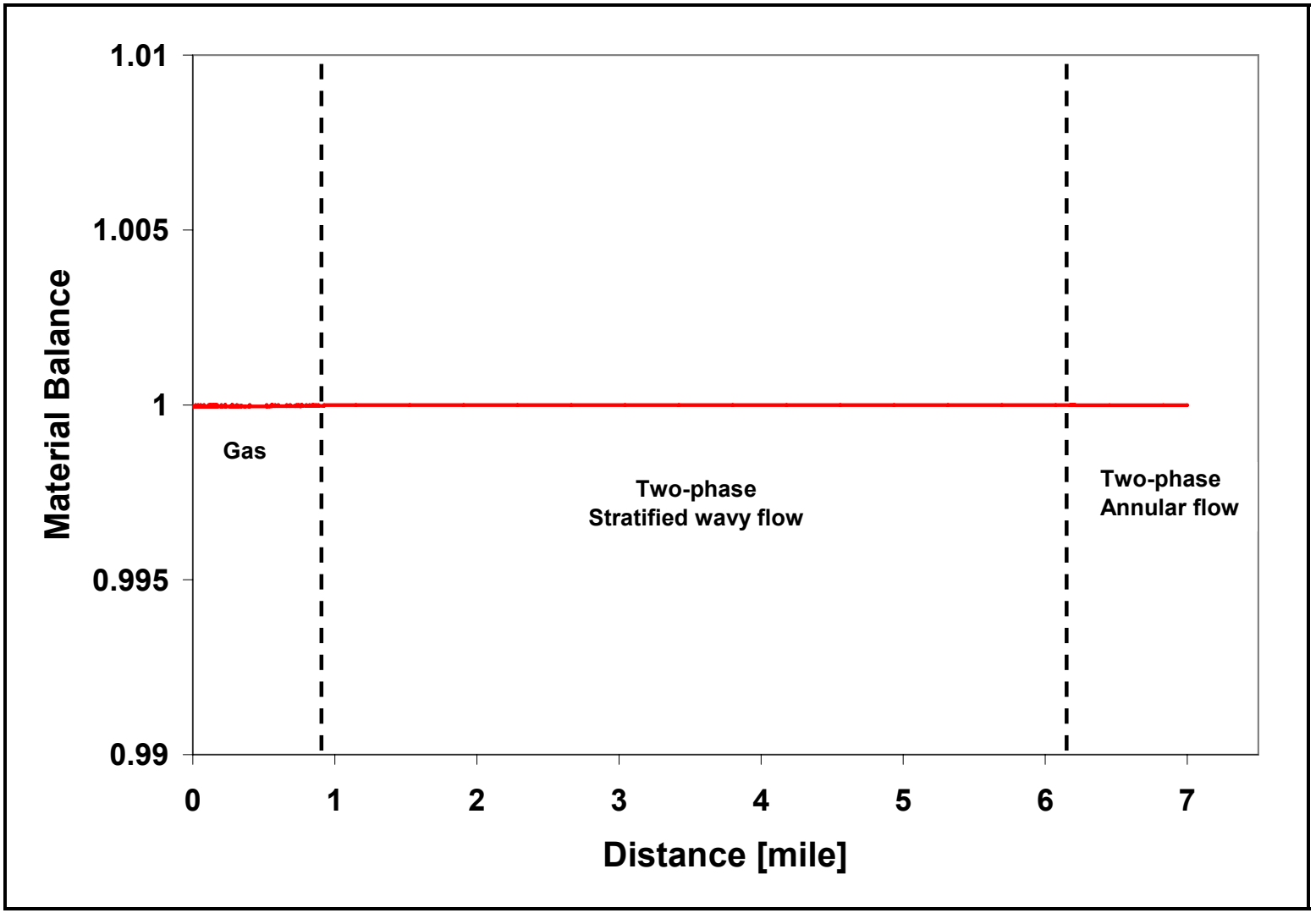

Figure 7.12 Cumulative material balance (proposed numerical experiment)

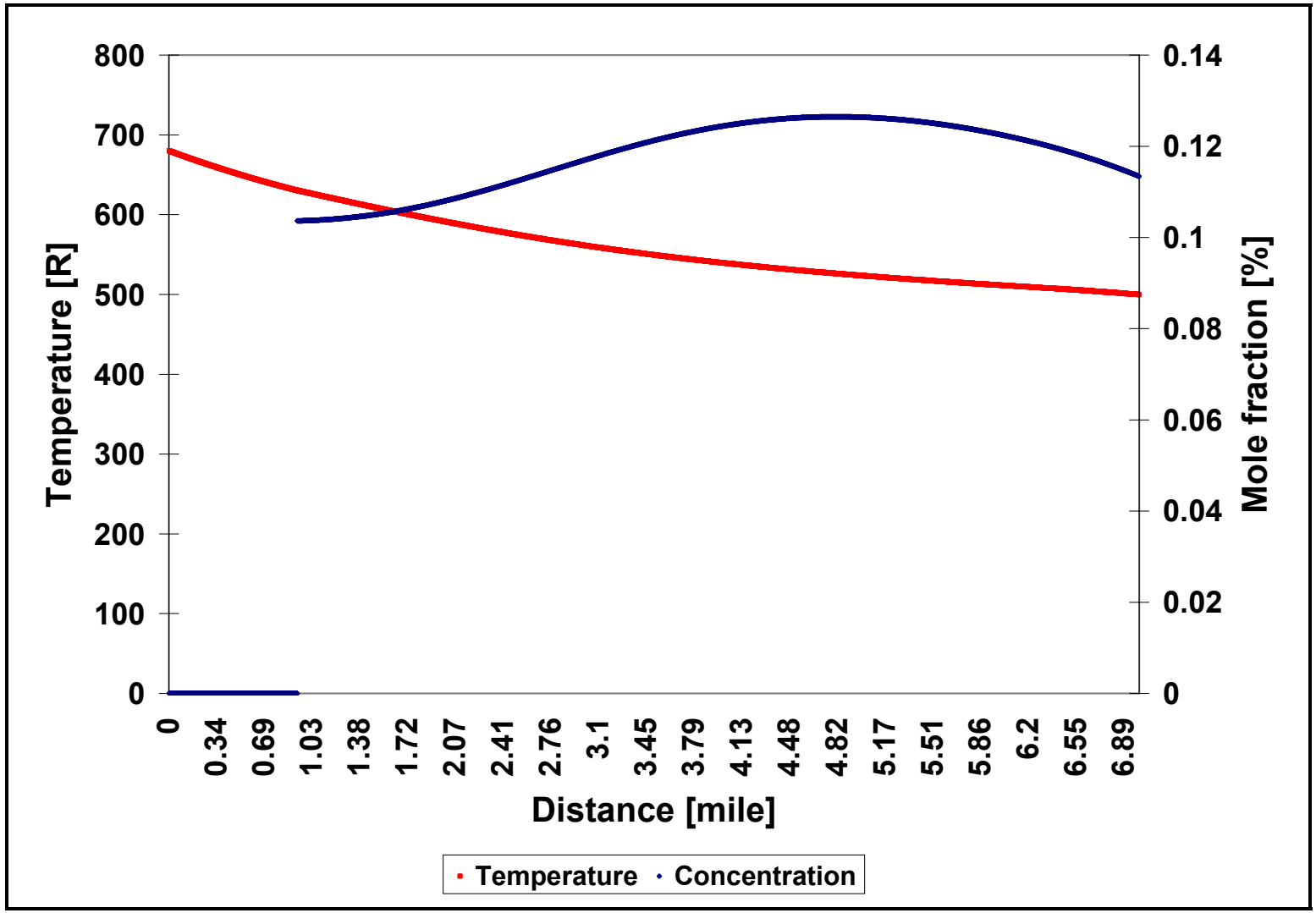

Figure 7.13 Methane concentration in the water stream (proposed numerical experiment)

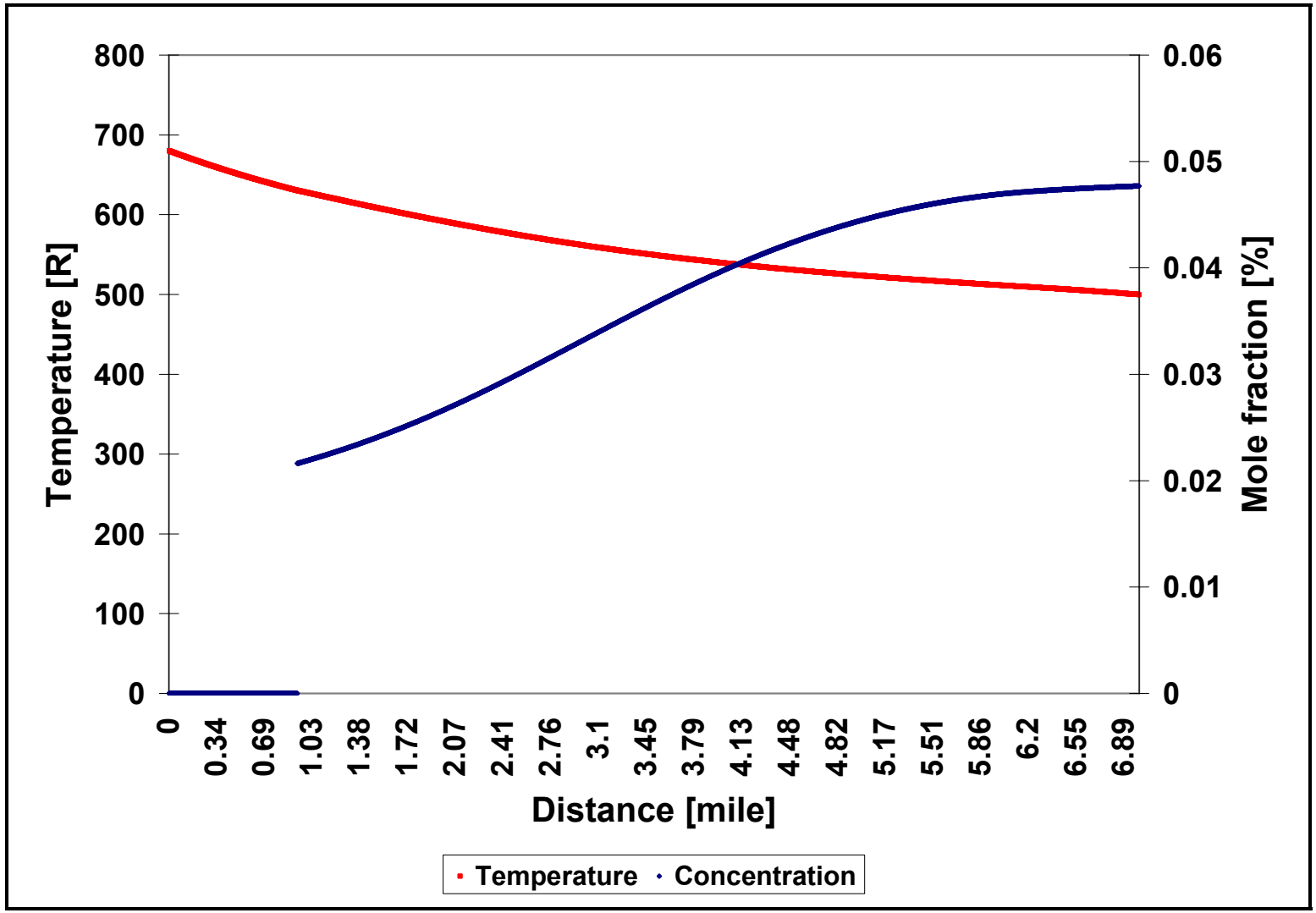

Figure 7.14 CO_2 concentration in the water stream (proposed numerical experiment)

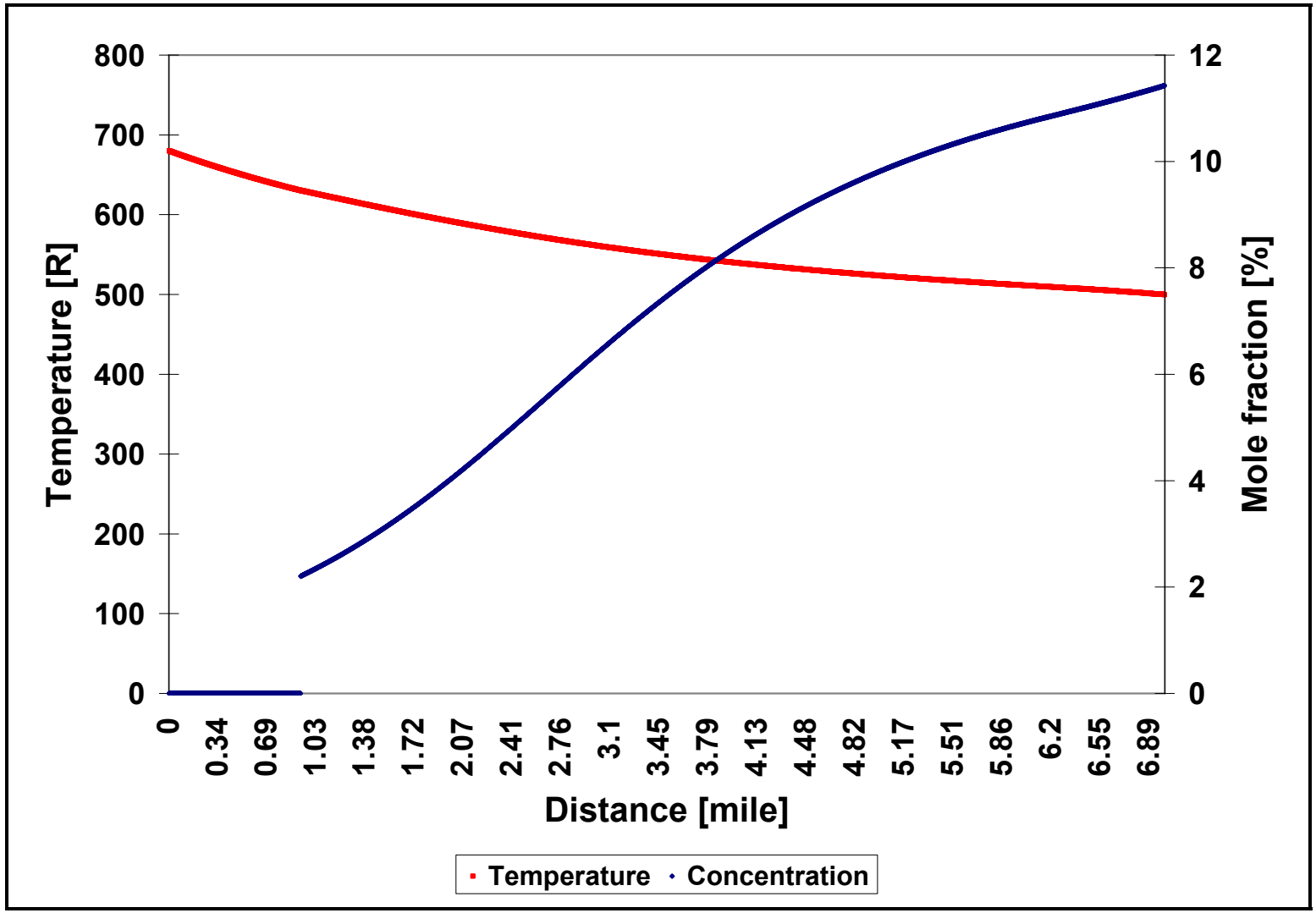

Figure 7.15 Methanol concentration in the water stream (proposed numerical experiment)

7.2 Two-phase (gas-condensate) flow

The current section evaluates the model performance for systems exhibiting two-phase (gas-condensate) flow. For that purpose, the present work revisits a field study presented by Mucharam (1990).

The field facility described by Mucharam is a 52000-ft long pipeline operated by Tenneco Company in Colombia. This gas transmission system is schematically represented in Figure 7.16. Gas, from fields K and T at *300 psia* and approximately *100 °F*, is the main feed for this pipeline.

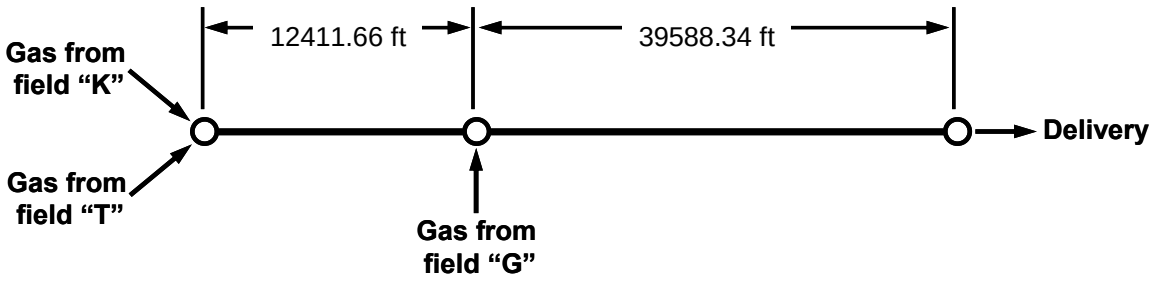

Figure 7.16 Schematic representation of the pipeline described by Mucharam

Figure 7.16 shows that the transmission line blends gas produced from three different fields (K, T and G). The first *12411.66 ft* of this pipeline transports *2.27 MMSCFD* of gas blended from fields K and T, while the rest of the pipe (*39588.34 ft*) carries *2.48 MMSCFD* of a gas that is a mixture of the streams K, T and G. The gas composition in each pipeline section is presented in Table 7.6.

Table 7.6 Composition of the gases blended from fields K, T and G

Component	Mix K+T	Mix K+T+G
Nitrogen	0.0085200	0.0084520
Carbon Dioxide	0.0263340	0.0260290
Methane	0.7797280	0.7792670
Ethane	0.0698040	0.0700790
Propane	0.0592040	0.0595780
i-Butane	0.0117280	0.0117720
n-Butane	0.0239890	0.0241040
i-Pentane	0.0082070	0.0082290
n-Pentane	0.0059740	0.0060020
Hexanes-plus	0.0065120	0.0064880

Table 7.6 shows that the gas compositions transported in the pipe contain high hexane-plus (C6+) fractions. The composition of the C6+ fractions is approximated as consisting of 47% of n-hexane, 36% of n-heptane and 17% of n-octane. This splitting approach is widely used in the gas industry and is based on empirical studies performed by one of the leading chromatograph manufacturers (Daniel®) (FERC, 2004). Table 7.7 presents the compositions of the gases transported after characterizing their C6+ fractions.

Table 7.7 Composition of the gases blended from fields K, T and G (Characterized)

Component	Mix K+T	Mix K+T+G
Nitrogen	0.0085200	0.0084520
Carbon Dioxide	0.0263340	0.0260290
Methane	0.7797280	0.7792670
Ethane	0.0698040	0.0700790
Propane	0.0592040	0.0595780
i-Butane	0.0117280	0.0117720
n-Butane	0.0239890	0.0241040
i-Pentane	0.0082070	0.0082290
n-Pentane	0.0059740	0.0060020
n-Hexane	0.0030606	0.0030494
n-Heptane	0.0023443	0.0023357
n-Octane	0.0011070	0.0011030

No commercial steel pipe has an internal diameter of 6 inches. Therefore, the internal pipe diameter indicated by Mucharam (1990) is clearly incorrect. The current study considers that the pipe has nominal diameter of 6 inches and a construction schedule of 80. This construction schedule is commonly selected when designing high-pressure gas pipelines that may transport water. The internal diameter of a 6" SCH 80 pipe is 5.461 inches. The absolute roughness of this old pipeline system is considered to be 0.0018 ft as suggested by Boriyantoro (1994).

The facility under study crosses a hilly region exhibiting over 100 elevation changes. Table 7.8 presents the elevation profile of the first 12410 ft of the pipeline, while Table 7.9 shows the terrain profile for the rest of the transmission line. The temperature in the area surrounding the pipeline has a maximum of about 105 °F during the day and a minimum of approximately 75 °F during the night (Mucharam, 1990).

Table 7.8 Terrain profile for the first pipe section

Length [ft]	*Elevation [ft]*	*Length [ft]*	*Elevation [ft]*	*Length [ft]*	*Elevation [ft]*
0.00	524.93	128.96	554.46	257.91	544.61
225.67	524.93	322.38	557.74	225.67	544.61
193.42	528.21	128.95	538.05	677.00	472.44
354.62	516.73	709.23	495.40	322.38	492.12
225.67	529.85	386.86	487.20	483.57	452.75
161.19	511.80	1096.10	459.31	322.38	482.28
805.95	567.58	419.09	465.87	225.66	462.59
419.10	538.05	290.15	449.47	161.19	459.31
483.57	564.30	306.26	442.91	161.19	439.63
161.19	557.74	660.88	492.12	644.77	459.31
225.66	544.62	1225.04	570.86		

Table 7.9 Terrain profile for the second pipe section

Length [ft]	*Elevation [ft]*	*Length [ft]*	*Elevation [ft]*	*Length [ft]*	*Elevation [ft]*
0.00	459.31	290.14	370.73	386.86	419.94
112.83	449.47	4706.76	370.73	322.38	403.54
660.88	524.93	1934.29	418.30	241.78	419.94
354.62	531.49	386.85	405.18	354.62	383.85
161.19	508.52	419.10	405.18	1386.24	462.59
580.28	521.65	515.81	418.30	225.66	452.75
548.05	587.26	128.95	434.71	419.10	472.44
193.43	587.26	967.14	434.71	386.86	452.75
338.50	603.67	644.76	459.31	155.23	462.59
483.57	505.24	225.67	452.75	231.62	451.11
386.86	557.74	354.62	475.72	838.19	454.39
386.85	505.24	1031.61	600.39	96.72	465.87
805.96	570.86	116.06	583.98	128.95	452.75
660.88	600.39	270.80	583.98	934.90	467.51
1096.09	505.24	386.86	515.09	161.19	452.75
1321.76	551.17	386.86	495.40	773.72	498.68
354.62	538.05	354.61	498.68	274.02	492.12
451.33	551.17	483.57	515.09	967.14	513.45
1160.57	383.85	612.53	495.40	322.38	508.52
386.86	426.51	161.19	511.80	322.38	538.05
677.00	377.29	354.62	459.31	1354.00	570.89
161.19	377.29	225.66	488.84	451.34	587.26
128.95	383.85	902.67	406.82	1579.66	574.14

The present field case is modeled as two independent pipe sections. This is because the first *12410 ft* and last *39590 ft* of pipe transport different gas flow rates and compositions. The pipeline is modeled considering that the outlet pressure of the first pipe is equal to the inlet pressure of the second line.

The current study evaluates the pipeline performance considering two scenarios. One scenario examines the day-time operation while the other analyzes the night-time behavior. In both scenarios the inlet gas temperature is considered to be equal to that of

the surroundings. This is based on the assumption that the gas feeding the pipeline had sufficient time to "cool down" before reaching the transmission line. In this study, the average gas temperatures are estimated as *98.7 °F* for the day and *89.8 °F* for the night.

Table 7.10 presents the "data sheet" of the field case analyzed. This "data sheet" summarizes the information used for modeling this case study.

Figure 7.17 plots the pipeline operating conditions on the phase envelope of the gas. As shown in this figure, the pipeline only operates in two-phase conditions. The dew point threshold is not contacted during the day or night-time operation. Moreover, the proximity between operating conditions and the dew point curve suggests that limited liquid accumulation takes place in the pipeline.

Mucharam (1990) analyzed the current case study assuming that mist flow conditions prevailed through the entire pipe. However, the current study determined that the gas turbulence is not sufficient to drag the liquid as entrained droplets, and identifies the prevailing flow pattern as stratified wavy. The difference in closure models makes comparison between Mucharam's model and the present work inappropriate.

Figures 7.18 through 7.22 present the hydrodynamic behavior for this system. These figures show the hydrodynamic profiles calculated for the two scenarios examined (day and night-time operation).

Table 7.10 Data sheet for the Tenneco field case

System ID: Mucharam Tenneco field [Stratified wavy flow]

First pipe section

Inlet Conditions

Day temperature	***558***	***R***
Night temperature	***549.5***	***R***
Pressure:	***300***	***psia***
Flow rate:	***2.27***	***MMSCFD***

Gas composition:
Table 9-7. (Mix K+T)

Pipe data

Diameter	***5.461***	***inches***
Abs. Roughness	***0.0018***	***ft***
Terrain Profile	***As shown in Table 9-8***	

Energy Data

U factor	***1***	***Btu/hr-ft2***
Surr. Temp. (Day)	***558***	***R***
Surr. Temp. (Night)	***549.5***	***R***

Second pipe section

Inlet Conditions

Day temperature	***558***	***R***
Night temperature	***549.5***	***R***
Pressure:	***Equal to the outlet of first section***	
Flow rate:	***2.48***	***MMSCFD***

Gas composition:
Table 9-7. (Mix K+T+G)

Pipe data

Diameter	***5.461***	***inches***
Abs. Roughness	***0.0018***	***ft***
Terrain Profile	***As shown in Table 9-9***	

Energy Data

U factor	***1***	***Btu/hr-ft2***
Surr. Temp. (Day)	***558***	***R***
Surr. Temp. (Night)	***549.5***	***R***

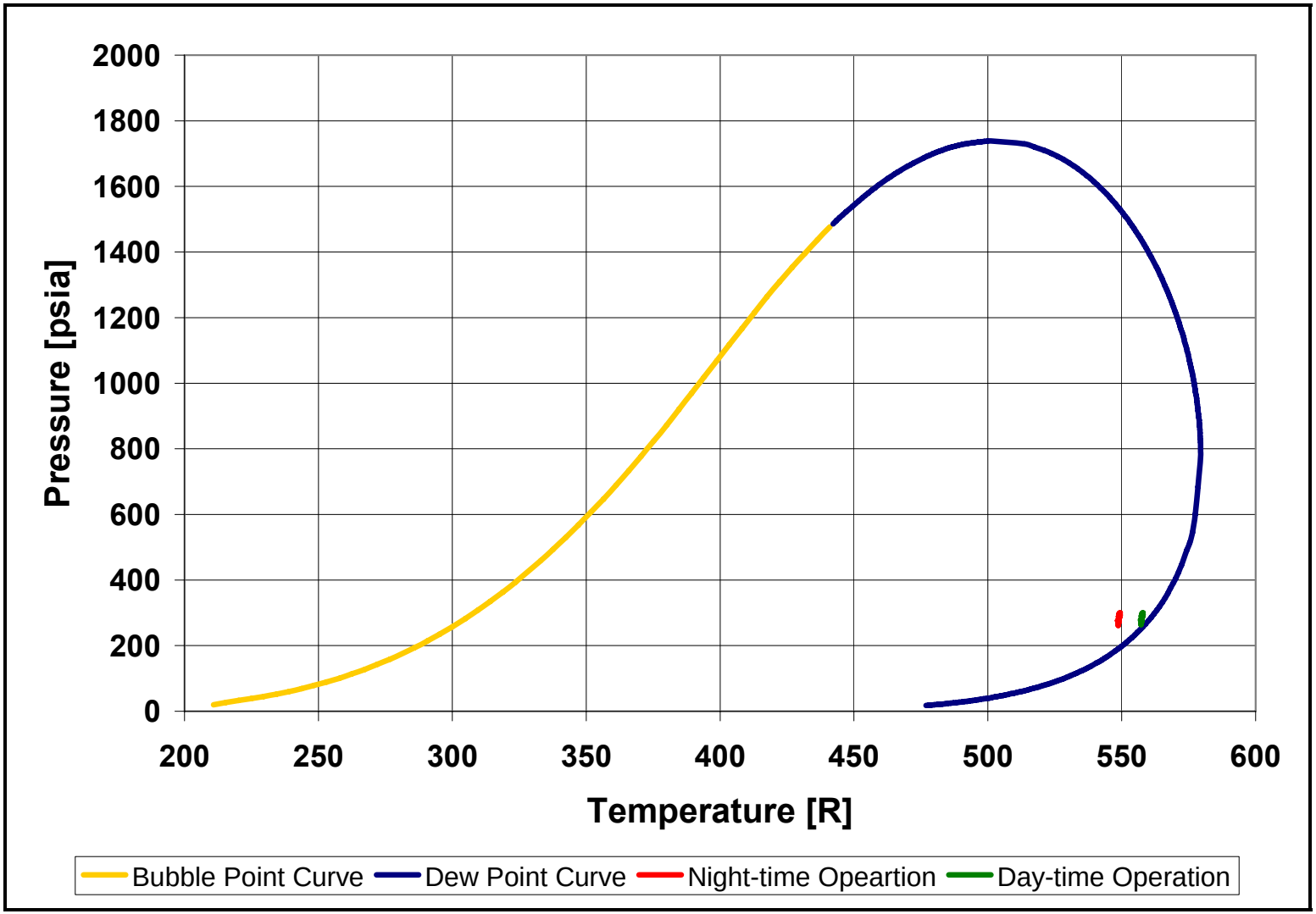

Figure 7.17 Operation profile of the pipeline system

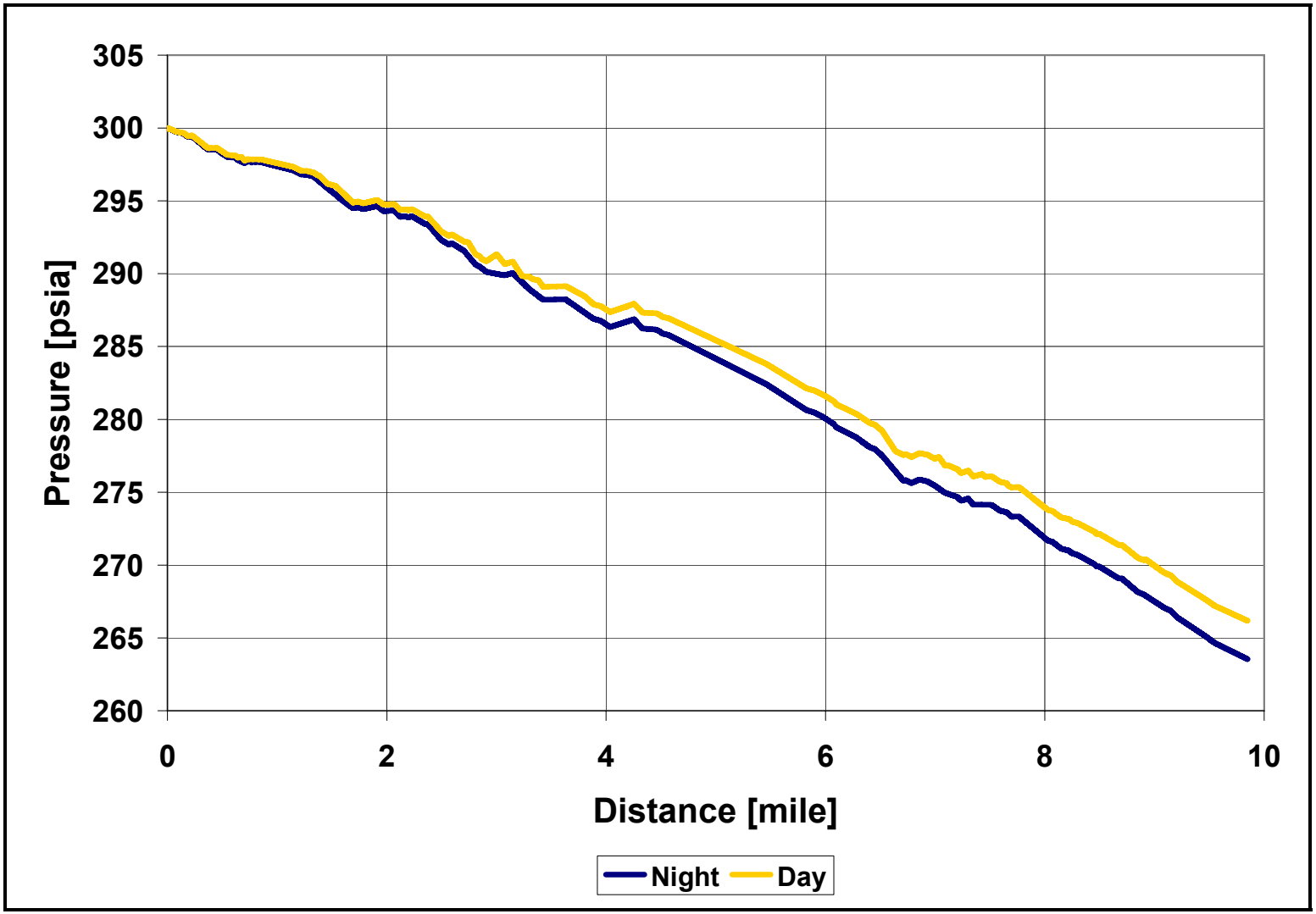

Figure 7.18 Pressure profile for the day and night operation

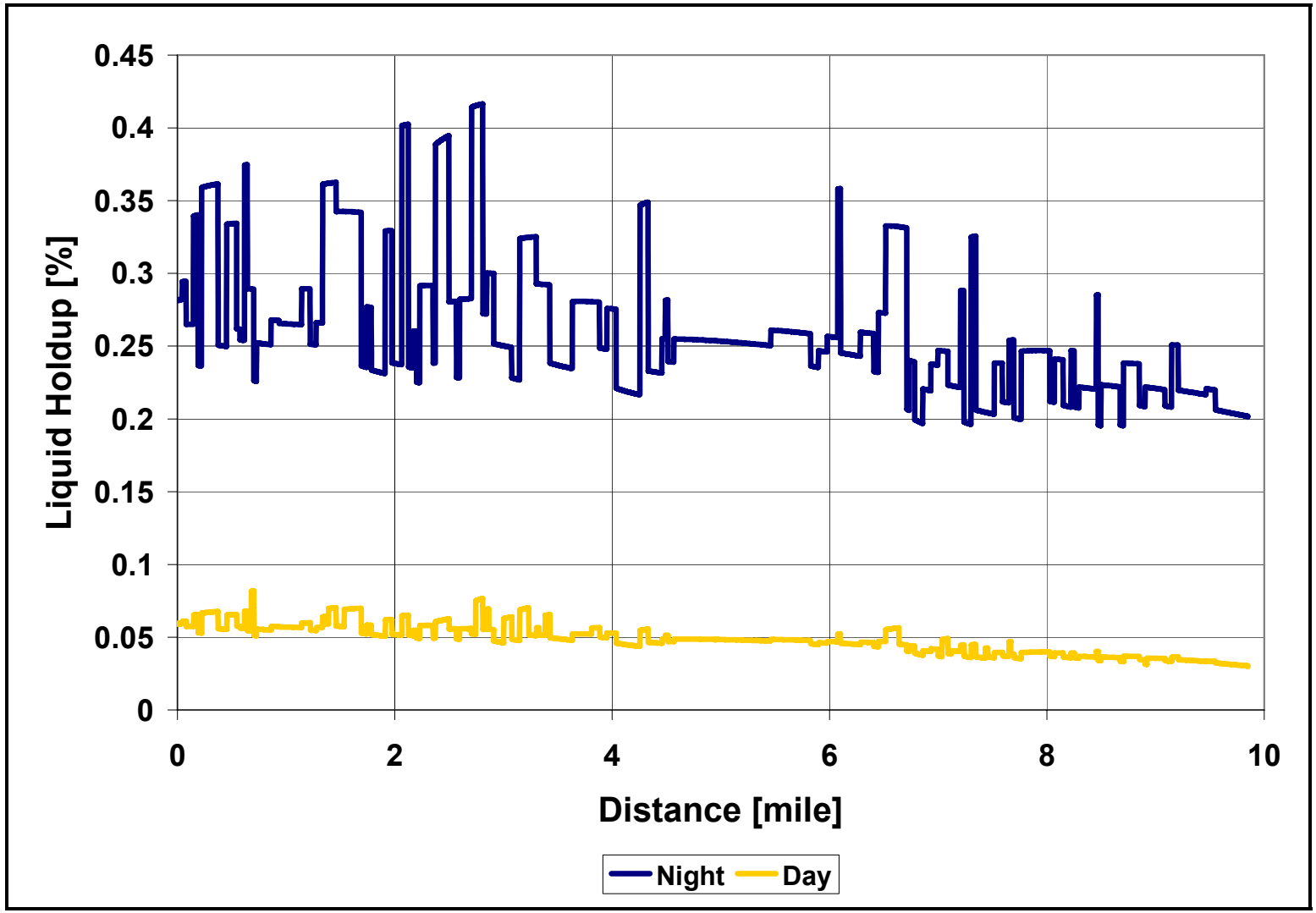

Figure 7.19 Predicted liquid holdup profile for the day and night scenarios

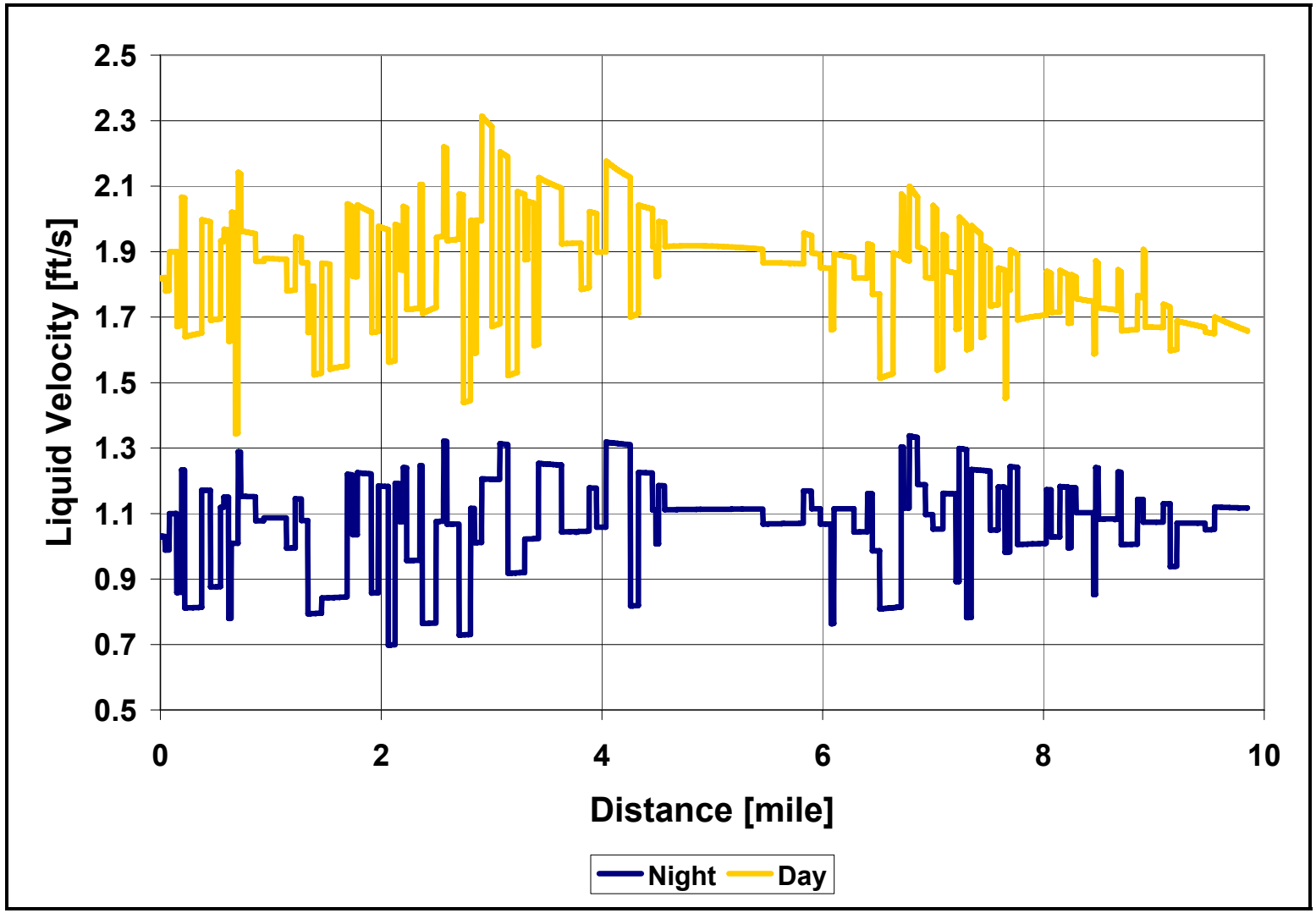

Figure 7.20 Predicted liquid velocity profiles during the day and night operations

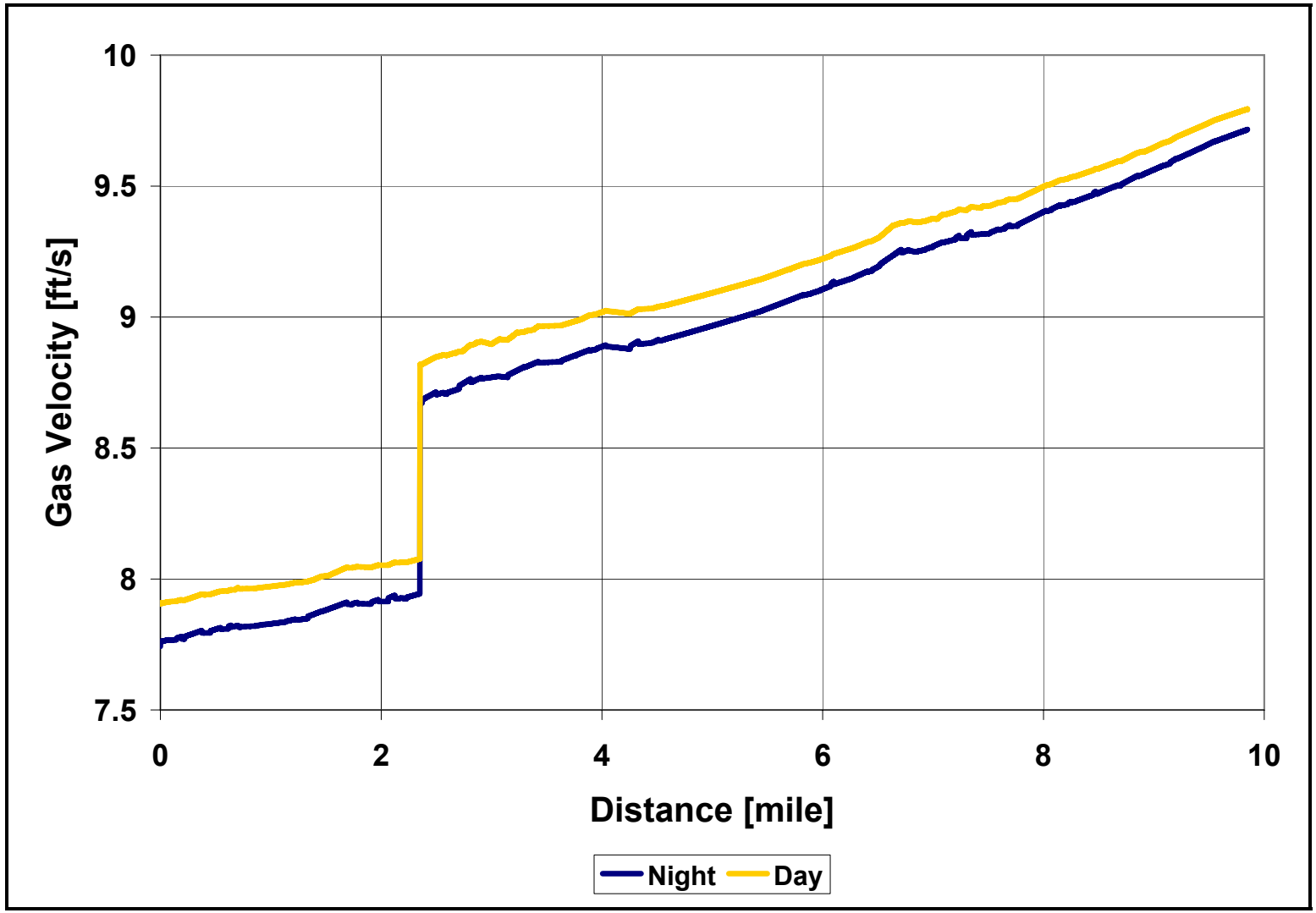

Figure 7.21 Gas velocity profiles for day and night conditions

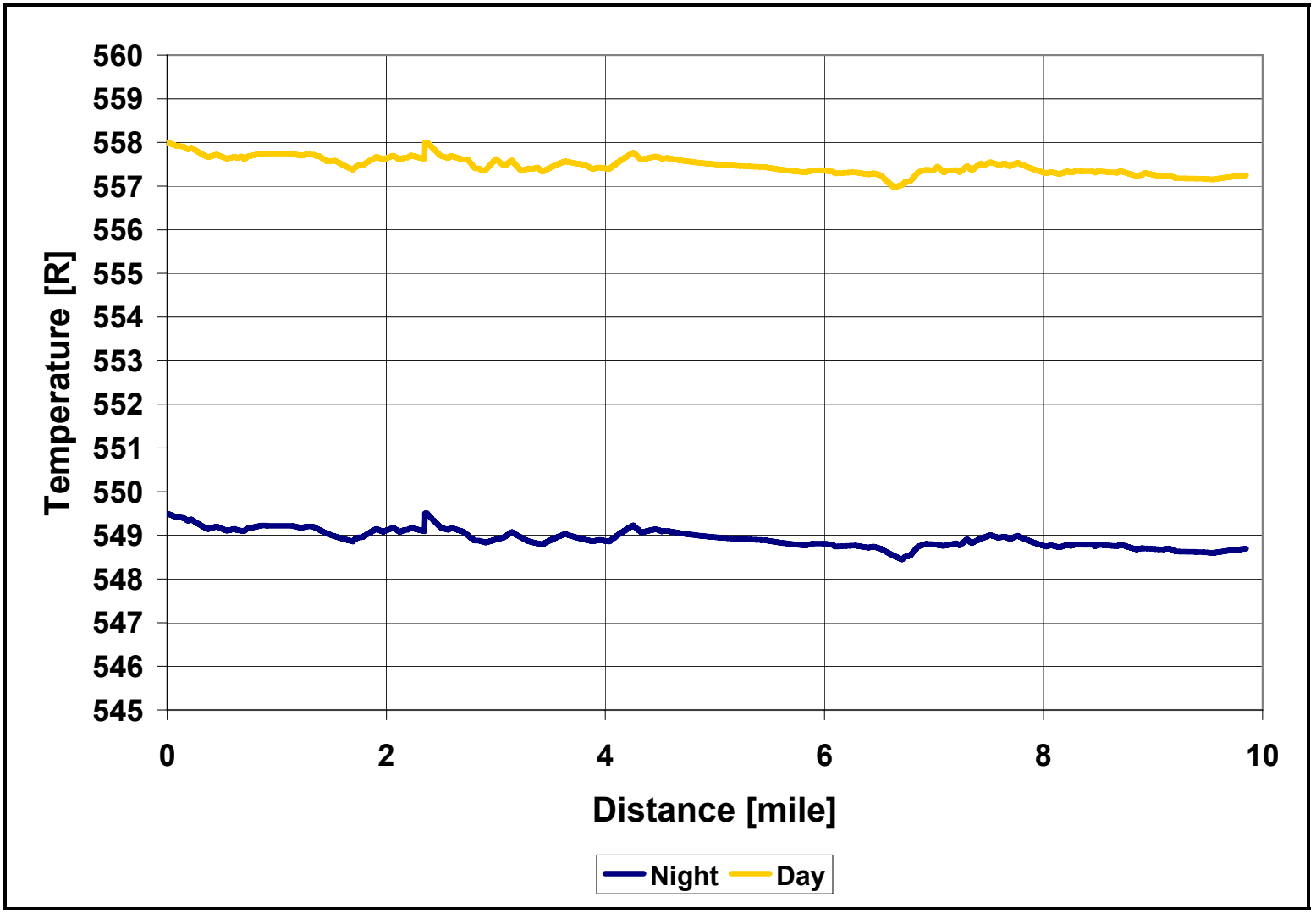

Figure 7.22 Temperature profiles predicted for the day and night scenarios

The model proves its capability of handling undulated terrain effects. The effect of gravitational forces is clearly reflected in the hydrodynamic model profiles (Figures 7.18 through 7.22). As expected, pressure drop gradient and liquid holdup decrease in downward inclined pipes and increase in upward inclined pipe segments. Liquid velocities rise in downhill pipes and decline when climbing uphill pipes.

Figure 7.18 presents the pressure profiles expected for the day and night-time scenarios. Pressure losses are expected to rise from *33.8 psi* during the day to *36.4 psi* during the night. The pressure drop variations occur due to liquid condensation/evaporation in the pipe caused by daily temperature changes. The average pressure drop predicted for this system is *35.1 psi*.

The pipeline operator reported a measured pressure drop of *50.0 psi* (Mucharam, 1990). However, in most field applications the pressure drop through the pipeline is estimated using bourdon-tube manometers. The accuracy of a reading obtained from a bourdon-tube manometer (0-500 psig range) could be as large as *+/- 20 psi*. Moreover, pipeline networks are very dynamic systems in which gas flow rates change rapidly due to the behavior of the market. In this field case, the flow rate passing through the system when the pressure drop was measured was not reported. It is known that a 20% increase in flow rate can raise pressure losses as much as 44%. The current work performs the calculations at the average flow rates reported by the operator. In summary, the pressure drop measured by the field personnel is a rough estimation. The pressure losses predicted by the model are in agreement with those estimated by the pipeline operator.

The impact of the gravitational forces on the liquid holdup predictions can be clearly observed in Figure 7.19. Liquid accumulates at the valleys and dissipates at the summits found along the topological profile of the pipeline. Gravitational effects have a larger impact during night-time operations. This is because greater liquid accumulation takes place at night.

During the night, liquid holdup reaches a maximum of *0.42%* at a point located *14820 ft* from the pipe inlet, and finds a minimum of *0.195%* at a distance of *45954 ft* from the pipe inlet. During the day, a maximum liquid holdup of *0.082%* is found at *3690 ft* from the pipe inlet, while a minimum of *0.03%* is predicted at the pipe outlet. The average liquid holdups calculated for day and night-time scenarios were *0.048%* and *0.26%* respectively.

The predicted liquid velocity profiles are presented in Figure 7.20. This plot shows that gravitational forces have a significant impact on the liquid velocity profiles. Gravity accelerates liquid flowing through downhill pipe segments, and decelerates liquid climbing uphill inclined sections.

Larger liquid velocities are predicted during the day-time conditions. Smaller liquid fractions are more easily dragged by the gas phase. Interfacial forces exert greater impact on systems transporting lower liquid loadings. The average liquid velocities for the day and night scenarios are *1.84 ft/s* and *1.07 ft/s* respectively.

Figure 7.21 presents gas velocities calculated along the pipe. For the day and night scenarios, a “sudden” increase in the gas velocity is predicted at *12410 ft* from the gas inlet. This “jump” appears due to additional gas entering the system from field G. As expected, gas velocities increase as pressure and gas density decline along the pipe. The maximum gas velocities are found at the pipe outlet and their values for day and night are *9.79 ft/s* and *9.71 ft/s* respectively.

The temperature during the day and night scenarios remained nearly constant along the entire pipe. The maximum temperature changes are less than *1 °F* along the entire pipe. However, limited “temperature recovery” effects are observed along the pipe. The “temperature recovery” is attributed to the conversion of the excess potential energy to internal energy (Sadegh & Adewumi, 2005). The predicted temperature profiles are shown in Figure 7.20.

Material balance calculations confirm the reliability of the model for handling two-phase (gas-condensate) flow in highly undulated terrain. The calculated material balance approximated *1.0* along the entire pipe. The maximum deviation obtained for this system was less than $5 \cdot 10^{-4}$.

Every four months the pipeline was pigged, and during that period *280 barrels* of condensate at atmospheric conditions were collected. Condensate volume is accurately measured because this fluid has a high commercial value.

The predicted condensate flow rates delivered by the pipe at outlet conditions were *1.26 bbl/day* for the day-time and *5.64 bbl/day* for the night-time scenario. In Colombia, days and nights last 12 hours all year long. Therefore, the daily average condensate production at pipe outlet conditions can be estimated as *3.45 bbl/day*. Over four months, the pipeline is predicted to deliver *414.33 bbls* of condensate at outlet conditions.

The condensate produced by the pipeline is “flashed” at atmospheric conditions. Therefore, a portion of the liquid delivered by the pipeline revaporizes when entering the atmospheric storage tank. Flash calculations revealed that *23.8%* of the condensate volume revaporizes during the day, while *27.01%* of the condensate becomes gas during the night-time operations. The predicted condensate volume at atmospheric conditions is *304.8 barrels*.

The condensate volumes measured by the field operator and predicted by the model present an outstanding match. The difference between the predicted and measured volumes is less than *9%*. The model over-predicted the condensate production by *24.8 barrels*. The difference between the predicted and measured condensate volumes could be attributed to evaporation losses in the liquid collection system.

This field case shows the capacity of the model for simulating two-phase (gas-condensate) flow in highly undulated terrain. The anticipated liquid delivery presents an

outstanding match when compared with that reported from the field, while pressure drop predictions are in agreement with field measurements.

For this particular field study, the pipeline operation is shown to be very sensitive to environmental temperature changes. During night-time operation, pressure losses rise *7.5%*, liquid accumulation increases *325.0%* and condensate delivery grows *438.0%*.

The current field case was also analyzed simplifying the pipeline elevation profile as two single-slope sections. Table 7.11 presents the details of the simplified elevation profile.

Table 7.11 Simplified pipeline elevation profile

Segment	Length [ft]	Inlet Elev. [ft]	Outlet Elev. [ft]
1	12,411.66	524.93	459.31
2	39,588.34	459.31	574.14

The results indicate that modeling this pipeline as two single-slope pipes is a good approximation. Pressure losses and liquid production yielded similar results than those presented for the highly undulating case. The anticipated pressure losses were *33.9 psi* during the day and *36.7 psi* at night, while the predicted condensate delivery was *313.5 barrels*.

The simplification of the elevation profile reduced the computational time required for the calculations, as it eliminated abrupt changes in gravitational forces along the pipeline.

7.3 Three-phase (gas-condensate-water) flow

The model's capacity for simulating three-phase (gas-condensate-water) flow was evaluated by revisiting the Tenneco field study presented by Mucharam (1990). In the previous section, this case study was analyzed neglecting the existence of water in the system and thus limiting the pipeline operation to two-phase (gas-condensate) flow. The current section takes into consideration the water delivered by the Tenneco field pipeline (*2.5 bbl/month*), and evaluates the occurrence of three-phase (gas-condensate-water) flow in the system.

The chromatographic analyses provided by the field operator did not report water content in the inlet gas compositions. The present study determined the water fraction in the inlet composition performing a sensitivity analysis. This sensitivity analysis consisted of varying the inlet water content until approximating the water produced by the pipe.

The inlet water fraction estimated was *0.3217%*. This water content is consistent with that commonly observed in typical pipeline operations. Pipeline-quality gas often transports small water fractions (less than *1%* mole). Table 7.12 present the estimated overall inlet compositions.

As shown in the previous section, considering this system as two single-slope pipes did not change the pressure drop or liquid production predictions, while the computational time required for performing the calculations was significantly reduced. Therefore, the transmission line is approximated as consisting of two single-slope

segments. Table 7.13 presents a “data sheet” summarizing the information used for modeling this field case.

Table 7.12 Composition of the inlet gas streams (Mucharam Tenneco field)

Component	Mix K+T	Mix K+T+G
Nitrogen	0.0084926	0.0084248
Carbon Dioxide	0.0262493	0.0259453
Water	0.0032170	0.0032170
Methane	0.7772196	0.7767591
Ethane	0.0695794	0.0698536
Propane	0.0590135	0.0593863
i-Butane	0.0116903	0.0117341
n-Butane	0.0239118	0.0240265
i-Pentane	0.0081806	0.0082025
n-Pentane	0.0059548	0.0059827
n-Hexane	0.0030508	0.0030400
n-Heptane	0.0023368	0.0023285
n-Octane	0.0011035	0.0010996

The model proves its capacity for detecting the existence of a second liquid phase in the pipe. As shown in Figure 7.23, the pipeline operates in the two-phase (gas-condensate) region during the day and in the three-phase (gas-condensate-water) region during the night.

The system is very sensible to daily temperature changes. Interestingly, water condenses, accumulates and flows only during the night. During the day, water does not condense in the pipe and all of it is transported in the gas stream.

Table 7.13 “Data sheet” of the Tenneco field pipeline case

System ID: Mucharam Tenneco field [Stratified wavy flow]

First pipe section

Inlet Conditions

Day temperature	***558***	***R***
Night temperature	***549.5***	***R***
Pressure:	***300***	***psia***
Flow rate:	***2.27***	***MMSCFD***

Gas composition:
Table 9-11. (Mix K+T)

Pipe data

Diameter	***5.461***	***inches***
Abs. Roughness	***0.0018***	***ft***
Terrain Profile	***Single Slope (-0.5283%)***	

Energy Data

U factor	***1***	***Btu/hr-ft2***
Surr. Temp. (Day)	***558***	***R***
Surr. Temp. (Night)	***549.5***	***R***

Second pipe section

Inlet Conditions

Day temperature	***558***	***R***
Night temperature	***549.5***	***R***
Pressure:	***Equal to the outlet of first section***	
Flow rate:	***2.48***	***MMSCFD***

Gas composition:
Table 9-11. (Mix K+T+G)

Pipe data

Diameter	***5.461***	***inches***
Abs. Roughness	***0.0018***	***ft***
Terrain Profile	***Single slope (0.29%)***	

Energy Data

U factor	***1***	***Btu/hr-ft2***
Surr. Temp. (Day)	***558***	***R***
Surr. Temp. (Night)	***549.5***	***R***

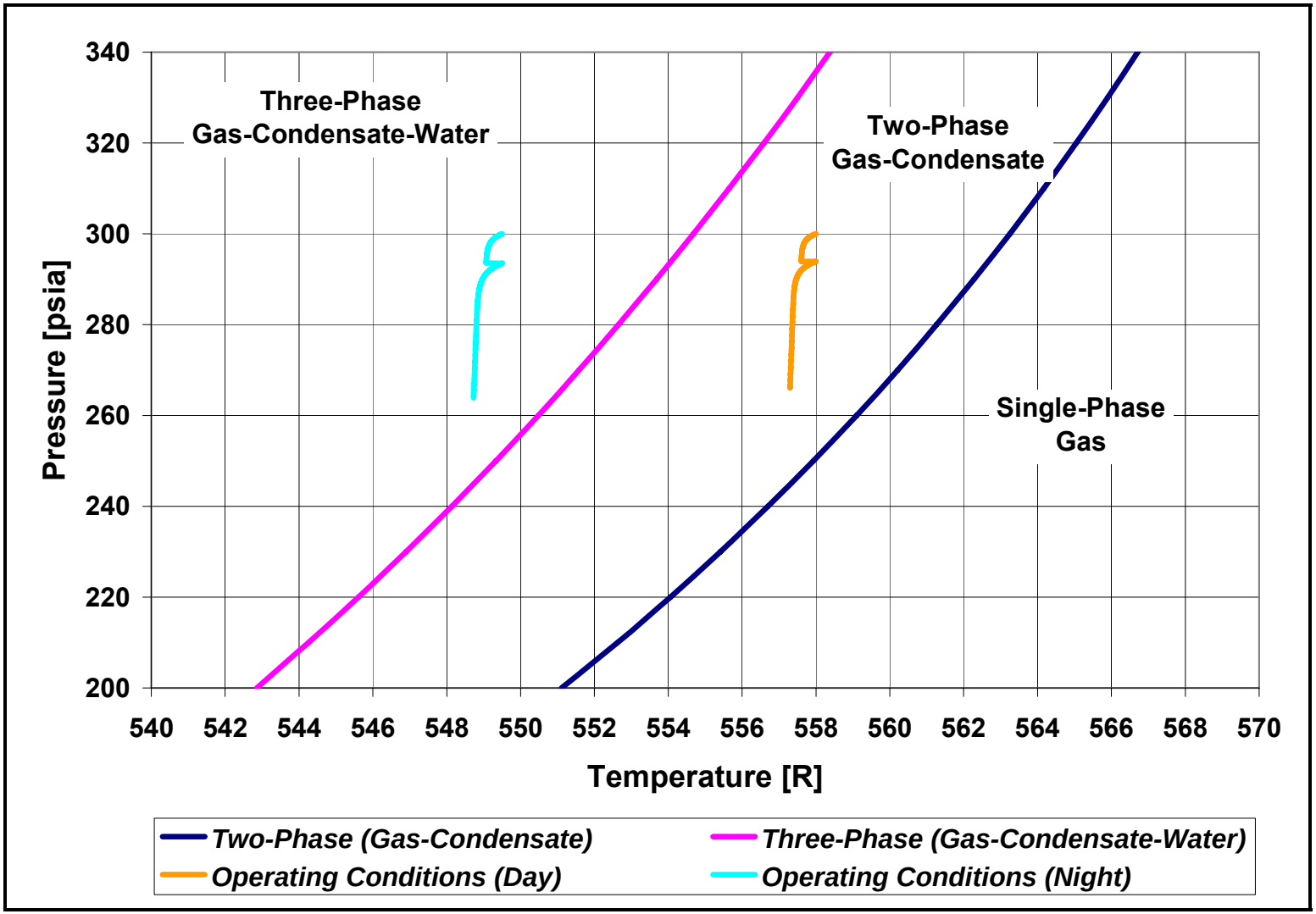

Figure 7.23 Operating conditions of the pipeline

During the day, two-phases (gas and condensate) travel in the pipe describing a stratified wavy flow pattern. During the night, three phases flow in the pipe describing a stratified wavy – stratified wavy flow regime. Water accumulates at the bottom of the pipe creating conditions for localized corrosion. The gas-condensate and condensate-water interfaces exhibit concave and wavy surfaces. The model predicts that the turbulence created in the condensate phase is enough to create waves in the condensate-water interface.

Figures 7.24 through 7.30 present the hydrodynamic behavior for this system. These figures show the hydrodynamic profiles calculated for the day and night-time scenarios.

Figure 7.24 shows the expected pressure profiles for the day and night-time scenarios. As indicated in the previous section, daily temperature changes promote liquid condensation/evaporation in the pipe. Liquid accumulation has a significant effect on the pressure losses across the pipe. Pressure losses rise from *33.85 psi* during the day to 35.92 *psi* during the night. The average pressure drop for this system is *34.9 psi*. The three-phase flow solution obtained for the night-time scenario nearly collapsed to the two-phase flow results. The limited amount of water in the system did not affect the pressure losses across the pipe significantly.

Figures 7.25 and 7.26 present the liquid holdup profiles for the day and night-time scenarios. During the night, condensate and water reach their maximum holdups (0.*251%*

and *0.0776%*) at *2750 ft* from the pipe inlet. During the day, the maximum condensate holdup (*0.057%*) is found at *2760* ft from the main gas supply. Interestingly, the maximum liquid holdups are not observed at the lowest elevation point in the pipe. This lowest elevation point in the pipe is the location where the "G" stream blends into the transmission line. Condensate tending to accumulate at that location is carried away by the additional gas blending in the system. Interfacial forces play a dominant role due to the limited liquid accumulation found in the system.

Figures 7.27 and 7.28 show the predicted liquid velocity profiles. During the night, the average condensate and water velocities are *1.23 ft/s* and *0.26 ft/s* respectively. The average condensate velocity during the day is *1.81 ft/s*. Interfacial forces play a dominant role on the velocity profiles. The injection of the "G" stream into the system accelerates liquid flow even though the pipe inclination changed to an upward orientation.

Figure 7.29 presents gas velocities calculated along the pipe. The maximum gas velocities for the day and night scenarios are *9.80 ft/s* and 9.69 ft/s respectively. These velocities are reached at the pipe outlet. As expected, a "sudden" increase in the gas velocity is predicted at the location where additional gas enters the system.

Temperature remained nearly constant along the entire pipe during the day and night. The maximum temperature variations along the entire pipe are less than *1°F*. The predicted temperature profiles are shown in Figure 7.30.

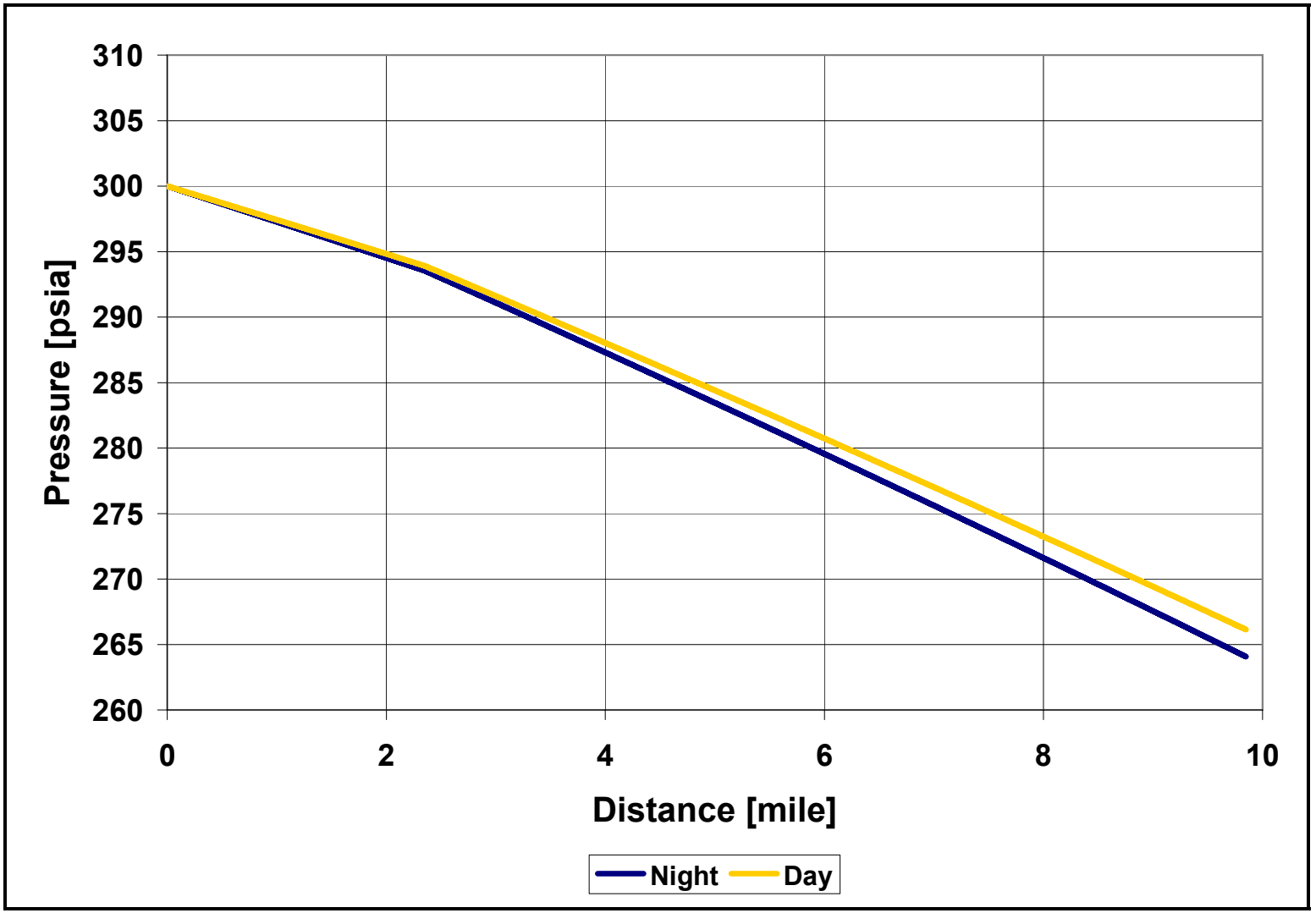

Figure 7.24 Pressure profile of the Tenneco field pipeline

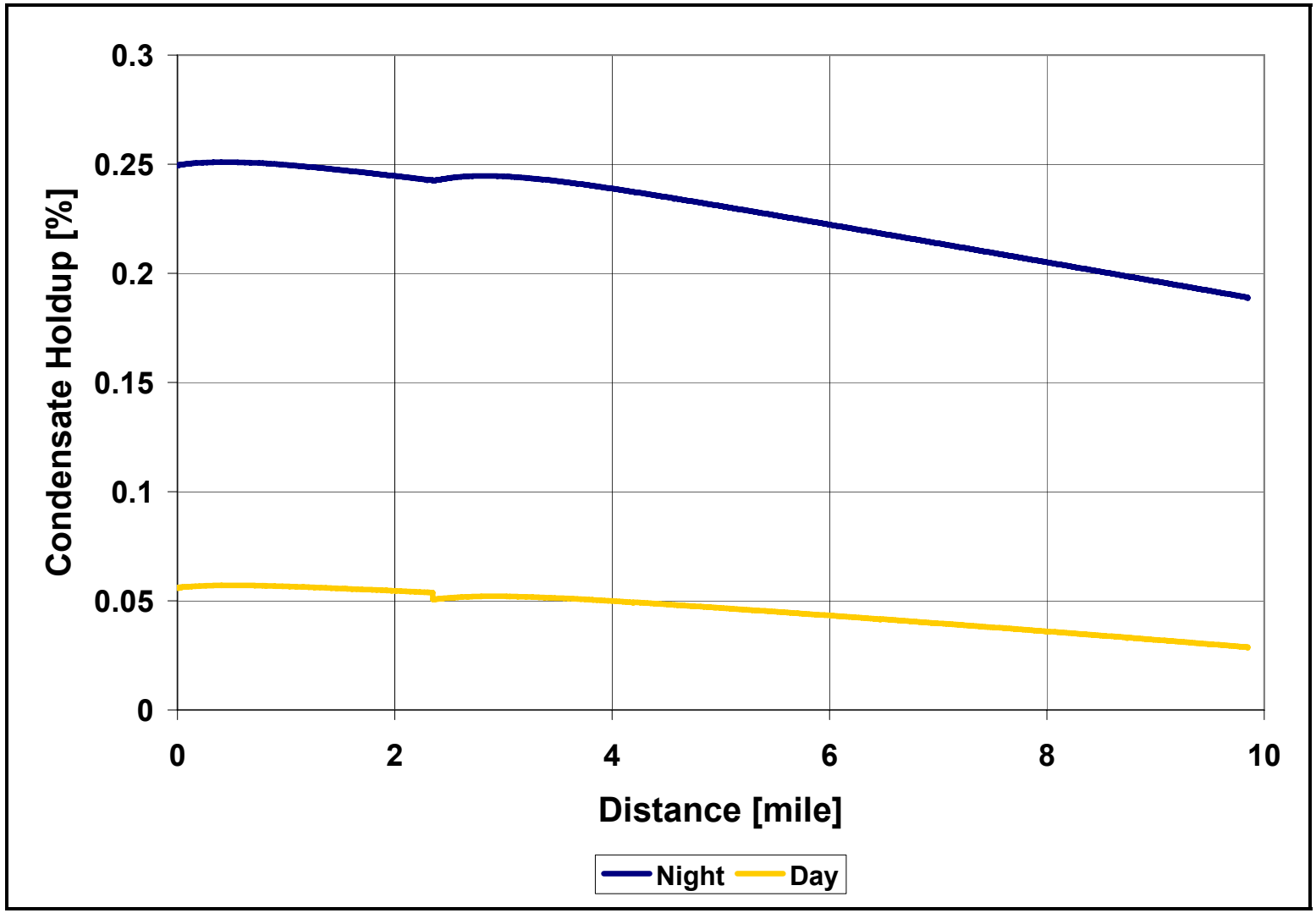

Figure 7.25 Condensate holdup profile for the Tenneco field pipeline

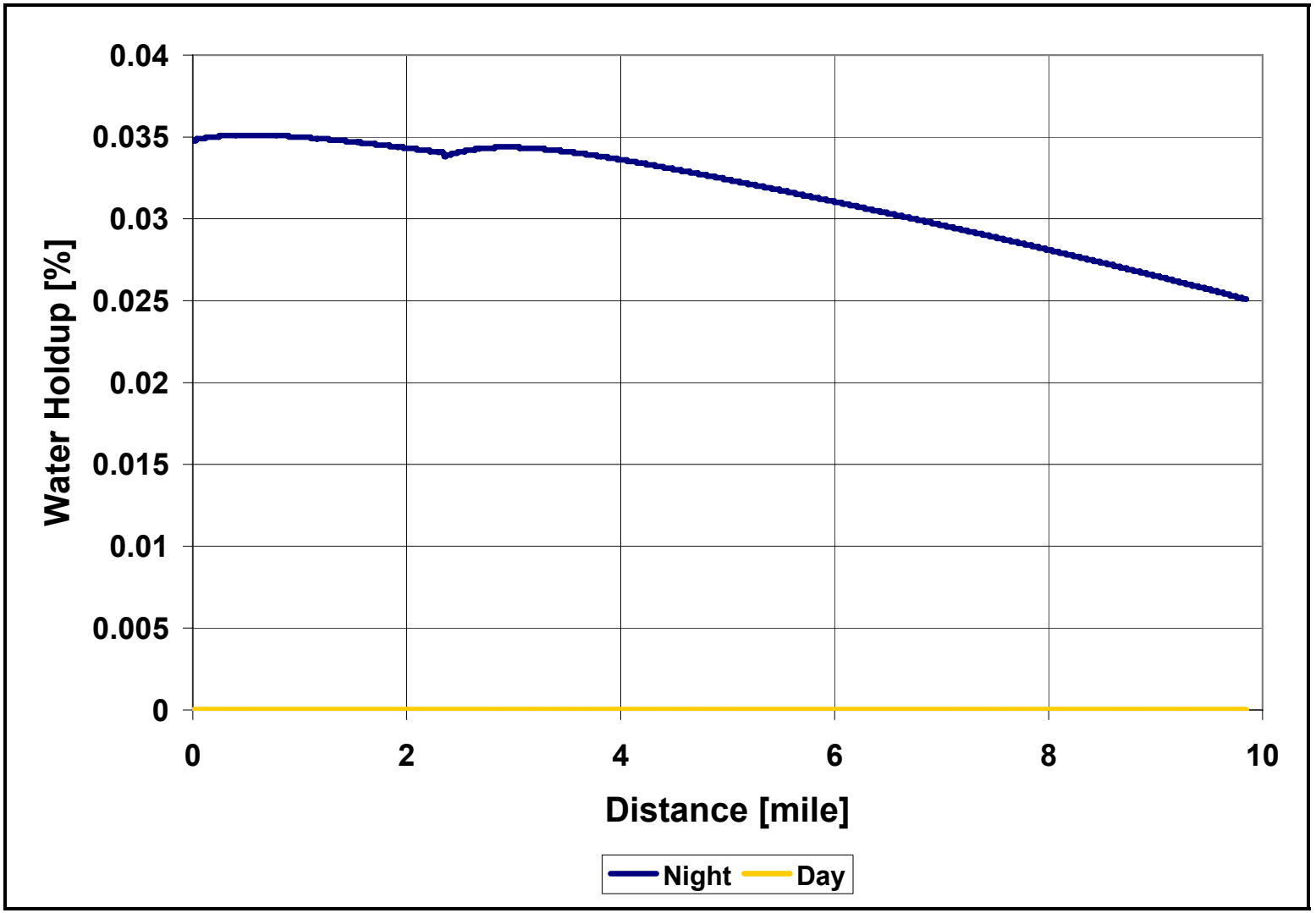

Figure 7.26 Water holdup profile for the Tenneco field pipeline

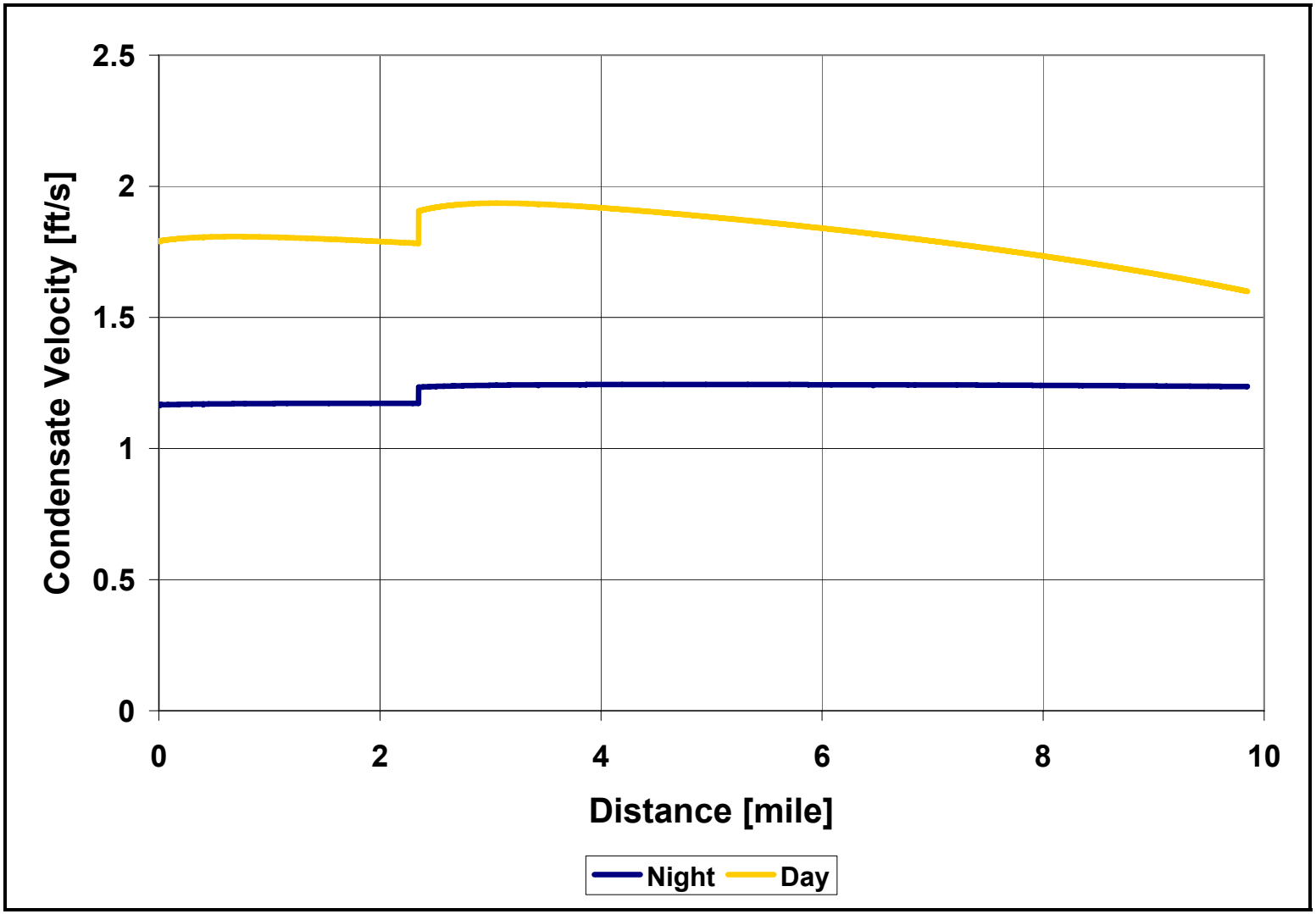

Figure 7.27 Condensate velocity profile for the Tenneco field pipeline

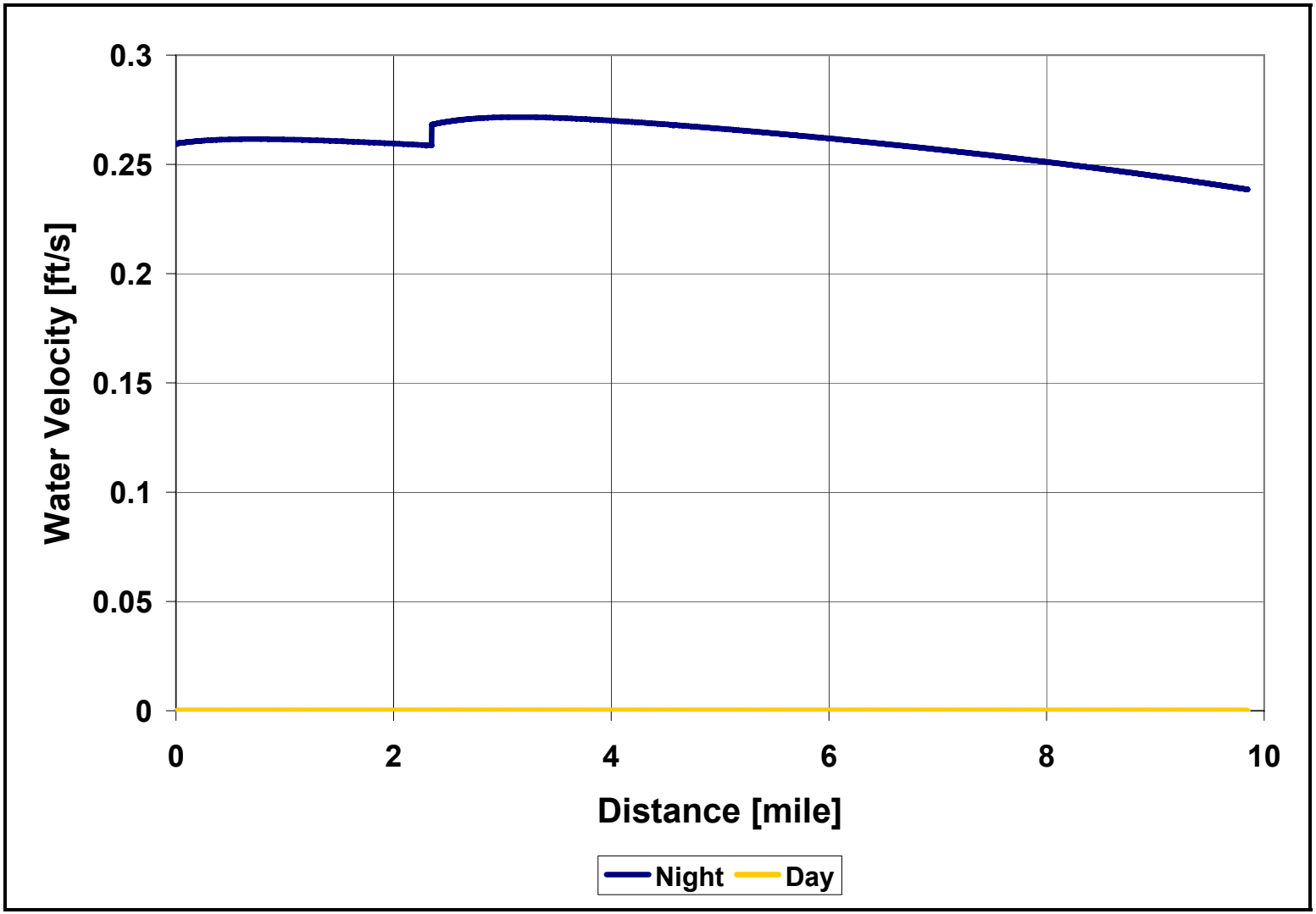

Figure 7.28 Water velocity profile for the Tenneco field pipeline

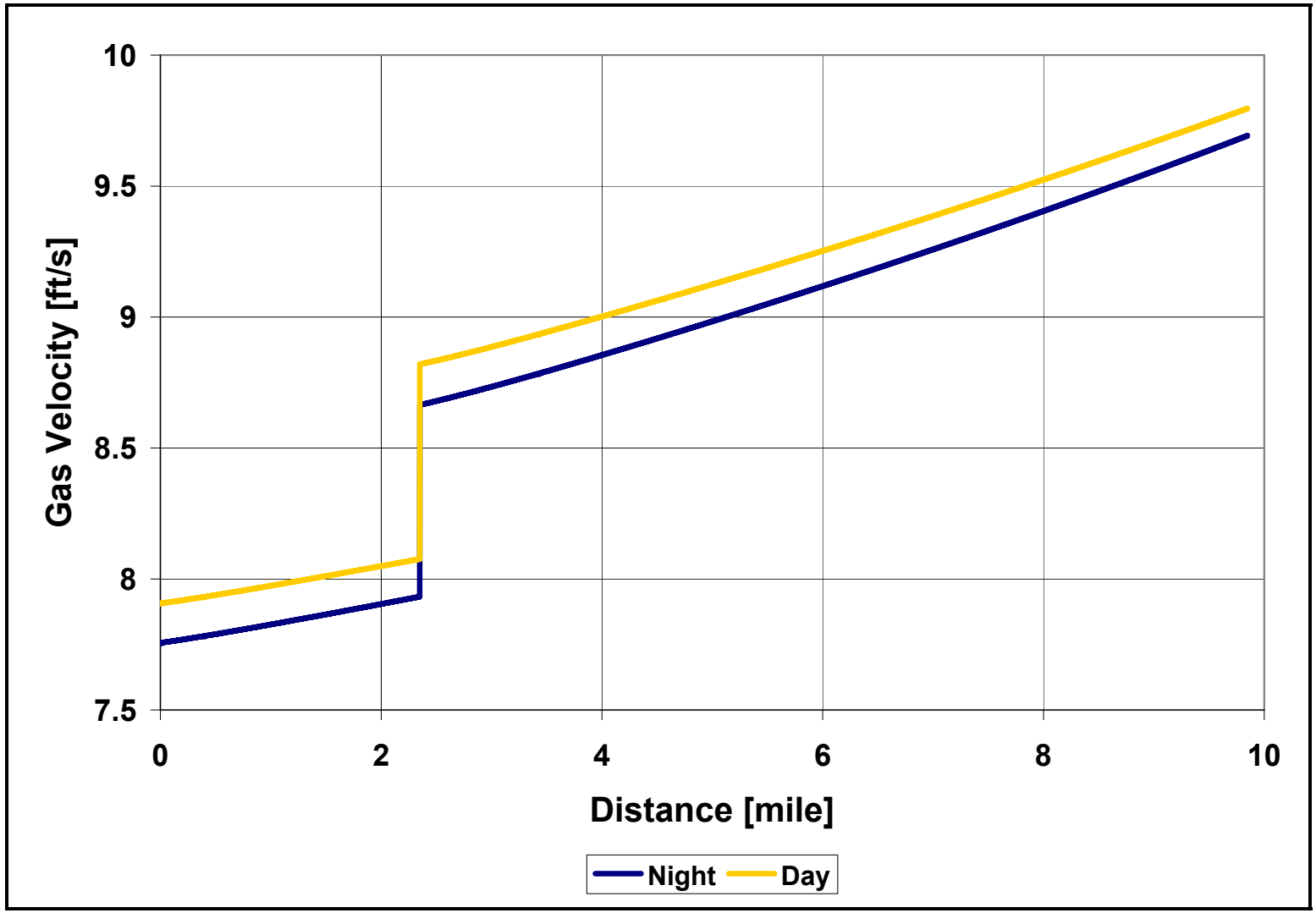

Figure 7.29 Gas velocity profile for the Tenneco field pipeline

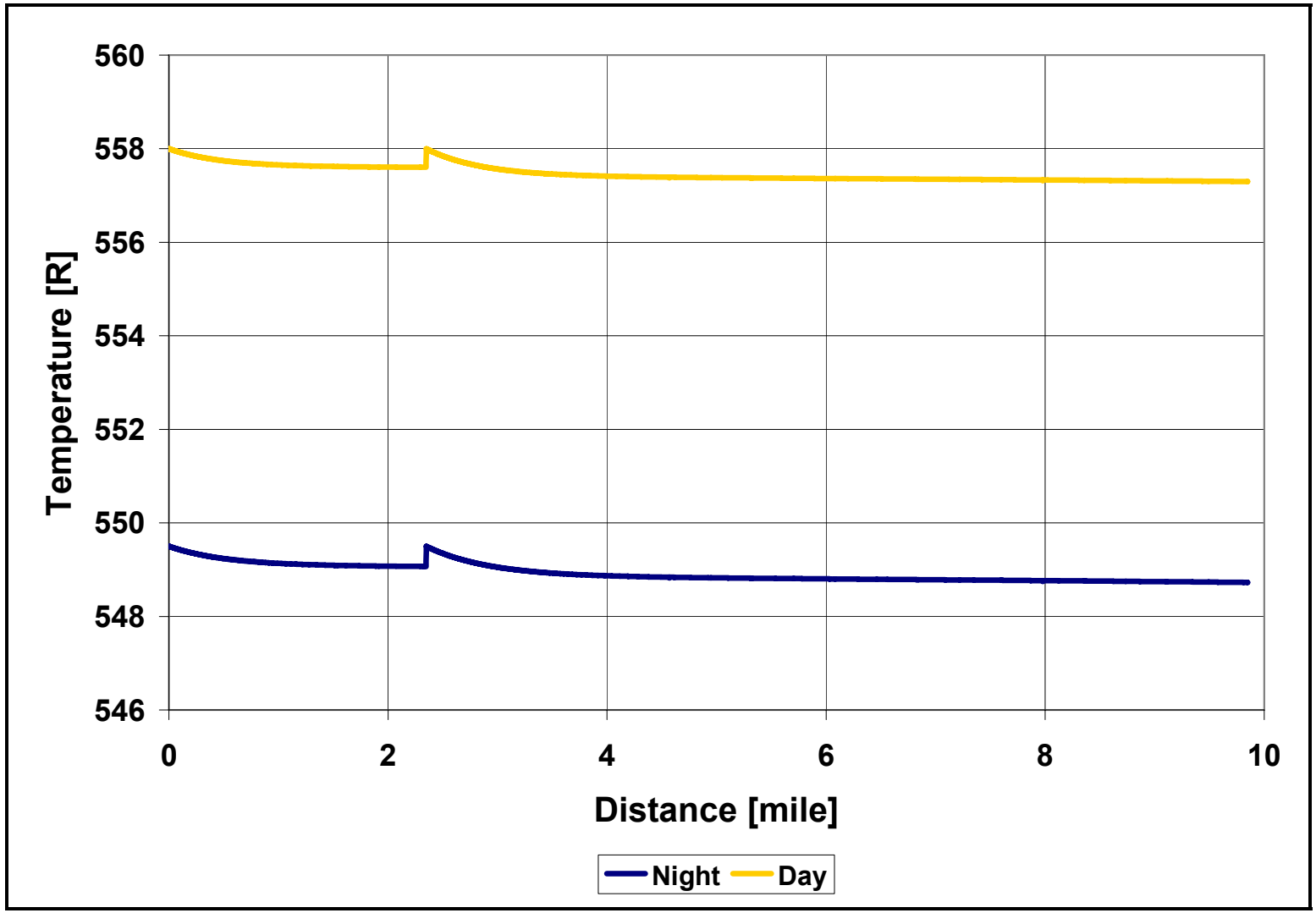

Figure 7.30 Temperature profile along the Tenneco field pipeline

Material balances verify the model reliability for performing three-phase (gas-condensate-water) flow calculations. The calculated material balance approximated *1.0* along the entire pipe, showing a maximum deviation of less than $5 \cdot 10^{-4}$.

At the pipe outlet conditions, the daily condensate and water production are *3.49 bbl/day* and *0.15 bbl/day* respectively. Over four months, the pipeline delivers *299.11 bbls* of condensate and *9.1 bbls* of water at atmospheric conditions. These liquid volumes are in excellent agreement with those measured by the field operator.

The predicted water production accurately matches the field measured volume (*10.0 bbls*), while the difference between the predicted and measured condensate production is less than *10%*. As indicated before, this difference could be attributed to evaporation losses in the liquid collection system.

This field case shows the capacity of the model for simulating three-phase (gas-condensate-water) flow. The predicted condensate and water production is in excellent agreement with the volumes reported from the field, while pressure drop predictions match field measurements. The model effectively predicted the prevailing three-phase flow pattern and the interfacial forces acting on the fluids.

7.4 Three-phase flow patterns and their transitions

The following section evaluates the model's capability to predict and adequately handle three-phase flow configurations. To this end, validation is sought by examining model behavior in a hypothetical flow system.

The hypothetical system consists of 1 ½ miles of commercial steel pipeline (*5.765" ID*) placed in a horizontal orientation. This pipeline is fed with gas consisting of light hydrocarbons and a small water fraction. The behavior of the piping system is analyzed by supplying different flow rates of this gas at *700 psia* and *40.33 °F*. Table 7.14 presents a "data sheet" providing the information required for modeling the system.

Table 7.14 "Data sheet" for the proposed three-phase hypothetical system

System ID: Three-phase numerical experiment

Inlet Conditions

Temperature:	***500***	***R***
Pressure:	***700***	***psia***
Flow rate:	***Variable***	

Gas composition:

Component	Mole
Water	0.020000
Methane	0.880000
n-Butane	0.080000
n-Heptane	0.020000

Pipe data

Diameter	***5.765***	***inches***
Abs. Roughness	***0.00015***	***ft***
Terrain Profile	***Horizontal***	

Energy Data

U factor	***1***	***Btu/hr-ft2***
Surr. Temp.	***500***	***R***

Five case studies were analyzed for this system, each one corresponding to a different inlet gas flow rate. The case studies yielded a wide range of operating conditions and a variety of flow configurations. Table 7.15 summarizes the prevailing flow configuration, pressure drop and temperature decline obtained for each case study.

Table 7.15 Summary of the results obtained for the three-phase hypothetical system

Case study	Flow Pattern	Q [MMSCFD]	ΔP [psi]	ΔT [°F]
A	SS-SS	0.46	0.026	0.0002
B	SW-SW	5.00	1.613	0.1023
C	SW-AN	10.00	12.325	1.0308
D	AN-AN / AN-MT	26.00	78.902	8.2658
E	AN-MT / MT-MT	42.00	323.234	42.9071

As shown in Table 7.15, the predicted sequence of flow pattern transitions is in agreement with that reported in the literature. Flow patterns transition gradually from a fully stratified configuration at low flow rates to fully disperse at high flow rates.

Energy losses rise dramatically as gas flow rates are increased. Friction increases proportionally to the square of the fluid velocities in the pipe. Moreover, case studies exhibiting high gas flow rates show large temperature drops due to the Joule-Thomson effect.

Case Study 'A'

Stratified smooth – stratified smooth (SS-SS) was the predicted flow configuration for this case study. This flow regime is commonly found in pipes handling low gas flow rates. In SS-SS flow, the gas turbulence is not sufficient to disturb the gas-condensate or condensate-water interfaces. Water and condensate travel stratified at the bottom of the pipe showing flat and smooth interfaces.

The current case study exhibits low fluid velocities. Gas, condensate and water travel along the entire pipe at *0.52 ft/s, 0.088 ft/s* and *0.018 ft/s* respectively. Low fluid velocities produce limited friction losses and therefore a small pressure drop across the pipe (*0.026 psi*). The small pressure drop yields to a negligible temperature decline due to the Joule-Thomson effect.

The operating conditions remain nearly invariable along the entire pipe making condensate and water holdups constant along the system. Condensate and water holdups are equal to *11.87%* and *2.8%* respectively.

Case Study 'B'

The predicted flow configuration for this case study is stratified wavy – stratified wavy (SW-SW). The model anticipates that the gas turbulence is sufficient to disturb the gas-oil and oil-water interfaces. Water and condensate travel stratified at the bottom of the pipe showing concave and rough interfaces.

Gas, condensate and water travel along the pipe at nearly unchanging velocities. These velocities are *5.97 ft/s, 0.69 ft/s* and *0.29 ft/s* respectively.

Pressure losses are significantly greater than the previous case (*1.613 psi*). However, they are still small and result in slight temperature drop.

Again, pressure and temperature remain nearly constant along the pipe making condensate and water holdups remain at a steady level along the system. Condensate accumulation represents *16.54%* of the pipe volume, while water occupies *1.91%* of the pipe bore.

Case Study 'C'

Stratified wavy – annular (SW-AN) is the flow configuration predicted for this case study. The model anticipates that the gas-condensate achieves annular flow while water is still traveling stratified at the bottom of the pipe.

In this case study, fluids traveling in the pipe exhibit moderate velocities. Gas enters the pipe with a velocity of *10.79 ft/s* and leaves it at *10.97 ft/s*. Condensate velocity increases from *2.58 ft/s* at the pipe inlet to *2.60 ft/s* at the outlet, and water enters the pipe with a velocity of *1.293 ft/s* and is delivered at *1.299 ft/s*.

Moderate fluid velocities have significant impact on the energy losses along the pipe. Pressure drops *12.325 psi* across the pipe, while temperature declines *1.03 °F* due to the Joule-Thomson effect.

Pressure and temperature changes along the pipe influence the hydrodynamic behavior of the fluids. Condensate accumulation goes from *8.84%* at the pipe inlet to *8.78%* at the outlet, and water holdup also declines from *0.867%* at the pipe inlet to *0.863%* at the delivery point.

Case Study 'D'

This case study shows the model's capacity for handling three-phase flow pattern transitions. Fluids travel along most of the pipe in an annular-annular configuration (AN-AN) and transition to annular – mist flow (AN-MT) at 7240 ft from the pipe inlet. During the flow pattern transition, gas detaches the condensate from the annulus and drags it as entrained droplets in the gas stream.

As shown in Figure 7.31, pressure and temperature profiles exhibit continuous trends even during the flow pattern transition. The pipeline exhibits a large pressure drop (*78.9 psi*) and temperature declines *8.26 °F* due to the Joule-Thomson effect.

As shown in Figure 7.32, condensate velocity increases abruptly during the flow pattern transition. Condensate goes from a velocity of *7.91 ft/*s to a velocity of *26.34 ft/s* as it passes from an annular to a mist flow pattern. The increase in condensate velocity

has significant effect on the interfacial (gas-condensate) forces which is reflected as a decline in gas velocity and an increase in water velocity.

Figure 7.33 shows that the flow pattern transition influences the liquid accumulation profiles. During the flow pattern transition, condensate holdup decreases from *7.64%* to *2.36%* while water accumulation declines from *0.89%* to *0.765%*. These hydrodynamic effects are caused by changes in interfacial forces.

Case Study 'E'

The current case study presents the model ability to handle dispersed flow patterns. The model's results show that the fluids enter the pipe in an annular mist (AN-MT) flow configuration and transition to mist-mist (MT-MT) flow at a point located 2400 ft from the pipe inlet. At the transition point, the gas velocity is able to detach most of the water from the pipe wall forming a fully dispersed flow pattern.

As shown in Figure 7.34, the system exhibits high energy losses. Pressure drops *323.23 psi* across the pipe, while temperature declines *42.91 °F* due to the Joule-Thomson effect. The temperature decline makes the system approach the freezing point of the aqueous phase at the pipe outlet.

Figure 7.35 shows that water velocity increases abruptly during the flow pattern transition. Water goes from a velocity of *8.27 ft/s* to a velocity of *41.88 ft/s* as it passes from an annular to a mist flow pattern. As shown in Figure 7.36, during the flow pattern

transition water accumulation declines as this fluid is accelerated along the pipe. Water holdup decreases proportionally to the increase in fluid velocity.

After the flow pattern transition, condensate and water travel entrained in the gas stream at different velocities. Water travels at a lower velocity because it exhibits larger droplet sizes.

Material balance calculations confirm the reliability of the model for handling three-phase flow configurations. The calculated material balance approximated *1.0* along the entire pipe for all cases analyzed. The maximum deviation in the cumulative material balance was less than $5 \cdot 10^{-4}$. The model proves capable of handling different three-phase flow configurations and their transitions.

The model proves capable of capturing the qualitative behavior of flow pattern transitions. The predicted sequence of flow pattern transitions is in agreement with that reported in the literature.

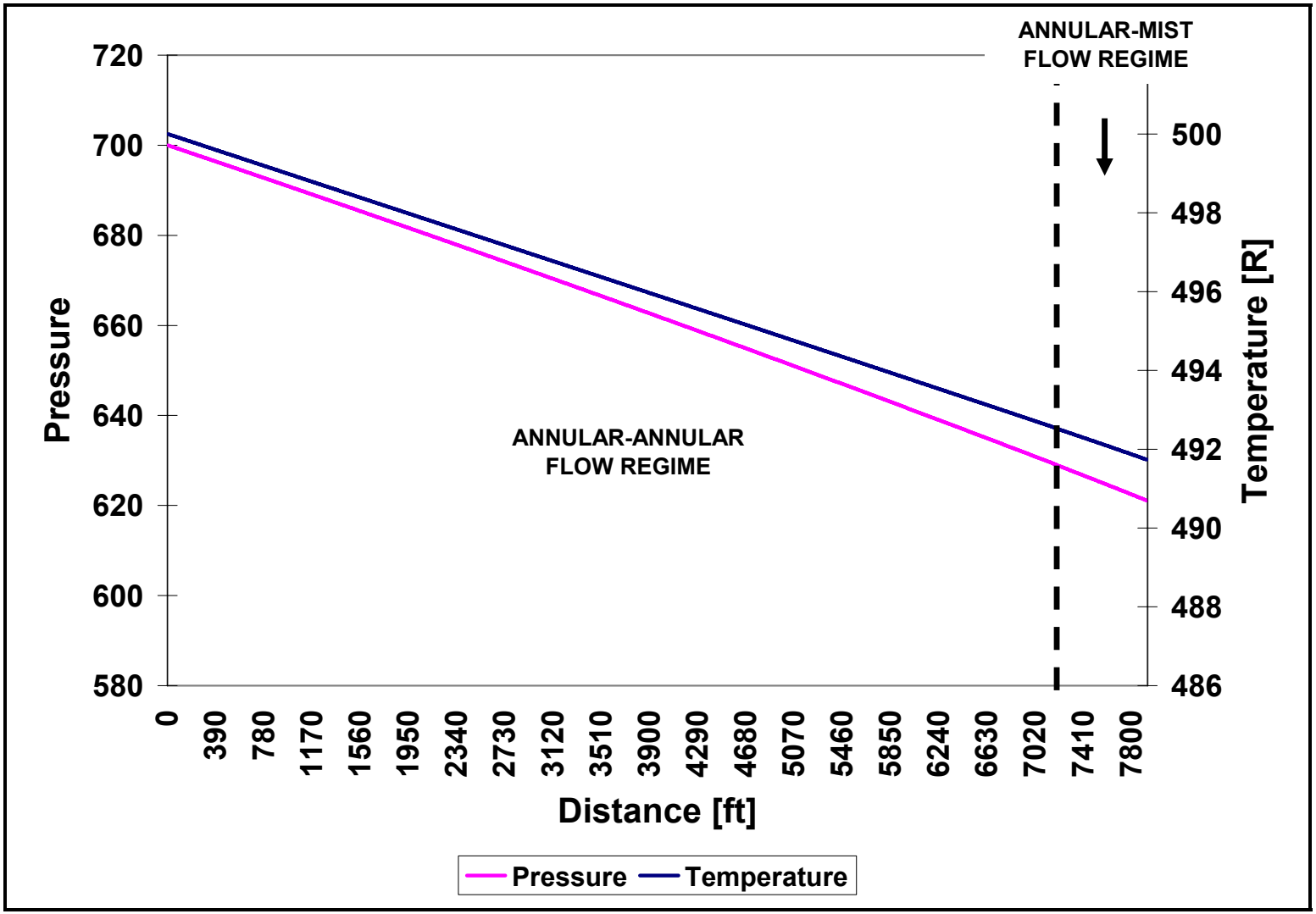

Figure 7.31 Operating conditions for case study D

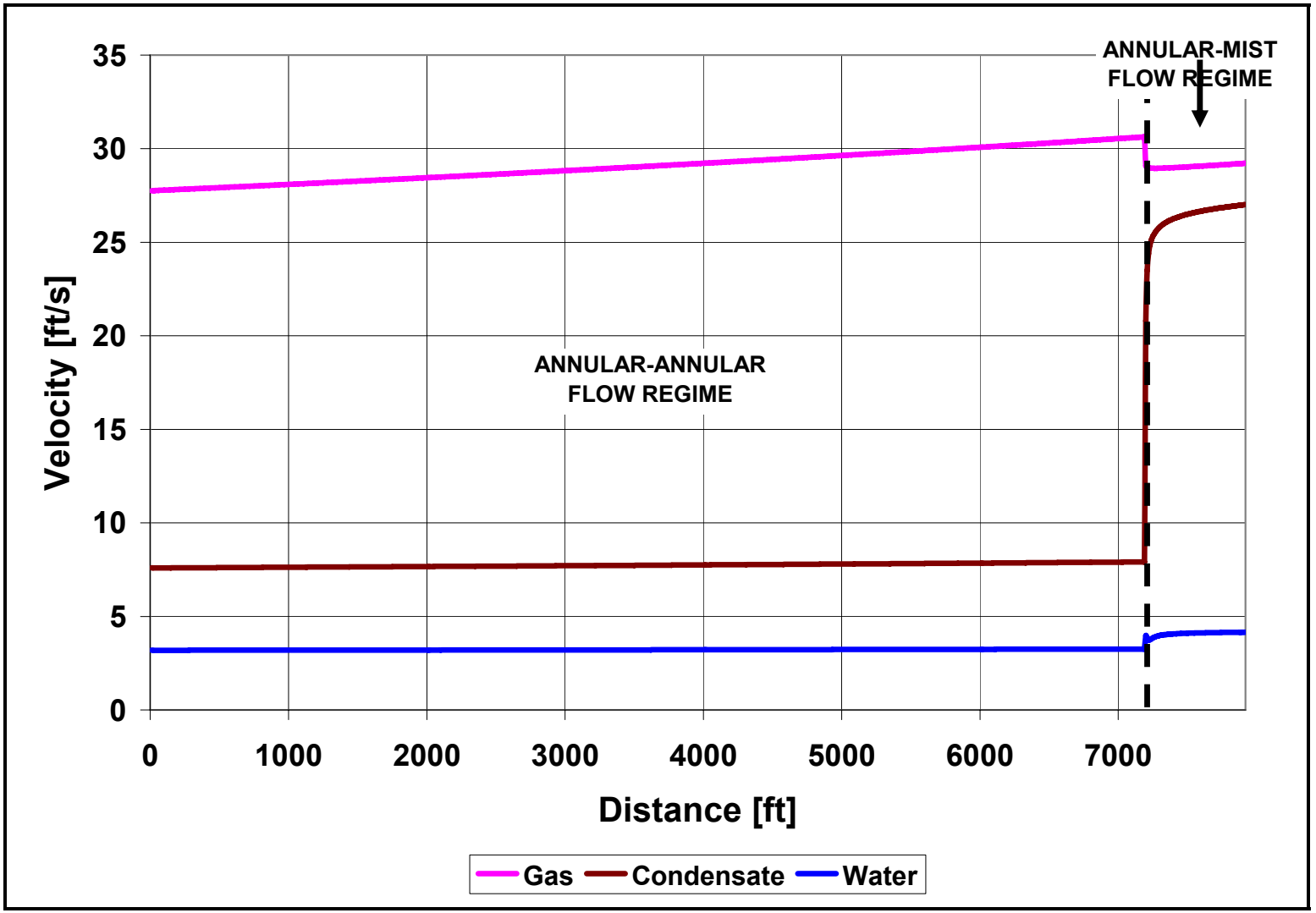

Figure 7.32 Velocity profile for case study D

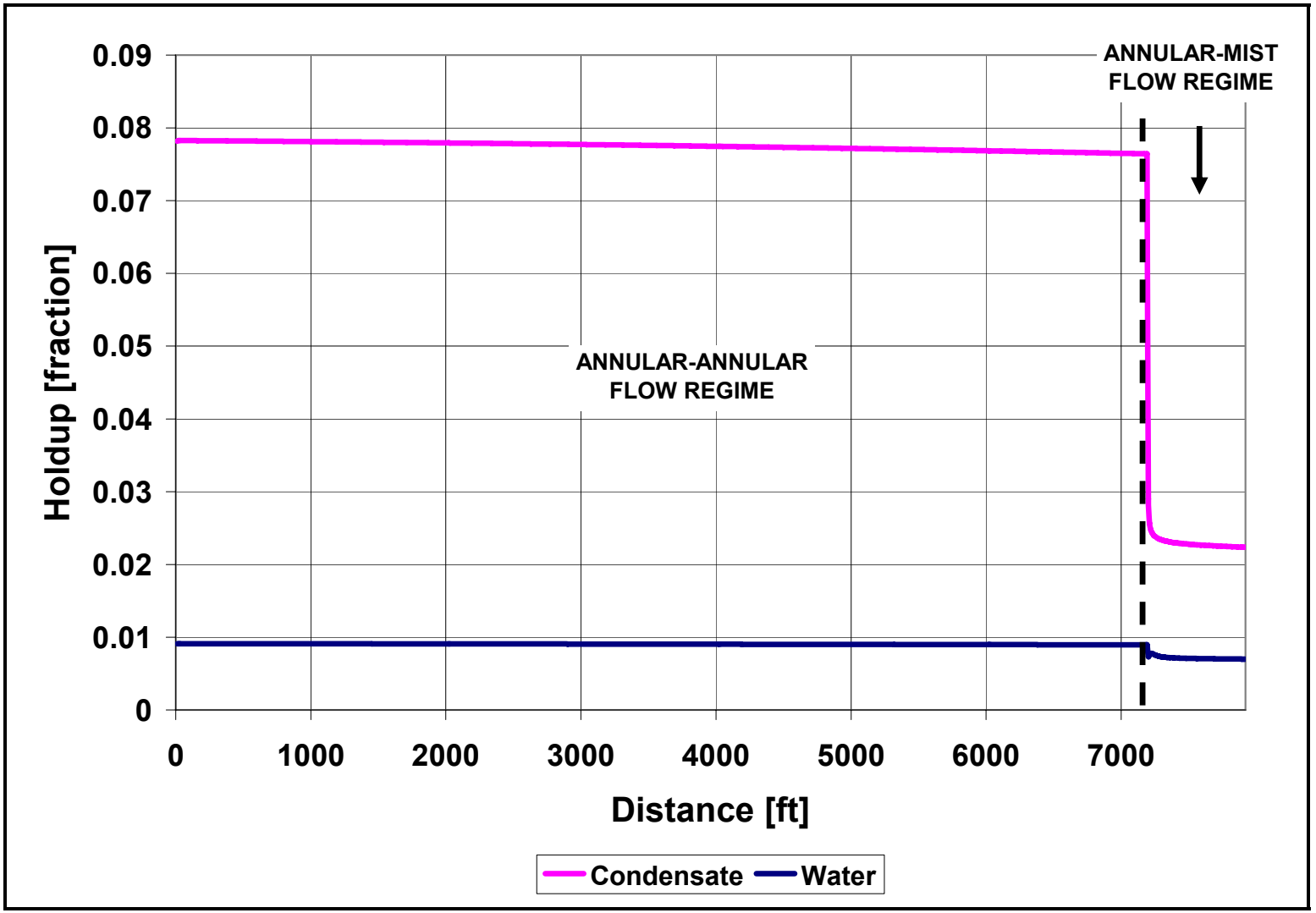

Figure 7.33 Holdup profile for case study D

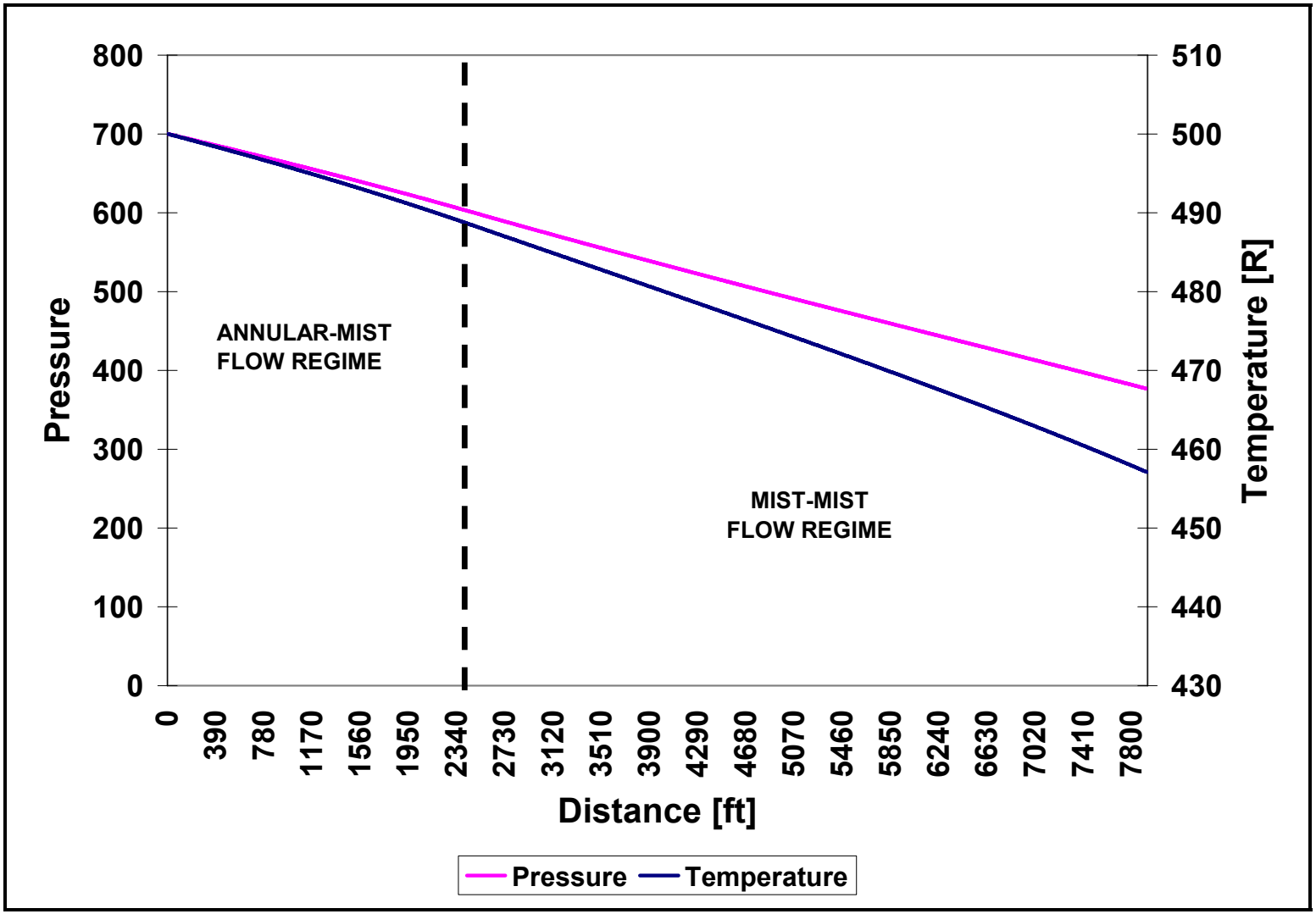

Figure 7.34 Operating conditions for case study E

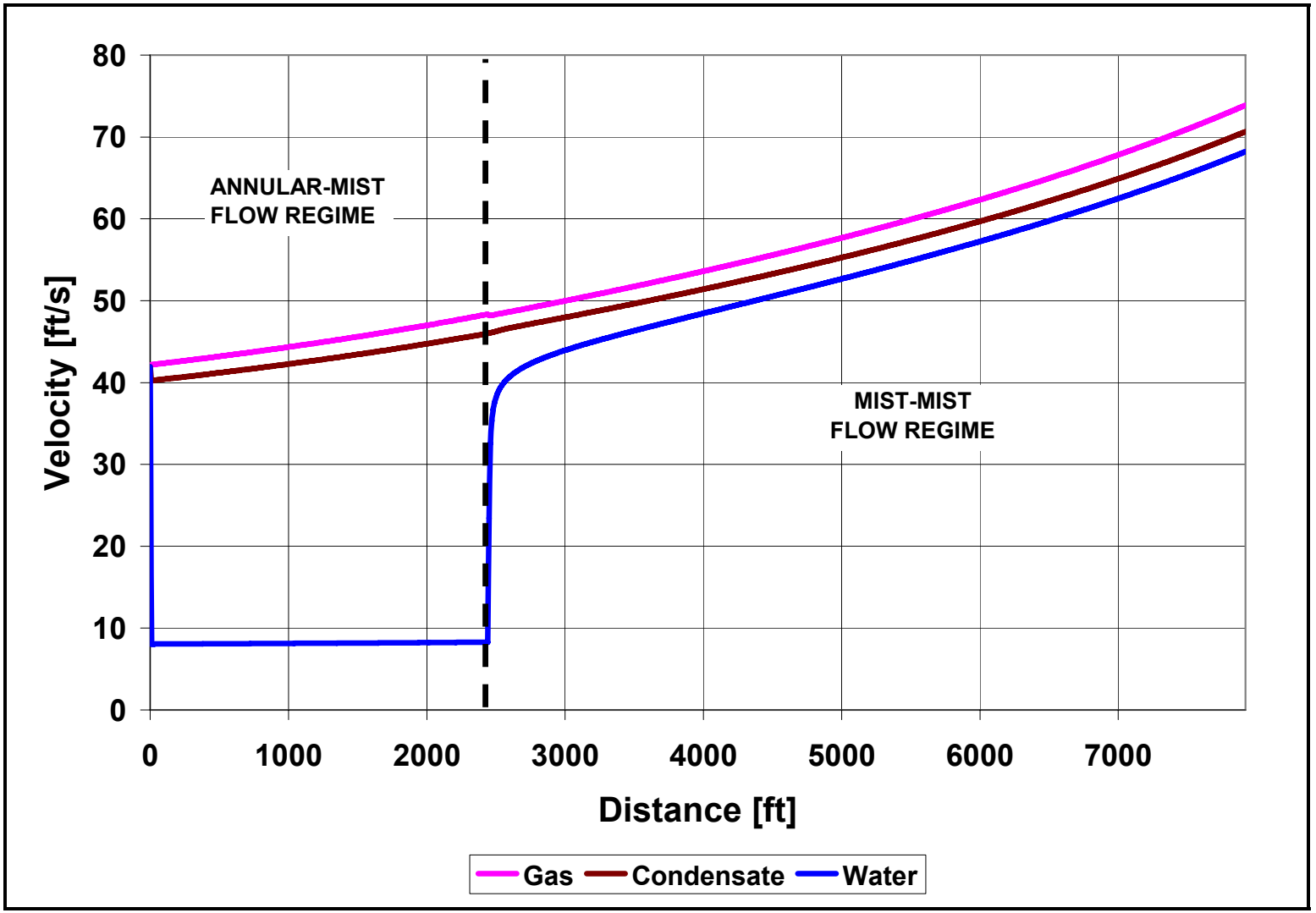

Figure 7.35 Velocity profile for case study E

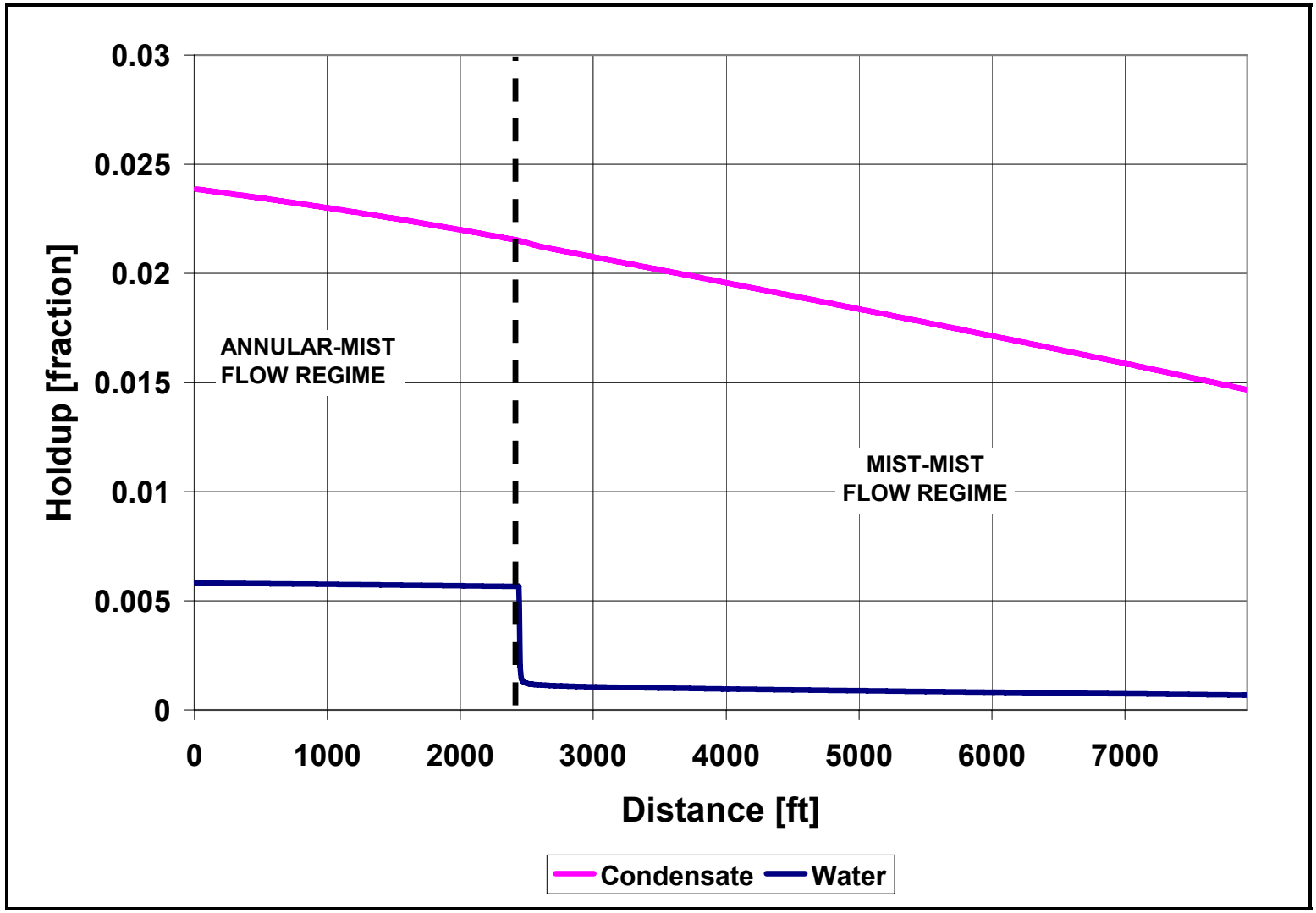

Figure 7.36 Holdup profile for case study E

CHAPTER 8

SUMMARY AND CONCLUSIONS

8.1 Summary

Three-phase flow is very common in the oil and gas industry. Most gas wells produce small fractions of condensate and water that are transported simultaneously to processing facilities. Even though this flow is of practical importance, very little progress has been made in understanding it.

The bulk of previous studies have sought to understand the mechanisms governing two-phase flow; for three-phase flow, simple extrapolation of two-phase flow is adopted due to the complexity of the problem. This approximation is erroneous for most practical cases. Three-phase flow is a challenging and complex problem. Modeling this flow involves the solution of complex thermodynamic and hydrodynamic mathematical formulations.

Three-phase flow (gas-condensate-water) poses serious problems for flow assurance engineers. The occurrence of this type of flow might reduce the flow capacity of a pipe, or provide the necessary conditions for forming substances that could adversely affect the hydraulic performance or the mechanical integrity of a piping system. Three-phase flow might set the conditions necessary for forming acids, hydrates, emulsions, waxes, or asphaltenes.

Engineers need a tool to understand how the fluids travel together, quantify the flow reduction in the pipe, and determine where, how much, and what type of liquid(s) form in a pipe. The current study addresses these needs, gaining a fundamental understanding of the thermodynamic and hydrodynamic mechanisms for two and three-phase flow.

The present work is the first attempt to develop a unified two-fluid model for two and three-phase flow in pipes. The model allows: 1) determination of flow reduction due to condensation of liquid(s) in a pipe, 2) assessment of the potential of forming substances that might affect the integrity of the pipe, and 3) evaluation of the possible measures for improving the deliverability of pipeline systems. The present study provides an novel tool that allows the Oil and Gas industry to save millions of dollars every year in the design, operation, and maintenance of pipeline systems.

8.2 Conclusions and recommendations

The unified two-fluid model developed is proven to be capable of handling systems exhibiting two-phase (gas-water and gas-condensate) and three-phase (gas-condensate-water) flow. Model predictions were compared against field and experimental data obtaining excellent matches.

Two-phase (gas-water) systems

The tool developed is the first capable of performing full-compositional modeling of systems exhibiting two-phase (gas-water) flow. The model does not require assuming, *"a priori"*, the existence of water. The model predicts the initial water condensation point in the pipeline, determines the concentration of different substances in the aqueous mixture,

and provides results for evaluating the effectiveness of acid/hydrate inhibition processes. The tool developed gives production engineers great detail about how much hydrate and corrosion inhibitors to inject and where, saving millions of dollars in the design, operation and maintenance of pipeline systems.

Two-phase (gas-condensate) systems

The current study demonstrates the model's capacity for simulating the behavior of gas-condensate systems. The model predicts pressure drop increases due to liquid condensation in the pipe, estimates the condensate composition, and handles different flow patterns and their transitions. Model predictions for systems exhibiting two-phase (gas-condensate) flow present excellent matches when compared with field data.

Three-phase (gas-condensate-water) systems

The present work proves the model's capacity for simulating the hydrodynamic behavior of systems exhibiting three-phase (gas-condensate-water) flow. Model predictions match field data. The model effectively predicted three-phase flow patterns and the forces acting on the fluids.

Currently, there is no generalized flow regime map for three-phase flow. The present work proposes a new approach for predicting the occurrence of three-phase (gas-condensate-water) flow patterns. This approach is based on expanding two-phase models and correlations for use in three-phase flow. The method developed proved capable of capturing the qualitative behavior of flow pattern transitions. The predicted sequence of

three-phase flow pattern transitions is in agreement with that reported in the literature. However, there is very limited data available for correlating flow pattern transitions in three-phase (gas-condensate-water) flow. Therefore, further research is still required for performing a quantitative evaluation of the theoretical approach proposed for estimating three-phase flow pattern transitions.

The present study classifies fully-separated three-phase flow patterns into eight idealized configurations. The geometry of these flow configurations was analyzed and closure relationships developed by expanding two-phase flow models and correlations for use in three-phase flow. These closure relationships effectively handled and predicted forces acting on the fluids. However, limited data is available for determining the forces involved in three-phase systems. Therefore, extensive experimental investigation is still required for an accurate determination of interfacial and frictional forces occurring in three-phase flow.

The model is capable of predicting the occurrence of three-phase flow conditions in the pipe. The tool predicts the formation of a second liquid phase in the system, determines its composition along with the prevailing flow configuration in the pipe.

The three-phase flow solution obtained for systems exhibiting very limited amounts of one liquid phase nearly collapses to the two-phase flow results. This fact reinforces the validity of the formulation for limit conditions.

Gravity effects

The algorithm developed is capable of handling undulated terrain effects with two- and three-phase flow systems. The effect of gravitational forces is clearly reflected in the resulting hydrodynamic profiles of the case studies analyzed. Pressure drop gradients and liquid holdups tend to decrease in downward inclined pipes and to increase in upward inclined pipe segments. Liquid velocities rise in downhill pipes and decline when climbing uphill pipes.

Flow patterns and their transitions

The model is capable of simulating the hydrodynamic behavior of single, two and three-phase flow in pipes. The number and type of phases present in the pipe is automatically determined by the thermodynamic model and the appropriate set of equations is invoked by the hydrodynamic tool. Moreover, the results show the model's ability to handle transitions from single to two-phase flow and from two to three-phase flow.

The current study includes most two and three-phase flow configurations expected for low liquid-loading conditions. The model automatically determines the prevailing flow pattern and simulates the system using an appropriate closure model. The closure models obtain good approximations of the forces acting on the fluids. However, it is also recognized that extensive research is still required for improving the accuracy of the closure models. Improvements to the closure relations may be addressed from several directions, of which some possibilities are discussed below.

For two-phase stratified flow, several researchers have noticed liquid detaching from the gas-liquid interface, droplets depositing in the upper parts of the pipe and rivulets draining down the pipe walls. Liquid deposition forms a “rough” surface in the “equivalent” gas conduit that has significant impact on the wall friction forces. Existing models for stratified wavy flow do not consider the effect of liquid deposition on the gas conduit’s roughness. The current study suggests that this roughness is greater than that of the pipe walls, and suggests that it can be related to the density and surface tension of the liquid deposited. Extensive experimental investigation is required for developing a model or correlations to take this effect into account.

Another effect observed in stratified flow is liquid droplet entrainment in the gas flow. Even though significant droplet entrainment has been reported by several researchers (Meng et al. (1999), Chen et al. (1997) and Sutharshan et al.(1995)) this study does not model this phenomenon. Stratified wavy flow conditions are far from satisfying Hinze’s criteria for diluted or dense dispersions. Therefore, the droplets detached from the liquid will eventually hit the pipe walls or return to the liquid bulk because the gas turbulence is not sufficient to support a stable dispersed flow pattern.

The current study suggests that a 7-equation formulation could be used for taking into account droplet entrainment in stratified flow. However, a model or correlation is still required for determining liquid entrainment fraction in that type of flow.

Several researchers in the field treat annular and mist flow as a combined configuration called annular-mist flow (Bendiksen et al. (1991), Issa & Tang (1994), Xiao et al. (1990) and Meng et al. (1999)). Their method treats the gas and entrained liquid droplets as a core pseudo-fluid of volumetric averaged properties. For this purpose, these authors assume that gas and entrained liquid travel at the same velocity (no-slip condition) and rely on empirical correlations for estimating the liquid entrainment fraction.

The present work proposes avoiding the no-slip assumption made in annular-mist flow by using the 7-equation formulation presented. However, it is still necessary to develop an accurate liquid entrainment correlation for the whole spectrum of annular and mist flow conditions.

The bulk of previous studies focused on the development of closure models for two-phase flow. Very little progress has been made in the development of a generalized three-phase flow regime map and closure relationships for three-phase flow. This work presents a new approach for determining flow pattern transitions in three-phase flow which proves to yield appropriate qualitative results. Moreover, closure models are proposed that effectively handle different three-phase flow patterns. However, limited experimental data is available in the literature for three-phase (gas-condensate-water) systems. Therefore, more experimental investigation is required for an accurate quantitative determination of flow patterns and modeling of forces occurring in three-phase flow.

The hydrodynamic behavior during flow pattern transitions is one of the most challenging problems still to be addressed in the two-fluid model. Assuming “sudden” flow pattern transitions implies abrupt discontinuities in the force profiles acting on the fluids. These discontinuities may lead to wrong holdup and velocity predictions. Pauchon et al. (1993) indicated that these force discontinuities are not compatible with the averaged nature of the equations of motion and suggested a protocol to avoid them. However, their approach fails to describe the physical mechanisms during flow pattern transitions. The current study recognizes the need for developing theoretical models for simulating the hydrodynamic behavior during flow pattern transitions in a pipe.

Material balances

Material balance calculations confirm the reliability of the 5 and 7-equation formulations for handling two and three-phase flow configurations. The calculated material balance approximated *1.0* along the entire pipe for all cases analyzed.

Performance of the thermodynamic model

The current study presents a thermodynamic model for performing multiphase flash calculations of typical gas well streams containing hydrocarbon mixtures, water, and hydrate inhibitors. The model proved capable of identifying the number and types of phases in equilibrium, estimating their composition, and quantifying their mass fraction in the system. The algorithm presented showed capable of performing Vapor-Liquid-equilibria (VLE), and Vapor-Liquid-Liquid-equilibria (VLLE) calculations. The hydrodynamic model was tested extensively to assess the capacity of the thermodynamic

tool for performing two and three-phase flash calculations. Millions of calculations were performed in this study obtaining accurate, fast and reliable results.

The results of the thermodynamic model evaluation are presented in appendix A. The model is capable of identifying the number of phases in equilibrium for all cases studied, and it performed two and three-phase flash calculations in a fast and reliable manner. The calculations proved to be appropriate for typical natural gas mixtures, which in some cases may contain significant fractions of non-hydrocarbon components (nitrogen, carbon dioxide, and helium). The calculations also showed an acceptable match when compared with experimental data, even for those systems that contain large fractions of polar components.

Numerical approach

Hydrodynamic modeling consists of solving the governing mass, momentum, and energy equations for different fluids traveling simultaneously in a pipe. The formulation of the governing equations for three-phase flow consists of seven ordinary differential equations. They include three mass conservation, three momentum balances, and one combined energy balance equations. This set of equations is solved numerically along the length of the pipe using the fifth-order Cash & Karp Runge-Kutta method. This method showed to be reliable and effective for performing two and three-phase flow calculations.

The present work develops the framework of a comprehensive thermo-hydrodynamic model capable of simulating two and three-phase flow in typical gas transmission

pipelines. Extension of this work could include modules for handling chemical reactions in acid forming systems and/or hydrate formation models. The flow model developed herein represents an outstanding tool that will allow flow assurance engineers to improve the design of lines, liquid collection, and separation facilities.

Moreover, future work in this research line may include extending the hydrodynamic and thermodynamic formulations proposed for performing wellbore flow simulation, and using the thermodynamic tool presented for better estimation of reservoir fluid properties in a compositional reservoir model.

REFERENCES

Açikgöz, M., França, F., and Laher Jr, R.T., An Experimental Study of Three-Phase Flow Regimes, International Journal of Multiphase Flow, v. 18, n. 3, pp. 327 - 336, 1992.

Adewumi, M.A. and Bukacek, R.F., Two-Phase Pressure Drop in Horizontal Pipelines, Journal of Pipelines, v. 5, pp. 1-14, 1985.

Adewumi, M.A., and Mucharam, L., Compositional Multiphase Hydrodynamic Modeling of Gas/Gas-Condensate Flow in Gas Pipelines, SPE Eastern Regional Meeting, Pittsburgh, October 1987.

Adewumi, M.A., Nor-Azlan, N. and Tian, S., Design Approach Accounts for Condensate in Gas Pipelines, SPE paper 26904 presented at the SPE Eastern Regional Conference and Exhibition held in Pittsburgh, Pennsylvania, November 2-4, 1993.

Agrawal, S.S., Gregory, G.A. and Govier, G.W., An Analysis of Horizontal Stratified Two-Phase Flow In Pipes, Canadian Journal of Chemical Engineering, v.51, pp. 280-286, 1973.

Andritsos, N., and Hanratty, T.J., Influence of Interfacial Waves in Stratified Gas-Liquid Flows, AIChE Journal, v. 33, pp. 444 - 454, 1987.

Ansari, A.M., Sylvester, N.D., Sarica, C., Shoham, O., and Brill, J.P., A Comprehensive Mechanistic Model for Upward Two-Phase Flow in Wellbores, SPE Paper 20630 presented at the SPE Annual Technical Conference and Exhibition held in New Orleans, Louisiana, September 23 - 26, 1990.

Antonini, G.E., Non-Isothermal Compositional Hydrodynamic Modeling of Gas and Condensate Flow in Pipelines, M.S. Thesis, The Pennsylvania State University, University Park, Pennsylvania, 2000.

Ayala, L.F., A Unified Two-Fluid Model for Multiphase Flow in Natural Gas Pipelines, M.S. Thesis, The Pennsylvania State University, University Park, Pennsylvania, 2001.

Baker, A., Nielsen, K., and Gabb, A., Pressure Loss, Liquid Holdup Calculations Developed, Oil and Gas Journal, pp. 55 - 69, 1988.

Baker, O., Design of Pipelines for the Simultaneous Flow of Oil and Gas, Oil and Gas Journal, v. 53, pp. 185, 1953.

Barnea, D., A Unified Model for Predicting Flow-Pattern Transitions for the Whole Range of Pipe Inclinations, International Journal of Multiphase Flow, v. 13, pp. 1-12, 1987.

Barnea, D., Shoham, O., and Taitel, Y., Flow Pattern Transition for Downward Inclined Two-Phase Flow; Horizontal to Vertical, Chemical Engineering Science, v.37, pp. 735-740, 1982.

Beggs, J.P., and Brill, H.D., A Study of Two-Phase Flow in Inclined Pipelines, Journal of Petroleum Technology, pp. 607-617, May 1973.

Bendiksen, K.H., Maines, D., Moe, R., and Nuland, S., The Dynamic Two-Fluid Model Olga, Theory and Application, SPE Paper 19451, SPE Production Engineering, pp. 171-180, May, 1991.

Boriyantoro, N.H., An Integrated Single / Multiphase Flow Model for Gas Condensate Pipelines, M.S. Thesis, The Pennsylvania State University, University Park, Pennsylvania, 1994.

Brady, C.J., Cunningham, J.R., and Wilson, G.M., Water-Hydrocarbon Liquid-Liquid-Vapor Equilibrium Measurements in 530 degrees F, Gas Processors Association Research Report 62, September, 1982.

Brauner, N., The Prediction of Dispersed Flow Boundaries in Liquid-Liquid and Gas-Liquid Systems, International Journal of Multiphase Flow, v.27, pp. 885-910, 2001.

Brill J. P., Arirachakaran, S.J., State of the Art in Multiphase Flow: Journal of Petroleum Technology, Volume 44, pp. 538 - 541, 1992.

Brodkey, R.S., The Phenomena of Fluid Motions, Addison-Wesley Publishing, Reading, MA, 1967.

Bunz, A. P., Dohrn, R., and Prausnitz, J. M., Three-Phase Flash Calculations for multicomponent Systems: Computers and Chemical Engineering. Volume 15, No. 1, pp. 47 - 51, 1991.

Campbell, A.N. and Anand, S.C., Densities, Excess Volumes, Surface Tensions, Viscosities and Dielectric Constants of the Systems: Methanol-Cyclohexane, Acetone-Methanol, Acetone-Cyclohexane, and Methanol-Cyclohexane-Acetone, Canadian Journal of Chemistry, v.50, n.8, pp. 1109 - 1114, April, 1972.

Carrillo, S., A Compositional Network Pipeline Model as a Tool for Decision Making, M.S. Thesis, The Pennsylvania State University, University Park, Pennsylvania, 1999.

Cash, J. R. and Karp, A. H., A variable order Runge-Kutta method for initial value problems with rapidly varying right-hand sides, ACM Transactions on. Mathematical Software, v.16, pp. 201-222, 1990.

Cawkwell, M.G., and Charles, M.E., Pressures, Temperatures Predicted for Two-Phase Pipelines, Oil and gas Journal, pp. 101-107, May 1985.

Chen, C.J., Ng, H.J., and Robinson, D.B., Solubility of Methanol or Glycol in Water-Hydrocarbon Systems, Gas Processors Association Research Report 117, March, 1988.

Chen, X., Cai, X., and Brill, J.P., Gas-Liquid Stratified Wavy Flow in Horizontal Pipelines, Journal of Energy Resources Technology, Transactions of the ASME, v.119, n.4, pp. 209-216, New York, 1997.

Cheremisinoff, N.P., and Davis, E.J., Stratified Turbulent-Turbulent Gas Liquid Flows, AIChE Journal, v. 25, pp. 48, 1979.

Chunxi, L., Wenchuan, W. and Zihao, W., A Surface Tension Model for Liquid Mixtures based on the Wilson Equation, Fluid Phase Equilibria, v. 175, pp. 185-196, 2000.

Clift, R., Grace, J.R., and Weber, M.E., Bubbles, Drops, and Particles, Academic Press, New York, 1978.

Colebrook, C.F., Turbulent Flow in Pipes with Particular Reference to the Transition Region between the Smooth and Rough Pipe Laws, Journal of the Institution of Civil Engineers (London, England), v. 11, pp. 133 - 156, 1939.

Danesh, A. and Noghrehkar, G. R., Hilly Country Gas-Condensate Pipelines, Report P-3062, Oil Service Company of Iran, August 1976.

Dukhovnaya, Y., One-Dimensional Compositional Modeling of Gas and Condensate Flow in Pipelines, M.S. Thesis, The Pennsylvania State University, University Park, Pennsylvania, 1996.

Dukler, A.E., Gas-Liquid Flow in Pipelines Research Results, AGA Project NX-28, May 1969.

Eaton, B.A., Andrews, D.E., Knowles, C.E., Silberberg, I. H., and Brown, K. E., The Prediction of Flow Patterns, Liquid Holdup, and Pressure Losses Occurring during Continuous Two-Phase Flow in Horizontal Pipelines, Trans. AIME, v. 240, pp. 815-828, 1967.

Eaton, B.A., The Prediction of Flow Patterns, Liquid Holdup and Pressure Losses Occurring During Continuous Two-Phase Flow in Horizontal Pipelines, Ph. D. Thesis, The University of Texas, Austin, TX, 1965.

Economou, I.G., and Donohue, M.D., Chemical, Quasi-Chemical and Perturbation Theories for Associating Fluids, A.I.Ch.E. Journal, Volume 37, n. 12, 1991.

Economou, I.G., and Tsonopoulos, C., Associating Models and Mixing Rules in Equations of State for Water / Hydrocarbon Mixtures, Chemical Engineering Science, Volume 52, n. 4, pp. 511 - 525, 1997.

Eltohami, E.S., Modeling of PCB Removal Processes from Natural Gas Transmission Lines, Ph.D. Thesis, The Pennsylvania State University, University Park, Pennsylvania, 2003.

Erdogmus, M., Development of a Modified Patel-Teja Equation of State, Ph. D. Thesis, The Pennsylvania State University, University Park, Pennsylvania, 2000.

Fanchi, J.R., Calculation of Parachors for Compositional Simulation: An Update, SPE Paper 19453, SPE Reservoir Engineering, August, 1990.

Fawcett, M.J., Evaluation of Correlations and Parachors To Predict Low Interfacial Tensions in Condensate Systems, SPE Paper 28611 presented at the SPE 69th Annual Technical Conference and Exhibition held in New Orleans, LA, September 25-29, 1994.

Fayed, A.S. and Otten, L., Comparing Measured and Calculated Multiphase Pressure Drop, Oil and Gas Journal, pp. 136-144, August, 1983.

Fehlberg, E., Classical fifth, sixth, seventh, and eighth order Runge Kutta formulas with stepsize control, Tech. Rep. TR R-287, NASA, 1968.

FERC NGC+ Liquid Hydrocarbon Drop Out Task Group, White Paper on Liquid Hydrocarbon Dropout in Natural Gas Infrastructure, February 28, 2005.

Ghosh, P., Prediction of Vapor-Liquid Equilibria Using Peng-Robinson and Soave-Redlich-Kwong Equations of State, Chemical Engineering Technology, Volume 22, n. 5, 1999.

Gonzalez, M.H., and Lee, A.L., Dew and Bubble Points of Simulated Natural Gases, Journal of Chemical and Engineering Data, v. 13, n. 2, pp. 172 - 176, 1968.

Gregory, G.A., and Aziz, K., Design of Pipelines for Multiphase (Gas/Gas-Condensate) Flow, Journal of Canadian Petroleum Technology, pp. 28-33, July 1975.

Grolman, E. and Fortuin, J.M.H, Gas-Liquid Flow in Slightly Inclined Pipes, Chemical Engineering Science, v.52, n.24, pp. 4461-4471, 1997a.

Grolman, E. and Fortuin, J.M.H, Liquid Holdup, Pressure Gradient, and Flow Patterns in Inclined Gas Liquid Pipe Flow, Experimental and Fluid Science, v.15, pp. 174-182, 1997b.

Guo, J.H., Luo, Y., Augustsson, A., Kashtanov, S., Rubensson, J.E., Shuh, D.K., Agren, H., and Nordgren, J., Molecular Structure of Alcohol-Water Mixtures, Physical Review Letters, v. 91, n. 15, pp. 157401, October, 2003.

Guzhov, A.I., Medvedev, V.F., and Savelev, V.A., Movement of Gas-Water-Oil Mixtures Through Pipelines, International Chemical Engineering, v.14, pp.713-714, 1974.

Hall, A.R.W., Multiphase Flow of Oil, Water and Gas in Horizontal Pipe, Ph. D. Thesis, Imperial College of Science, Technology and Medicine, University of London, UK, 1992.

Hart, J., Hamersma, P.J. and Fortuin, J.M., Correlations Predicting Pressure Drop and Liquid Holdup During Horizontal Gas-Liquid Pipe Flow with a Small Liquid Holdup, International Journal of Multiphase Flow, v.15, pp. 947-964, 1989.

Heidemann, R. A., 1974, Three-phase equilibria using equations of state: AIChE Journal, Volume 20, 844 - 855, September 1974.

Herning, F. and Zipperer, L., Calculation of the Viscosity of Technical Gas Mixtures from the Viscosity of Individual Gases, Gas U. Wasserfach, v. 79, n. 49, pp. 69, 1936.

Hinze, J., Fundamentals of the Hydrodynamic Mechanism of Splitting in Dispersion Processes, AICHE Journal, v.1, n.3, pp.289-295, 1955.

Hough, E.W. and Stegemeier, G.L., Correlation of Surface and Interfacial Tension of Light Hydrocarbons in the Critical Region, SPE Journal, pp. 259-263, December, 1961.

Huang, S. S., Leu, A. D., Ng, H. J., and Robinson D. B., The phase behavior of two mixtures of methane, carbon dioxide, hydrogen sulfide, and water: Fluid Phase Equilibria, Volume 19, p.p. 21 - 32, 1985.

Hubbard, M.G. and Dukler, A.E., The Characterization of Flow Regimes for Horizontal Two-Phase Flow, Proc. Heat Transfer and Fluid Mechanics Conference, Santa Clara, California, pp. 100-121, 1966.

Hughes, E.D, Lyczkowski, R.W. and McFadden, J.H., An Evaluation of State-of-the-Art Two-Velocity Two-Phase Flow Models and their Applicability to Nuclear Transient Analysis, Volume 2: Theoretical Basis, Electric Power Research Institute EPRI NP-143, 1976.

Hugill, J.A. and van Welsenes, A.J., Surface Tension: A Simple Correlation for Natural Gas and Condensate Systems, Fluid Phase Equilibria, v.29, pp. 383-390, 1986.

Huron, M. J., and Vidal, J., New Mixing Rules in Simple Equations of State for Representing Vapor-Liquid-Equilibria of Strongly Non-Ideal Mixtures: Fluid Phase Equilibria, Volume 3, pp. 255, 1979.

Isdale, J.D., Easteal, A.J., and Woolf, L.A., Shear Viscosity of Methanol + Water Mixtures Under Pressure, International Journal of Thermophysics, Volume 6, n. 5, pp. 439 - 451, 1985.

Ishii, M. and Mishima, K., Droplet Entrainment Correlation in Annular Two-Phase Flow, International Journal of Heat and Mass Transfer, v.32, n.10, pp. 1835-1846, 1989.

Issa, R.I. and Tang, Z.F., Prediction of Pressure Drop and Holdup in Gas-Liquid Flow in Pipes using the Two-Fluid Model, SPE Paper 22534 (Unsolicited), 1991.

Jamari, S., Experimental Study of the Stratified/Slug-Annular Flow Regime Transition in Two-Phase (air-liquid) Flow in a Horizontal Pipe, Ph. D. Thesis, Imperial College of Science, Technology and Medicine, London, United Kingdom, 2006.

Jeffreys, H., On the Formation of Water Waves by Wind, Proceedings of the Royal Society, A110, pp. 241, 1926.

Jossi, J.A., Stiel, L.I., and Thodos, G., The Viscosity of Pure Substances in the Dense Gaseous and Liquid Phases, AIChE Journal, Volume 8, pp. 59, 1962.

Kaya, A.S., Sarica, C., and Brill, J.P., Comprehensive Mechanistic Model of Two-Phase Flow in Deviated Wells, SPE Paper 56522 presented at the SPE Annual Technical Conference and Exhibition held in Houston, Texas, October 3 - 6, 1999.

Khor, S.H., Mendes-Tatsis, M.A., and Hewitt, G.F., One-Dimensional Modeling of Phase Holdups in Three-Phase Stratified Flow, International Journal of Multiphase Flow, v. 23, n. 5, pp. 885 - 897, 1997.

Khor, S.H., Three-Phase Liquid-Liquid-Gas Stratified Flow In Pipelines, Ph. D. Thesis, Imperial College of Science, Technology and Medicine, London, United Kingdom, 1998.

Kowalski, J.E., Wall and Interfacial Shear Stresses in Stratified Flow in a Horizontal Pipe, AIChE Journal, v. 33, n. 2, pp. 274 - 281, 1987.

Kristensen, J.N., and Christensen, P.L., A Combined Soave-Redlich-Kwong and NRTL Equation for Calculating the Distribution of Methanol between Water and Hydrocarbon Phases, Fluid Phase Equilibria, v. 82, pp. 199 - 206, 1993.

Laflin, G.C., and Oglesby, K.D., An Experimental Study On The Effects of Flowrate, Water Fraction and Gas-Liquid Ratio on Air-Oil-Water Flow In Horizontal Pipes, B. Sc. Thesis, University of Tulsa, USA.

Lee, A.H., and Jepson, W.P., Experimental Study of Flow Pattern of Oil-Water-Gas Mixture in Horizontal Pipelines, Corrosion / 92, NACE International Annual Conference and Exposition, Paper 92194, Nashville, TN, April, 1992.

Lee, A.L., Gonzalez, M.H., and Eakin, B.E., The Viscosity of Natural Gases, SPE Paper 1340, Journal of Petroleum Technology, 997-1000, August 1966.

Lee, S.T. and Chien, M.C.H., A New Multicomponent Surface Tension Correlation Based on Scaling Theory, SPE Paper 12643 presented at the SPE/DOE Symposium on Enhanced Oil Recovery, Tulsa, Oklahoma, April 15-18, 1984.

Lindeloff, N., and Michelsen, M.L., Phase Envelope Calculations for Hydrocarbon-Water Mixtures, SPE Paper 77770, presented at the SPE Annual Technical Conference and Exhibition held in San Antonio, Texas, September 29 - October 2, 2003.

Lockhart, R.W., and Martinelli, R.C., Proposed Correlations of Data for Isothermal Two-Phase, Two-Component Flow in Pipes, Chemical Engineering Progress, v. 45, pp. 39 - 48, January 1949.

Lohrenz, J., Bray, B. and Clark, C., Calculating Viscosities of Reservoir Fluids from their Compositions, SPE Paper 915, Journal of Petroleum Technology, pp. 1171-1176, October 1964.

Lunde, K., Nuland, S., and Lingelem, M., Aspects of Three-Phase Flows in Gas Condensate Pipelines, 6th Conference on Multiphase Production, Cannes, France, June 16 -18, 1993.

Macleod, D.B., On a relation between surface tension and density, Transactions of the Faraday Society, v.19, pp. 38-42, 1923.

Malinowski, M.S., An Experimental Study of Oil-Water and Oil-Water-Gas Flowing Mixtures in Horizontal Pipes, M.S. Thesis, University of Tulsa, Oklahoma, 1975.

Mandhane, J.M., Gregory, G.A., and Aziz, K., A Flow Pattern Map for Gas-Liquid Flow In Horizontal Pipes, International Journal of Multiphase Flow, v.1, pp. 537-553, 1974.

Martinez, A.F., Two-Phase Gas-Condensate Flow in Pipeline Open-Network Systems, M.S. Thesis, The Pennsylvania State University, University Park, Pennsylvania, 1994.

Mc Ketta, J.J., and Katz, D.L., Methane-n-Butane-Water System in Two- and Three-Phase, Industrial and Engineering Chemistry, v. 40, n. 5, pp. 853 - 863, 1948.

Meissner, H.P. and Michaels, A.S., Surface Tensions of Pure Liquids and Liquid Mixtures, Industrial and Engineering Chemistry, v.41, n.12, pp. 2781-2787, December, 1949.

Meng, W., Chen, X.T., Kouba, G.E., Sarica, C., and Brill, J.P., Experimental Study of Low Liquid Loading Gas-Liquid Flow in Near Horizontal Pipes, SPE Paper 56466 presented at the SPE Annual Technical Conference and Exhibition held in Houston, TX, October, 1999.

Michelsen, M.L., A Modified Huron-Vidal Mixing Rule for Cubic Equations of State, Fluid Phase Equilibria, Volume 60, pp. 213, 1990.

Michelsen, M.L., Calculation of Multiphase Equilibrium, Computers and Chemical Engineering, Volume 18, n. 7, pp. 545 - 550, 1994.

Michelsen, M.L., Some Aspects of Multiphase Calculations, Fluid Phase Equilibria, Volume 30, pp. 15 - 29, 1986.

Michelsen, M.L., The Isothermal Flash Problem. Part I. Stability, Fluid Phase Equilibria, Volume 9, pp. 1-19, 1982a.

Michelsen, M.L., The Isothermal Flash Problem. Part II. Phase Split Calculation, Fluid Phase Equilibria, Volume 9, pp. 21-40, 1982b.

Miqueau, C., Mendiboure, B., Graciaa, A. and Lachaise, J., Modeling of the Surface Tension of Multicomponent Mixtures with the Gradient Theory of Fluid Interfaces, Industrial and Engineering Chemistry - Research, v.44, pp. 3321 - 3329, 2005.

Miya, M., Woodmansee, D.E., and Hanratty, T.J., A Model for Roll Waves in Gas-Liquid Flow, Chemical & Engineering Science, v. 26, pp. 1915, 1971.

Mollerup, J.M., A Note on the Derivation of Mixing Rules from Excess Gibbs Free Energy Models, Fluid Phase Equilibria, Volume 25, pp. 323 - 326, 1986.

Mucharam, L., Adewumi M.A., and Watson, R.W., Study of Gas Condensation in Transmission Pipelines with a Hydrodynamic Model, SPE Paper 18234, SPE Production Engineering, v. 5, n. 3, August 1990.

Mucharam, L., and Adewumi M.A., Compositional Multiphase Hydrodynamic Modeling of Gas/Gas-Condensate Dispersed Flow in Gas Pipelines, SPE Paper 17056, SPE Production Engineering, v. 5, n. 1, pp. 85 - 90, February 1990.

Mucharam, L., One-Dimensional Compositional Modeling of Gas and Condensate Flow in Pipelines, Ph. D. Thesis, The Pennsylvania State University, University Park, Pennsylvania, 1990.

Nasr-El-Din, H.A., Al-Otaibi, M.B., Al-Aamri, A.M. and Ginest, N., Surface Tension of Completion Brines, SPE Paper 93421 presented at the SPE International Symposium on Oilfield Chemistry held in Houston, TX, February 2-4, 2005.

Nelson, P. A., Rapid Phase Determination in Multiple-Phase Flash Calculations: Computers and Chemical Engineering, Volume 11, No. 6, pp. 581-591, 1987.

Nordin, N., Multiphase Equilibria of PCB-Contaminated Natural Gas Systems, Ph. D. Thesis, The Pennsylvania State University, University Park, Pennsylvania, 1997.

Oliemans, R.V., Pots, B.F. and Trompe, N., Modeling of Annular Dispersed Two-Phase Flow in Vertical Pipes, International Journal of Multiphase Flow, v.12, n.5, pp. 711-732, 1986.

Orbey, H., and Sandler, S.I., Modeling Vapor-Liquid Equilibria - Cubic Equations of State and Their Mixing Rules, Cambridge University Press, United Kingdom, 1998.

Pan, L., High Pressure Three-Phase (Gas-Liquid-Liquid) Flow, Ph. D. Thesis, Imperial College of Science, Technology and Medicine, University of London, UK, 1996.

Pan, L., Jayanti, S., and Hewitt, G.F., Flow Patterns, Phase Inversion, and Pressure Gradient in Air-Oil-Water Flow in a Horizontal Pipe, Proceedings of the 2nd International Conference on Multiphase Flow held in Kyoto, Japan, April 3 - 7, 1995.

Parikh, J.S., Bukacek, R.F., Graham, L., and Leipziger, S., Dew and Bubble Point Measurements for a Methane-Ethane-Propane Mixture, Journal of Chemical and Engineering Data, v. 29, pp. 301 - 303, 1984.

Passut, C.A. and Danner, R.P., Correlation of Ideal Gas Enthalpy, Heat Capacity, and Entropy, Industrial & Engineering Chemical Process Design and Development, v. 11, n. 4, pp. 543 - 546, 1972.

Patel, N. C., and Teja, A. S, A new cubic equation of state for fluids and fluid mixtures: Chemical Engineering Science. Volume 37, No. 3, pp. 463 - 473, 1982.

Pauchon, C., Dhulesia, H., Lopez, D., and Fabre, J., TACITE: A Comprehensive Mechanistic Model for Two-Phase Flor, Paper presented at the 6th International Conference on Multiphase Production, Cannes, France, June 16-18, 1993.

Pedersen, K. S., Blilie, A.L., and Meisingset, K.K., PVT Calculations on Petroleum Reservoir Fluids Using Measured and Estimated Compositional Data for the Plus Fraction, Industrial & Chemical Engineering Research, Volume 31, pp. 1378 - 1384, 1992.

Pedersen, K. S., Michelsen, M.L., and Fredheim, A.O., Phase Equilibrium Calculations for Unprocessed Well Streams Containing Hydrate Inhibitors, Fluid Phase Equilibria, Volume 126, pp. 13 - 28, 1996.

Pedersen, K. S., Milter, J., and Rasmussen, C.P., Mutual Solubility of Water and a Reservoir Fluid at High Temperatures and Pressures - Experimental and Simulated Data, Fluid Phase Equilibria, Volume 189, pp. 85 - 97, 2001.

Pedersen, K.S., Thomassen, P., and Fredenslund, A., Characterization of Gas Condensate Mixtures, Advanced Thermodynamics, v. 1, pp. 137 - 152, 1989.

Peng D. Y., and Robinson, D. B., 1976, Two and three phase equilibrium calculations for systems containing water: The Canadian Journal of Chemical Engineering, v. 54, 595 - 599, December 1976b.

Peng D. Y., and Robinson, D. B., Two and three phase equilibrium calculations for coal gasification and related processes: The Canadian Journal of Chemical Engineering, Volume 54, 393 - 414, December 1980.

Peng D.Y. and Robinson D.B., A New Two-Constant Equation of State, Industrial Engineering & Chemistry Fundamentals, v. 15, n.1, 1976a.

Poling, B.E., Prausnitz, J.M., and O'Connell, J.P., The Properties of Gases and Liquids, McGraw Hill, fifth edition, 2001.

Press, W.H., Teukolsky, S.A., Vetterling, W.T., and Flannery, B.P., Numerical Recipes in Fortran: The Art of Scientific Computing, Cambridge University Press, Second edition, Second Reprint, pp. 701 - 716, 1994.

Rachford, H.H. Jr., and Rice, J.D., Procedure for Use of Electrical Digital Computers in Calculating Flash Vaporization Hydrocarbon Equilibrium, Journal of Petroleum Technology, v.4, sec.1, p.19, and sec. 2, p.3, October, 1952.

Redlich, O., and Kwong, J.N., On the Thermodynamics of Solutions. V. An Equation of State, Fugacities of Gaseous Solutions, Chemistry Review, Volume 44, pp. 233 - 244, 1949.

Renon, H., and Prausnitz, J.M., Local Composition in Thermodynamic Excess Functions for Liquid Mixtures, A.I.Ch.E. Journal, v. 14, pp. 135 - 144, 1968.

Risnes, R., Dalen, V., and Jessen, J.I., Phase Equilibrium Calculations in the Near-Critical Region, Elsevier Sequoia, SA, Proceedings of the European Symposium on EOR, pp. 329-350, Lausanne, 1981.

Roberts, I., Modeling and Experimental Studies of Transient Stratified Multiphase Flows, Ph. D. Thesis, Imperial College of Science, Technology and Medicine, University of London, UK, 1996.

Sadegh, A.A. and Adewumi, M.A., Temperature Distribution in Natural Gas/Condensate Pipelines Using a Hydrodynamic Model, SPE Paper 97978 presented at the SPE Eastern Regional Meeting held in Morgantown, WV, September 14-16, 2005.

Sastri, S.R.S. and Rao, K.K., A Simple Method to Predict Surface Tension of Organic Liquids, The Chemical Engineering Journal, v.59, pp. 181-186, 1995.

Schechter, D.S. and Guo, B., Parachors Based on Modern Physics and Their Uses in IFT Prediction of Reservoir Fluids, SPE Reservoir Evaluation & Engineering, June, 1998.

Shinta A. A., Firoozabadi, A., Equation of State Representation of Aqueous Mixtures Using an Association Model: The Canadian Journal of Chemical Engineering, Volume 73, June, 1995.

Shinta, A.A., and Firoozabadi, A., Predicting Phase Behavior of Water / Reservoir-Crude Systems With the Association Concept, SPE Paper 27872, presented at the SPE Western Regional Meeting held in Long Beach, California, March 23 - 25, 1994.

Soave, G., Equilibrium Constants from a Modified Redlich-Kwong Equation of State, Chemical Engineering Science, v. 27, pp. 1197, 1972.

Sobocinski, D.P., Horizontal Co-Current Flow of Water, Gas-Oil and Air, M.S. Thesis, University of Oklahoma, 1955.

Sprow, F.B. and Prausnitz, J.M., Surface Tension of Simple Liquid Mixtures, Transactions of the Faraday Society, v.62, pp. 1105, 1966a.

Sprow, F.B. and Prausnitz, J.M., Surface Tensions of Simple Liquids, Transactions of the Faraday Society, v.62, pp. 1097, 1966.

Stapelberg, H.H., and Mewes, D., The Flow of Two Immiscible Liquids and Air in a Horizontal Pipe - Pressure Drop and Flow Regimes, European Two-Phase Flow Group Meeting, Varese, May 21 - 24, 1990b.

Stapelberg, H.H., and Mewes, D., The Flow of Two Immiscible Liquids and Air in a Horizontal Pipe, Advances in Gas-Liquid Flow, pp. 89-96, 1990a.

Stapelberg, H.H., and Mewes, D., Three-Phase Flow (Oil, Water, Gas) in Horizontal Tubes, Proceeding of the International Conference on Multiphase Flows, Tsukuba, Japan, September 24-27, 1991.

Suarez, J.T., Torres-Marchal, C. and Rasmussen, P., Prediction of Surface Tensions of Nonelectrolyte Solutions, Chemical and Engineering Science, v.44, n.3, pp. 782-786, 1989.

Sugden, S., The Variation of Surface Tension with Temperature and some Related Functions, Journal of Chemical Society, v.125, pp. 32, 1924.

Sutharshan, B., Kawaji, M. and Ousaka, A., Measurement of Circumferential and Axial Liquid Film Velocities in Horizontal Annular Flow, International Journal of Multiphase Flow, v.21, n.2, pp.193-206, 1995.

Szyszkowski, B. von, Capillary Properties of Aqueous Solutions of Fatty Acids, Z. Physik. Chem., v.64, pp. 385, 1908.

Taitel, Y., and Dukler A.E., A Model for Predicting Flow Regime Transitions in Horizontal and Near Horizontal Gas Liquid Flow, A.I.Ch.E. Journal, v. 22, n. 1, pp. 47 - 55, 1976.

Taitel, Y., Barnea, D., and Brill, J.P., Stratified Three-Phase Flow in Pipes, International Journal of Multiphase Flow, v. 21, pp. 53 - 60, 1995.

Tamura, M., Kurata, M. and Odani, H., Practical Method for Estimating Surface Tension of Solutions, Journal of the American Chemical Society, v.28, pp. 83-88, 1955.

Teja, A.S., and Rice, P., Generalized Corresponding States Method for the Viscosities of Liquid Mixtures, Industrial & Engineering Chemistry Fundamentals, v. 20, pp. 77 - 81, 1981.

Trebble, M. A., A Preliminary Evaluation of Two and Three Phase Flash Initiation Procedures: Fluid Phase Equilibria, v. 53, pp. 113-122, 1989.

Ulke, A., A Study of a Two-Component Two-Phase Flow System in One Dimension, Eds. Veziroglu, T.N. and Bergles, A.E., Multi-Phase Flow and Heat Transfer III, Part A, Fundamentals, Elsevier, pp. 59-77, 1984.

Van Der Waals, J. (1873), The Equation of State for Gases and Liquids, Nobel Lectures in Physics, Volume 1, pp. 254 - 265, Elsevier, Amsterdam, 1967.

Vidal, J., Thermodynamics - Applications in Chemical Engineering and the Petroleum Industry, Technip Editions, pp. 301, Paris, 2003.

Vincent, P.A., and Adewumi M.A., Engineering Design of Gas-Condensate Pipelines with a Compositional Hydrodynamic Model, SPE Paper 18543, SPE Production Engineering, v. 5, n. 4, pp. 381 - 386, November 1990.

Vincent, P.A., One-Dimensional Compositional Modeling of Gas and Condensate Flow in Pipelines, M.S. Thesis, The Pennsylvania State University, University Park, Pennsylvania, 1988.

Wallis, G.B., One-Dimensional Two-Phase Flow, McGraw-Hill Book Company, 1969.

Weinaug, C.F. and Katz, D.L., Surface Tension of Methane-Propane Mixtures, Industrial and Engineering Chemistry, v.25, 32, 1943.

Weismann, J., Duncan, D., Gibson, J., and Crawford, T., Effects of Fluid properties and Pipe Diameter on Two-Phase Flow Patterns in Horizontal Lines, International Journal of Multiphase Flow, v.5, pp. 437-462, 1979.

Wilkes, J.O., Fluid Mechanics for Chemical Engineers, Prentice Hall PTR Upper Saddle River, New Jersey, pp. 142 - 143, 1999.

Wong, D.S. and Sandler, S.I., A Theoretically Correct Mixing Rule for Cubic Equations of State, AIChE Journal, v. 38, n. 5, pp. 671 - 680, May 1992.

Xiao, J., A Comprehensive Mechanistic Model for Two-Phase Flow in Pipelines, M.S. Thesis, University of Tulsa, Tulsa, Oklahoma, 1990.

Xiao, J.J, Shoham, O. and Brill, J.P., A Comprehensive Mechanistic Model for Two-Phase Flow in Pipelines, SPE Paper 20631 presented at the SPE Annual Technical Conference and Exhibition in New Orleans, LA, September 23-26, 1990.

Xiao, J.J, Shoham, O. and Brill, J.P., Evaluation of Interfacial Friction Factor Prediction Methods for Gas/Liquid Stratified Flow, SPE Paper 22765 presented at the SPE Annual Technical Conference and Exhibition in Dallas, TX, October 6-9, 1991.

Yakoumis, I.V., Kontogeorgis, G.M., Voutsas, E.C., and Tassios, D.P., Vapor-Liquid Equilibria for Alcohol/Hydrocarbon systems Using the CPA Equation of State, Fluid Phase Equilibria, Volume 130, pp. 31 - 47, 1997.

Zhang, H.Q., and Sarica, C., Unified Modeling of Gas/Oil/Water Pipe Flow - Basic Approaches and Preliminary Validation, SPE Paper 95749 presented at the SPE Annual Technical Conference and Exhibition held in Dallas, Texas, October 9 - 12, 2005.

Zhibao, L., Lu, B.C., A Molecular Model for Representing Surface Tension for Polar Liquids, Chemical Engineering Science, v.56, pp. 6977-6987, 2001.

Zhibao, L., Shiquan, S., Meiren, S., Jun, S., Prediction of Surface Tension of Binary and Multicomponent Non-electrolyte Liquid Mixtures by UNIFAC Group Contribution Method, Journal of Chemical Industry and Engineering (China), v.1, pp. 17-24, 1991.

Zuo, Y.X. and Stenby, E.H., Corresponding-States Parachor Models for the Calculation of Interfacial Tensions, The Canadian Journal of Chemical Engineering, v.75, pp. 1130-1137, 1997.

APPENDIX A

MATRIX FORM OF THE GOVERNING EQUATIONS

FOR THREE-PHASE FLOW

The set of ordinary differential equations for modeling three-phase flow in pipes can be written in a matrix form as follows:

$$\begin{bmatrix} a_{11} & a_{12} & 0 & a_{14} & 0 & a_{16} & a_{17} \\ a_{21} & a_{22} & 0 & a_{24} & 0 & a_{26} & a_{27} \\ a_{31} & 0 & a_{33} & a_{34} & 0 & 0 & a_{37} \\ a_{41} & 0 & a_{43} & a_{44} & 0 & 0 & a_{47} \\ a_{51} & 0 & 0 & 0 & a_{55} & a_{56} & a_{57} \\ a_{61} & 0 & 0 & 0 & a_{65} & a_{66} & a_{67} \\ a_{71} & a_{72} & a_{73} & a_{74} & a_{75} & a_{76} & a_{77} \end{bmatrix} \frac{d}{dx} \begin{bmatrix} P \\ v_g \\ v_{Lh} \\ \alpha_{Lh} \\ v_{Lw} \\ \alpha_{Lw} \\ T \end{bmatrix} = \begin{bmatrix} 0 \\ b_2 \\ 0 \\ b_4 \\ 0 \\ b_6 \\ b_7 \end{bmatrix} \qquad \text{(A.1)}$$

The governing equations were organized in order to avoid the appearance of zeros in the main diagonal of the matrix. The elements in matrices $[A_m]$ and $[B_m]$ are calculated in field units using the following expressions:

$$a_{11} = \alpha_g v_g \left(\frac{\partial \rho_g}{\partial P} \right)_T - G_m \left(\frac{\partial f_{mg}}{\partial P} \right)_T$$

$$a_{12} = \alpha_g \rho_g$$

$$a_{14} = -\rho_g v_g$$

$$a_{16} = -\rho_g v_g$$

$$a_{17} = \alpha_g v_g \left(\frac{\partial \rho_g}{\partial T} \right)_P - G_m \left(\frac{\partial f_{mg}}{\partial T} \right)_P$$

$$a_{21} = \frac{\alpha_g v_g^2}{g_c} \left(\frac{\partial \rho_g}{\partial P} \right)_T + 144 \alpha_g$$

$$a_{22} = \frac{2 \alpha_g \rho_g v_g}{g_c}$$

$$a_{24} = -\frac{\rho_g v_g^2}{g_c}$$

$$a_{26} = -\frac{\rho_g v_g^2}{g_c}$$

$$a_{27} = \frac{\alpha_g v_g^2}{g_c} \left(\frac{\partial \rho_g}{\partial T} \right)_P$$

$$a_{31} = \alpha_{Lh} v_{Lh} \left(\frac{\partial \rho_{Lh}}{\partial P} \right)_T - G_m \left(\frac{\partial f_{mLh}}{\partial P} \right)_T$$

$$a_{33} = \alpha_{Lh} \rho_{Lh}$$

$$a_{34} = \rho_{Lh} v_{Lh}$$

$$a_{37} = \alpha_{Lh} v_{Lh} \left(\frac{\partial \rho_{Lh}}{\partial T} \right)_P - G_m \left(\frac{\partial f_{mLh}}{\partial T} \right)_P$$

$$a_{41} = \frac{\alpha_{Lh} v_{Lh}^2}{g_c} \left(\frac{\partial \rho_{Lh}}{\partial P} \right)_T + 144 \alpha_{Lh}$$

$$a_{43} = \frac{2 \alpha_{Lh} \rho_{Lh} v_{Lh}}{g_c}$$

$$a_{44} = \frac{\rho_{Lh} v_{Lh}^2}{g_c}$$

$$a_{47} = \frac{\alpha_{Lh} v_{Lh}^2}{g_c} \left(\frac{\partial \rho_{Lh}}{\partial T} \right)_P$$

$$a_{51} = \alpha_{Lw} v_{Lw} \left(\frac{\partial \rho_{Lw}}{\partial P} \right)_T - G_m \left(\frac{\partial f_{mLw}}{\partial P} \right)_T$$

$$a_{55} = \alpha_{Lw} \rho_{Lw}$$

$$a_{56} = \rho_{Lw} v_{Lw}$$

$$a_{57} = \alpha_{Lw} v_{Lw} \left(\frac{\partial \rho_{Lw}}{\partial T} \right)_P - G_m \left(\frac{\partial f_{mLw}}{\partial T} \right)_P$$

$$a_{61} = \frac{\alpha_{Lw} v_{Lw}^2}{g_c} \left(\frac{\partial \rho_{Lw}}{\partial P} \right)_T + 144 \alpha_{Lw}$$

$$a_{65} = \frac{2 \alpha_{Lw} \rho_{Lw} v_{Lw}}{g_c}$$

$$a_{66} = \frac{\rho_{Lw} v_{Lw}^2}{g_c}$$

$$a_{67} = \frac{\alpha_{Lw} v_{Lw}^2}{g_c} \left(\frac{\partial \rho_{Lw}}{\partial T} \right)_P$$

$$a_{71} = \left\{ \begin{array}{l} \alpha_g v_g \left[H_g + \frac{v_g^2}{2 g_c J} \right] \left(\frac{\partial \rho_g}{\partial P} \right)_T + \alpha_{Lh} v_{Lh} \left[H_{Lh} + \frac{v_{Lh}^2}{2 g_c J} \right] \left(\frac{\partial \rho_{Lh}}{\partial P} \right)_T \\ + \alpha_{Lw} v_{Lw} \left[H_{Lw} + \frac{v_{Lw}^2}{2 g_c J} \right] \left(\frac{\partial \rho_{Lw}}{\partial P} \right)_T \\ - \left[\alpha_g v_g \rho_g \eta_g Cp_g + \alpha_{Lh} v_{Lh} \rho_{Lh} \eta_{Lh} Cp_{Lh} + \alpha_{Lw} v_{Lw} \rho_{Lw} \eta_{Lw} Cp_{Lw} \right] \end{array} \right\}$$

$$a_{72} = \alpha_g \rho_g \left[H_g + \frac{3 v_g^2}{2 g_c J} \right]$$

$$a_{73} = \alpha_{Lh} \rho_{Lh} \left[H_{Lh} + \frac{3 v_{Lh}^2}{2 g_c J} \right]$$

$$a_{74} = \rho_{Lh} v_{Lh} \left[H_{Lh} + \frac{v_{Lh}^2}{2 g_c J} \right] - \rho_g v_g \left[H_g + \frac{v_g^2}{2 g_c J} \right]$$

$$a_{75} = \alpha_{Lw} \rho_{Lw} \left[H_{Lw} + \frac{3 v_{Lw}^2}{2 g_c J} \right]$$

$$a_{76} = \rho_{Lw} v_{Lw} \left[H_{Lw} + \frac{v_{Lw}^2}{2 g_c J} \right] - \rho_g v_g \left[H_g + \frac{v_g^2}{2 g_c J} \right]$$

$$a_{77} = \left\{ \begin{array}{l} \alpha_g v_g \left[H_g + \frac{v_g^2}{2 g_c J} \right] \left(\frac{\partial \rho_g}{\partial T} \right)_P + \alpha_{Lh} v_{Lh} \left[H_{Lh} + \frac{v_{Lh}^2}{2 g_c J} \right] \left(\frac{\partial \rho_{Lh}}{\partial T} \right)_P \\ + \alpha_{Lw} v_{Lw} \left[H_{Lw} + \frac{v_{Lw}^2}{2 g_c J} \right] \left(\frac{\partial \rho_{Lw}}{\partial T} \right)_P \\ - \left[\alpha_g v_g \rho_g Cp_g + \alpha_{Lh} v_{Lh} \rho_{Lh} Cp_{Lh} + \alpha_{Lw} v_{Lw} \rho_{Lw} Cp_{Lw} \right] \end{array} \right\}$$

$$b_2 = -F_{gg} - F_{wg} - F_{ig-Lh}$$

$$b_4 = -F_{gLh} - F_{wLh} + F_{ig-Lh} - F_{iLh-Lw}$$

$$b_6 = -F_{gLw} - F_{wLw} + F_{iLh-Lw}$$

$$b_7 = Q_{st} - \frac{1}{J}\left(v_g b_2 - v_{Lh} b_4 + v_{Lw} b_6\right)$$

In the previous expressions, J is an energy conversion factor equal to $778.17\ lbf - ft/Btu$ and g_c is a unit conversion factor equal to $32.174\ lbm/ft/lbf - s^2$.

APPENDIX B

MATRIX FORM OF THE GOVERNING EQUATIONS

FOR TWO-PHASE FLOW

The set of ordinary differential equations for modeling two-phase flow in pipes can be expressed in a matrix form as:

$$\begin{bmatrix} a_{11} & a_{12} & 0 & a_{14} & a_{15} \\ a_{21} & a_{22} & 0 & a_{24} & a_{25} \\ a_{31} & 0 & a_{33} & a_{34} & a_{35} \\ a_{41} & 0 & a_{43} & a_{44} & a_{45} \\ a_{51} & a_{52} & a_{53} & a_{54} & a_{55} \end{bmatrix} \frac{d}{dx} \begin{bmatrix} P \\ v_g \\ v_l \\ \alpha_g \\ T \end{bmatrix} = \begin{bmatrix} 0 \\ b_2 \\ 0 \\ b_4 \\ b_5 \end{bmatrix} \qquad \text{(B.1)}$$

The governing equations were organized in order to avoid the appearance of zeros in the main diagonal of the matrix. The elements in matrices $[A_m]$ and $[B_m]$ are calculated in field units using the following expressions:

$$a_{11} = \alpha_g v_g \left(\frac{\partial \rho_g}{\partial P} \right)_T - G_m \left(\frac{\partial f_{mg}}{\partial P} \right)_T$$

$$a_{12} = \alpha_g \rho_g$$

$$a_{14} = \rho_g v_g$$

$$a_{15} = \alpha_g v_g \left(\frac{\partial \rho_g}{\partial T} \right)_P - G_m \left(\frac{\partial f_{mg}}{\partial T} \right)_P$$

$$a_{21} = \frac{\alpha_g v_g^2}{g_c}\left(\frac{\partial \rho_g}{\partial P}\right)_T + 144\alpha_g$$

$$a_{22} = \frac{2\alpha_g \rho_g v_g}{g_c}$$

$$a_{24} = \frac{\rho_g v_g^2}{g_c}$$

$$a_{25} = \frac{\alpha_l v_l^2}{g_c}\left(\frac{\partial \rho_l}{\partial T}\right)_P$$

$$a_{31} = \alpha_l v_l\left(\frac{\partial \rho_l}{\partial P}\right)_T - G_m\left(\frac{\partial f_{ml}}{\partial P}\right)_T$$

$$a_{33} = \alpha_l \rho_l$$

$$a_{34} = -\rho_l v_l$$

$$a_{35} = \alpha_l v_l\left(\frac{\partial \rho_l}{\partial T}\right)_P - G_m\left(\frac{\partial f_{ml}}{\partial T}\right)_P$$

$$a_{41} = \frac{\alpha_l v_l^2}{g_c}\left(\frac{\partial \rho_l}{\partial P}\right)_T + 144\alpha_l$$

$$a_{43} = \frac{2\alpha_l \rho_l v_l}{g_c}$$

$$a_{44} = -\frac{\rho_l v_l^2}{g_c}$$

$$a_{45} = \frac{\alpha_l v_l^2}{g_c}\left(\frac{\partial \rho_l}{\partial T}\right)_P$$

$$a_{51} = \begin{Bmatrix} \alpha_g v_g \left[H_g + \frac{v_g^2}{2 g_c J} \right] \left(\frac{\partial \rho_g}{\partial P} \right)_T + \alpha_l v_l \left[H_l + \frac{v_l^2}{2 g_c J} \right] \left(\frac{\partial \rho_l}{\partial P} \right)_T \\ - \left[\alpha_g v_g \rho_g \eta_g Cp_g + \alpha_l v_l \rho_l \eta_l Cp_l \right] \end{Bmatrix}$$

$$a_{52} = \alpha_g \rho_g \left[H_g + \frac{3 v_g^2}{2 g_c J} \right]$$

$$a_{53} = \alpha_l \rho_l \left[H_l + \frac{3 v_l^2}{2 g_c J} \right]$$

$$a_{54} = -\rho_l v_l \left[H_l + \frac{v_l^2}{2 g_c J} \right] + \rho_g v_g \left[H_g + \frac{v_g^2}{2 g_c J} \right]$$

$$a_{55} = \begin{Bmatrix} \alpha_g v_g \left[H_g + \frac{v_g^2}{2 g_c J} \right] \left(\frac{\partial \rho_g}{\partial T} \right)_P + \alpha_l v_l \left[H_l + \frac{v_l^2}{2 g_c J} \right] \left(\frac{\partial \rho_l}{\partial T} \right)_P \\ - \left[\alpha_g v_g \rho_g Cp_g + \alpha_l v_l \rho_l Cp_l \right] \end{Bmatrix}$$

$$b_2 = -F_{gg} - F_{wg} - F_i$$

$$b_4 = -F_{gl} - F_{wl} + F_i$$

$$b_5 = Q_{st} - \frac{1}{J} \left(v_g b_2 - v_{Lh} b_4 \right)$$

In the previous expressions, J is an energy conversion factor equal to $778.17\ lbf - ft/Btu$ and g_c is a unit conversion factor equal to $32.174\ lbm/ft/lbf - s^2$.

APPENDIX C

MATRIX FORM OF THE GOVERNING EQUATIONS

FOR SINGLE PHASE (GAS) FLOW

The set of ordinary differential equations for modeling gas flow in pipes can be expressed in a matrix form as:

$$\begin{bmatrix} a_{11} & a_{12} & a_{13} \\ a_{21} & a_{22} & 0 \\ a_{31} & a_{32} & a_{33} \end{bmatrix} \frac{d}{dx} \begin{bmatrix} P \\ v_g \\ T \end{bmatrix} = \begin{bmatrix} 0 \\ b_2 \\ b_3 \end{bmatrix} \qquad \text{(C.1)}$$

The governing equations were organized in order to avoid the appearance of zeros in the main diagonal of the matrix. The elements in matrices $[A_m]$ and $[B_m]$ are calculated in field units using the following expressions:

$$a_{11} = v_g \left(\frac{\partial \rho_g}{\partial P} \right)_T$$

$$a_{12} = \rho_g$$

$$a_{13} = v_g \left(\frac{\partial \rho_g}{\partial T} \right)_P$$

$$a_{21} = 144$$

$$a_{22} = \frac{\rho_g v_g}{g_c}$$

$$a_{31} = -\rho_g v_g \eta_g Cp_g$$

$$a_{32} = \frac{\rho_g v_g^2}{g_c J}$$

$$a_{33} = \rho_g v_g Cp_g$$

$$b_2 = -F_g - F_w$$

$$b_3 = Q_{st} - \frac{1}{J}\left(v_g b_2\right)$$

In the previous expressions, J is an energy conversion factor equal to 778.17 $lbf - ft/Btu$ and g_c is a unit conversion factor equal to 32.174 $lbm/ft/lbf - s^2$.

APPENDIX D

SOLUTION OF THE RACHFORD-RICE EQUATION

USING THE NEWTON-RAPHSON METHOD

As shown in section 4.3.3, the application of a material balance to a two-phase system allows deriving the next expression:

$$Q(LA) = \sum_{i=1}^{n} \frac{c_i (1 - K_i)}{K_i + LA(1 - K_i)} = 0$$

In this expression, *Ki* represents the distribution coefficients, while *LA* is the liquid molar fraction in the system. This expression was originally derived by Rachford & Rice (1952), and it is a non-linear expression that requires a numerical procedure for its solution.

This work solves this equation using the Newton-Raphson method. This method consists of finding successive estimates of the unknown (*LA*) by the iterative calculation of:

$$LA^{new} = LA^{old} - \frac{Q(LA)}{Q'(LA)}$$

Where:

The derivative of the objective function with respect to the liquid molar fraction is expressed as:

$$Q'(LA) = \sum_{i=1}^{n} \frac{c_i (1 - K_i)^2}{[K_i + LA(1 - K_i)]^2} = 0$$

This method requires repeating the calculation procedure until the values of *LA* are within a specified tolerance. Then, convergence has been achieved and the value of *LA* has, therefore, been properly determined. The convergence criterion employed in this work is:

$$\left| LA^{new} - LA^{old} \right| < 1 \cdot 10^{-10}$$

APPENDIX E

VALIDATION OF THE MULTIPHASE EQUILIBRIA MODEL

Multiphase flow modeling of unprocessed gas well streams requires the determination of the physical and thermodynamic properties of the fluids flowing in a pipe. The estimation of these properties allows engineers to quantify energy losses and determine where, how much, and the type of liquid that will accumulate in a pipe.

A multiphase equilibria model is a core tool for a good representation of the hydrodynamic behavior of the fluids being transported. The objective of this thermodynamic tool is to determine the composition of the fluids that exist in a pipe. This information is used for estimating the physical and thermodynamic fluid properties required by a hydrodynamic model. The properties required by the hydrodynamic model include density, viscosity, and mass fraction of the different phases being formed.

This work presents a model for performing multiphase flash calculations of typical gas well streams containing hydrocarbon mixtures, water, and hydrate inhibitors. This model is capable of identifying the number and types of fluid phases in equilibrium, estimating their composition, and quantifying their mass fraction in the system. The algorithm presented is capable of performing Vapor-Liquid-equilibria (VLE), Liquid-Liquid-equilibria (LLE), and Vapor-Liquid-Liquid-equilibria (VLLE) calculations.

In this chapter, this model is tested. The tests proposed are intended to validate the results obtained for VLE and VLLE calculations.

This chapter contains two sections. The first section analyzes the results obtained for VLE calculations, while the second section discusses the results obtained for VLLE calculations.

E.1 Validation of Two-phase Vapor-Liquid-Equilibria calculations

The tests in this section are aimed at verifying the accuracy of the flash calculations, and also verify that the thermodynamic tool developed can successfully identify the formation of single phases (vapor or liquid). For this reason, it was decided to test the model calculating bubble and dew points along the phase envelope of typical natural gas mixtures.

E.1.1 Case Studies

Ten gas mixtures where selected as benchmark for testing the accuracy of the calculations. These mixtures contain hydrocarbons, nitrogen, carbon dioxide, helium, and other non-hydrocarbons typically found in natural gas. For each of these gas mixtures, several bubble and dew points were calculated and the results compared with data available. The case studies include:

a) Synthetic composition used by Michelsen (1981a). This composition was used by Michelsen for testing the accuracy of his phase stability criterion.

b) Experimental data provided by Parikh et al. (1984) for a mixture containing methane, ethane, and propane.

c) Experimental data provided by Lee & Gonzalez (1968) for three natural gas mixtures.

d) Five typical gas compositions found in the field. These compositions have been extensively studied by the American Gas Association, and they are typically used as a benchmark for verifying the accuracy of compressibility factor calculations performed for gas metering applications (AGA standard No. 8). The phase envelope determination of these mixtures was performed using commercial software (PhasePro®). This software has been extensively tested by the natural gas industry, and it is currently used by hundreds of companies in the field finding satisfactory results. Table E.1 indicates the composition of the gas mixtures analyzed.

E.1.2 Results

Figures E.1 to E.10 summarize the results and compare them with the data available. These figures show an excellent match between the VLE calculations and the data available. The algorithm successfully calculated more than 100 dew and bubble points of different mixtures, demonstrating the capacity of the algorithm to identify the occurrence of single phases (Vapor/Liquid). The model was capable of identifying phase distribution and calculated phase split even near the critical point. In most cases, the

bubble and dew point temperature calculations are within 2 °F of the data available. This difference between experimental data and the calculations is acceptable, given that the experimental procedure employed by the authors referenced required visual determination of bubble and dew points. In practice, sometimes it is difficult to visualize the occurrence of the first droplet of liquid or bubble of vapor.

In general, the results are in excellent agreement for all the mixtures analyzed. Even for those that contain significant molar fractions of non-hydrocarbon components (nitrogen, carbon dioxide and helium).

Table E.1 Composition of the gas mixtures analyzed (Mole fractions)

	Composition									
Component	Michelsen	Parikh	Lee et al. S-1	Lee et al. S-2	Lee et al. S-3	Amarillo	Gulf Coast	Ekofisk	High N2	High N2-CO2
Methane	0.943000	0.851100	0.862000	0.959000	0.950000	0.906724	0.965222	0.859063	0.814410	0.812118
Ethane	0.027000	0.100700	0.064000	0.026000	0.026000	0.045279	0.018186	0.084919	0.033000	0.043030
Propane	0.007400	0.048200	0.024000	0.000100	0.007800	0.008280	0.004596	0.023015	0.006050	0.008950
i-Butane	0.000000	0.000000	0.000000	0.000000	0.000000	0.001037	0.000977	0.003486	0.001000	0.001510
n-Butane	0.004900	0.000000	0.004600	0.000000	0.000000	0.001563	0.001007	0.003506	0.001040	0.001520
i-Pentane	0.000000	0.000000	0.000000	0.000000	0.000000	0.000321	0.000473	0.000509	0.000000	0.000000
n-Pentane	0.002700	0.000000	0.000900	0.000000	0.000000	0.000443	0.000324	0.000480	0.000000	0.000000
n-Hexane	0.001000	0.000000	0.008700	0.000000	0.000000	0.000393	0.000664	0.000000	0.000000	0.000000
n-Heptane	0.000000	0.000000	0.000100	0.000000	0.000000	0.000000	0.000000	0.000000	0.000000	0.000000
Nitrogen	0.014000	0.000000	0.034000	0.015000	0.016000	0.031284	0.002595	0.010068	0.134650	0.057021
Helium	0.000000	0.000000	0.001700	0.000000	0.000000	0.000000	0.000000	0.000000	0.000000	0.000000
Carbon Dioxide	0.000000	0.000000	0.000000	0.000000	0.000000	0.004676	0.000596	0.014954	0.009850	0.075851

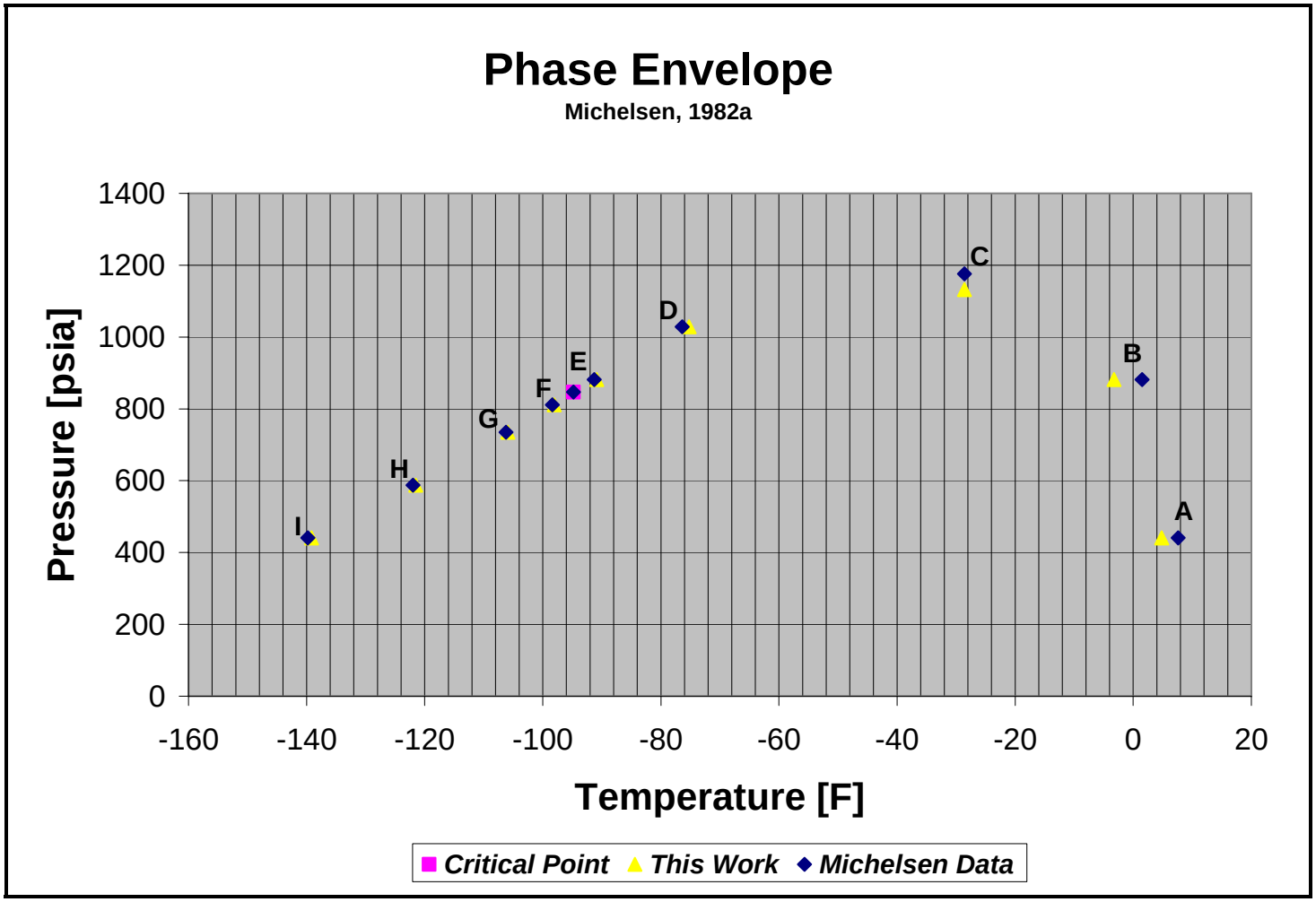

Figure E.1 Results for the synthetic composition suggested by Michelsen (1982a)

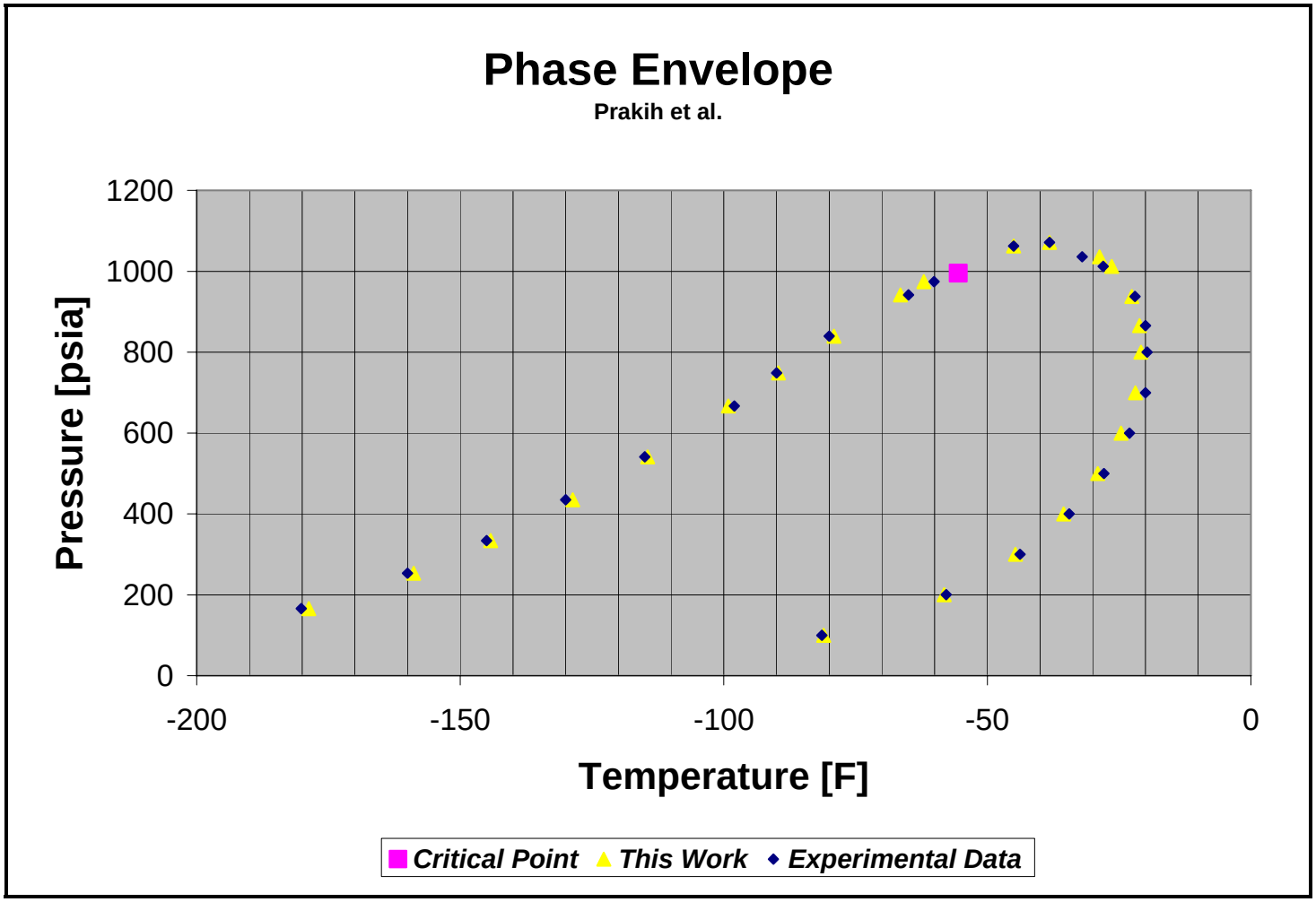

Figure E.2 Results for the composition analyzed by Parikh et al. (1984)

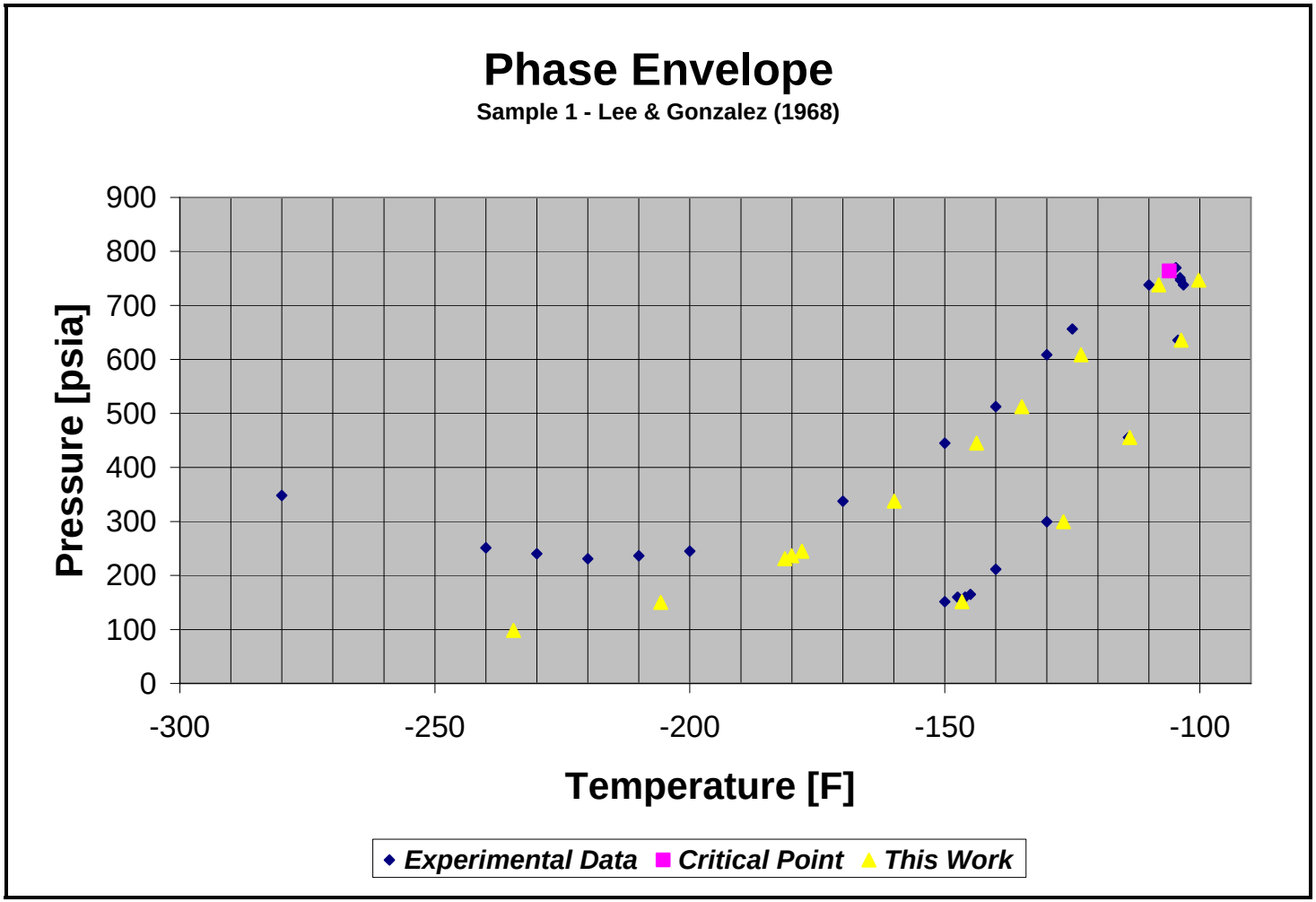

Figure E.3 Results for Sample 1 analyzed by Lee et al. (1968)

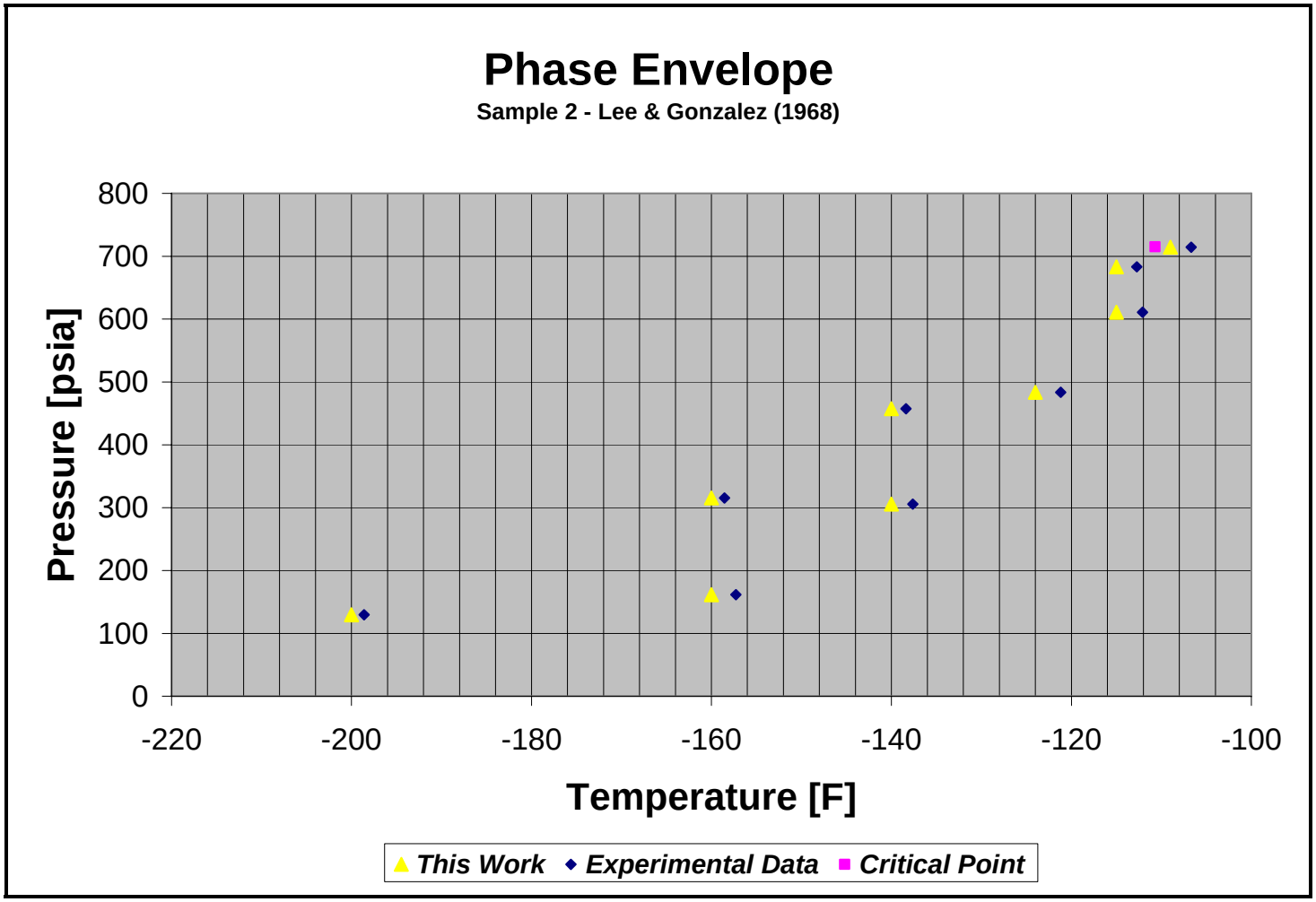

Figure E.4 Results for Sample 2 analyzed by Lee et al. (1968)

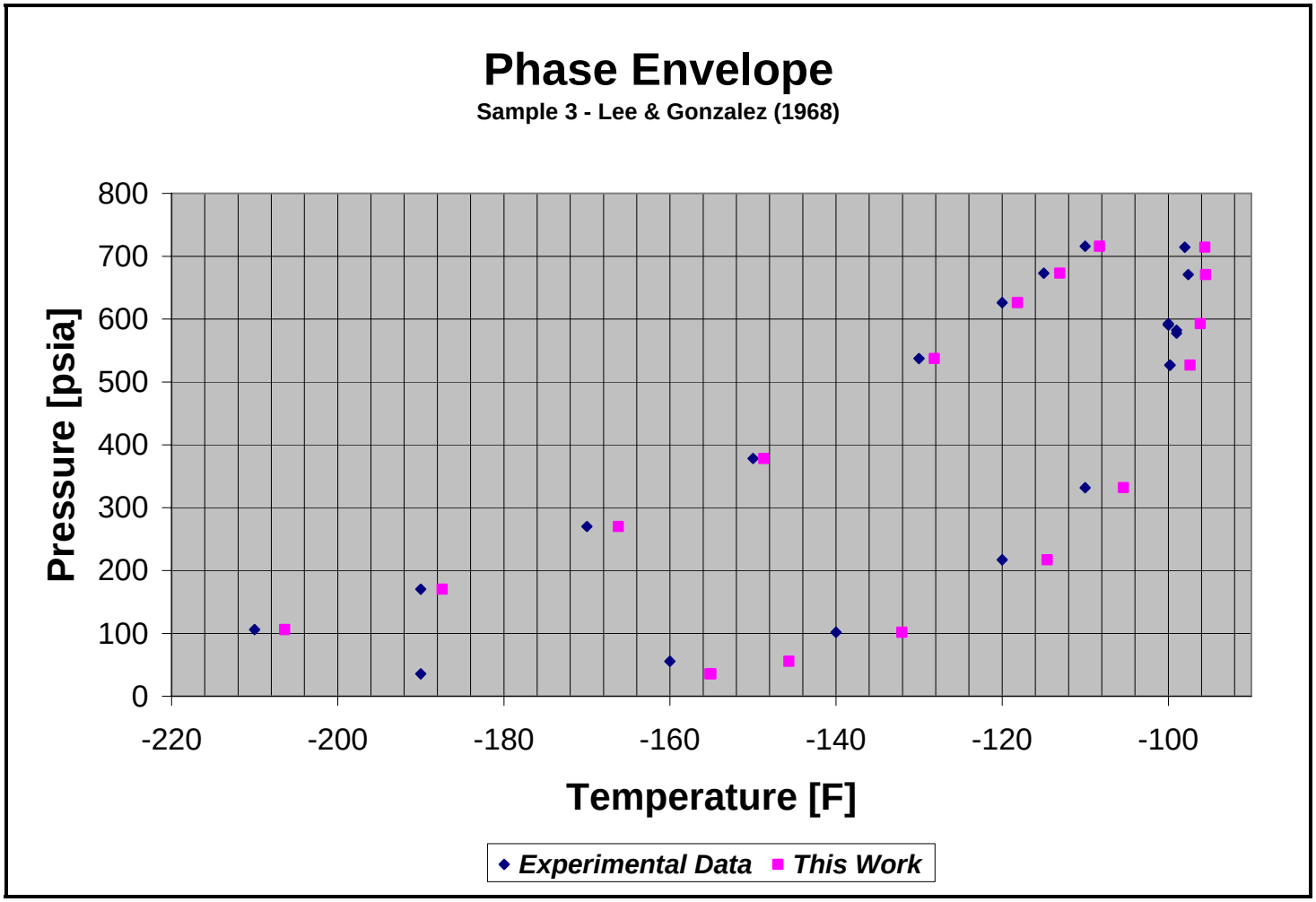

Figure E.5 Results for Sample 3 analyzed by Lee et al. (1968)

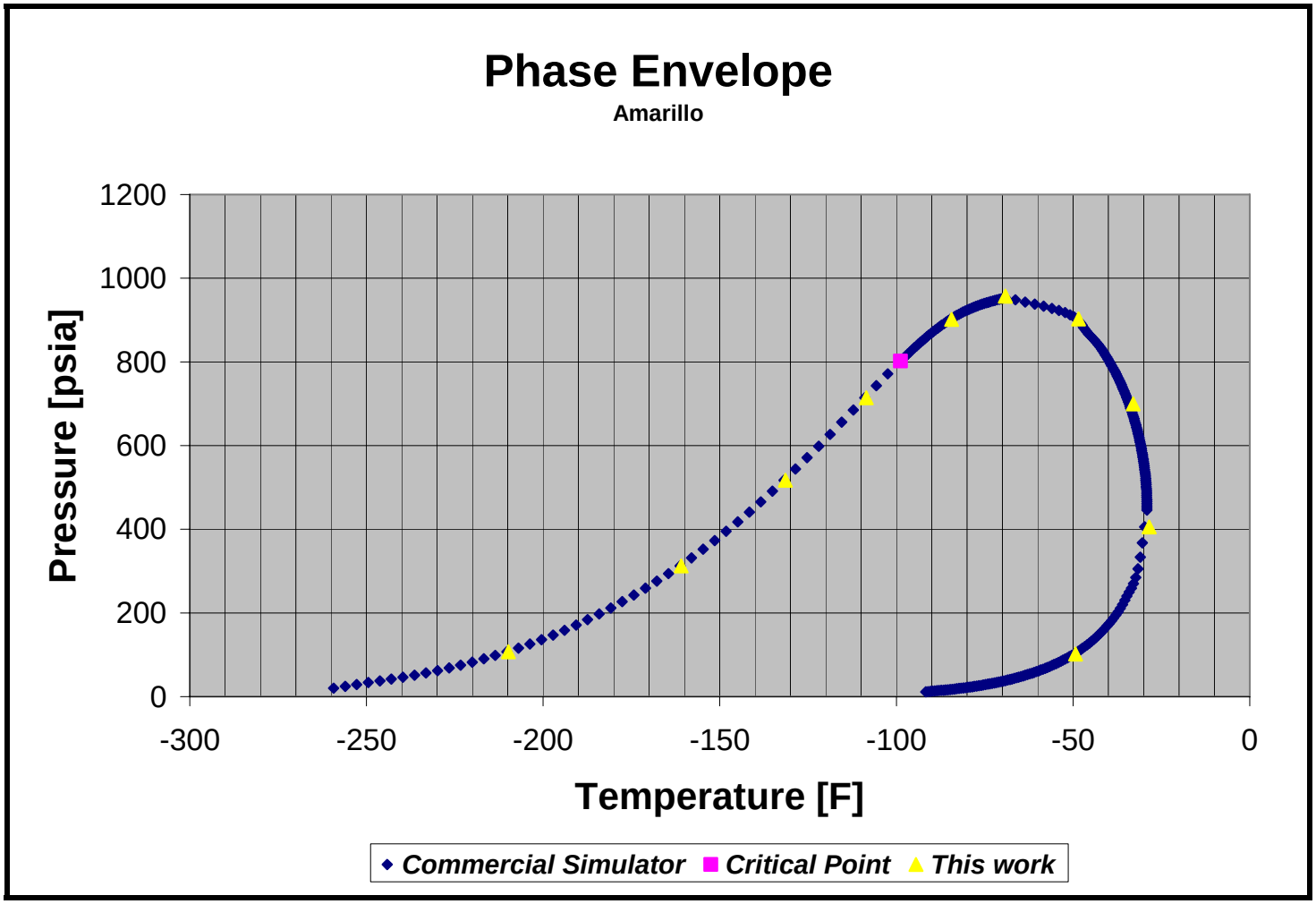

Figure E.6 Results for the Amarillo composition

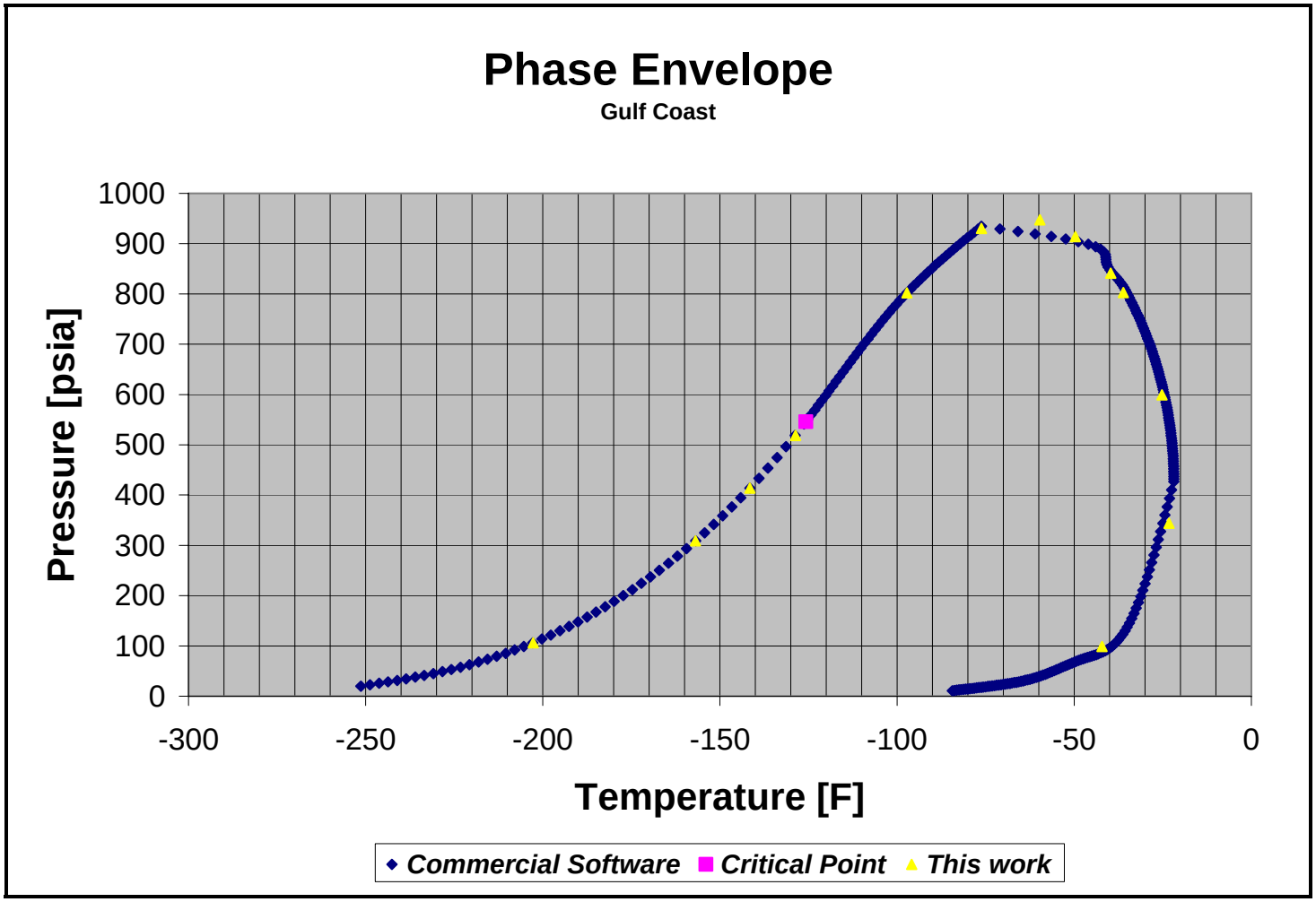

Figure E.7 Results for the Gulf Coast composition

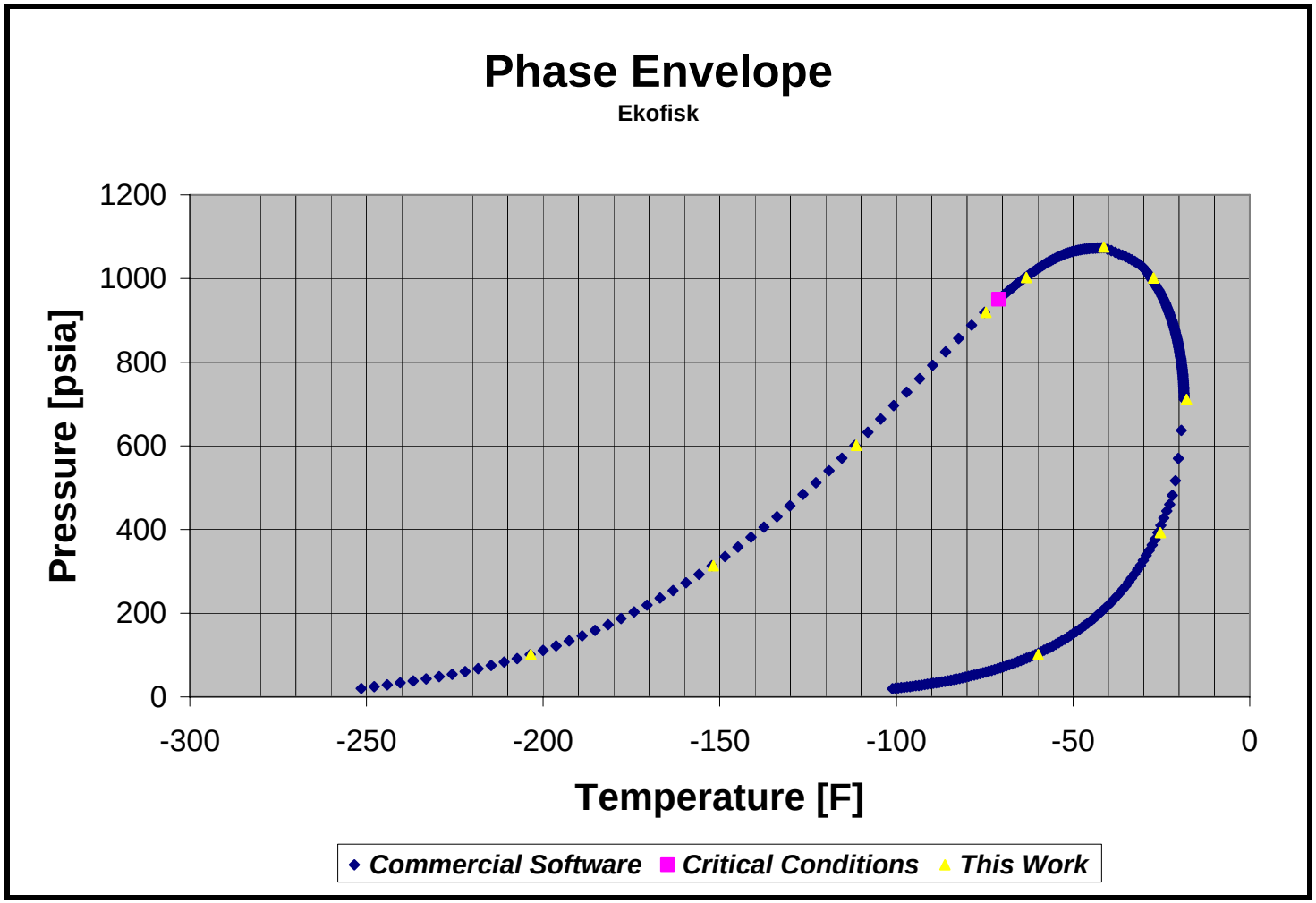

Figure E.8 Results for the Ekofisk composition

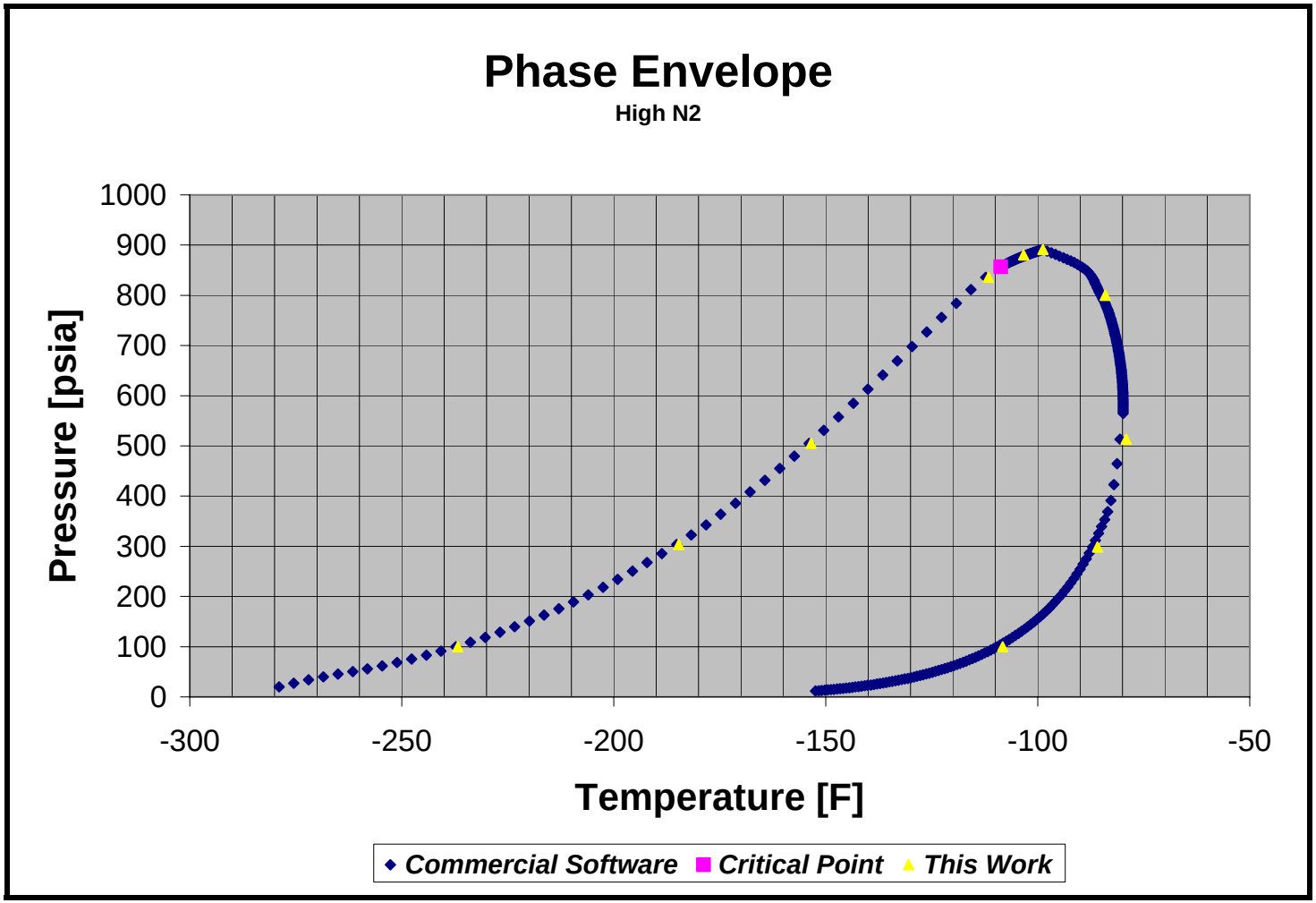

Figure E.9 Results for a typical composition containing 13% of Nitrogen

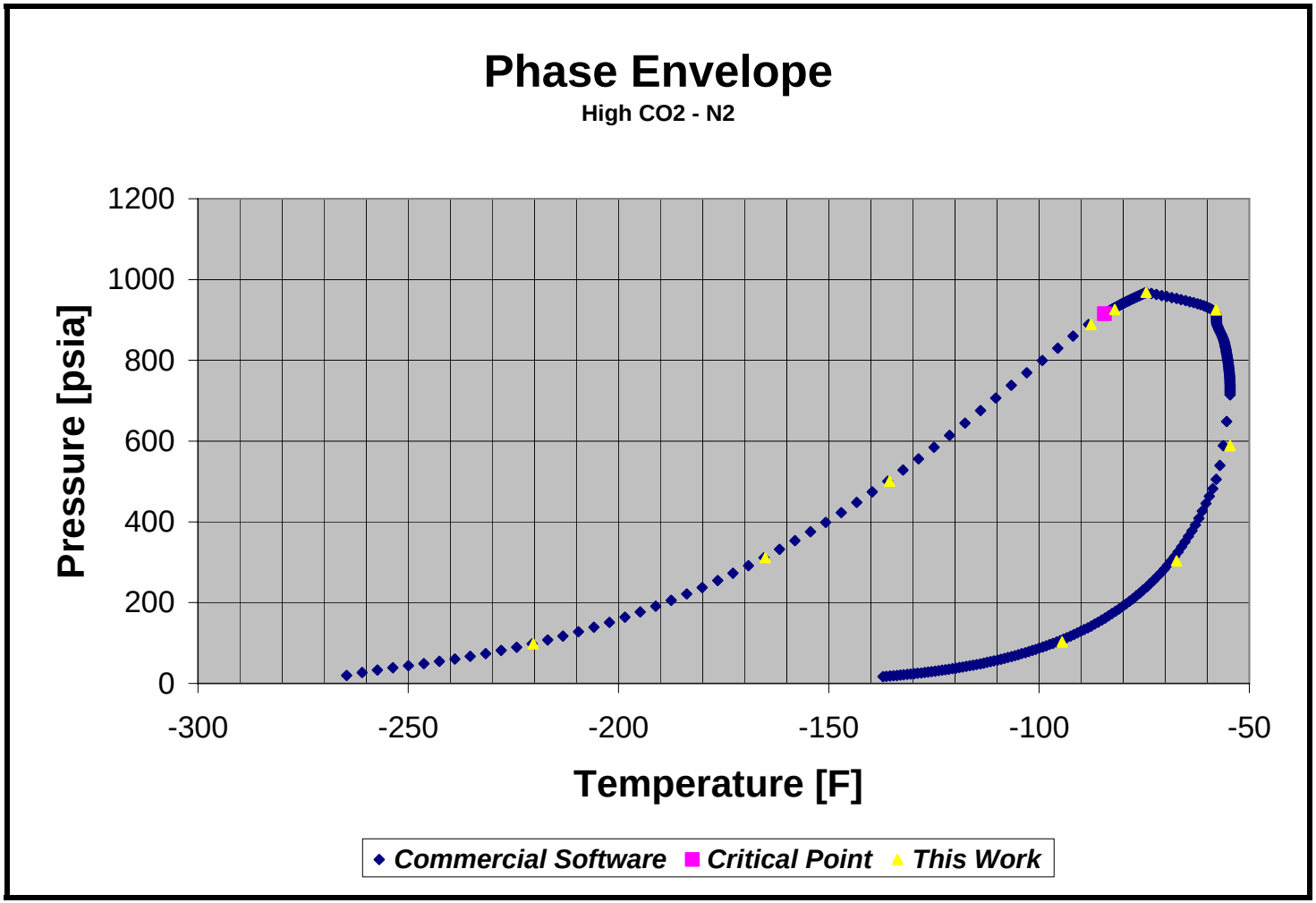

Figure E.10 Results for a composition containing 5.7% of Nitrogen and 7.5% of CO_2

E.2 Validation of Three-phase Vapor-Liquid-Liquid-Equilibria calculations

Numerical simulation of multiphase flow of unprocessed gas well streams demands the development of a multiphase equilibria model capable of representing the behavior of strongly non-ideal mixtures. These mixtures contain hydrocarbons, water, and in some cases methanol as hydrate inhibitor.

This thermodynamic model has to prove to be fast and reliable for two and three-phase Vapor-Liquid-Liquid equilibrium calculations. This section is intended to show that the algorithm is capable of determining the correct number of phases, and verify the accuracy of the flash calculations.

E.2.1 Case Studies

Several data sets were used for benchmarking the model. These data sets include:

a) Numerical experiments performed by Michelsen (1993).
b) Numerical experiments performed by Heidemann (1974). This includes the determination of three-phase condensation curves.
c) Experimental data published by Mc Ketta & Katz (1948) for a ternary system containing methane, n-butane, and water.
d) Experimental data published by Chen et al. (1988) for a quaternary system containing methane, n-heptane, water, and methanol.
e) Experimental data provided by Pedersen et al. (1996) for complex mixtures containing gas-condensate, water, and methanol.

E.2.2 Results

The first test of the algorithm compares the results with a numerical experiment performed by Michelsen (1993). Michelsen performed three-phase flash calculations on a system containing 20% ethane, 50% propane, 20% n-Butane, and 10% water. He used the SRK EOS, and assumed zero for all binary interaction coefficients. This test verifies the ability of the model for predicting the three phases. The results obtained for the mole fractions of the phases present are very similar to those reported by Michelsen. Table E.2 summarizes and compares the results obtained with those provided by Michelsen.

Table E.2 Comparison of the results for the synthetic comp. suggested by Michelsen

Michelsen (1993) Hyd. - water mix. - P= 73.480 psia and T= 504.0 R			
Mole Fraction	**Michelsen**	**Calc.**	**Dev. [%]**
Hyd.Liquid	*28.20*	*29.61*	*-4.99*
Water Liquid	*9.90*	*9.87*	*0.27*
Vapor	*61.90*	*60.52*	*2.23*

The model was benchmarked against additional numerical experimentation performed by Heidemann (1974). Heidemann used a synthetic water – paraffin system suggested by Erbar (1973) to test the ability of his thermodynamic model to perform three-phase flash calculations using the same EOS for all phases. Tables E.3 and E.4 compare the results obtained by Heidemann with the model calculations. The results are in good agreement. The molar fraction of the three phases identified exhibit an excellent match. However, the mutual solubilities of water/hydrocarbons are not in good agreement with those predicted by Heidemann. This is due to the well known fact that the classical mixing rules employed by Heidemann cannot accurately represent the mutual solubility of hydrocarbon-water.

Table E.3 Molar fraction of the phases predicted by Heidemann (1974)

Number of Moles	Heidemann	Calc.	Dev. [%]
Hyd.Liquid	*62.96*	*61.66*	*2.07*
Water Liquid	*28.91*	*28.04*	*3.02*
Vapor	*58.13*	*60.30*	*-3.74*

Table E.4 Comparison of the results of the flash calculations

Heidemann (1974) Hydrocarbon - water mixture - P = 350 psia and T= 300 F

		Hyd. Rich Liquid		*Aqueous Liquid*		*Vapor*	
Component	***Feed***	***Heidemann***	***Calc.***	***Heidemann***	***Calc.***	***Heidemann***	***Calc.***
C3	***25***	*7.93*	*8.09*	---	*0.00207*	*17.07*	*16.90*
n-C4	***25***	*11.55*	*11.21*	---	*0.00130*	*13.45*	*13.79*
n-C5	***30***	*17.74*	*17.30*	---	*0.00036*	*12.26*	*12.70*
n-C6	***10***	*7.03*	*6.89*	---	*0.00004*	*2.97*	*3.11*
n-C8	***20***	*17.27*	*17.01*	---	*0.00002*	*2.73*	*2.99*
Water	***40***	*1.44*	*1.16*	*28.91*	*28.03233*	*9.65*	*10.81*

Heidemann (1974) also calculated three-phase condensation curves for the synthetic water-paraffin system proposed. Figure E.11 illustrates the results obtained by this author and compares them with the calculations performed. This figure shows an excellent agreement between the model results and the calculations performed by Heidemann. It also shows that the model can determine the range of temperatures at which three-phases coexist in equilibrium and the molar fraction of the phases present. This figure illustrates that for temperatures lower than 405 K only two liquid phases (LLE) coexist, while for temperatures higher than 440 K there is Vapor-Liquid equilibrium (hydrocarbon-rich liquid/ vapor).

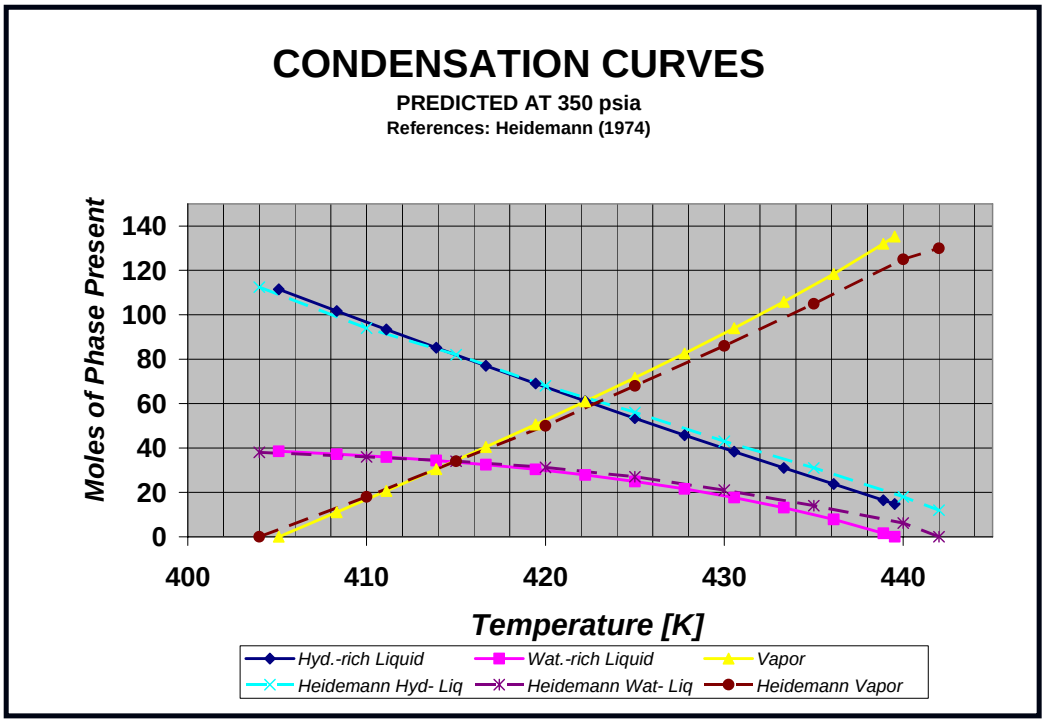

Figure E.11 Comparison of the condensation curves

The results discussed thus far show the capacity of the model for predicting the occurrence of vapor-liquid-liquid equilibrium, and performing three-phase flash calculations. However, they do not provide a good basis to determine whether the model can predict the compositions of the phases present within a reasonable range.

Three sets of experimental data were selected for verifying the accuracy of the phase compositions predicted when performing three-phase flash calculations of hydrocarbon-water mixtures. The first of these data sets corresponds to the data measured by Mc Ketta and Katz (1948) for systems containing methane, n-butane, and water. Table E.5 presents a comparison between the data measured by these researchers and the model calculations. This table presents the results of twelve multiphase flash calculations

performed at different pressures and a temperature of 100 °F. The results show that the model can predict, reasonably well, the compositions of the three phases present. The model performs an acceptable prediction of the mole fraction for the most abundant (dominant) components for all phases present. For intermediate pressures (474 to 1880 psia) the predictions of these mole fractions are within 3 % of those reported experimentally. For low pressures (200 and 212 psia) the model shows larger deviations in the prediction of the composition of the dominant mole fractions of all phases. These deviations are due to the fact that the model uses the Huron-Vidal mixing rules. However, this range of pressures is not that typically encountered in offshore gas production operations. The model losses accuracy in the prediction of the mole fractions of the dominant components for high pressure (1880 psia and above) calculations. This is because the system is approaching the critical locus tending to form two liquid phases. Even though the calculations are performed in the proximity of the critical conditions the deviations are still within an acceptable range (approximately 20%).

The model exhibits some deviations in the prediction of the mutual solubilities of hydrocarbon-water. Even though the absolute deviations seem to be large (Up to 40%) the absolute value of the differences is small. In most cases, the prediction of the water in the hydrocarbon-rich phase and hydrocarbons in the water-rich phase is within 30%. These deviations are considered to be acceptable for the purposes of this study, since they will not have a significant effect on the calculation of the physical and thermodynamic properties of the fluid phases present in equilibrium.

Additional validation of the model was performed comparing results with experimental data of a quaternary system (methane, n-heptane, water, and methanol) presented by Chen et al. (1988). This case study represents an extreme test for the model since the fraction of polar components (water and methanol) in the overall mixture is more than 37% for all test compositions. In this case study, six flash calculations were performed for different hydrocarbon-water-methanol mixtures at approximately 1000 psia, and different temperatures (14 °F, 68 °F, and 122 °F). Tables E.6 to E.11 present a comparison of the model results with the experimental data. These tables show that the calculations are in good agreement with the experimental data. The model predicts reasonably well the mole fractions of the most abundant components in all the phases.

Table E.5 Model results vs. experimental data presented by Mc Ketta & Katz (1948)

Mc Ketta & Katz (1948) Three-phase Equilibria (C1 + n-C4 + Water) @ T=100 F

		Hydrocarbon-rich Liquid			Water-rich Liquid			Vapor		
Pressure [psia]	**Comp.**	**Exp.**	**Calc**	**Dev [%]**	**Exp.**	**Calc**	**Dev [%]**	**Exp.**	**Calc**	**Dev [%]**
631	C1	0.207600	0.205190	1.16	0.000649	0.000921	-41.96	0.871000	0.859788	1.29
	n-C4	0.792400	0.793964	-0.20	0.000059	0.000049	17.93	0.129000	0.138381	-7.27
	Water	0.000838	0.000847	-1.07	0.999290	0.999030	0.03	0.001840	0.001831	0.46
202	C1	0.069400	0.055229	20.42	0.000264	0.000263	0.30	0.785000	0.698596	11.01
	n-C4	0.930600	0.943945	-1.43	0.000087	0.000056	36.11	0.215000	0.296483	-37.90
	Water	0.000654	0.000826	-26.32	0.999650	0.999682	0.00	0.005080	0.004921	3.12
1406	C1	0.450500	0.459707	-2.04	0.001505	0.001813	-20.50	0.858000	0.865734	-0.90
	n-C4	0.549500	0.539407	1.84	0.000045	0.000039	14.07	0.142000	0.133188	6.21
	Water	0.000864	0.000886	-2.55	0.998450	0.998148	0.03	0.001028	0.001078	-4.88
979	C1	0.307000	0.320413	-4.37	0.001051	0.001365	-29.85	0.865000	0.875426	-1.21
	n-C4	0.693000	0.678723	2.06	0.000065	0.000044	32.48	0.135000	0.123243	8.71
	Water	0.000871	0.000864	0.77	0.998884	0.998591	0.03	0.001315	0.001332	-1.27
474	C1	0.147900	0.151547	-2.47	0.000720	0.000696	3.40	0.847000	0.837444	1.13
	n-C4	0.852100	0.847614	0.53	0.000080	0.000051	36.08	0.153000	0.160246	-4.74
	Water	0.000809	0.000839	-3.74	0.999200	0.999253	-0.01	0.002315	0.002310	0.22
212	C1	0.048000	0.058856	-22.62	0.000299	0.000280	6.48	0.712500	0.710277	0.31
	n-C4	0.952000	0.940318	1.23	0.000051	0.000055	-9.31	0.287500	0.285016	0.86
	Water	0.000692	0.000827	-19.45	0.999650	0.999665	0.00	0.004850	0.004707	2.95
1838	C1	0.624000	0.617905	0.98	0.001805	0.002177	-20.61	0.814000	0.819906	-0.73
	n-C4	0.376000	0.381185	-1.38	0.000033	0.000034	-3.43	0.186000	0.179131	3.69
	Water	0.000824	0.000910	-10.41	0.998162	0.997789	0.04	0.000858	0.000962	-12.18
1900	C1	0.669000	0.647715	3.18	0.001818	0.002223	-22.26	0.777000	0.805060	-3.61
	n-C4	0.331000	0.351371	-6.15	0.000030	0.000034	-13.68	0.223000	0.193988	13.01
	Water	0.000831	0.000914	-9.99	0.998150	0.997744	0.04	0.000841	0.000951	-13.19
1910	C1	0.697500	0.653069	6.37	0.001852	0.002230	-20.40	0.749000	0.802095	-7.09
	n-C4	0.302500	0.346016	-14.39	0.000028	0.000033	-19.44	0.251000	0.196955	21.53
	Water	0.000832	0.000915	-9.95	0.998120	0.997737	0.04	0.000831	0.000950	-14.27
1912	C1	0.713000	0.654166	8.25	0.001852	0.002231	-20.48	0.739000	0.801476	-8.45
	n-C4	0.287000	0.344919	-20.18	0.000028	0.000033	-19.37	0.261000	0.197575	24.30
	Water	0.000835	0.000915	-9.57	0.998120	0.997735	0.04	0.000835	0.000949	-13.68
1880	C1	0.642000	0.637548	0.69	0.001822	0.002208	-21.19	0.804000	0.810429	-0.80
	n-C4	0.358000	0.361540	-0.99	0.000031	0.000034	-7.41	0.196000	0.188616	3.77
	Water	0.000828	0.000913	-10.21	0.998150	0.997758	0.04	0.000841	0.000955	-13.54
1220	C1	0.386000	0.398733	-3.30	0.001290	0.001630	-26.35	0.879000	0.873068	0.67
	n-C4	0.614000	0.600390	2.22	0.000060	0.000041	31.92	0.121000	0.125769	-3.94
	Water	0.000820	0.000876	-6.89	0.998650	0.998329	0.03	0.001060	0.001163	-9.72

Table E.6 Model results vs. exp. data presented by Chen et al. (1988) – Mixture 1

Phase compositions at P=1002.94 psia and T=14 °F

		Hydrocarbon Liquid Phase			Vapor Phase			Aqueous Phase		
Component	**Feed**	**Exp**	**Calc**	**% Dev**	**Exp**	**Calc**	**% Dev**	**Exp**	**Calc**	**% Dev**
Water	**36.59**	**0.017**	**0.016**	**-5.9**	**-**	**0.0070**		**76.390**	**76.48000**	**0.1**
Methanol	**11.10**	**0.128**	**0.326**	**60.7**	**0.0185**	**0.0192**	**3.6**	**23.140**	**22.95700**	**-0.8**
Methane	**31.39**	**36.480**	**40.790**	**10.6**	**99.8400**	**99.8200**	**0.0**	**0.458**	**0.55200**	**17.0**
n-Heptane	**20.92**	**63.380**	**58.850**	**-7.1**	**0.1270**	**0.1530**	**17.0**	**0.011**	**0.00412**	**-63.2**

Table E.7 Model results vs. exp. data presented by Chen et al. (1988) – Mixture 2

Phase compositions at P=1003.95 psia and T=14 °F

		Hydrocarbon Liquid Phase			Vapor Phase			Aqueous Phase		
Component	**Feed**	**Exp**	**Calc**	**% Dev**	**Exp**	**Calc**	**% Dev**	**Exp**	**Calc**	**% Dev**
Water	16.80	0.028	0.023	-19.1	-	0.0047		42.690	42.50038	-0.4
Methanol	22.08	0.489	0.687	28.8	0.0333	0.0369	9.8	55.600	55.37202	-0.4
Methane	36.67	36.590	40.796	10.3	99.8300	99.8049	0.0	1.630	2.01496	19.1
n-Heptane	24.45	62.900	58.704	-7.1	0.1240	0.1535	19.2	0.077	0.11263	31.3

Table E.8 Model results vs. exp. data presented by Chen et al. (1988) – Mixture 3

Phase compositions at P=1000.76 psia and T=68 °F

		Hydrocarbon Liquid Phase			Vapor Phase			Aqueous Phase		
Component	**Feed**	**Exp**	**Calc**	**% Dev**	**Exp**	**Calc**	**% Dev**	**Exp**	**Calc**	**% Dev**
Water	39.09	0.035	0.051	30.9	-	0.0460		76.500	76.62000	0.2
Methanol	11.86	0.373	0.633	41.1	0.0905	0.0960	5.7	23.170	22.85000	-1.4
Methane	29.43	30.660	33.600	8.8	99.5000	99.4200	-0.1	0.322	0.51050	36.9
n-Heptane	19.62	68.930	65.720	-4.9	0.3690	0.4375	15.7	0.004	0.00455	23.1

Table E.9 Model results vs. exp. data presented by Chen et al. (1988) – Mixture 4

Phase compositions at P=1003.66 psia and T=68 °F

		Hydrocarbon Liquid Phase			Vapor Phase			Aqueous Phase		
Component	**Feed**	**Exp**	**Calc**	**% Dev**	**Exp**	**Calc**	**% Dev**	**Exp**	**Calc**	**% Dev**
Water	19.00	0.045	0.069	35.2	-	0.0300		43.050	42.74918	-0.7
Methanol	24.95	1.230	1.035	-18.8	0.1640	0.1923	14.7	55.450	55.27487	-0.3
Methane	33.63	30.240	33.600	10.0	99.4400	99.3404	-0.1	1.390	1.83026	24.1
n-Heptane	24.42	68.480	65.296	-4.9	0.3700	0.4373	15.4	0.115	0.14568	21.1

Table E.10 Model results vs. exp. data presented by Chen et al. (1988) – Mixture 5

Phase compositions at P=1025.42 psia and T=122 °F

		Hydrocarbon Liquid Phase			Vapor Phase			Aqueous Phase		
Component	**Feed**	**Exp**	**Calc**	**% Dev**	**Exp**	**Calc**	**% Dev**	**Exp**	**Calc**	**% Dev**
Water	39.17	0.150	0.138	-8.1	-	0.2100		77.050	76.86000	-0.2
Methanol	11.88	1.050	1.060	0.9	0.4320	0.3534	-22.2	22.610	22.62000	0.0
Methane	29.37	28.900	29.910	3.4	98.4600	98.3100	-0.2	0.328	0.50660	35.3
n-Heptane	19.58	69.900	68.880	-1.5	0.9340	1.1290	17.3	0.010	0.00543	-82.4

Table E.11 Model results vs. exp. data presented by Chen et al. (1988) – Mixture 6

Phase compositions at P=1021.07 psia and T=122 °F

		Hydrocarbon Liquid Phase			Vapor Phase			Aqueous Phase		
Component	**Feed**	**Exp**	**Calc**	**% Dev**	**Exp**	**Calc**	**% Dev**	**Exp**	**Calc**	**% Dev**
Water	18.64	0.183	0.177	-3.3	-	0.1300		43.400	43.10526	-0.7
Methanol	24.46	2.580	1.946	-32.6	0.7940	0.7453	-6.5	54.800	54.93987	0.3
Methane	34.12	28.880	29.640	2.6	98.1100	97.9951	-0.1	1.600	1.76656	9.4
n-Heptane	22.75	68.360	68.237	-0.2	0.9470	1.1227	15.6	0.180	0.18831	4.4

The results show some deviations in the prediction of the mutual solubilities of hydrocarbon-water/methanol. These deviations reach in some cases 35%. Even though these deviations seem to be large, the absolute value of the differences in molar fraction is small (Less than 0.4% in all cases). Therefore, these deviations are considered to be acceptable for the purposes of this study because they will not have a significant effect on the estimation of the physical and thermodynamic properties of the fluids.

Finally, the model predictions were compared with experimental data presented by Pedersen et al. (1996) for a complex system containing gas-condensate, water, and methanol. Tables E.12 and E.13 present the results of these tests. These tables show that the calculations are in good agreement with the experimental data. The model appropriately predicted the mole fraction of the three phases. The mole fraction of the dominant components in all phases is within 1.8 % of those reported experimentally. The mole fraction of methanol in hydrocarbon-rich liquid, and the vapor phase exhibit certain deviation. However, it is still acceptable for the purposes of this study. The maximum absolute difference in terms of molar fraction is 0.165 %.

Table E.12 Model results vs. exp. data presented by Pedersen et al. (1996) - Case 1

Pedersen et al. (1996) Mixture 2 - Case 1 - P = 874.57756 psia and T= 498.15 R

		Hyd. Rich Liquid			Aqueous Liquid			Vapor		
Component	**Feed**	**Exp.**	**Calc.**	**Dev. [%]**	**Exp.**	**Calc**	**Dev. [%]**	**Exp.**	**Calc**	**Dev. [%]**
Hydrocarbons	84.69	99.812	99.587	0.23	---	0.610	---	99.957	99.937	0.02
Methanol	2.99	0.201	0.366	-81.99	18.68	18.917	-1.27	0.0429	0.043	0.51
Water	12.32	---	0.048	---	81.32	80.473	1.04	---	0.020	---

Table E.13 Model results vs. exp. data presented by Pedersen et al. (1996) – Case 2

Pedersen et al. (1996) Mixture 2 - Case 2 - P = 2174.1157 psia and T= 505.53 R

		Hyd. Rich Liquid			Aqueous Liquid			Vapor		
Component	**Feed**	**Exp.**	**Calc**	**Dev. [%]**	**Exp.**	**Calc**	**Dev. [%]**	**Exp.**	**Calc**	**Dev. [%]**
Hydrocarbons	64.05511	99.812	99.755	0.06	---	0.878	--	99.931	99.889	0.04
Methanol	6.720914	0.188	0.199	-5.79	18.68	18.347	1.78	0.0687	0.082	-18.65
Water	29.22397	--	0.046	--	81.32	80.775	0.67	---	0.029	--

Typically, the model required less than 20 iterations to reach a solution. However, the algorithm may require up to 200 iterations for calculations performed near critical conditions. The maximum time required for a single flash calculation was less than 2 seconds in a computer with a Pentium 4 (2.8 GHz) processor.

E.3 Conclusions

This model proved to be capable of identifying the number of phases present in equilibrium for all cases studied. It performed two and three-phase flash calculations in a fast and reliable manner.

The model showed to provide an excellent match for Vapor-Liquid equilibria of hydrocarbon systems. It successfully calculated more than 100 dew and bubble points of different mixtures, proving to be fast and reliable even for dew and bubble point calculations near the critical point. The calculations proved to be appropriate for typical natural gas mixtures, which in some cases may contain significant fractions of non-hydrocarbon components (nitrogen, carbon dioxide, and helium).

The results illustrate the capacity of the model in performing reliable three-phase flash calculations. The calculations showed an acceptable match when compared with experimental data, even for those systems that contain large fractions of polar components. Therefore, it can be concluded that the model performs an acceptable representation of the thermodynamic behavior of complex hydrocarbon-water/methanol mixtures.

VITA

Jose S. Zaghloul

Jose S. Zaghloul received a B.S. degree in Mechanical Engineering from Universidad Central de Venezuela (1994). After graduation, he worked for Petroleos de Venezuela (PDVSA) for six years. In PDVSA, he was dedicated to design and develop major oil and gas production and transmission facilities.

In 2001, Mr. Zaghloul started his graduate studies in Petroleum and Natural Gas Engineering at Penn State University where he obtained his Master of Science degree in 2002. After graduation, he continued his doctoral studies in the same program at Penn State.

During his graduate studies several recognitions were awarded to Mr. Zaghloul. They include: Joseph and Anna Rubash Graduate Fellowship (2001), Outstanding Teaching Assistant Award (2004), Graduate Student Merit Award (2005), and the Centennial Research Award in Earth and Mineral Sciences (2006).

Mr. Zaghloul is a member of the Society of Petroleum Engineers (SPE), and the American Society of Mechanical Engineers (ASME). His research interests include reservoir engineering, fluid phase equilibria and multiphase flow.